

THEORETICAL AND COMPUTER SIMULATION STUDIES OF CHEMICAL EVENTS IN SOLUTION

Thesis Submitted for the Degree of
Doctor of Philosophy (Science)

of

Jadavpur University

By

Hemant Kumar Kashyap



Department of Chemical, Biological and Macromolecular Sciences
S. N. Bose National Centre for Basic Sciences
Block-JD, Sector-III, Salt Lake City
Kolkata-700098, INDIA
October 2009

CERTIFICATE FROM THE SUPERVISOR(S)

This is to certify that the Thesis entitled “*Theoretical and Computer Simulation Studies of Chemical Events in Solution*” submitted by Sri **Hemant Kumar Kashyap**, who got his name registered on 1st October 2007 for the award of Ph. D. (Science) degree of Jadavpur University, is absolutely based upon his own work under the supervision of **Dr. Ranjit Biswas** at S. N. Bose National Centre for Basic Sciences, Kolkata, India and that the neither this thesis nor any part of it has been submitted for either any degree /diploma or any other academic award anywhere before.

Dr. Ranjit Biswas
Thesis Supervisor

*To
My Grand Family*

Acknowledgement

I spent about five years or so at S. N. Bose National Centre for Basic Sciences (SNBNCBS), Kolkata, as a research scholar in the department of Chemical, Biological and Macromolecular Sciences (CBMS). Working here was enormous fun. This thesis work was indeed not possible without the help and support from the people in my nearest solvation shells and I am pleased to acknowledge their efforts in this regard.

First and foremost, I express my eternal gratitude to my research supervisor Prof. Ranjit Biswas for his sharp guidance, encouragement and honing my scientific skills. His kind affection has always motivated me to perform my best at all the time. I learnt from him how to handle various aspects of scientific problems by using my knowledge and intuitions. Apart from a supervisor I always found a good friend in him.

I am thankful to Prof. B. M. Deb, IISER, Kolkata, for his consistent encouragement. He has always been a source of inspiration to me, be it academic or non-academic. I offer my thanks to Prof. Jaydeb Chakrabarti for his help and advice. I really enjoyed all the frank discussions with him on various topics during my research work here. I thank to my Post-MSc. coursework teachers, especially to Profs. Surajit Sengupta and Tanushree Saha Dasgupta, for building up my basic knowledge at the initial phase of my research. I thank Prof. Gautam Gangopadhyay, Head, Dept. of CBMS, for his valuable support whenever needed. My thanks are due to Prof. Priya Mahadevan for her kind support and encouragement. I thank all the members of my Thesis Committee for their critical suggestions and help. I thank all the faculty members of the department and the Centre for support, encouragement and necessary stimulation. I thank Prof. A. K. Raychaudhuri, Director, SNBNCBS, for providing correct atmosphere to do science here.

I thank Profs. Biman Bagchi, IISc, Bangalore, and Mark Maroncelli, Pennsylvania State University, USA, for constant support and encouragement. I am thankful to Prof. Srabani Roy and her students, Arijit Roy, in IIT, Kharagpur, for helping me in learning the basics of simulation techniques in the beginning of my Ph. D. work. I thank Prof. Pratim Chatraj, IIT, Kharagpur and Prof. Amlendu Chandra, IIT, Kanpur, for valuable suggestions and advices.

I thank all the non-academic staff members of the Centre for their immense help while my stay at SNBNCBS.

I offer my thanks to my labmates - Tuhin Pradhan, Harun Al Rasid Gazi, Biswajit, Gichhait, Snehasis Daschakraborti, Tamishira Paul, Madhumita Basu and Bidyut Akhuli. It is really motivating and good to see that every one around us is working hard with full

dedication. I must thank other two members of our group Dr. Parijat Das and Rwitaban for their vital support. Special thanks to Tuhin, Biswajit and Snehasis for taking extreme care of me while I was in Hospital.

I don't have formal words to express my feelings to my friends - Iliyas, Pawan, Avishek, Alisher, Washim, Anil, Mukesh, Pradeep, Manoj, Ajay, Amit, Tushar, Sharad, Vikram, Niraj, Mainak, Shailesh, Irfan, Chinmay, Susmita, Amit (Das), Urbashi, Kinshuk, Biswajit (Das), Abhinandan, Rajiv and Sudip. They have been always with me with full support irrespective of my conditions.

I was grateful to have seniors like Manirul Ali, Abishek Chaudhury, Kartik Tarafdar, Debabrata Dutta, Mrinal Kanti Bera, Navin Chandra, Abhishek Pandey, and Venkat Kamlakar. I learnt a lot from them. It's my pleasure to thank visiting faculty, Dr. Kuntal Chakrabarti, and Postdoc, Dr Rajni Kant. They have been always educative and enthusiastic for my research progress.

I really miss my school teacher Late Girija Shankar Saini who was the prime person for building my carrier in Science.

I am lucky to have my maternal uncle Mr. Ramesh Chandra. I learnt from him how to execute my liabilities with perfection.

And finally, I express my heartfelt thanks and deep sense of gratitude to my grand parents, father (Mr. M. P. Kashyap), mother (Mrs. B. Devi), uncle (Mr. B. K. Kashyap), aunt (Mrs. G. Devi), sisters (Ranjana, Meenu and Puja) and brothers (Tinku, Monu and Sonu), and "Pooja" for their patience and deep affection towards me. I owe a lot to them.

Abstract

In this Thesis we have presented detailed theoretical and computer simulation studies on several equilibrium and dynamical processes that occur in solution phase. The systems involved are pure and mixed-solvents, electrolyte solutions and room temperature ionic liquids (RTIL). A microscopic theory, known as extended molecular hydrodynamic theory (EMHT), has been generalized in order to study ion transport and solvation dynamics in the above systems. An integral equation theory, based on the mean spherical approximation (MSA), has been developed to study the preferential solvation in mixed-solvent electrolyte solutions. The contributions to the dynamic Stokes' shift of a dipolar probe dissolved in RTIL have been separated and analyzed. In addition, the reasons for the failure of dielectric relaxation based theories in describing the Stokes' shift dynamics in the ionic liquids are discussed. Effects of spatial heterogeneity of the structure on ion transport in water-*tert* butyl alcohol (TBA) mixture have been explored.

In the first chapter of the Thesis an introduction of the present work along with the review of relevant literature has been provided. Chapter 2 contains the results of our theoretical study of limiting ionic conductivity of singly charged ions in liquid formamide and dynamical solvent response toward a photoexcited dipolar solute dissolved in the same medium. The calculated results are compared with existing experimental results to check the predictive power of the simple theoretical scheme for this complex liquid. Chapter 3 discusses our studies on ion diffusion in aqueous mixtures of *tert* butyl alcohol (TBA). In chapter 4 a semi-molecular theory based on mean spherical approximation (MSA) model has been developed for a system of ions dissolved in a mixture of asymmetric (different sizes and dipole moments) dipolar solvents. Solvation dynamics and dynamic Stokes' shift of dipolar probes in ionic liquids of different types have been studied in chapters 5 and 6. The origin of fast and slow time scales in solvation dynamics and their relation to the observed large dynamic Stokes' shifts in these liquids have been explored in these chapters. Molecular dynamics simulation studies of water-TBA mixtures covering a wide composition range have been carried out and the results are discussed in chapter 7. Chapter 8 then ends with a general conclusion where a few research problems have been suggested for future study.

List of Publications

- (1) “*Limiting Ionic Conductivity and Solvation Dynamics in Formamide*” by **Hemant K. Kashyap**, Tuhin Pradhan and Ranjit Biswas, **J. Chem. Phys.** *125*, 174506, **2006**.
- (2) “*Ions in a Binary Asymmetric Dipolar Mixture: Mole Fraction Dependent Born Energy of Solvation and Partial Solvent Polarization Structure*” by **Hemant K. Kashyap** and Ranjit Biswas, **J. Chem. Phys.** *127*, 184502, **2007**.
- (3) “*Non-ideality in Born Free Energy of Solvation in Alcohol-Water and Dimethylsulfoxide-Acetonitrile Mixtures: Solvent Size Ratio and Ion Size Dependence*” by **Hemant K. Kashyap** and Ranjit Biswas, **J. Chem. Sci.** *119*, 391, **2007**.
- (4) “*Dipolar Solvation Dynamics in Room Temperature Ionic Liquids: An Effective Medium Calculation Using Dielectric Relaxation Data*” by **Hemant K. Kashyap** and Ranjit Biswas, **J. Phys. Chem. B** *112*, 12431, **2008**.
- (5) “*Solvation Dynamics of Dipolar Solute in Room Temperature Ionic Liquids: Separation of Ion-dipole and Dipole-dipole Interaction contributions*” by **Hemant K. Kashyap** and Ranjit Biswas, **J. Phys. Chem. B**, **2009** (in press).
- (6) “*Molecular Dynamics Simulation Studies of Water – Tertiary Butyl Alcohol (TBA) Binary Mixtures: Mole-fraction Dependent Correlation Functions, Static Dielectric Constants, and Diffusion Coefficients*” by **Hemant K. Kashyap** and Ranjit Biswas, (**submitted**).
- (7) “*Limiting Ionic Mobility in Tertiary Butyl Alcohol (TBA)-Water Mixture*” by **Hemant K. Kashyap** and Ranjit Biswas, (**submitted**).
- (8)* “*Solvation Dynamics in Ionic Liquids: Temperature Dependence*” by **Hemant K. Kashyap** and Ranjit Biswas, (**in preparation**).

(9)* “*Stokes’ Shift and Its Dynamics in Ternary Ionic Melt Mixtures: Experiment and Theory*” by Biswajit Guchhait, Harun A. R. Gazi, **Hemant K. Kashyap** and Ranjit Biswas, (**in preparation**).

(10)* “*Solvation and Rotational Dynamics in Electrolyte Solutions of Binary Polar Solvent Mixtures*” by Harun A. R. Gazi, **Hemant K. Kashyap** and Ranjit Biswas, (**in preparation**).

* *Not included in this Thesis*

Contents

Chapter 1: Introduction.....	13
Chapter 2: Ionic Conductivity and Solvation Dynamics in Formamide.....	25
2.1 Introduction.....	25
2.2 The Molecular Theory.....	29
2.2.1 Limiting Molar Ionic Conductivity.....	30
2.2.2 Dipolar Solvation Dynamics.....	33
2.3 Calculation Procedure.....	34
2.3.1 Calculation of Generalized Rate of Solvent Polarization Relaxation, $\sum_{lm}(k, z)$	34
2.3.2 Calculation of Static Correlation Functions.....	37
2.3.2.1 Solvent Dipole-dipole Direct Correlation Functions, $c(110, k)$ and $c(111, k)$	37
2.3.2.2 Ion-dipole Direct Correlation Function, $c_{id}^{10}(k)$	38
2.3.2.3 Solute Dipole – Solvent Dipole Direct Correlation Function, $c_{sd}^{10}(k)$	40
2.4 Results & Discussion.....	40
2.4.1 Limiting Molar Ionic Conductivity and Temperature Dependence.....	40
2.4.2 Solvation Dynamic and Temperature Dependence.....	46
2.5 Conclusion.....	48
References.....	51
Chapter 3: Limiting Ionic Conductivity in Water – Tertiary Butyl Alcohol (TBA) Mixtures: Alcohol Molefraction Dependence.....	56
3.1 Introduction.....	56
3.2 Theory.....	59
3.3 Calculation Procedure.....	60
3.3.1 Calculation of Static Correlation Functions.....	60
3.3.2 Calculation of the Longitudinal Component of Generalized Rate of	

Solvent Polarization Relaxation, $\sum_{10}(k, z)$	63
3.4 Numerical Results and Discussion	65
3.4.1 Li ⁺ in Water-TBA	65
3.4.2 Na ⁺ in Water-TBA	67
3.4.3 K ⁺ in Water-TBA	68
3.4.4 C ₁ in Water-TBA	68
3.4.5 C ₄ in Water-TBA	68
3.5 Conclusion	71
References	73
Chapter 4: Ion Solvation in Asymmetric Binary Dipolar Mixture...	77
4.1 Introduction	77
4.2 Theoretical Formulation	80
4.2.1 Model Description	81
4.2.2 Interaction Potentials among Different Species	81
4.2.3 Ornstein-Zernike (OZ) Relations for the System of Ions in Binary Mixture	82
4.2.4 MSA Closure	82
4.2.5 Multiplication Table for 1, E_i , D_{ij} and Δ_{ij}	83
4.2.6 Ion-solvent and Solvent-solvent Correlation Functions in Electrolyte Solution of Binary Dipolar Mixture	83
4.2.7 Born Free Energy of Solvation of an Ion in Binary Dipolar Mixture	87
4.2.8 Solvent Partial Polarization Densities of an Ion at Infinite Dilution in a Binary Dipolar Mixture	92
4.3 Results & Discussion	92
4.3.1 Born Free Energy of Solvation	93
4.3.1.1 Born Free Energy in Model Binary Mixtures	93
4.3.1.2 Born Free Energy in Alcohol-Water Mixtures	95
4.3.1.3 Born Free Energy in DMSO-Acetonitrile Mixtures	101
4.3.2 Partial Polarization Densities	103
4.3.2.1 Partial Polarization Densities in Alcohol-Water Mixtures	103
4.3.2.2 Partial Polarization Densities in DMSO-Acetonitrile Mixtures	108
4.3.3 Comparison with Experiments	109
4.4 Conclusion	113

Appendix.....	115
References.....	116

Chapter 5: Dipolar Solvation Dynamics in Dipolar Room

Temperature Ionic Liquids.....	119
5.1 Introduction.....	119
5.2 Computational Details.....	124
5.3 Results & Discussion.....	127
5.3.1 DCS in [bmim][PF ₆]	128
5.3.2 DCS in [bmim][BF ₄]	130
5.3.3 C153 in [bmim][PF ₆]	132
5.3.4 4-AP in [bmim][PF ₆]	134
5.3.5 DCS in [bmim][DCA]	134
5.3.6 DCS in [hmim][BF ₄].....	135
5.4 Probe Dependence of Solvation Dynamics in RTILs.....	135
5.5 Conclusion.....	138
References and Notes.....	141

Chapter 6: Solvation Dynamics in Room Temperature Ionic Liquids: Role of Dipole-dipole and Dipole-ion Interactions.....144

6.1 Introduction.....	144
6.2 The Molecular Theory.....	148
6.2.1 Total Solvation Response Function, $S_E(t)$	148
6.2.2 Solvation Response Function due to Solute Dipole and Solvent Dipole Interaction, $S_{sd}(t)$	152
6.2.3 Solvation Response Function due to Solute Dipole and Solvent Charge (Ion) Interaction, $S_{si}(t)$	153
6.3 Results & Discussion.....	155
6.3.1 Imidazolium Ionic Liquids: Stokes' Shift and Dynamics.....	155
6.3.2 Phosphonium Ionic Liquids: Stokes' Shift and Dynamics.....	155
6.3.3 Continuum Model and Present Theory.....	171
6.4 Conclusion.....	174
References and Notes	180

Chapter 7: Molecular Dynamics Simulation Studies of Water –

Tertiary Butyl Alcohol (TBA) Mixtures: Equilibrium and Dynamical Properties.....	185
7.1 Introduction.....	185
7.2 Models and Simulation Details.....	187
7.3 Results & Discussion.....	189
7.3.1 Equilibrium Properties.....	189
7.3.1.1 Potential Energies.....	189
7.3.1.2 Site-site Radial Distribution Functions.....	191
7.3.1.3 Orientational Distribution Functions.....	194
7.3.1.4 Dielectric Constant.....	196
7.3.2 Dynamical Properties.....	197
7.3.2.1 Velocity Autocorrelation Functions.....	197
7.3.2.2 Mean Square Displacement	199
7.3.2.3 Self Diffusion Coefficient.....	201
7.3.2.4 Mutual Diffusion Coefficient.....	201
7.4 Summary and Conclusion.....	206
References.....	208
Chapter 8: Concluding Remarks and Future Problems.....	211
8.1 Future Problems.....	213
8.1.1 Electrolyte Concentration Dependence of Molar Ionic Conductivity in Mixed Solvents.....	213
8.1.2 Ionic Conductivity of Multivalent Ions in Pure Solvents.....	214
8.1.3 Solvation and Rotational Dynamics in Electrolyte Solutions of Mixed Solvents.....	214
8.1.4 Solvation and Rotational Dynamics in (Amide + Salt) Mixtures.....	214
8.1.5 Electron Transfer Reactions in Room Temperature Ionic Liquids.....	215
8.1.6 Solvation Dynamics in Common Dipolar Solvents Using DCS as Probe.....	215
References	217
Appendix I.....	218
Appendix II.....	222
Appendix III.....	227

Chapter 1

Introduction

Chemical reactions constitute a central part both in chemistry and biology.¹⁻¹⁷ Usually, such reactions involve exchange of atoms or groups, rearrangement of groups around a double bond, transfer of charge or a proton, enzyme-catalyzed cleavage of a bio-active moiety, micellization, polymerization or even protein folding. These reactions, more often than not, occur in solution phase where more than one solvent component may be present. Many of the above chemical reactions can be understood in terms of potential energy surface where a sizeable barrier separates the product from the reactant. Understanding the role of a medium on a given reaction then revolves around understanding the medium-induced modifications of the reaction barrier and passage of the reactant to the product through the barrier region. Therefore, reaction in solution phase is modified via both the static and dynamic medium effects.

Solvent static effects on a reaction involve the modification of the barrier height via the solvent polarity. The dynamical part of the solvent influence on the rate of a given reaction depends on how fast the solvent molecules solvate both the reactants and products. How a given reaction dynamically couples to its solvent environment depends on the solvation time scales. In ultrafast solvents like water, alcohol and acetonitrile, these time scales range from tens of femtosecond to few picoseconds.^{4,18-19} In usual time resolved fluorescence spectroscopic techniques these time scales are probed by monitoring the fluorescence emission frequency of a laser excited fluorescent molecule.^{4,18-19} As inter-diffusion and preferential solvation significantly slows down the dynamics in binary mixtures than in pure solvents, solvent effects on chemical reactions are expected to be more complex in binary liquid mixtures.²⁰⁻²⁵ The advantage of solvent mixtures over pure solvents is that by changing the composition of the mixture one can tune the polarity, solubility, viscosity and many of its static and dynamic properties. Similar advantage is with electrolyte solution where one can change the average polarity of the medium by changing the electrolyte

concentration in the solution. In addition to electrolyte-induced modification in solution polarity, the interactions of the reactant with the dissociated ions, ion-pairs and, other charged and neutral species can significantly alter both the rate and yield of a chemical reaction.²⁶ Another class of solvent - room temperature ionic liquids- which can act both as electrolyte and solvent are now emerging as a useful alternative reaction media because of its high thermal stability, low volatility and a broad liquid range.²⁷⁻³³ Because of these reasons, attention is now shifted from pure to mixed solvents, electrolyte solutions and room temperature ionic liquids. However, an important feature has always been to explore how different *dynamically* these complex systems are from the relatively better understood conventional polar solvents at ambient condition. As will be seen later, this has also been one of our goals with the calculations performed for several systems considered in this Thesis.

Apart from controlling the reaction rate, dynamics of solvation has also been found to play an important role in ion transport processes.^{14-15,34-37} An extended molecular hydrodynamic theory, which was developed earlier to study polar solvation dynamics in simple dipolar solvents, has been found to be very successful in predicting the experimentally measured limiting ionic mobility of small uni-positive ions in several complex polar solvents, such as, water and monohydroxy alcohols. These studies have indicated a very close connection between the ultrafast solvation response and ion diffusion in these dipolar solvents. Solvents of more complex character where, in addition to intermolecular hydrogen bonding, some degree of polymerization also exists (for example, formamide), have not been considered earlier for exploring the inter-connection between the dynamic solvation response and ionic mobility.

Another interesting problem related to ion transport is the experimentally observed non-monotonic alcohol mole fraction dependence of limiting ionic conductivity of alkali metal ions in the water-rich region of aqueous mixtures of tertiary butyl alcohol.³⁸ Eventhough these results are known for a pretty long time, one does not know what are the contributions of the solution structure and dynamics to these observed dependence. If one considers the mole fraction dependence of either viscosity or dielectric relaxation times in this region,³⁸⁻³⁹ one does not find any non-linearity in them. However, the available dielectric relaxation data³⁹ does indicate presence of a stretching exponent which may be a signature of the microscopic

heterogeneity present in water-TBA mixtures. Extensive experimental⁴⁰⁻⁴⁸ and computer simulation⁴⁹⁻⁵⁷ studies have revealed microscopic solution heterogeneity in these mixtures and alcohol mole-fraction induced solution structural transition from the tetrahedral water-like hydrogen bonding network to alcohol-like zigzag structure. One therefore wonders what could be the possible effects of such structural aspects on the polarization structure around an ion moving through an aqueous mixture of TBA. Since in such a mixture microscopic heterogeneity is induced by the hydrophobic interaction and polarization structure around an ion in it is governed by the preferential solvation, it becomes a non-trivial task to include all these aspects in a simple analytical theory that desires to explain the experimentally observed ionic conductivity. Moreover, no theory exists in the literature that even qualitatively describes static structural aspects of a ‘homogeneous’ solution where three distinct components – two different dipolar solvent species and ions – are present in a single solution phase. In this Thesis an attempt has been made to develop a semi-molecular theory based on the mean spherical approximation (MSA) formalism in order to calculate the microscopic polarization around an ion dissolved in a binary polar mixture.

As expected, the theory that assumes *a priori* the solution homogeneity cannot describe properly the solution structure that is expected to possess microscopic heterogeneity due to hydrophobic and/or H-bonding interactions. Since interaction among the tertiary butyl groups in TBA molecules leads to domain formation in aqueous water-TBA mixtures, an MSA type description for the static correlations is bound to be inaccurate. As a result, the use of these correlations as input for the calculations of ion mobility lead to insufficient depiction of the composition dependence of limiting ionic conductivity in water-TBA mixtures. Logically then one should carry out computer simulation studies with realistic interaction potential functions for these mixtures at various compositions and use the simulated static correlations to explore the reasons that render the non-monotonic composition dependence of the limiting ionic conductivity. One can of course set up extended reference interaction site model (XRISM) calculations for the solution static structure factor but that is also a numerically extensive technique. Considering all these, molecular dynamics simulation studies of water-TBA mixtures have been carried out for several TBA mole fractions. These simulations serve at least two purposes. First, it

supplies semi-accurate static correlations required for the calculations of limiting ionic conductivity. Second, it provides an opportunity to study the alcohol mole fraction dependence of the self and crossed diffusion coefficients in these mixtures. The availability of experimental results for some of these mixtures makes a direct comparison with simulated results possible and thus provides an opportunity to test the ability of the model potentials (used in simulation studies here) for describing the structural aspects of real solutions.

Since the quest for suitable reaction media continues, newer systems emerge with certain physico-chemical properties that possess distinct advantages over the conventional organic solvents or their mixtures. Room temperature ionic liquids, and salts that become liquid ~ 10 - 20 K above the room temperature are now increasingly used as alternative reaction media not only in laboratory for organic synthesis⁵⁸ but also in chemical industries for large scale production.²⁷⁻²⁸ Electrolyte solutions in binary polar solvent mixtures,⁵⁹ and mixtures of inorganic salts with acetamide and substituted acetamide⁶⁰ are also other examples which have been in use as alternative reaction media. While some measurements on dynamical aspects of ionic liquids have begun to emerge, similar studies for electrolyte solutions of binary solvent mixtures and solutions of acetamide with inorganic salts are still lacking. For example, there exists only one dielectric relaxation study of (acetamide + NaSCN) mixture even though such mixtures are very interesting systems as the degree of super-cooling depends on the identity and charge of the ions. Dynamic Stokes' shift measurements and dielectric relaxation studies of several imidazolium ionic liquids have revealed the presence of extremely fast times scales which are reminiscent of those in conventional dipolar solvents. These results as well as the observation of large Stokes' shifts for dipolar solute probes dissolved in these highly viscous liquids of low dielectric constant fuels the debate as what could be the possible reasons for such fast time scales and large dynamic Stokes' shifts. An attempt has been made in the present Thesis to separate out the dipole-dipole and dipole-ion contributions to the observed shifts. In addition, the origin of fast time scales in some of the ionic liquids has been investigated and relationship between solvation energy relaxation of an excited dipolar solute and the frequency dependent dielectric function of these explored. Note that earlier studies have found strong interconnection between the solvation dynamics and dielectric relaxation for common dipolar solvents.³⁴

The present Thesis is therefore divided in several chapters where the next chapter (chapter 2) contains the results on our theoretical studies of limiting ionic conductivity and solvation dynamics in formamide at room temperature. Note the calculation method used here is based on a self-consistent extended molecular hydrodynamic theory (EMHT) developed earlier³⁴⁻³⁷ to study similar problems in simple polar solvents. The calculated results are compared with experimental data.⁶¹ The temperature dependence of total ionic conductivity of a given uni-univalent electrolyte in formamide and solvation dynamics of a dissolved dipolar probe have also been studied. The effects of dynamic polar solvation response on ionic conductivity have been investigated by studying the time dependent progress of solvation of a polarity probe dissolved in formamide. The intermolecular libration⁶²⁻⁶³ bands which are often detected in the range of 100-200 cm^{-1} in formamide are systematically incorporated in the calculation to investigate their role in determining both the conductivity and the ultrafast polar solvation response in formamide.

The same EMHT theory is then used to describe the observed composition dependence of the limiting ionic conductivity of monovalent ions in aqueous mixtures of TBA.³⁸ The numerical results and their comparisons with experimental data are provided in chapter 3. The effects of spatial heterogeneity in water-TBA solutions on ionic mobility are incorporated via using the simulated static correlations as input to the theory. This leads to a very good agreement between theory and experiments and indicate that it is the solution structure that plays the key role in producing the non-monotonic composition dependence of limiting ionic conductivity of alkali metal ions in the water-rich region of aqueous solutions of TBA.

Chapter 4 describes a semi-molecular theory (based on the MSA model⁶⁴⁻⁶⁵) developed to investigate the role of partial solvent polarization densities on Born free energy of solvation for an ion dissolved in a completely asymmetric binary dipolar mixture. The differences in solvent diameters, dipole moments and ionic size are incorporated systematically within the MSA framework.⁶⁶⁻⁷⁰ Subsequently, the theory is used to investigate the role of ion-solvent and solvent-solvent size ratios in determining the non-ideality in Born free energy of solvation of a uni-positive rigid ion in alcohol-water (associating solvents) and dimethylsulfoxide-acetonitrile (non-

associating solvents) mixtures where the solvent components are represented *only* by their molecular diameters and dipole moments.

Chapters 5 and 6 describe the numerical results obtained by using a semi-molecular theory for studying solvation dynamics and dynamic Stokes' shift in several imidazolium and phosphonium ionic liquids. The theory developed for this study is also described in detail in these chapters. Recent solvation dynamics experiments with common dipolar solvation probes in imidazolium ionic liquids (dipolar) have revealed large dynamic Stokes' shifts and biphasic solvation energy relaxations.⁷¹⁻⁷⁹ For non-dipolar ionic liquids such as phosphonium cation based ionic liquids the dynamic Stokes' shift is rather small and solvation energy relaxation is found to be a single stretched-exponential decay function with a time constant of about couple of a nanosecond. The theory presented in these chapters has been able to explain the experimental results with surprising accuracy. The validity of the dynamic continuum model for describing the solvation dynamics in these ionic liquids have also been tested and reasons for failure described.

It has already been mentioned that extensive experimental⁴⁰⁻⁴⁸ and simulation⁴⁹⁻⁵⁷ studies have already been carried out to investigate the structural and dynamical aspects of water-TBA mixtures. But most of them were concentrated towards low TBA concentration region and less attention has been given to alcohol-rich region where several interesting properties of the mixture have been also reported. For example neutron diffraction experiment of Bowron *et al.* reveals the clustering of water molecules in this region.⁴² Interestingly the viscosity vs TBA molefraction curve also shows a shallow minimum near the concentrated alcohol composition.³⁸ Therefore, although the static and dynamic properties of these mixtures are well characterized, a comprehensive understanding of the anomalous features in alcohol-rich region is still lacking. In chapter 7 all atom flexible models of water and TBA have been used to carry out molecular dynamics (MD) simulations for water-TBA over whole composition range at 300K temperature. The simulated pair distribution functions for various sites of water and TBA molecules have been calculated in order to study the microscopy structure of these mixtures. Simulated static dielectric constants for the mixture (from orientational correlation functions as well as collective dipole-moment fluctuation) have been compared with the experimental

data. Self diffusion coefficients of the constituent solvent molecules have been calculated using velocity autocorrelation function (VACF) and mean square displacement (MSD), and compared with available experimental results. In addition the simulated results for mutual (crossed) diffusion coefficient in the mixture have also been presented in this chapter.

A brief concluding remark of this thesis work is presented in chapter 8. In addition, we have discussed a few research problems in this chapter which may be studied in future.

References

1. P. J. Rossky and J. D. Simon, *Nature* **370**, 263 (1994).
2. M. Maroncelli, J. MacInnis and G. R. Fleming, *Science* **243**, 1674 (1989).
3. A. E. Bragg, M. C. Cavanagh and B. J. Schwartz, *Science* **321**, 1817 (2008).
4. R. Jimenez, G. R. Fleming, P. V. Kumar and M. Maroncelli, *Nature* **369**, 471 (1994).
5. G. vander Zwan and J. T. Hynes, *Chem. Phys.* **152**, 169 (1991).
6. (a) J. D. Simon, *Pure & Appl. Chem.* **62**, 2243 (1990); (b) J. D. Simon, *Acc. Chem. Res.* **21**, 128 (1988).
7. G. R. Fleming and P. G. Wolynes, *Phys. Today* **43**, 36 (1990).
8. J. T. Hynes, *Annu. Rev. Phys. Chem.* **36**, 573 (1985).
9. R. F. Grote and J. T. Hynes, *J. Chem. Phys.* **73**, 2715 (1980).
10. G. A. Voth and R. M. Hochstrasser, *J. Phys. Chem.* **100**, 13034 (1996).
11. (a) R. A. Marcus and N. Sutin, *Biochem. Biophys. Acta* **811** 275 (1985); (b) H. Sumi and R. A. Marcus, *J. Chem. Phys.* **84**, 4894 (1986).
12. (a) S. Mukamel and Y. J. Yan, *Acc. Chem. Res.* **22**, 301 (1989); (b) S. Mukamel, *Adv. Chem. Phys.* **70**, 165 (1988).
13. G. L. Closs and J. R. Miller, *Science* **240**, 440 (1988).
14. B. Bagchi, *Annu. Rev. Phys. Chem.* **40**, 115 (1989).
15. B. Bagchi and A. Chandra, *Adv. Chem. Phys.* **80**, 1 (1991).
16. B. Bagchi and N. Gayathri, *Adv. Chem. Phys.* **107**, 1 (1999).
17. M. W. Makinen, S. A. Schichman, S. C. Gill and H. B. Gray, *Science* **222**, 929 (1983).
18. C. F. Chapman and M. Maroncelli, *J. Phys. Chem.* **95**, 9095 (1991).
19. M. L. Horng, J. A. Gardecki, A. Papazyan and M. Maroncelli, *J. Phys. Chem.* **99**, 17311 (1995).
20. A. Chandra, *Chem. Phys. Lett.* **235**, 133 (1995).
21. (a) S. Chowdhuri and A. Chandra, *J. Chem. Phys.* **119**, 4360 (2003); (b) S. Chowdhuri and A. Chandra, *J. Chem. Phys.* **123**, 234501 (2005).
22. R. Gupta and A. Chandra, *J. Chem. Phys.* **127**, 024503 (2007).
23. T. J. F. Day and G. N. Patey, *J. Chem. Phys.* **110**, 10937(1999).
24. H. Li, S. Arzhantsev and M. Maroncelli, *J. Phys. Chem. B* **111**, 3208 (2007).
25. J. A. Gardecki and M. Maroncelli, *Chem. Phys. Lett.* **301**, 571 (1999).

26. T. Pradhan, H. A. R. Gazi and R. Biswas, *J. Chem. Phys.* **131**, 054507 (2009).
27. R. D. Rogers and K. R. Seddon, *Ionic Liquids: Industrial Application for Green Chemistry*, American Chemical Society Symposium Series 818, American Chemical Society: Washington, DC, 2002.
28. P. Wasserscheid and T. Welton, *Ionic Liquids in synthesis*; Wiley-VCH: New York, 2003.
29. H. Jin, X. Li and M. Maroncelli, *J. Phys. Chem. B* **111**, 13473 (2007).
30. H. Jin, G. A. Baker, S. Arzhantsev, J. Dong and M. Maroncelli, *J. Phys. Chem. B* **111**, 7291 (2007).
31. H. Jin, B. O'Hare, J. Dong, S. Arzhantsev, G. A. Baker, J. F. Wishart, A. J. Benesi and M. Maroncelli, *J. Phys. Chem. B* **112**, 81 (2008).
32. Y. Wang and G. A. Voth, *J. Am. Chem. Soc.* **127**, 12192 (2005).
33. Z. Hu and C. J. Margulis, *Proc. Natl. Acad. Sci. U. S. A.* **103**, 831 (2006).
34. B. Bagchi and R. Biswas, *Adv. Chem. Phys.* **109**, 207 (1999) and references therein.
35. B. Bagchi, *J. Chem. Phys.* **95**, 467 (1991).
36. (a) R. Biswas, S. Roy and B. Bagchi, *Phys. Rev. Lett.* **75**, 1098 (1995); (b) R. Biswas and B. Bagchi, *J. Chem. Phys.* **106**, 5587 (1997); (c) R. Biswas and B. Bagchi, *J. Am. Chem. Soc.* **119**, 5946 (1997); (d) R. Biswas and B. Bagchi, *J. Phys. Chem.* **100**, 1238 (1996); (e) R. Biswas and B. Bagchi, *J. Phys. Chem.* **100**, 4261 (1996).
37. B. Bagchi and R. Biswas, *Acc. Chem. Res.* **31**, 181 (1998).
38. T. L. Broadwater and R. L. Kay, *J. Phys. Chem.* **74**, 3802 (1970).
39. S. Mashimo and N. Miura, *J. Chem. Phys.* **99**, 9874 (1993).
40. S. Dixit, J. Crain, W. C. K. Poon, J. L. Finney and A. K. Soper, *Nature*, **416**, 829 (2002).
41. (a) D. T. Bowron and J. L. Finney, *J. Phys. Chem. B* **111**, 9838 (2007); (b) D. T. Bowron, J. L. Finney and A. K. Soper, *J. Phys. Chem. B* **102**, 3551 (1998).
42. D. T. Bowron and S. D. Moreno, *J. Chem. Phys.* **117**, 3753 (2002).
43. M. Nakada, O. Yamamuro, K. Maruyama and M. Misawa, *J. Phys. Soc. Jpn.* **76**, 054601 (2007).
44. V. Calandrini, A. Deriu, G. Onori, R. E. Lechner and J. Pieper, *J. Chem. Phys.* **120**, 4759 (2004).

45. (a) Y. Koga, Chem. Phys. Lett. **111**, 176 (1984); (b) Y. Koga, Can. J. Chem. **66**, 1187 (1988); (c) Y. Koga, Can. J. Chem. **66**, 3171 (1988).
46. (a) K. Iwasaaki and T. Fusiyaama, J. Phys. Chem. **81**, 1908 (1977); (b) K. Iwasaaki and T. Fusiyaama, J. Phys. Chem. **83**, 463 (1979).
47. F. Franks and D. J. G. Ives, Q. Rev. Chem. Soc. **20**, 1 (1966).
48. M. Brai and U. Kaatz, J. Phys. Chem. **90**, 8946 (1992).
49. K. Nakanishi, K. Ikari, S. Okazaki and H. Touhara, J. Chem. Phys. **80**, 1656 (1984).
50. H. Tanaka, K. Nakanishi and H. Touhara, J. Chem. Phys. **81**, 4065 (1984).
51. I. Omelyan, A. Kovalenko and F. Hirata, J. Theo. Compu. Chem. **2**, 193 (2003).
52. M. E. Lee and N. F. A. van der Vegt, J. Chem. Phys. **122**, 114509 (2005).
53. E. S. Ferrari, R. C. Burton, R. J. Davey and A. Gavezzotti, J. Comput. Chem. **27**, 1211 (2006).
54. A. Parera, F. Sokolic, L. Almasy and Y. Koga, J. Chem. Phys. **124**, 124515 (2006).
55. M. Kiselev and Ivlev, J. Mol. Liq. **110**, 193 (2004).
56. (a) P. G. Kusalik, A. P. Lyubartsev, D. L. Bergman, and Aatto Laaksonen, J. Phys. Chem. B. **104**, 9526 (2000); (b) P. G. Kusalik, A. P. Lyubartsev, D. L. Bergman, and Aatto Laaksonen, J. Phys. Chem. B **104**, 9533 (2000).
57. S. Paul and G. N. Patey, J. Phys. Chem. B **110**, 10514 (2006).
58. A. K. Chakraborti and S. R. Roy, J. Am. Chem. Soc. **131**, 6802 (2009).
59. H. A. R. Gazi, H. K. Kashyap and R. Biswas (in preparation).
60. B. Guchhait, H. A. R. Gazi, H. K. Kashyap and R. Biswas (in preparation).
61. J. Thomas and D. F. Evans, J. Phys. Chem. **74**, 3812 (1970).
62. O. F. Nielsen, P. A. Lund and E. Praestgaard, J. Chem. Phys. **77**, 3878 (1982).
63. Y. J. Chang and E. W. Castner, Jr., J. Chem. Phys. **99**, 113 (1993).
64. C. G. Gray and K. E. Gubbins, *Theory of Molecular Liquids*, Clarendon: Oxford, 1984).
65. J. P. Hensen and I. R. McDonald, *Theory of Simple Liquids*, Academic Press: San Diego, CA, 1986.
66. M. S. Wertheim, J. Chem. Phys. **55**, 4291 (1971).
67. S. A. Adelman and J. M. Deutch, J. Chem. Phys. **59**, 3971 (1973).
68. D. Isbister and R. Bearman, J. Mol. Phys. **28**, 1297 (1974).

69. L. Blum, J. Chem. Phys. **61**, 2129 (1974).
70. P. T. Cummings and L. Blum, J. Chem. Phys. **85**, 6658(1986).
71. S. Arzhantsev, H. Jin, G. A. Baker and M. Maroncelli, J. Phys. Chem. B **111**, 4978 (2007).
72. (a) R. Karamkar and A. Samanta, J. Phys. Chem. A **106**, 4447 (2002); (b) R. Karamkar and A. Samanta, J. Phys. Chem. A **106**, 6670 (2002).
73. J. A. Ingram, R. S. Moog, N. Ito, R. Biswas and M. Maroncelli, J. Phys. Chem. B **107**, 5926 (2003).
74. N. Ito, S. Arzhantsev and M. Maroncelli, Chem. Phys. Lett. **396**, 83 (2004).
75. (a) A. Paul and A. Samanta, J. Phys. Chem. B **111**, 4724 (2007); (b) A. Paul and A. Samanta, J. Phys. Chem. B **111**, 1957 (2007).
76. A. Samanta, J. Phys. Chem. B **110**, 13704 (2006).
77. (a) P. K. Mandal and A. Samanta, J. Phys. Chem. B **109**, 15172 (2005); (b) P. K. Mandal, M Sarkar and A. Samanta, J. Phys. Chem. B **108**, 9048 (2004); (c) R. Karamkar and A. Samanta, J. Phys. Chem. A **107**, 7340 (2003).
78. B. L. Bhargava and S. Balasubramanian, J. Chem. Phys. **123**, 144505 (2005).
79. (a) M. N. Kobrak, J. Chem. Phys. **125**, 064502 (2006); (b) M. N. Kobrak and V. Znamenskiy, Chem. Phys. Lett. **395**, 127 (2004); (c) M. N. Kobrak, J. Chem. Phys. **127**,184507 (2007).

Chapter 2

Ionic Conductivity and Solvation

Dynamics in Formamide

2.1 Introduction

Formamide and its substituted derivatives are strongly associating molecular liquids and therefore constitute an important class of solvents.¹⁻¹⁷ These liquids are characterized by large values of permanent dipole moments and dielectric constants. These solvents are also strong hydrogen bond (H-bond) donors and stronger H-bond acceptors than water. Owing to its unique H-bonding capability, formamide can exist as both cyclic dimers and linear chain oligomers in liquid phase at room temperature. The structures of formamide in its gas,¹⁸ amorphous,¹⁹ crystalline,²⁰ and liquid phases have also been investigated through experiments,¹⁷⁻³⁰ simulations³¹⁻³⁵ and theoretical calculations.^{13,14} Recently, several authors have looked at equilibrium and excited state dynamics of formamide by using non-linear spectroscopic techniques.³⁻⁷ All these activities are partially motivated by the fact that formamide can be used as a model system for studying the hydrogen bonding interactions that occur between amido protons on a hydrated protein backbone. The aqueous mixture of formamide³⁶⁻³⁸ could be an excellent model system for studying hydrogen bonding interactions that may occur in hydrated protein chains. Since formamide contains important structural units like carbonyl and amino groups as well as peptide bond, this molecule stands as the simplest building block for amide based catenane and rotaxane systems that are used as excellent molecular templates for tailoring materials with user-defined properties.³⁹⁻⁴² It is also predicted that the coupling between the low frequency vibrations in formamide may play an important role for conformational changes and enzymatic actions in biological systems.⁴³⁻⁴⁴ For example, an out-of-plane vibrational mode of a hydrogen bonded system is likely to be involved in a conformational change in a biologically relevant moiety.

The investigation of ion transport and solvation processes in formamide is crucial because of the following reasons. A considerable amount of understanding about the role of ion-solvent interaction and the role of structure and dynamics of solvent in determining ion mobility can be achieved by studying ion transport in electrolyte solutions.⁴⁵⁻⁵³ The discovery of biphasic polar solvation response⁴⁹⁻⁵³ has motivated further studies to answer the following question: To what extent can the ultrafast solvation response of sub-pico-second time scale control a diffusive process like ion conductance which takes place on a time scale of tens of pico-seconds or even longer?

One of the central quantities in the study of transport properties in electrolyte solutions is the ionic conductance (Λ). In the low concentration limit of strong electrolytes where the dissociation is assumed to be complete, the concentration dependence of conductivity in solutions of polar solvents such as formamide, substituted amides, water, acetonitrile and alcohols is described by the Kohlrausch's law as follows:⁴⁵⁻⁴⁸

$$\Lambda_m = \Lambda_0 - \kappa\sqrt{c} \quad , \quad (2.1)$$

where Λ_m represents the equivalent molar conductivity, Λ_0 is its limiting value at infinite dilution, κ is a coefficient that is found to depend more on the nature of the electrolyte than on its specific identity. Extrapolation of Λ_m to zero ion concentration produces Λ_0 .

The equivalent conductivity at infinite dilution, Λ_0 , is essentially related to the ion mobility U under the influence of externally applied weak electric field in the following manner:⁴⁵⁻⁴⁷

$$\Lambda_0 = UF = |q| \frac{F}{\zeta} = \frac{|q|F}{A\eta_0 r_{ion}} \quad , \quad (2.2)$$

where F stands for Faraday constant and q the charge on the ion. ζ is the ionic friction coefficient. The third equality in the above equation arises if one assumes that

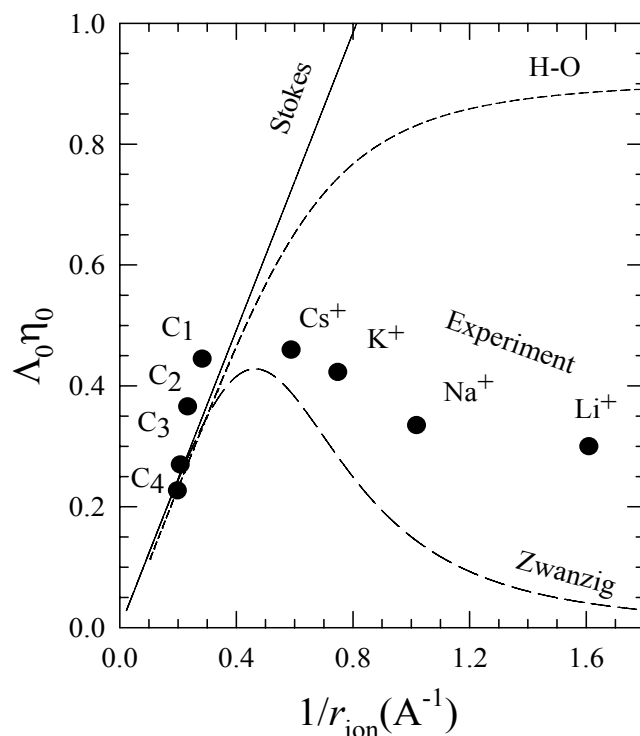


Figure 2.1: Comparison between the experimental results (*solid circles*) of Walden product ($\Lambda_0\eta_0$) for the uni-positive alkali, and tetra-alkyl ammonium ions as a function of inverse of crystallographic radius (r_{ion}^{-1}) for formamide at room temperature with the predicted values of Stokes's law (*solid line*), Hubbard-Onsager theory (*short dashed line*), and continuum theory of Zwanzig (*long dashed line*). Here, the tetra-alkyl ammonium ions are represented by C₁-C₄ where C_n = (C_nH_{2n+1})₄N⁺; n is from 1 to 4. The experimental data shown here are taken from J. Thomas and D. F. Evans, *J. Phys. Chem.*, **74**, 3812 (1970).

the friction experienced by an ion with crystallographic radius, r_{ion} , moving through a solvent with viscosity, η_0 , can be obtained from hydrodynamics by using the Stokes' law. A is a constant and the value of which depends upon boundary conditions (slip or stick). This immediately tells us that $\Lambda_0\eta_0$ is proportional to the inverse of the crystallographic radii of the ions in a given solvent. This is known as the *Walden's rule* and was found to be valid for large singly charged ions.⁴⁵⁻⁴⁸ However, as the ions become smaller, the deviation becomes larger leading to stronger non-monotonic ion size dependence. This is shown in Fig. 2.1.

Initially, the break down of Walden's rule was explained in terms of *solvent-berg* model.^{45,46} This model assumes that the solvent molecules in the first solvation shell around the ion are rigidly bound to it and hence the effective radius is much larger

than the crystallographic radius of the bare ion. This bigger size automatically reduces the mobility of the ion. The effective size of such composite unit increases in size as ion becomes smaller. However, this model fails to explain the limiting ionic conductivity of ions for which the ion-solvent size ratio approaches to unity.

Later, Born suggested that in addition to the mechanical (bare) friction, the ion experiences retardation due to the coupling of its electric field with solvent polarization while moving through the solvent.⁵⁴ This additional friction is termed as dielectric friction in Born's model and therefore the total friction on the ion is a sum of bare friction and dielectric friction. Fuoss, Boyd and Zwanzig further developed the dielectric friction model,⁵⁵⁻⁵⁷ and Zwanzig, after incorporating the electrohydrodynamic effects, obtained an expression where dielectric friction varies inversely as the volume of the ion. The prediction of Zwanzig's theory⁵⁷ for ions in formamide is shown in Fig. 2.1. In all these models, the solvent was treated as a structure-less continuum characterized by frequency dependent dielectric function and a single Debye relaxation time, τ_D .

Hubbard and Onsager studied the ion mobility within the framework of continuum picture⁵⁸ and their self-consistent theoretical approach led to the following expression for total friction^{59,60}

$$\frac{1}{\zeta_{total}} = \int_{r_{ion}}^{\infty} \frac{dr}{4\pi r^2 \eta(r)}, \quad (2.3)$$

where r is the distance from the surface of the ion, and $\eta(r)$ is the distance dependent viscosity given as,⁴⁷ $\eta(r) = \eta_0 [1 + \tau_D q^2 (\epsilon_0 - \epsilon_\infty) / 16\pi \eta_0 \epsilon_0^2 r^4]$. The prediction from H-O theory, shown in Fig. 2.1, indicates that this theory is also inadequate for predicting the experimental limiting ionic conductivities of small ions in formamide. It was later shown empirically that the limiting ionic conductivity could be partially controlled by the solvent diffusion that is related to variety of molecular motions as well as coupling between them.⁶¹

Subsequently, Wolynes and coworkers⁶²⁻⁶⁴ developed a theory that took into account the ion-solvent interactions, microscopic structure around an ion to describe the ion

conductivity. However, this theory also neither include the full dynamics of the liquid nor the effects of the self-motion of the ion and therefore enjoyed a limited success.

Recently, a generalized molecular theory has been developed by Bagchi and co-workers^{52, 66-69} that incorporates the complex dynamics of polar solvents as well as the self motion of the ion. This theory has been found to predict successfully the experimental results in water, D₂O, acetonitrile and alcohols. We have used this theory to calculate the Λ_0 in formamide. It is to be noted here that the above theory predicts a dynamic cooperativity of solvent translational modes which affects the conductivity in a non-linear way.⁵²

Computer simulation studies for ion conductance in neat amide solvents have not been performed so far, even-though ion-transport in some other solvent systems have been simulated.⁷⁰⁻⁷² The complex nature of the solvent and non-availability of proper model-potential might be the reasons for this. However, Rode *et al.* studied the limiting ionic mobility of small, rigid ions such as Na⁺ cation in aqueous mixture of formamide by using the molecular dynamics simulation⁷¹ method. These authors found in this work that the cation is preferentially solvated by formamide molecules which is in agreement with the existing NMR data.

The motivation for studying the ion transport and solvation dynamics in formamide comes further from the following facts. First, experimental results for both limiting ionic conductivity and solvation dynamics in liquid formamide at room temperature are available. Second, it would be interesting to explore the effects of the intermolecular vibration (libration) bands in the range of 100-200 cm⁻¹ that have been observed repeatedly in the low frequency Raman studies of amide systems. One wonders here whether this low frequency motion could contribute to the initial fast solvent reorganization and hence makes the solvation energy relaxation ultrafast. This is important as we have observed earlier that inclusion of these bands gives rise to better prediction of both limiting ionic conductance and solvation dynamics in polar solvents, such as water, D₂O and N-Methyl amides^{52,66-69,73,74} However, we are not aware of any experiment that indicates fraction wise contribution of these bands (one at ~110 cm⁻¹ and another at ~200 cm⁻¹) to the dielectric dispersion from ϵ_∞ to square

of the refractive index in liquid formamide. Therefore, we have assumed that the band at 110 cm^{-1} is responsible for the missing part as indicated above. We have performed calculations both with and without this band to see its effect. Third, the total limiting ionic conductance (Λ_{total}) in formamide shows interesting temperature dependence. In the above molecular theory, the temperature dependence enters through the generalized rate of solvent polarization relaxation (via the frequency dependent dielectric relaxation data), and solute-solvent and solvent-solvent static correlation functions. One would therefore like to see whether the above molecular theory could explain the observed temperature dependence of Λ_{total} in formamide.

As already mentioned,⁷⁵ solvation dynamics is intimately related to the ion transport processes and hence study of solvation dynamics is crucially important for understanding the microscopic mechanism of ion conductance. For example, consider the motion of Li^+ in a solvent with $\tau_D \sim 40 \text{ ps}$. By using the experimental value of Λ_0 for Li^+ in formamide in the following expression, $D = A_0 (k_B T / q^2 N_A)$, one obtains the diffusion coefficient of Li^+ as $\sim 2.4 \times 10^{-6} \text{ cm}^2 \text{ s}^{-1}$. This, after inserting into the Einstein relation, produces $\langle l^2 \rangle^{1/2} = \sqrt{6D\tau_D} = 0.24 \text{ nm}$. This is the diffusion displacement of lithium ion over a time period of 40 ps. However, the displacement of this ion with mobility $U = 9.4 \times 10^{-5} \text{ cm}^2 \text{ V}^{-1} \text{ s}^{-1}$ in the direction of the applied field $E=1 \text{ Vcm}^{-1}$ is $l_E = UE\tau_D = 3.8 \times 10^{-8} \text{ nm}$ at typical experimental conditions. Interestingly, this value is seven orders less in magnitude than the calculated value of $\langle l^2 \rangle^{1/2}$. This means that the motion of the ion between the electrodes is very irregular and the limiting ionic conductivity is determined by random collisions of the moving ion with the solvent environment and thus both by structure and dynamics.^{71,72}

The organization of the rest of the chapter is as follows. Sec. 2.2 contains the details of the molecular theory that has been used here. Method of calculation is discussed briefly in section 2.3. Numerical results along with discussion are presented in Sec. 2.4. The chapter ends with a conclusion in section 2.5.

2.2 The Molecular Theory

2.2.1 Limiting Molar Ionic Conductivity

The microscopic theory used here is based on the following picture.^{52,66-69} As an ion moves in a liquid medium it experiences fluctuating forces from two separate sources. First, force comes from the short range interaction with the surrounding solvent molecules. This force is primarily repulsive in nature. The friction originating from this part is termed bare friction, ζ_{bare} . This friction can be calculated from solvent viscosity (η_0) and the crystallographic radius of the ion (r_{ion}) by using Stokes' law as follows: $\zeta_{bare} = A\eta_0 r_{ion}$, where the value of A could be 4π or 6π depending upon boundary condition (slip or stick). This is clearly an approximation as hydrodynamics may not be true for an ion which is smaller in size than the solvent. However, it has been seen that the contribution from this part is small for smaller ions therefore the error made in this approximation is not significant.⁶²⁻⁶⁴ The second part of the fluctuating force originates from the long range ion-dipole interaction. The ion experiences retardation due to the coupling of its electric field with solvent polarization while moving through the solvent.⁵⁴ This gives rise to a friction, coined by Born, called as dielectric friction (ζ_{df}). Therefore, the total friction on the ion is can be expressed as follows:⁵⁴

$$\zeta_{total} = \zeta_{bare} + \zeta_{df} \quad (2.4)$$

Therefore, the primary idea of this theory comes from Born's assumption of dielectric friction.⁵⁴ Here we neglect the cross correlation between repulsive short range and attractive long range ion-dipole interactions. This is also an approximation first proposed by Wolynes and has been extensively used in subsequent works.⁶²⁻⁶⁵ However, the validity of this approximation is also questioned when the long range interactions are large enough and the frictional contribution due to cross correlation becomes of the order of magnitude.⁷⁶ The dielectric friction is calculated from force auto correlation function (FACF) using Kirkwood formula which is given by⁷⁷

$$\zeta_{df} = \frac{1}{3k_B T} \int dt \langle \Delta \mathbf{F}_{id}(0) \cdot \Delta \mathbf{F}_{id}(t) \rangle \quad (2.5)$$

where $\Delta\mathbf{F}_{id}(t)$ is the time dependent fluctuating force acting on the ion due to ion-dipole interaction and $k_B T$ is the Boltzmann's constant times temperature. $\langle \dots \rangle$ denotes the ensemble average. The density functional theory (DFT) provides an expression for the effective fluctuating potential, and therefore the force, on the ion in terms of space and orientation dependent density. The expression for the fluctuating force density on the ion due to ion-dipole interaction is given by^{52,53}

$$\Delta\mathbf{F}_{id}(\mathbf{r}, t) = k_B T n_{ion}(\mathbf{r}, t) \nabla \int d\mathbf{r}' d\mathbf{\Omega}' c_{id}(\mathbf{r}; \mathbf{r}', \mathbf{\Omega}') \delta\rho_d(\mathbf{r}', \mathbf{\Omega}', t) \quad (2.6)$$

where $n_{ion}(\mathbf{r}, t)$ is the number density of ion, $\delta\rho_d(\mathbf{r}, \mathbf{\Omega}) = \rho_d(\mathbf{r}, \mathbf{\Omega}) - \rho_d^0/4\pi$ is the space (\mathbf{r}), orientation ($\mathbf{\Omega}$) and time (t) dependent fluctuation in the average number density ρ_d^0 of the pure solvent, and $c_{id}(\mathbf{r}; \mathbf{r}', \mathbf{\Omega}')$ is the space and orientation dependent ion-dipole direct correlation function (DCF). DCF describes the effective interaction between the ion and the dipolar solvent molecules. Now the space and orientation dependent number density and DCF are expanded in spherical harmonics. We then use the standard Gaussian decoupling approximation to obtain the microscopic expression for the frequency dependent dielectric friction as^{52,66-69}

$$\zeta_{df}(z) = \frac{2k_B T \rho_d^0}{3(2\pi)^2} \int_0^\infty dt e^{-zt} \int_0^\infty dk k^4 S_{ion}(k, t) |c_{id}^{10}(k)|^2 S_{solvent}^{10}(k, t) \quad (2.7)$$

where $c_{id}^{10}(k)$ is the Fourier transform of the longitudinal component of static ion-dipole DCF and $S_{solvent}^{10}(k, t)$ the longitudinal component of the *orientational dynamic structure factor* of the pure solvent. In the definition of above correlation function k is taken parallel to the z axis. $S_{ion}(k, t)$ denotes the self-dynamic structure factor of the ion. The interesting feature of the above equation is that it couples single particle motion to the collective dynamics of the solvent via ion-dipole direct correlation function. In the above equation the self-dynamic structure factor of the ion is assumed to be given by⁵²

$$S_{ion}(k, t) = \exp[-D_r^{ion} k^2 t] = \exp\left[-\left(\frac{k_B T}{\zeta_{bare} + \zeta_{df}}\right) k^2 t\right] \quad (2.8)$$

where the diffusion coefficient of the ion, D_T^{ion} , itself depends on the total friction.

The orientational dynamic structure factor of the pure solvent is calculated by using the following expression⁵²

$$S_{solvent}^{10}(k,t) = \frac{1}{4\pi 3Y} \left[1 - \frac{1}{\varepsilon_L(k)} \right] L^{-1} [z + \Sigma_{10}(k,z)]^{-1} \quad (2.9)$$

where L^{-1} stands for Laplace inversion. $3Y$ is the polarity parameter of the solvent which is related to the dipole-moment, μ , and density, ρ_d^0 , of the solvent by the relation, $3Y = (4\pi / 3k_B T) \mu^2 \rho_d^0$. $\varepsilon_L(k)$ is the longitudinal component of wave number dependent dielectric function. $\Sigma_{10}(k,z)$ is the longitudinal ($l=1, m=0$) component of the generalized rate of orientational polarization density relaxation of the solvent. The calculation of $\Sigma_{10}(k,z)$ is rather complex. It is determined by the static orientational structure, frequency dependent dielectric function $\varepsilon(z)$, translational diffusion coefficient of the solvent molecule. The expression for the generalized rate of orientational polarization density relaxation, $\Sigma_{lm}(k,z)$, and other details are given in section 2.3.1 and also in Appendix I.

In the $z=0$ limit, Eq. (2.7) provides the following expression for macroscopic dielectric friction (i.e. $\zeta_{df}(z=0) \equiv \zeta_{df}$)^{52, 66-69}

$$\zeta_{df} = \frac{2k_B T \rho_0}{3(2\pi)^2} \frac{1}{4\pi 3Y} \int_0^\infty dk k^4 |c_{id}^{10}(k)|^2 \left[1 - \frac{1}{\varepsilon_L(k)} \right] \frac{1}{D_T^{ion} k^2 + \Sigma_{10}(k, D_T^{ion} k^2)} \quad (2.10)$$

Since the diffusion coefficient of the ion, D_T^{ion} itself depends on the total friction, the above equation for ζ_{df} must be solved self-consistently. Once ζ_{df} is calculated self-consistently the limiting molar ionic conductivity in infinite dilution is obtained by

using the relation $\Lambda_0 = \frac{qF}{RT\zeta_{total}}$, where R is the Avogadro number times the Boltzmann constant.

2.2.2 Dipolar Solvation Dynamics

Let us consider a mixture of dipolar solute and solvent. As the solute is dissolved in the solvent the equilibrium structure of the pure solvent is disturbed and causes density inhomogeneity in the solute-solvent composite system. In this state one can write excess part of free energy functional for the whole solute-solvent system. Then the expression for the excess solvation energy of the solute, which is essentially the excess effective potential energy of solute due to its fluctuating interaction with the surrounding solvent molecules, is obtained by taking functional differentiation the free energy functional and equating it equal to zero for the equilibrium condition (see Appendix II).

The probe molecules (solute) that are frequently used in solvation dynamics experiments are often massive and contain several aromatic rings and therefore several times bigger than a solvent molecule. This means that the probe solute remains practically immobile during the course of solvation and therefore the solvation becomes that of an immobile solute. Therefore, we use the expression for the position (\mathbf{r}), orientation ($\mathbf{\Omega}$) and time (t) dependent total fluctuating solvation energy for a fixed solute which is written as^{52,78}

$$\Delta E_{sol}(\mathbf{r}, \mathbf{\Omega}, t) = -k_B T \int d\mathbf{r}' d\mathbf{\Omega}' c_{sd}(\mathbf{r}, \mathbf{\Omega}; \mathbf{r}', \mathbf{\Omega}') \delta\rho_d(\mathbf{r}', \mathbf{\Omega}', t) \quad (2.11)$$

where $c_{sd}(\mathbf{r}, \mathbf{\Omega}; \mathbf{r}', \mathbf{\Omega}')$ is the position and orientation dependent solute-solvent direct correlation functions. Then a tedious but straight forward algebra (given in Appendix II) leads to the following expression for the normalized solvation energy auto correlation function for a fixed solute^{75,78}

$$S(t) = \frac{\int_0^\infty dk k^2 \left\{ |c_{sd}^{10}(k)|^2 \left[1 - \frac{1}{\varepsilon_L(k)} \right] L^{-1} [z + \Sigma_{10}(k, z)]^{-1} + 2 |c_{sd}^{11}(k)|^2 [\varepsilon_T(k) - 1] L^{-1} [z + \Sigma_{11}(k, z)]^{-1} \right\}}{\int_0^\infty dk k^2 \left\{ |c_{sd}^{10}(k)|^2 \left[1 - \frac{1}{\varepsilon_L(k)} \right] + 2 |c_{sd}^{11}(k)|^2 [\varepsilon_T(k) - 1] \right\}} \quad (2.12)$$

where $c_{sd}^{10}(k)$ and $c_{sd}^{11}(k)$ are the longitudinal and transverse components of the wave number dependent dipole-dipole direct correlation function, respectively and have been calculated using MSA. $\varepsilon_L(k)$ and $\varepsilon_T(k)$ are longitudinal and transverse components of wave number dependent dielectric constant, respectively. $\Sigma_{lm}(k, z)$ denotes the $(l, m)^{th}$ component of the wave number and frequency dependent generalized rate of solvent orientational polarization density relaxation.

We have used above equation to calculate the decay of the normalized solvation energy auto-correlation function, $S(t)$, of a dipolar probe coumarin 153 (C153) in formamide at 283.15 K, 298.15 K and 328.15 K.

2.3 Calculation Procedure

2.3.1 Calculation of Generalized Rate of Solvent Polarization

Relaxation, $\Sigma_{lm}(k, z)$

The calculation of the generalized rate of solvent orientational polarization density relaxation, $\Sigma_{lm}(k, z)$, is non-trivial task and somewhat involved. The detailed derivation of this quantity has already been presented elsewhere^{52,73} and also provided in Appendix I. The expression for the generalized rate of orientational polarization density relaxation is given by^{52,73}

$$\Sigma_{lm}(k, z) = \frac{k_B T k^2 f(llm, k)}{M \sigma^2 [z + \Gamma_T(k, z)]} + \frac{k_B T l(l+1) f(llm, k)}{I [z + \Gamma_R(k, z)]} \quad (2.13)$$

where σ , M and I are the diameter, mass and average moment of inertia of the solvent molecule, respectively. $\Gamma_T(k, z)$ and $\Gamma_R(k, z)$ are the wavenumber and frequency dependent translational and rotational memory kernels, respectively. $f(lm, k) = 1 - (\rho_d^0 / 4\pi)(-1)^m c(llm, k)$, describes the (1, 1, 0), (1, 1, 1) and (1, 1, -1) components of the orientational static structure of the dipolar solvent.

Of these two frictional memory kernels, the calculation of $\Gamma_T(k, z)$ is somewhat easier and has been obtained from the isotropic liquid dynamic structure factor, $S(k, z)$,

using the relation,⁵²
$$\frac{k_B T}{M\sigma^2[z + \Gamma_T(k, z)]} = \frac{S(k)[S(k) - zS(k, z)]}{k^2 S(k, z)}$$
 with

$$S(k, z) = \frac{S(k)}{z + D_T^{Solvent} k^2 / S(k)}$$
. In the present calculation the translational diffusion

coefficient ($D_T^{Solvent}$) of a solvent molecule has been obtained from the liquid viscosity using the slip hydrodynamic boundary condition. The solvent static structure factor, $S(k)$, is calculated by using Percus-Yevick (PY) hard sphere direct correlation function, $c_{PY}(k)$ as: $S(k) = [1 - \rho_d^0 c_{PY}(k)]^{-1}$. The other details regarding the calculation of $\Gamma_T(k, z)$ have been described in Refs.52 and 67 and also in Appendix I.

The rotational memory kernel $\Gamma_R(k, z)$ has been obtained by using the scheme developed earlier for underdamped liquids.^{52,73} In this scheme the k-dependence of $\Gamma_R(k, z)$ have been neglected and therefore the kernel $\Gamma_R(k, z)$ is replaced by $\Gamma_R(k = 0, z)$. The function $\Gamma_R(k = 0, z)$ is then directly connected to the frequency dependent dielectric function $\varepsilon(z)$ as follows

$$\frac{2f(110, k = 0)k_B T}{I[z + \Gamma_R(k, z)]} = \frac{z\varepsilon_0[\varepsilon(z) - \varepsilon_\infty]}{\varepsilon_\infty[\varepsilon_0 - \varepsilon(z)]} \quad (2.14)$$

where ε_0 the static dielectric constant of the medium and ε_∞ is $\varepsilon(z)$ in high frequency limit. Similarly, $\sum_{11}(k, z)$ can be obtained from the experimental dielectric relaxation data but only after replacing $f(110, k = 0)$ by $f(111, k = 0)$.

Table 2.1: Dielectric relaxation parameters for formamide at different temperatures

Temperature (K)	ϵ_0	τ_1 (ps)	β_1 (DC) ^(a)	ϵ_1 ^(b)	n_D ^(c)	n_D^2
288.15	113.42	55.6	0.91	5.62	1.447	2.094
298.15	109.56	40.3	0.94	5.71	1.447	2.094
328.15	98.75	22.1	0.94	4.80	1.447	2.094

(a) Davidson-Cole (DC) relaxation. (b) The dispersion ($\epsilon_1 - n_D^2$) is assumed to carry out by the librational band at 110 cm^{-1} for all the three temperatures studied here. (c) n_D represents the refractive index.

The experimental data for the frequency dependent dielectric function of formamide at three different temperatures are described by the following rather general expression⁷⁹

$$\epsilon(z) = \epsilon_\infty + \frac{(\epsilon_0 - \epsilon_1)}{[1 + (z\tau_1)^{1-\alpha_1}]^{\beta_1}} \quad (2.15)$$

where z is Laplace frequency, ϵ_0 is the static dielectric constant, $\epsilon_1 = \epsilon_\infty$ is its limiting value at high frequency, τ_1 is the relaxation time constant with shape parameters $0 \leq \alpha_1 < 1$ and $0 < \beta_1 \leq 1$.

For our calculation in formamide, we have used dielectric relaxation data measured by J. Berthel and coworkers⁸⁰ who recorded the frequency dependent dielectric function in the range of 0.2 – 89 GHz. The details of the dielectric relaxation data are summarized in Table 2.1. The interesting aspect of these data is that they are best fitted to a single Davidson-Cole (DC, $\alpha_1 = 0, \beta_1 < 1$) equation at all the three temperatures studied here. It should also be noted that at these temperatures the value of the measured ϵ_∞ is approximately 5. Therefore, the dispersion, $(\epsilon_\infty - n_D^2) = (5 - 2.1) \approx 3$, (n_D being the refractive index) is *missing* in these data due to the limited resolution available to these authors. However, it has been seen earlier⁷⁴ that such missing component can make the solvation energy relaxation faster and hence contribute in an important manner to both the ultrafast polar solvation response and ionic conductivity

in formamide. The experimental study of Chang and Castner³ by using optical-heterodyne detected optical Kerr effect (OKE) spectroscopy has revealed that formamide contains librational modes with frequencies centered at ~ 110 and ~ 200 cm^{-1} . These findings have also been corroborated by other authors.^{8,9} The works of Cho *et al.*⁸¹ and McMorrow and Lotshaw⁸² have shown the connection between dynamics measured by OKE and TDFSS (time dependent fluorescence Stokes' shift) measurements. We therefore assume that the librational mode detected at ~ 110 cm^{-1} takes part in both the polar solvation energy relaxation and limiting ionic conductivity in formamide at all the temperatures studied here. In addition, we have assumed that this librational mode is an overdamped one.^{52-53,75}

2.3.2 Calculation of Static Correlation Functions

2.3.2.1 Solvent Dipole-dipole Direct Correlation Functions, $c(110, k)$ and $c(111, k)$

The solvent orientational static correlation function, $c(110, k)$, is calculated by using the mean spherical approximation (MSA) model for a pure solvent.⁸³ Then proper corrections at both $k \rightarrow 0$ and $k \rightarrow \infty$ limits are used to obtain the wavenumber dependent dielectric function $\varepsilon_L(k)$. Subsequently, the longitudinal component of the wave number dependent dielectric function, $\varepsilon_L(k)$ obtained by the following exact relation⁵²⁻⁵³

$$\left[1 - \frac{1}{\varepsilon_L(k)} \right] = \frac{3Y}{1 - (\rho_d^0 / 4\pi)c(110, k)} \quad (2.16)$$

For intermediate wavenumbers ($k\sigma \rightarrow 2\pi$), we have used the above equation while for $k \rightarrow \infty$ we have used a Gaussian function which begins at the second peak height of $[1 - 1/\varepsilon_L(k)]$ to describe the behaviour at large k . As described earlier,^{52,53,65} this procedure removes the wrong wavenumber behaviour of static correlations described by the MSA.

We have obtained the transverse component of the solvent dipole-dipole direct correlation function, $c(111, k)$, directly from the MSA. Then the transverse component

of wave number dependent dielectric function $\varepsilon_T(k)$ is obtained by using the following relation^{52,53}

$$[\varepsilon_T(k) - 1] = \frac{3Y}{1 + (\rho_d^0 / 4\pi)c(111, k)} \quad (2.17)$$

The corrections at wave number $k \rightarrow 0$ in the correlation functions were done to ensure that $\varepsilon_L(k=0) = \varepsilon_T(k=0)$ are equal to experimental dielectric constant of formamide which is around ~ 113 .

2.3.2.2 Ion-dipole Direct Correlation Function, $c_{id}^{10}(k)$

The ion-dipole direct correlation function, $c_{id}^{10}(k)$, is calculated using the procedure of Chan *et al.*⁸⁴ for electrolyte solution in the limit of zero ion concentration. We first calculate the solvent microscopic polarization, $P_{mic}(r)$, around an ion using following relation⁸⁴

$$P_{mic}(r) = \frac{(\varepsilon_0 - 1)ze}{4\pi\varepsilon_0 r^2} \left[1 - r \frac{dF(r)}{dr} + F(r) \right] \quad (2.18)$$

where ε_0 is static dielectric constant of pure solvent, e the electronic charge and z the valency of the ion. The microscopic correction of polarization through the dimensionless quantity $F(r)$ is important feature of this equation. The behaviour of the microscopic solvent polarization, $P_{mic}(r)$, around different ions has been shown in Fig. 2.2. It evident from Fig. 2.2 that polarization density around an ion is oscillatory in nature and maximum at ion-solvent contact. Note the difference in $P_{mic}(r)$ value for ions with different size. Polarization density at the contact as wells other solvation shells is maximum for smaller ion such as Li^+ and is minimum for larger ion like tetra-butyl ammonium ion, C_4^+ . Once the $P_{mic}(r)$ value is calculated we then use Eqs. 3.67, 3.57 and 3.15b of Ref. 84 to obtain $c_{id}^{10}(k)$.

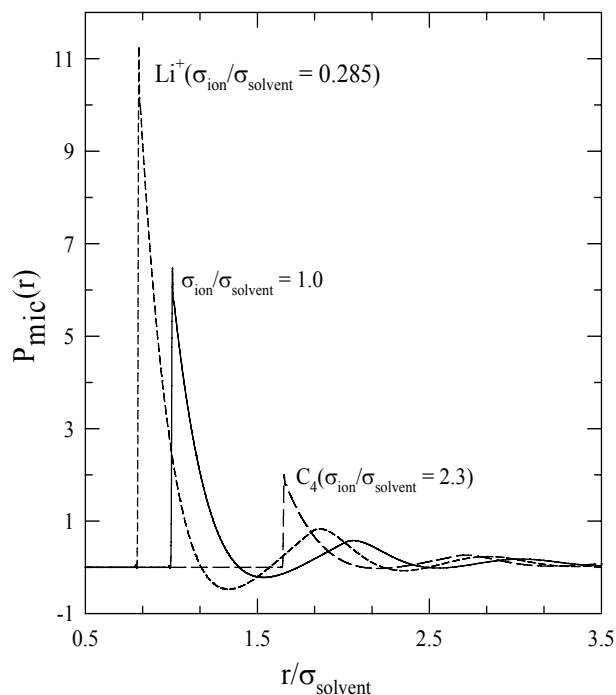


Figure 2.2: The microscopic polarization, $P_{mic}(r)$, (scaled by $\sqrt{k_B T / \sigma_{solvent}^3}$) of solvent around an ion as a function distance r (scaled by solvent diameter $\sigma_{solvent}$) from the centre of the ion. Note the difference in polarization for different ion-solvent (formamide) size ratios. A small negative value of $P_{mic}(r)$ is also seen which may mean that formamide molecules just outside the first salvation shell are oriented in a direction opposite to those inside the shell.

Table 2.2: Solvent parameters needed for the theoretical calculation at different temperatures.

Temperature (K)	Diameter (Å)	μ (D)	Density (g/cm ³)	Viscosity (cP)
283.15	4.36	3.72 ^(a)	1.1508	5.00
298.15	4.36	3.72	1.1296	3.31
328.15	4.36	3.72 ^(a)	1.1296 (298.15K) ^(b)	1.833 (325.15K) ^(b)

(a) The values of μ at temperatures 283.15 and 328.15 K are not available and hence the value of μ at 298.15 K is used for calculations at the other two temperatures. (b)The values in the parenthesis in the ‘Density’ and ‘Viscosity’ columns indicate the temperatures at which these properties were measured.

Here we would like to mention that since MSA is a linear theory, any modification in the solvent structure around an ion through nonlinear interactions in a solvent of high dielectric constant and dipole moment will be completely missed.⁸⁴ Therefore, the calculated polarization structure around an ion in formamide, as shown in Fig. 2.2, may not be quantitatively correct. However, the calculation of ion-dipole direct correlation functions by using MSA may still be justified because the predictions are semi-quantitative in nature with correct trends. Furthermore, there is no other simple theory which is analytically tractable as MSA to describe ion-dipole system better than this.

2.3.2.3 Solute Dipole- Solvent Dipole Direct Correlation Function, $c_{sd}^{10}(k)$

The value of $c_{sd}^{10}(k)$ is calculated by using the MSA model for a binary mixture of dipolar liquids. This model was solved by Isbister and Bearman.⁸⁵ Here we have assumed that the formamide is host solvent in which the dipolar probe solute (C153) is present in the limit of zero concentration. The parameters necessary for obtaining these static correlations have been given in Table 2.2.

2.4 Results & Discussion

2.4.1 Limiting Molar Ionic Conductivity and Temperature

Dependence

Here we present the results of the calculated limiting molar ionic conductivities in formamide at three temperatures, namely, at 283.15, 298.15 and 328.15 K. A comparison between theory and experiments⁸⁶ shall be shown wherever possible. In Fig. 2.3 we show the calculated value of the *Walden product*, $\Lambda_0\eta_0$, plotted against the inverse of the crystallographic radius of the ion, r_{ion}^{-1} , in formamide at room temperature. The *solid line* represents the predictions from the present theory. For comparison, available experimental data (*solid circles*) are shown in the same figure.

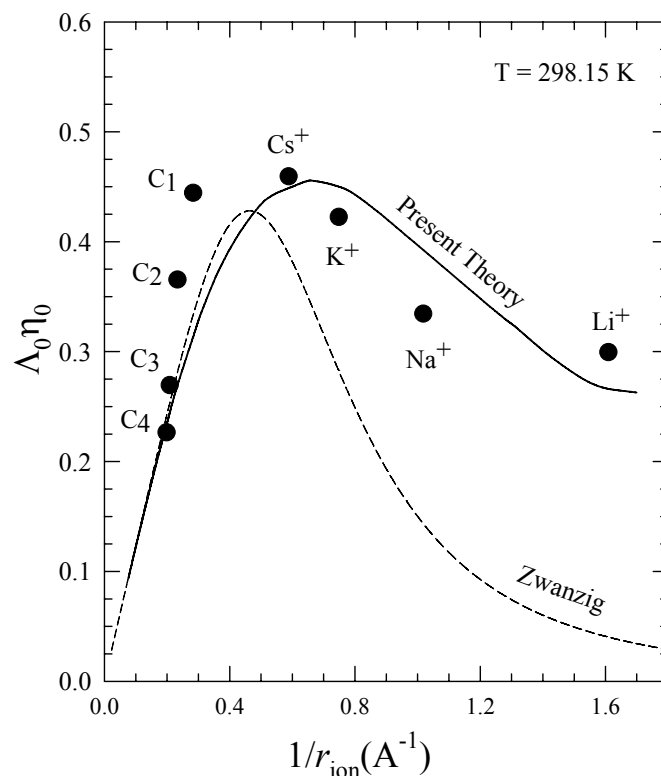


Figure 2.3: The limiting values of Walden product ($\Lambda_0\eta_0$) for the alkali, and tetra-alkyl ammonium ion as a function of inverse of crystallographic radius (r_{ion}^{-1}) in formamide at room temperature. The *solid line* represents the prediction of the present microscopic theory, the *solid circles* denote the experimental results, and the *short dashed line* represents Zwanzig theory.

It is clear that the theory agrees well with the experiments. However, the predicted peak position of the *Walden product* with respect to r_{ion}^{-1} is slightly shifted towards the smaller ions. Fig. 2.3 also shows the calculated values of the *Walden product* for uni-positive ions in formamide predicted by the continuum theory of Zwanzig. It is interesting to note that the theory of Zwanzig⁵⁷ fails completely for small ions like Na^+ and Li^+ . This is probably due to the neglect of the microscopic structure of the liquid around the moving ion and also not accounting for the fast components of the liquid dynamics that are often exhibited in the recent frequency dependent dielectric relaxation measurements.⁸⁰

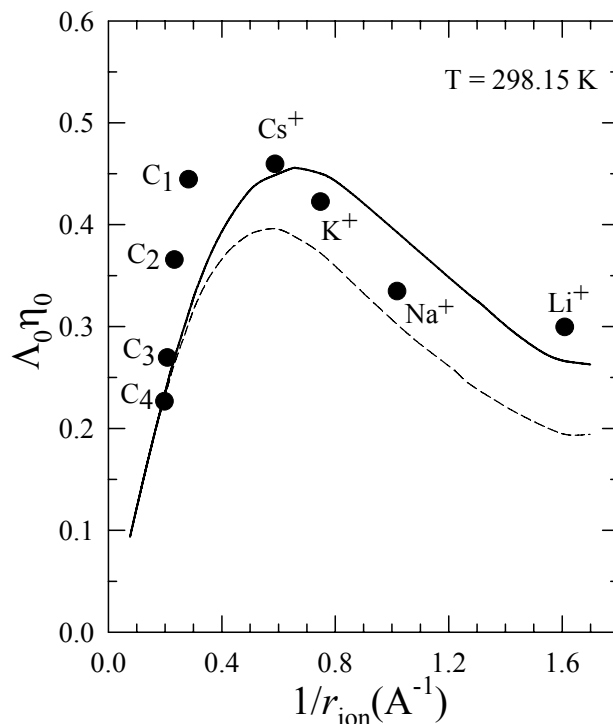


Figure 2.4: The effect of libration band (110 cm^{-1}) on the limiting ionic conductivity in formamide at room temperature. The values of Walden product, $\Lambda_0 \eta_0$, are plotted as a function of the inverse of crystallographic radius of the ions. The *solid line* represents the prediction of the present theory with the contribution of the libration band at 110 cm^{-1} to the dielectric relaxation data of formamide is considered. Experimental *Walden products* for different ions are denoted by *solid circles*. The *short dashed line* represents the prediction of the present theory without the contribution from the libration band.

The effects of the intermolecular vibration (libration) band with a frequency centered at 110 cm^{-1} on the limiting ionic conductivity are shown in Fig. 2.4. The *solid* and *dashed* lines represent the calculations with and without this band, respectively. As evident from this figure, the agreement between the theory and experiments⁸⁶ becomes *poor* if the contribution of this band to the *complete* dielectric relaxation of formamide is neglected. This has been observed *earlier* for water and deuterated water (D_2O) also.^{52,66-69,73} As we will see in the next section, this band also contributes *significantly* to the time dependent progress of solvation of a dipolar probe in formamide.

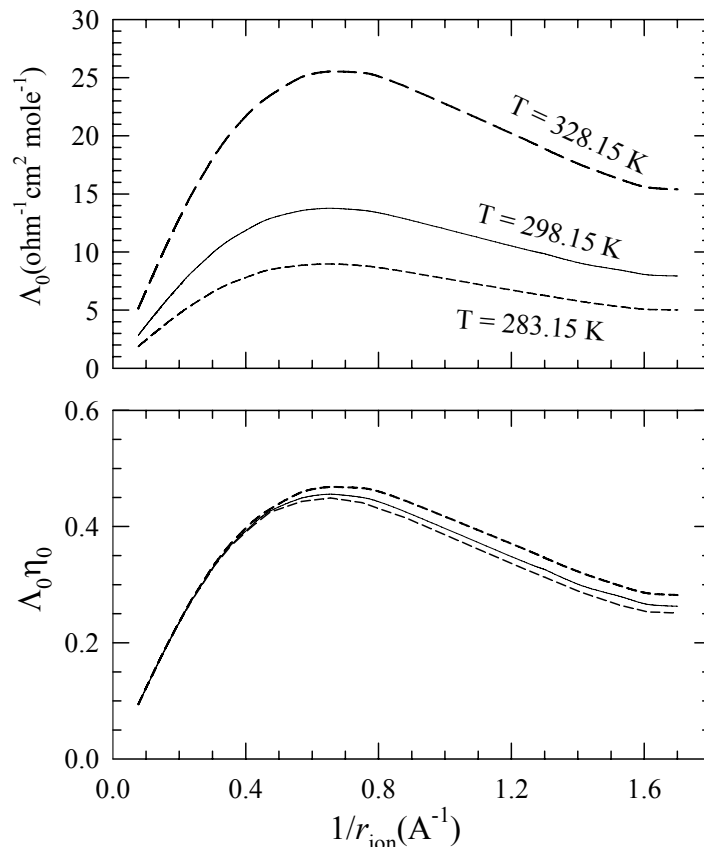


Figure 2.5: *Upper panel:* Temperature dependent limiting ionic conductance, Λ_0 , for uni-positive ions as a function of the inverse of the crystallographic ionic radius (r_{ion}^{-1}). The *short dashed line*, *solid line*, and *long dashed line* represent the predictions of the present molecular theory at 283.15, 298.15, and 328.15 K, respectively. *Lower panel:* The temperature dependence of the Walden Product for same ions at these three temperatures. The representations remain the same as in the upper panel.

The limiting ionic conductivity, Λ_0 , calculated for three different temperatures 283.15, 298.15 and 328.15 K in formamide are shown in the *upper panel* of Fig. 2.5. The temperature dependent solvent parameters needed for the above calculation are summarized in Table 2.2. Note in the above figure that the calculation predicts a strong temperature dependence of limiting ionic conductivity in formamide. Since the present theory uses the experimentally measured frequency dependent dielectric relaxation data as an input, such strong temperature dependence originates primarily from the dielectric relaxation parameters obtained at different temperatures. This means that the zero frequency dielectric friction, $\zeta_{df}(z=0)$, is responsible for the observed temperature dependence. We would like to mention here that the calculated

Table 2.3: $\Lambda_0^T \eta_0$, the total ionic conductivity at infinite dilution ($\Lambda_0^T = \Lambda_0^+ + \Lambda_0^-$) multiplied with the solvent viscosity (η_0), for 1:1 electrolytes in formamide: temperature dependence

Salts	Experiment $\Lambda_0^T \eta_0$ (298.15K)/ $\Lambda_0^T \eta_0$ (283.15K)	Present theory ^(a) $\Lambda_0^T \eta_0$ (298.15K)/ $\Lambda_0^T \eta_0$ (283.15K)	Present theory ^(b) $\Lambda_0^T \eta_0$ (298.15K)/ $\Lambda_0^T \eta_0$ (328.15K)
NaCl	1.04	1.02	0.96
KCl	0.98	1.01	0.97
KBr	0.98	1.01	0.97
Me ₄ NI	0.98	1.01	0.99
Et ₄ NI	0.98	1.01	0.99
Pr ₄ NBr	0.99	1.01	0.99
Pr ₄ NI	0.99	1.01	0.99
Bu ₄ NBr	1.01	1.01	0.99
Bu ₄ NI	1.02	1.01	0.99
i-Am ₃ BuNI	0.99	1.00	0.99

(a) Values for solvent viscosity (η_0) at these temperatures are given in the last column of Table 2.2.

(b) Theoretical predictions presented in this column could not be compared with experiments due to nonavailability of experimental data at 328.15 K.

values of Λ_0 could not be compared with the experiments at 283.15 K and 328.15 K because of the non-availability of experimental data at these temperatures. We could, however, compare the total limiting ionic conductivities ($\Lambda_0^T = \Lambda_0^+ + \Lambda_0^-$) of several 1:1 strong electrolytes in this liquid at 298.15 K. Such a comparison is shown in Table 2.3 where the ratio between the values of $\Lambda_0^T \eta_0$ obtained at 298.15 and 283.15 K is presented for both experiment and theory. It is evident from the table that the theory agrees well with experiments at 283.15K. The ratios of $\Lambda_0^T \eta_0$ have also been calculated for temperatures at 298.15 and 328.15 K for same set of electrolytes.

Since viscosity also depends upon temperature, it would be interesting to see how the *Walden product* for these uni-positive ions varies with temperature in formamide. The lower panel of Fig. 2.5 shows the variation of the *Walden product* with temperature

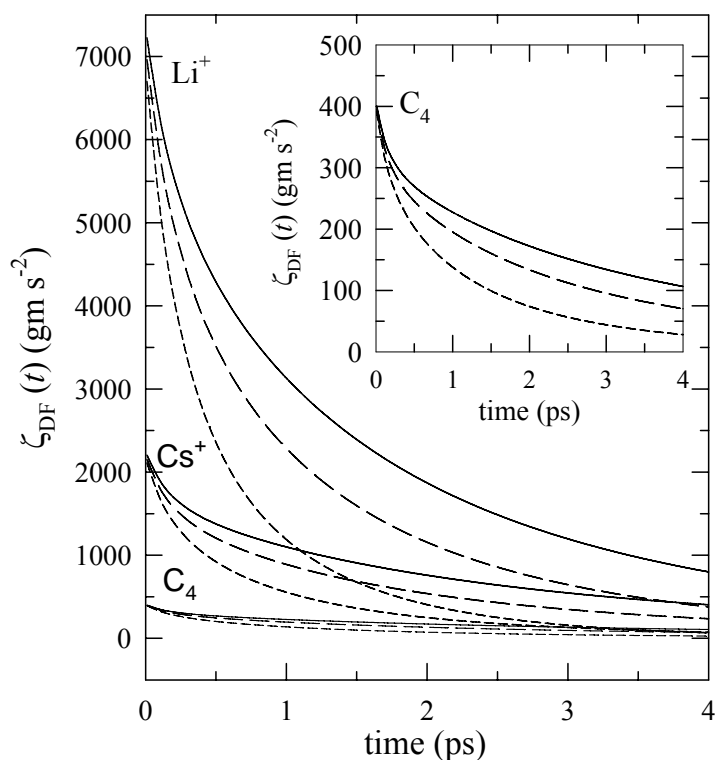


Figure 2.6: The time dependent dielectric friction, $\zeta_{\text{DF}}(t)$, experienced by Li^+ , Cs^+ , and C_4 ions as a function of time t at 283.15 K (solid lines), 298.15 K (long dashed lines) and 328.15 K (short dashed lines).

for these ions. Note here that the temperature dependence in viscosity *offsets* the strong temperature dependence exhibited by the limiting ionic conductivity shown in the upper panel and hence the *Walden product* becomes almost *insensitive* to the change in temperature.

We now come back to the discussion on the temperature dependence of dielectric friction. The time dependent dielectric friction experienced by Li^+ , Cs^+ , and C_4 ions while diffusing through formamide at 283.15 K, 298.15 K and 328.15 K are shown in Fig. 2.6. For clarity, the dependence for the largest ion C_4 is also shown in the *inset*. As expected, the value for the time dependent dielectric friction at the zero time for the smallest ion Li^+ is largest while that for the largest ion C_4 is smallest. Also, note that the rate of the decay of time dependent dielectric friction becomes slower as one decreases the temperature.

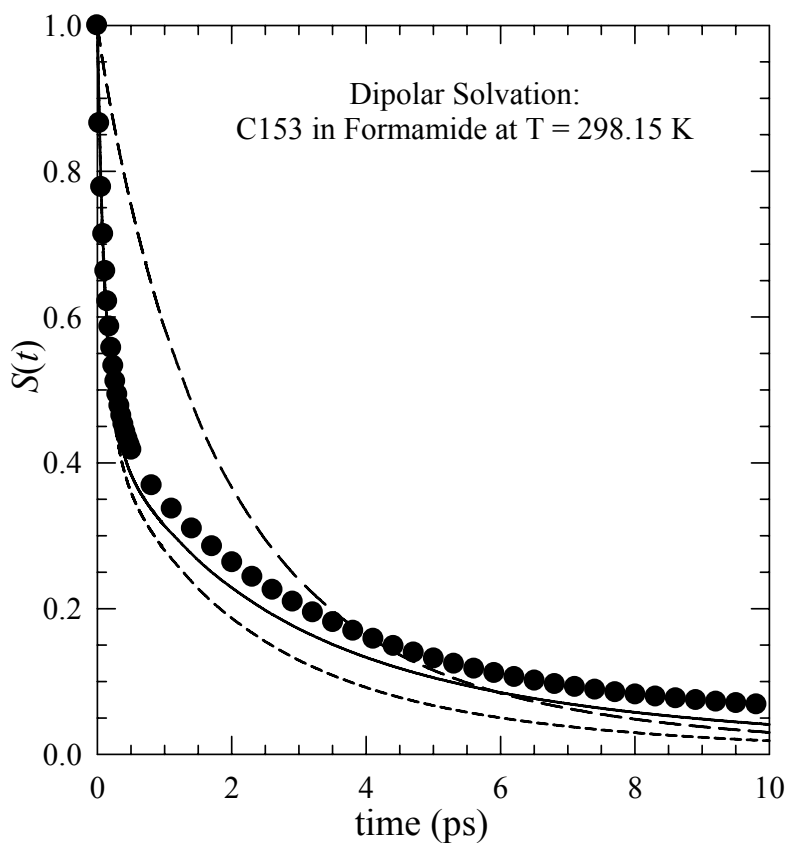


Figure 2.7: The normalized solvation energy time auto-correlation function, $S(t)$, for a dipolar solute probe (Coumarin 153) dissolved in formamide at 298.15 K is shown as a function of time. The calculated results are denoted by the *lines (solid, short dashed and long dashed)* while the experiments are by the *filled circle*. The theoretical prediction represented by the *long dashed line* is calculated by using the experimental dielectric relaxation data supplied in Ref. 80. The *short dashed line* is obtained by adding the contribution of the libration band at 110 cm^{-1} band to this dielectric Relaxation data. The *solid line* is obtained by considering the contribution of the libration band and also freezing the translation motion of solvent molecules. Note that the agreement with experiments (*solid circles*) becomes better upon freezing the solvent translational motion.

2.4.2 Solvation Dynamics and Temperature Dependence

We now present the numerical results of solvation dynamics of an excited dipolar probe, C153 in formamide at three different temperatures and also compare with the experimental data provided by Horng *et al.*⁵⁰. We will also present results here to

show the effects of the intermolecular vibration band at 110 cm^{-1} on the time dependent progress of solvation of an instantaneously excited dipolar probe in formamide. The effect of this band on ionic conductivity is already shown in the previous section.

In Fig. 2.7 we compare the decay of the normalized solvation energy auto-correlation function, $S(t)$ obtained by using Eq. (2.12) at 298.15 K with those from the experiments by Horng *et al.*⁵⁰. It is evident from the figure that the predicted decay of the normalized solvation energy correlation function (*solid line*) agrees rather well with the experiments (*solid circles*). Note here that the numerical results represented by the *solid* and the *short dashed* lines are obtained by properly incorporating the contributions from the 110 cm^{-1} band to the complete dielectric relaxation of formamide at 298.15 K. In addition, the solvent molecules are assumed to be *translationally immobile* for the calculated decay represented by the *solid line*. The *long dashed* line represents the calculated decay without the 110 cm^{-1} band. It is interesting to note that the experimentally observed short time dynamics is *completely missed* if the contribution from this band is neglected in the present theory. We would also like to mention here that when the solvent molecules are translationally mobile, the decay at long time ($>1\text{ ps}$) predicted by the present theory is faster than what has been observed in experiments. This may be explained as follows. Formamide in the liquid phase can exist as cyclic dimers and linear chain oligomers³⁻³⁵ and therefore these large units would be much less mobile (translation) than a single formamide molecule. Consequently, the solvent reorganization around the excited solute (C153) via translational diffusion becomes sluggish and hence the decay rate becomes slower at long time. However, this does not affect the relaxation at short times ($<1\text{ ps}$) because the initial part of the polar solvation energy relaxation is dictated by the intermolecular vibration band (in formamide it is peaked at 110 cm^{-1}) which is *collective* in nature.

In Fig. 2.8 we present the calculated decay of the solvation energy auto-correlation function $S(t)$ at 283.15 K (*solid line*), 298.15 K (*long dashed line*) and 328.15 K (*short dashed line*). We have assumed here that the librational mode remains peaked

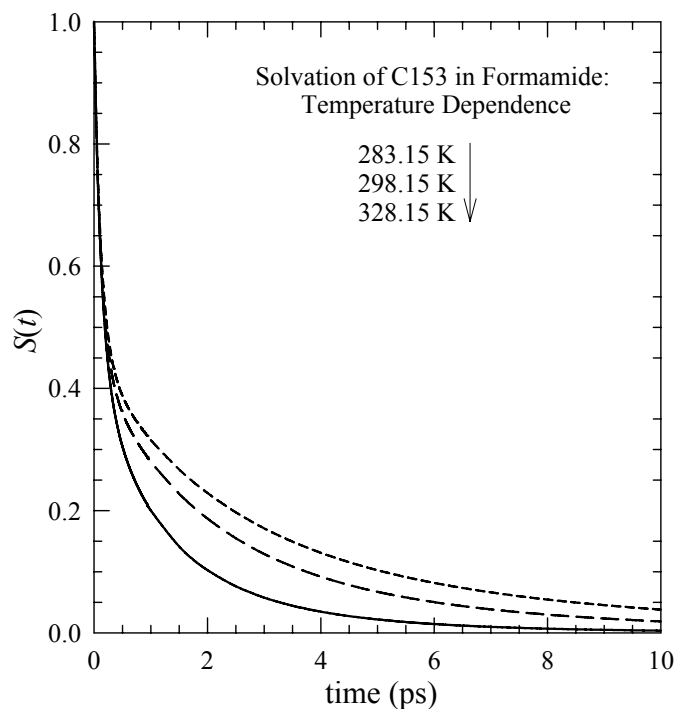


Figure 2.8: The effect of temperature on polar solvation energy relaxation in formamide. The normalized solvation energy auto-correlation function, $S(t)$, calculated for coumarin 153 in formamide at 283.15 K (*short dashed line*), 298.15 K (*long dashed line*) and 328.15 K (*solid line*) are shown as a function of time (t). Note here that in these calculations, the contributions of the libration band as well as those from the solvent translational mode have been incorporated. In addition, no temperature dependence of the libration band is considered.

at 110 cm^{-1} at all the temperatures studied here. As a consequence of this approximation, at short time the calculated rate of the decay of the normalized solvation energy auto-correlation function becomes the same for these three temperatures. The long time decay, however, becomes slower as the temperature decreases. In all the calculations presented in Fig. 2.8, the solvent molecules are assumed to be translationally mobile.

2.5 Conclusion

Let us summarize the main results presented in this chapter. We have calculated limiting molar ionic conductivity of uni-positive ions in formamide at three different temperatures by using a microscopic theory. The results predicted by the theory are

found to be in good agreement with the relevant experimental data. The non-monotonic size-dependence of Walden product in formamide has been explained satisfactorily by the present theory as was done earlier for water, deuterated water, acetonitrile and monohydroxy alcohols.^{52,66-69} We have also calculated the total limiting ionic conductance of several 1:1 strong electrolytes in formamide at three different temperatures and compared with the available experimental data. We have also studied solvation dynamics of a dipolar solute probe (C153) in formamide in order to investigate the effects of dynamical solvent modes on the ionic mobility in this liquid. A satisfactory agreement between the predicted and experimentally observed decay rates of normalized solvation energy auto-correlation function, $S(t)$, has been found at 298.15 K. Such a comparison for two other temperatures could not be made due to non-availability of experimental results at these temperatures.

The role of the libration mode centred at 110 cm^{-1} in determining the time scale of the fast component of the polar solvation energy relaxation in formamide and its subsequent effects on ion mobility have also been investigated here. We have found that the fast component of the solvation energy relaxation is totally missed if one switches off the contributions coming from the libration mode. This switching off also over-estimates the friction on a moving ion and hence lowers the value of its conductivity at infinite dilution in formamide. We would, however, like to mention here that the coupling of this band to both the solvation dynamics and ionic conductivity through dielectric relaxation is purely an assumption. This assumption together with the results obtained here might be regarded as a feedback to dielectric relaxation studies of liquid formamide. This is because the results of this study indicate that there might be another relaxation step with a time constant present in subpicosecond regime. Further experiments with more sophisticated technique, such as terahertz pulse transmission spectroscopy,⁸⁷ may be employed to reveal such a fast time scale in the dielectric relaxation of formamide at temperatures studied here.

The success of the theory might be lying in the use of the experimentally measured dielectric relaxation data as an input in solvent dynamic structure factor which takes care, at least *partially*, of the complex interactions that are present in the solvent. And, the present theory accounts for the microscopic structure of the solvent and includes the microscopic polarization around a solute ion in a consistent manner.

However, we would like to mention here that in our calculation of dielectric friction, we have neglected the cross-correlation between forces arising out of short-range (*hard*) and long-range (*soft*) interactions. This might be erroneous since recent simulation studies by Kumar and Maroncelli⁷⁶ have revealed the non-separability of frictions arising out of these interactions. This could be a potential source of fatal error and calculations using such scheme may not reflect the correct picture. Their simulation results also demonstrate that whenever the long-range interactions are large enough to significantly affect the friction, the frictional contribution due to the cross-correlation between the short-range and long-range forces is of the same magnitude as the friction coming solely from the long-ranged interactions. One therefore needs to develop a theory that will account for the cross-correlations in some consistent manner and yet will remain analytically simple such as the present one. This is definitely a challenging task.

References

1. J. C. Evans, *J. Chem. Phys.* **22**, 1228 (1954).
2. C. C. Costain and J. M. Dowling, *J. Chem. Phys.* **32**, 1228 (1960).
3. Y. J. Chang and E. W. Castner, Jr., *J. Chem. Phys.* **99**, 113 (1993).
4. J. Park, J. H. Ha and M. Hochstrasser, *J. Chem. Phys.* **121**, 7281 (2004).
5. J. H. Ha, Y. S. Kim and R. M. Hochstrasser, *J. Chem. Phys.* **124**, 064508 (2006).
6. Y. L. Li, L. Huang, R. J. D. Miller, T. Hasegawa and Y. Tanimura, *J. Chem. Phys.* **128**, 234507 (2008).
7. M. Lima, R. Chelli, V. V. Volkov and R. Righini, *J. Chem. Phys.* **130**, 204518 (2009).
8. K. Goossens, L. Smeller and K. Heremans, *J. Chem. Phys.* **99**, 5736 (1993).
9. O. F. Nielsen, P. A. Lund and E. Praestgaard, *J. Chem. Phys.* **77**, 3878 (1982).
10. A. Engdahl and B. Nelander and P. Astrand, *J. Chem. Phys.* **99**, 4894 (1993).
11. R. Ludwig, F. Weinhold and T. C. Farrar, *J. Chem. Phys.* **103**, 3636 (1995).
12. S. Chalmet and M. F. R. Lopez, *J. Chem. Phys.* **111**, 1117 (1999).
13. E. Tsuchida, *J. Chem. Phys.* **121**, 4740 (2004).
14. D. H. A. ter Steege, C. Lagrost, W. J. Buma, D. A. Leigh and F. Zerbetto, *J. Chem. Phys.* **117**, 8270 (2002).
15. M. Oguni and C. A. Angell, *J. Chem. Phys.* **78**, 7334 (1983).
16. A. Mortensen, O. F. Nielsen, J. Yarwood and V. Shelley, *J. Phys. Chem.* **98**, 5221 (1994).
17. R. Ludwig, J. Bohmann and T. C. Farrar, *J. Phys. Chem.* **99**, 9681 (1995).
18. (a) R. J. Kurland and E. B. Wilson, *J. Chem. Phys.* **27**, 585 (1957); (b) C. C. Costain and J. M. Dowling, *J. Chem. Phys.* **32**, 158 (1960).
19. S. Nasr and L. Bosio, *J. Chem. Phys.* **108**, 2297 (1998)
20. J. Ladel and B. Post, *Acta Crystallogr.* **7**, 559 (1954).
21. R. J. de Sando and G. H. Brown, *J. Phys. Chem.* **72**, 1088 (1968).
22. E. D. Stevens, *Acta Crystallogr.* **B34**, 544 (19784).
23. F. J. Weismann, M. D. Zeidler, H. Bartognolli and P. Chieux, *Mol. Phys.* **57**, 345 (1986)
24. M. Kitano and K. Kuchitsu, *Bull. Chem. Soc. Jpn.* **47**, 67 (1974).

25. S. L. Whittenburg, V. K. Jain and S. J. McKinnon, *J. Phys. Chem.* **90**, 1004 (1986).
26. E. Hirota, R. Sugisaki, C. J. Nielsen and G. O. Sorensen, *J. Mol. Spectrosc.* **49**, 251 (1974).
27. J. Barthel, K. Buchner, J. B. Gill and M. Kleebauer, *Chem. Phys. Lett.* **167**, 62 (1990).
28. J. Barthel and K. Buchner, *Pure Appl. Chem.* **63**, 1473 (1991).
29. T. Drakenberg and S. Forsen, *J. Phys. Chem.* **74**, 1 (1970).
30. M. I. Bugar, T. E. Amour and D. Fiat, *J. Phys. Chem.* **55**, 1049 (1981).
31. D. H. Christensen, R. N. Kortzeborn, B. Bak and J. J. Led, *J. Chem. Phys.* **53**, 3912 (1970).
32. W. L. Jorgensen and C. J. Swenson, *J. Am. Chem. Soc.* **107**, 569(1985).
33. K. P. Sagarik and R. Ahlrichs, *J. Chem. Phys.* **86**, 5117 (1987).
34. E. M. C. Lago and M. A. Rios, *J. Chem. Phys.* **110**, 6782 (1999).
35. J. Gao, J. J. Pavelites and D. Habibollazadeh, *J. Phys. Chem.* **100**, 2689 (1996).
36. Y. P. Puhovski and B. M. Rode, *J. Phys. Chem. B* **102**, 2920 (1995).
37. M. A. M. Cordeiro, W. P. Santana, R. Cusinato and J. M. M. Cordeiro, *J. Mol. Struct.* **759**, 159 (2006).
38. M. D. Elola and B. M. Ladanyi, *J. Chem. Phys.* **125**, 184506 (2006).
39. D. A. Leigh, A. Murphy, J. P. Smart and A. M. Z. Slawin, *Angew Chem. Int. Ed. Engl.* **36**, 728 (1997).
40. D. A. Leigh and A. Murphy, *Chem. Ind.* **178** (1999).
41. V. Bermudez, N. Capron, T. Gase, F. G. Gatti, F. Kajzar, D. A. Leigh, F. Zerbetto and S. Zhang, *Nature (London)* **406**, 608 (2000).
42. A. M. Brouwer, C. Frochot, F. G. Gatti, D. A. Leigh, L. Mottier, F. Paolucci, S. Roffia and G. W. H. Wurpel, *Science* **291**, 2124 (2001).
43. (a) O. F. Nielsen, P. A. Lund and E. Praestgaard, *J. Chem. Phys.* **75**, 1586 (1981); (b) O. F. Nielsen, P. A. Lund and E. Praestgaard, *J. Raman Spectrosc.* **9**, 286 (1980).
44. O. F. Nielsen, P. A. Lund and S. B. Petersen, *J. Am. Chem. Soc.* **104**, 1991 (1982).
45. S. Glasstone, *An Introduction to Electrochemistry* (Litton Education Publishing, New York, 1942); J. O'M Bockris and A. K. N. Reddy, *Modern*

- Electrochemistry* (Plenum, New York, 1973); P. W. Atkins, *Physical Chemistry* (Oxford University Press, 1994) 5th Ed., Part III, Ch. 24.
46. H. S. Harned and B. B. Owen, *The Physical Chemistry of Electrolyte Solutions*, (Reinhold, New York, 1958) 3rd Ed.
47. (a) H. S. Frank, *Chemical Physics of Ionic Solutions* (Wiley, New York, 1956); R. A. Robinson and R. H. Stokes, *Electrolyte Solutions* (Butterworth, London, 1959); (b) R. L. Kay in *Water: A Comprehensive Treatise*, ed. F. Franks (Plenum, New York, 1973), Vol. 3.
48. R. L. Kay and D. F. Evans, *J. Phys. Chem.* **70**, 2325 (1966).
49. R. Jimenez, G. R. Fleming, P. V. Kumar and M. Maroncelli, *Nature* (London) **369**, 471 (1994); M. Maroncelli, J. McInnis and G. R. Fleming, *Science* **243**, 1674 (1989).
50. M. L. Horng, J. A. Gardecki, A. Papazyan and M. Maroncelli, *J. Phys. Chem.* **99**, 17311 (1995).
51. D. Bingemann and N. P. Ernsting, *J. Chem. Phys.* **102**, 2691 (1995); N. P. Ernsting, N. E. Konig, K. Kemeter, S. Kovalenko and J. Ruthmann, *AIP Conf. Proc.* **441** (1995).
52. B. Bagchi and R. Biswas, *Adv. Chem. Phys.* **109**, 207 (1999) and references therein.
53. (a) B. Bagchi and A. Chandra, *Adv. Chem. Phys.* **80**, 1 (1991); (b) B. Bagchi, *Annu. Rev. Phys. Chem.* **40**, 115 (1989).
54. M. Born, *Z. Phys.* **1**, 45 (1920).
55. R. M. Fuoss, *Proc. Natl. Acad. Sci.* **45**, 807 (1959).
56. (a) R. H. Boyd, *J. Chem. Phys.* **35**, 1281 (1961); (b) R. H. Boyd, **39**, 2376 (1963).
57. (a) R. Zwanzig, *J. Chem. Phys.* **38**, 1603 (1963); (b) R. Zwanzig, **52**, 3625 (1970).
58. (a) J. B. Hubbard and L. Onsager, *J. Chem. Phys.* **67**, 4850 (1977); (b) J. B. Hubbard, *J. Chem. Phys.* **68**, 1649 (1978).
59. J. B. Hubbard and P. G. Wolynes, in *The Chemical Physics of Solvation*, Ed. R. Dogonadze et al. (Elsevier, NY, 1988) Part C, Chap. 1, p. 33.
60. (a) J. B. Hubbard and R. F. Kayser, *J. Chem. Phys.* **74**, 3535 (1981); (b) J. B. Hubbard and R. F. Kayser, *J. Chem. Phys.* **76**, 3377 (1982).

61. Y. M. Kessler, R. S. Kumeev, I. I. Vaisman, R. B. Lyalina and R. H. Bratishko, *Ber. Bunsenges. Phys. Chem.* **93**, 770 (1989).
62. P. G. Wolynes, *J. Chem. Phys.* **68**, 473 (1978).
63. P. Colonomos and P. G. Wolynes, *J. Chem. Phys.* **71**, 2644 (1979).
64. P. G. Wolynes, *Annu. Rev. Phys. Chem.* **31**, 345 (1980).
65. B. Bagchi, *J. Chem. Phys.* **95**, 467 (1991).
66. R. Biswas, S. Roy and B. Bagchi, *Phys. Rev. Lett.* **75**, 1098 (1995).
67. R. Biswas and B. Bagchi, *J. Chem. Phys.* **106**, 5587 (1997).
68. R. Biswas and B. Bagchi, *J. Am. Chem. Soc.* **119**, 5946 (1997).
69. B. Bagchi and R. Biswas, *Acc. Chem. Res.* **31**, 181 (1998).
70. (a) S. H. Lee and J. C. Rasaiah, *J. Chem. Phys.* **101**, 6964 (1994); (b) S. H. Lee and J. C. Rasaiah, *J. Phys. Chem.* **100**, 1420 (1996).
71. Y. P. Puhovski and B. M. Rode, *J. Chem. Phys.* **107**, 6908 (1997).
72. Y. P. Puhovski and B. M. Rode, *J. Chem. Phys.* **102**, 2920 (1995).
73. (a) S. Roy and B. Bagchi, *J. Chem. Phys.* **99**, 1310 (1993); (b) S. Roy and B. Bagchi, *J. Chem. Phys.* **99**, 9938 (1993); (c) N. Nandi, S. Roy and B. Bagchi, *J. Chem. Phys.* **102**, 1390 (1995).
74. R. Biswas and B. Bagchi, *J. Phys. Chem.* **100**, 1238 (1996).
75. H. K. Kashyap, T. Pradhan and R. Biswas, *J. Chem. Phys.* **125**, 174506 (2006).
76. P. V. Kumar and M. Maroncelli, *J. Chem. Phys.* **112**, 5370 (2000).
77. J. G. Kirkwood, *J. Chem. Phys.* **14**, 180 (1946).
78. R. Biswas and B. Bagchi, *J. Phys. Chem.* **100**, 4261 (1996).
79. See, for example, *Theory of Electric Polarization*, 78th ed., edited by C. J. F. Bottcher and P. Bordewijck (Elsevier, Amsterdam, 1978), Vol. II.
80. J. Barthel, R. Buchner and B. Wurm, *J. Mol. Liq.* **98-99**, 51 (2002).
81. M. Cho, S. J. Rosenthal, N. F. Scherer, L. D. Ziegler and G. R. Fleming, *J. Chem. Phys.* **96**, 5033 (1992).
82. D. McMorro and T. Lotshaw, *J. Phys. Chem.* **95**, 10395 (1991).
83. C. G. Gray and K. E. Gubbins, *Theory of Molecular Fluids* (Clarendon, Oxford, 1984), Vol. I.
84. D. Y. C. Chan, D. J. Mitchel and B. Ninham, *J. Chem. Phys.* **70**, 2946 (1979).
85. (a) D. Isbister and R. Bearman, *J. Mol. Phys.* **28**, 1297 (1974); (b) S. A. Adelman and J. M. Deutch, *J. Chem. Phys.* **59**, 3971 (1973).

86. J. Thomas and D. F. Evans, *J. Phys. Chem.* **74**, 3812 (1970).
87. J. T. Kindt and C. A. Schumuttenmaer, *J. Phys. Chem.*, **100**, 10373 (1996).

Chapter 3

Limiting Ionic Conductivity in Water-Tertiary Butyl Alcohol (TBA) Mixtures: Alcohol Mole Fraction Dependence

3.1 Introduction

Experimental studies of ionic conductivity in aqueous tertiary butyl alcohol (TBA) solutions have revealed that at room temperature in the limit of low TBA mole fraction, the Walden product (WP), $\Lambda_0\eta_0$, of uni-positive rigid ions shows a non-monotonic TBA mole fraction dependence.¹ The $\Lambda_0\eta_0$ versus TBA mole fraction (X_{TBA}) curve shows a peak at $X_{\text{TBA}}=0.10$ where several anomalous properties of the water-TBA mixture have been reported.¹⁻¹⁷ The peak values of the $\Lambda_0\eta_0$ versus X_{TBA} curve has been attributed to the *structure-breaking* power of the ions in the aqueous alcohol mixtures. However, the limiting ionic conductivity of relatively large tetra-alkyl ammonium ions show *linear* composition dependence and has been explained in terms of *hydrophobic hydration*.¹ These experimental findings are summarized in Fig. 3.1.

Neutron diffraction,²⁻⁴ X-ray scattering,⁶ light scattering⁷ experiments and computer simulation⁸⁻¹⁷ studies of water-TBA mixture have suggested that the self association of TBA molecules due to hydrophobic interaction between alkyl groups of TBA is responsible for the observed anomalies in various thermodynamic properties in water-rich compositions. Salt solutions can be used both to stabilize and destabilize hydrophobic surfaces causing low-polar molecules to become more (salting-in) or less (salting-out) soluble.¹⁸⁻²⁰ Therefore, the presence of ions in aqueous alcohol mixture can significantly modify the structure of the mixture and can alter many of the

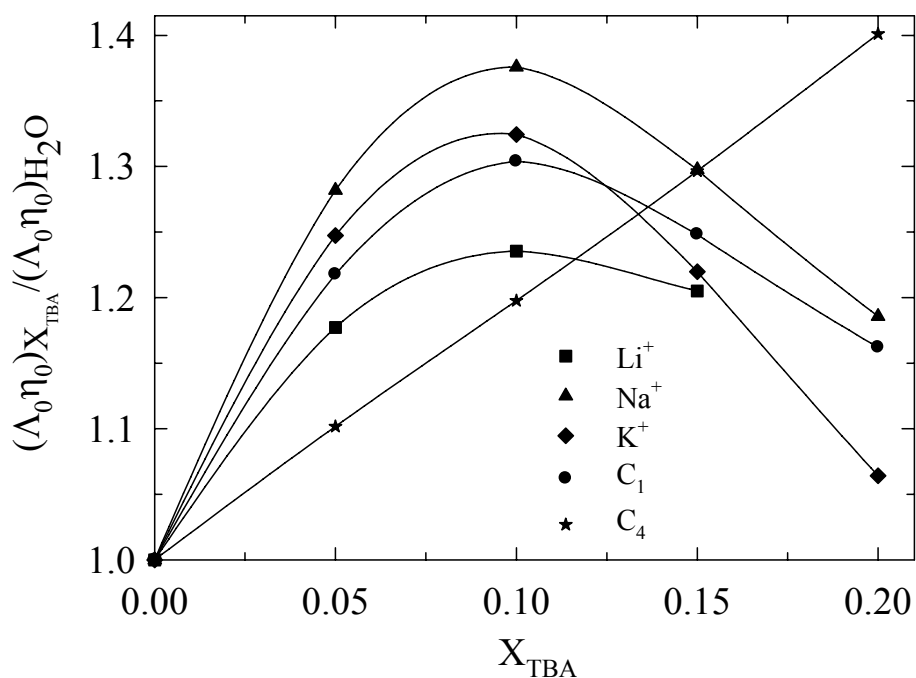


Figure 3.1: Experimental Walden products for cations in water-TBA mixture relative to its value for pure water. The data has been taken from Broadwater and Kay (J. Phys. Chem. **74**, 3802 (1970)).

solution properties. Also, the local enrichment of one solvent component around the ion, so-called *preferential solvation*,²¹⁻²² can have profound effects on its conductivity. For, if the ion is solvated more by water then the motion of the ion would be different than if it is solvated preferentially by TBA molecules. The extent of the effect of the preferential solvation may change with the composition of the mixture.²¹

As we have noticed in the last chapter, theoretical studies on ionic conductivity in pure polar solvents have been able to explain the break-down of the Stokes' law for small uni-positive ions in terms of ion-solvent interaction, microscopic structure of the unperturbed solvent and its natural dynamics.²³⁻⁴⁰ However, similar theoretical studies for binary mixtures are very few even-though there exists a large amount of experimental data.⁴¹⁻⁵⁰ Ibuki and Nakahara tested the Hubbard-Onsager (HO) theory for ionic conductivity in ethanol-water⁵¹ and dioxane-water⁵² mixtures. These authors have found that HO theory does reasonably well in predicting the friction coefficients

for alkali metal ions as function of solvent composition. The phenomenological approach of Apelblat to calculate the limiting molar ionic conductances for appreciable number of aqueous and non-aqueous mixtures seems to be working well.⁵³ Even though the above approach is able to predict the experimental data, it does not provide any molecular level explanations in terms of ion-solvent and solvent-solvent interactions and also the dynamics of solution mixtures. Wang and Anderko developed a model to calculate self-diffusivity of the ions, and therefore conductivity, in the mixed solvent electrolyte solutions.⁵⁴ However, the model proposed by them involves adjustable parameters to match the experimental limiting molar ionic conductivity in mixed solvents and therefore lacks a systematic microscopic description of ion conductivity in mixed solvents.

In this chapter we have calculated limiting molar ionic conductivity of alkali metal ions, Li^+ , Na^+ , K^+ , and organic ions, tetra-methyl-ammonium, C_1 and tetra-butyl-ammonium, C_4 , in water-TBA mixtures in the water-rich region of the mixture composition. The predicted results are then compared with the available experimental data.¹ Each composition studied here is assumed to be an effective single-component dipolar solvent defined by experimental density with dipole-moment μ given by $\mu^2 = (1 - X_{TBA})\mu_W^2 + X_{TBA}\mu_{TBA}^2$ where X_{TBA} denotes the mole-fraction of TBA, μ_W and μ_{TBA} the dipole-moments of pure water and TBA, respectively.⁵⁵ The static structure of the mixture has been obtained from molecular dynamics simulation (see chapter 7).¹⁷ This is done in order to incorporate the structural complexity of such binary mixtures in a way much better than simply using the MSA for ion in dipolar mixtures.²¹ The effects of solution heterogeneity also enters into the calculation as experimental dielectric relaxation data are used as inputs to the theory for predicting the limiting ionic conductivity at a given TBA mole-fraction.

The organization of the rest of the chapter is as follows: In section 3.2 we give an overview of the theoretical details. Calculation procedure is discussed briefly in section 3.3. Numerical results with discussion are presented in section 3.4. Finally the chapter ends with conclusion in section 3.5.

3.2 Theory

In binary dipolar mixtures, the bare friction, ζ_{bare} , may still be approximated by the Stokes' law, $\zeta_{bare} = A\eta_0 r_{ion}$, η_0 being the solution viscosity. The coefficient A has been taken to be 4π (*slip* boundary condition) for all the ions considered here. The mode-coupling expression for dielectric friction, ζ_{df} , in binary dipolar mixtures can be derived as done before for pure dipolar solvents. We write the excess free energy functional for the total system (ion + binary mixture) as^{39,55}

$$\begin{aligned} \beta\Delta F[n_{ion}(\mathbf{r}), \rho_a(\mathbf{r}, \mathbf{\Omega})] = & \int d\mathbf{r} n_{ion}(\mathbf{r}) [\ln \frac{n_{ion}(\mathbf{r})}{n_{ion}^0} - 1] + \sum_{a=1}^2 \int d\mathbf{r} d\mathbf{\Omega} \rho_a(\mathbf{r}, \mathbf{\Omega}) [\ln \frac{\rho_a(\mathbf{r}, \mathbf{\Omega})}{\rho_a^0 / 4\pi} - 1] \\ & - \frac{1}{2} \int d\mathbf{r} d\mathbf{r}' c_{ii}(\mathbf{r}; \mathbf{r}') \delta n_{ion}(\mathbf{r}) \delta n_{ion}(\mathbf{r}') \\ & - \frac{1}{2} \sum_{a,b=1}^2 \int d\mathbf{r} d\mathbf{\Omega} d\mathbf{r}' d\mathbf{\Omega}' c_{ab}(\mathbf{r}, \mathbf{\Omega}; \mathbf{r}', \mathbf{\Omega}') \delta \rho_a(\mathbf{r}, \mathbf{\Omega}) \delta \rho_b(\mathbf{r}', \mathbf{\Omega}') \\ & - \sum_{a=1}^2 \int d\mathbf{r} d\mathbf{r}' d\mathbf{\Omega}' c_{ia}(\mathbf{r}; \mathbf{r}', \mathbf{\Omega}') \delta n_{ion}(\mathbf{r}) \delta \rho_a(\mathbf{r}', \mathbf{\Omega}') \end{aligned} \quad (3.1)$$

where $\delta n_{ion}(\mathbf{r}) = n_{ion}(\mathbf{r}) - n_{ion}^0$ and $\delta \rho_a(\mathbf{r}, \mathbf{\Omega}) = \rho_a(\mathbf{r}, \mathbf{\Omega}) - \rho_a^0 / 4\pi$, are the fluctuations of solute dipole and solvent dipole of a^{th} type densities about their bulk values, respectively. Minimizing the above free energy functional for equilibrium condition we get the following expression for the effective force density acting on the ion due to ion-dipole interactions as^{39,55}

$$\Delta F_i(\mathbf{r}, t) = k_B T n_{ion}(\mathbf{r}, t) \nabla \sum_{a=1}^2 \int d\mathbf{r}' d\mathbf{\Omega}' c_{ia}(\mathbf{r}; \mathbf{r}', \mathbf{\Omega}') \delta \rho_a(\mathbf{r}', \mathbf{\Omega}', t) \quad (3.2)$$

Now, as done in chapter 2 by using the Kirkwood formula⁵⁶ of force autocorrelation function and the standard Gaussian decoupling approximation⁵⁷ we obtain the following expression for the macroscopic dielectric friction⁵⁵

$$\zeta_{df} = \frac{2}{3} \frac{k_B T}{(2\pi)^2} \sum_{a,b} \sqrt{\rho_a^0 \rho_b^0} \int_0^\infty dk k^4 S_{ion}(k, t) c_{ia}^{10}(k) c_{ib}^{10}(-k) S_{ab}^{10}(k, t) \quad (3.3)$$

where ρ_a^0 is number density of a^{th} type dipolar component of the mixture. $S_{ion}(k, t)$ denotes the self-dynamic structure factor of the ion. $c_{ia}^{10}(k)$ is the Fourier transform of the longitudinal component of static ion-dipole direct correlation function (DCF) due interaction between the ion and a^{th} type dipole. $S_{ab}^{10}(k, t)$ is partial solvent dynamic structure factor. The solution static structure factor may be assumed to be given by the mean spherical approximation (MSA) or the hypernetted chain (HNC) theories. However, the calculation of the partial dynamic structure factor, $S_{ab}^{10}(k, t)$, is rather daunting task if one wants to consider the microscopic dynamics of the system. It will be evident later in this chapter that static correlation functions obtained from MSA for electrolyte solution in binary dipolar mixtures^{21,58} is not sufficient to predict the correct structure of water-TBA mixture. Therefore, as discussed above, we have approximated water-TBA mixture as an effective dipolar one-component medium. This leads to the above expression for dielectric friction (Eq. 3.3) to reduce to that for a single component system as described in chapter 2.

3.3 Calculation Procedure

3.3.1 Calculation of Static Correlation Functions

The ion-dipole DCF, $c_{id}^{10}(k)$, is calculated using the procedure of Chan *et al.*⁵⁹ for electrolyte solution in the limit of zero ion concentration (see section 2.3.2.2 for more details). The longitudinal component of wave number dependent dielectric function $\varepsilon_L(k)$ has been obtained from our own molecular dynamics simulation studies¹⁷ done using all atom models for water and TBA (see chapter 7). The function $\varepsilon_L(k)$ is related with dipolar symmetry projections, $h^{11l}(r)$, as⁶⁰

$$\left[1 - \frac{1}{\varepsilon_L(k)}\right] = 3Y \left\{1 + \frac{1}{3} \rho \tilde{h}^{110}(k) + \frac{2}{3} \rho \tilde{h}^{112}(k)\right\} \quad (3.4)$$

where $\tilde{h}^{11l}(k)$ is the Fourier-Hankel transform of the projection $h^{11l}(r)$ as

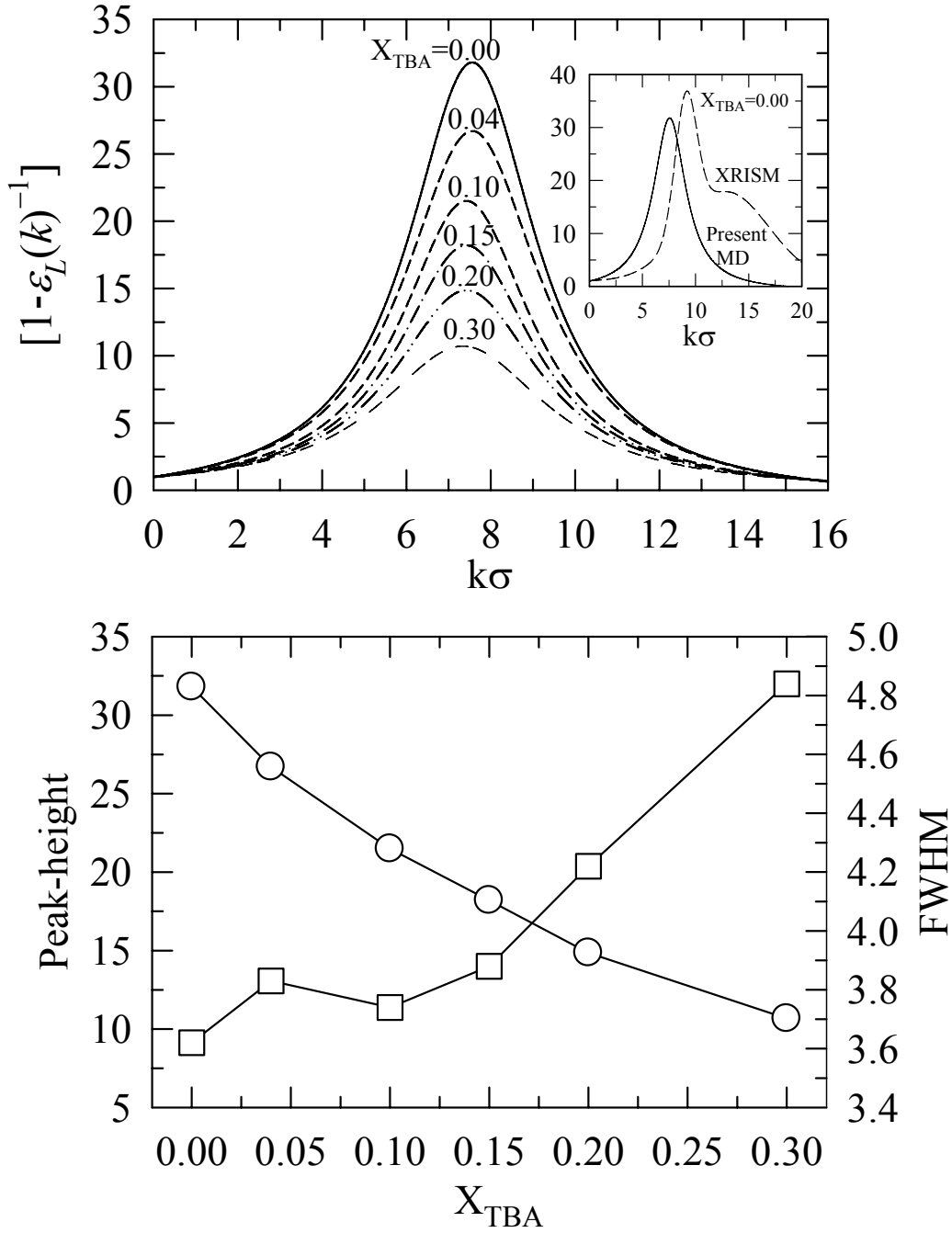


Figure 3.2: *Upper panel:* Simulated Longitudinal component wavenumber dependent dielectric function, $\varepsilon_L(k)$, as a function of wavenumber, $k\sigma$, at different composition of water-TBA mixture. The present MD result for pure water is compared with that from extended reference interaction site model (XRISM) in the *inset* of the figure. Note that $\sigma = 2.8\text{\AA}$ in the present calculation while it is 3.15\AA in XRISM. *Lower panel:* Essential features of $[1 - \varepsilon_L(k)]^{-1}$: *Open circles* and *open squares* are peak-height and full width at half maximum (FWHM) of the function, respectively.

$$\tilde{h}^{1l}(k) = 4\pi i^l \int_0^{\infty} r^2 j_l(kr) h^{1l}(r) dr \quad (3.5)$$

and j_l is the spherical Bessel function of order l . $h^{1l}(r)$ is calculated from the weighted sum of dipolar symmetry projections of pair distribution for each species pairs (water-water, water-TBA, TBA-TBA) of the mixture as:⁶⁰

$$h^{1l}(r) = \sum_{i,j} \frac{x_i x_j \mu_i \mu_j}{\mu^2} h_{ij}^{1l}(r),$$

where x_i and μ_i are molefraction and the dipole-

moment of species i , respectively and $h_{ij}^{1l}(r)$ is dipolar symmetry coefficients for a pair of molecules of species i and j . Other details about the function $h^{1l}(r)$ can be found in chapter 7. Note here that only first peak of the simulated $[1-1/\varepsilon_L(k)]$ with proper corrections at both $k \rightarrow 0$ and $k \rightarrow \infty$ limits has been used for the calculation of limiting ionic conductivity.³⁹ The simulated $[1-1/\varepsilon_L(k)]$ versus wavenumber k curve at various molfraction of TBA is shown in the upper panel of Figure 3.2. The simulated $[1-1/\varepsilon_L(k)]$ at zero TBA mole-fraction has been compared with that from extended reference interaction site model (XRISM) calculation by Raineri and coworkers⁶¹ and is shown in the *inset* of the same panel. Note that the peak value of $[1-1/\varepsilon_L(k)]$ from XRISM is more pronounced than that of MD simulation. Also, the peak position from XRISM is slightly shifted towards larger value of $k\sigma$. This because the value of σ is greater in XRISM calculation than that in our MD simulation. The characteristics of the $[1-1/\varepsilon_L(k)]$ at different molefractions are plotted in the lower panel of Fig. 3.2. It should be noticed that the peak height of $[1-1/\varepsilon_L(k)]$ curve decreases with increasing TBA molefraction. The full width at half maximum (FWHM) of the $[1-1/\varepsilon_L(k)]$ curve increases from pure water to $X_{\text{TBA}}=0.04$ then slightly decreases at $X_{\text{TBA}}=0.10$ and increases again with further increase of TBA concentration. Note also that the second peak in $[1-1/\varepsilon_L(k)]$ calculated from XRISM is having negligible contribution in predicting the limiting molar ionic conductivity.

3.3.2 Calculation of the Longitudinal Component of Generalized

Rate of Solvent Polarization Relaxation, $\sum_{10}(k, z)$

As described in chapter 2 (Eq. 2.13) the wave number and frequency dependent generalized rate of solvent polarization relaxation, $\sum_{10}(k, z)$, contains two dissipative kernels – the rotational kernel ($\Gamma_R(k, z)$) and the translational kernel ($\Gamma_T(k, z)$).^{39, 62-64} The translational dissipative kernel, $\Gamma_T(k, z)$, has been calculated by using the isotropic dynamic structure factor of the effective dipolar medium while the rotational kernel $\Gamma_R(k, z)$ at $k \rightarrow 0$ limit is directly related to the experimentally determined frequency dependent dielectric function, $\varepsilon(z)$ and is given by Eq. 2.14. For other details about the calculation see section 2.3.1 of chapter 2.

The dielectric relaxation function that has been used in the calculation expressed as follows:

$$\varepsilon(z) = \varepsilon_\infty + \sum_{i=1}^2 \frac{S_i}{[1 + (z\tau_i)^{\beta_i}]^{\alpha_i}} + \sum_{j=3}^5 \frac{S_j \Omega_j}{[z + \Omega_j^2 + z\gamma_j]} \quad (3.6)$$

where z is Laplace frequency, ε_∞ is the limiting value of $\varepsilon(z)$ at high frequency τ_j the relaxation time for the S_j dispersion. The parameters α_i and β_i determine the shape of a relaxation spectrum. Ω_j and $\gamma_j = 2\Omega_j$ stand respectively for the resonance frequency and the damping constant for the contribution coming from high frequency modes that has been described using the damped harmonic oscillator model. For our calculation in TBA-water mixture, we have used dielectric relaxation data measured by Mashimo and coworkers⁶⁵ who recorded the frequency dependent dielectric function in the range of 1 MHz – 20 GHz. The dielectric relaxation parameters used in the calculation are given in Table 3.1. These data have been best fitted to a single non-Debye relaxation process. As shown in Fig. 3.3 that the relaxation time, τ_1 , is linearly increasing with increasing TBA mole fraction but the exponents, α_1 and β_1 , deviate from linearity as one adds TBA in water. The deviation from unity as well as from linearity of these exponents clearly indicates the

Table 3.1: Dielectric relaxation parameters used in the calculation ^(a)

	$X_{TBA}=0.00$	$X_{TBA}=0.04$	$X_{TBA}=0.10$	$X_{TBA}=0.15$	$X_{TBA}=0.20$	$X_{TBA}=0.30$
ϵ_0	78.30	70.3	54.0	45.6	40.1	28.1
S_1	72.12	66.0	51.2	42.2	37.1	25.0
$\tau_1(\text{ps})$	8.32	19.95	31.62	42.66	50.12	74.13
α_1	1	0.822	0.776	0.731	0.734	0.738
β_1	1	0.989	0.979	0.946	0.955	0.958
S_2	1.69	-	-	-	-	-
$\tau_2(\text{ps})$	1.02	-	-	-	-	-
α_2	1	-	-	-	-	-
β_2	1	-	-	-	-	-
S_3	0.29	0.1	-	-	-	-
$\Omega_3(\text{cm}^{-1})$	69.3	69.3	-	-	-	-
S_4	2.10	2.1	-	-	-	-
$\Omega_4(\text{cm}^{-1})$	193	193	-	-	-	-
S_5	0.33	0.28	0.95	1.05	1.12	1.20
$\Omega_5(\text{cm}^{-1})$	685	685	685	685	685	685
n_D^2	1.77	1.82	1.85	1.86	1.88	1.90

(a) The relaxation parameters for the slowest dispersion step have been taken from Mashimo *et al.*⁶⁵ except for pure water for which the relaxation parameters have been taken from ref. 39.

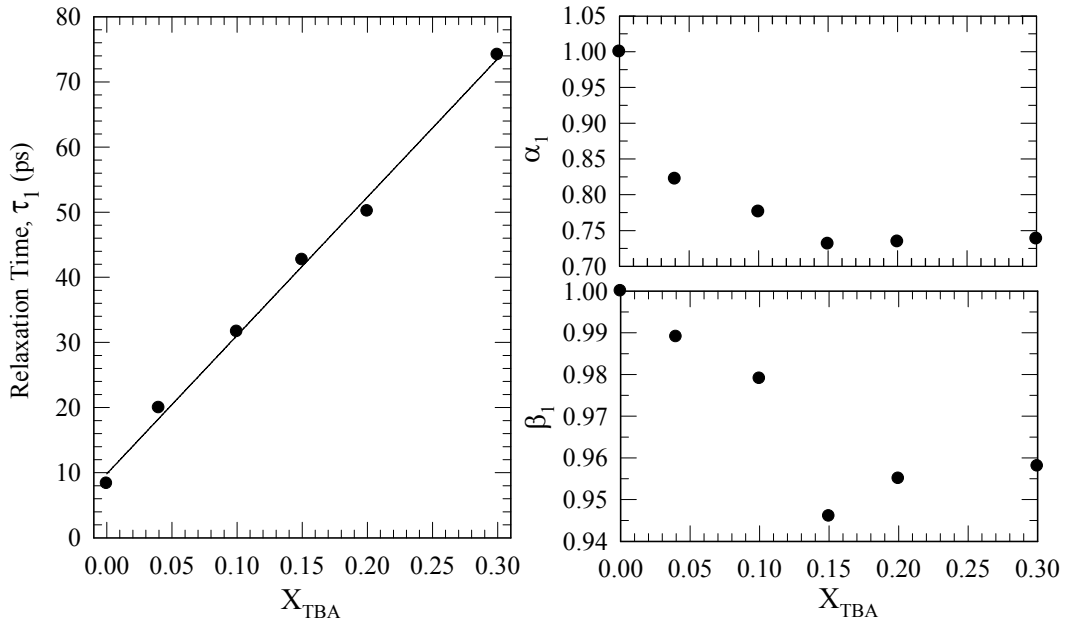


Figure 3.3: The dielectric relaxation parameters for the slowest dispersion step as a function of TBA mole fraction.

growth of solution heterogeneity upon addition of TBA in the aqueous mixture. It should also be noted that the measured ε_∞ is approximately 3 to 5 for all the TBA mole-fractions studied here. Therefore, the dispersion, $\varepsilon_\infty - n_D^2$ (n_D being the refractive index), is *missing* in these data due to the limited resolution available to these authors. However, it has been observed before that such missing relaxations have played an important role in determining both the ionic conductivity and the early part of the solvation dynamics in pure solvents³⁹ and therefore could be crucial in such mixtures as well. In our calculation we have assumed that the librational bands that are present in pure water account for the relaxation from ε_∞ to n_D^2 at all the composition studied here. The other essential parameters required in the calculation are provided in Table 3.2.

3.4 Numerical Results and Discussion

3.4.1 Li⁺ in Water-TBA

In Fig. 3.4 we have shown the calculated limiting molar ionic conductivity, Λ_0 and Walden product, $\Lambda_0\eta_0$, for Li⁺ ion as functions of TBA molefraction, X_{TBA} , in aqueous TBA mixture and compared with the experimental results. The theoretical results are shown by *open circles* and experimental results by *filled circles*. The predicted values of Λ_0 and $\Lambda_0\eta_0$ with the static correlations calculated from MSA for ions in dipolar mixture^{21,58} are shown by *open triangles*. We shall keep this notation fixed hereafter. The experimental data are taken from the works of Broadwater and Kay.¹ It is quite evident from the upper panel of this figure that the predictions from the present theory are appreciably good at all the composition studied here. Also, as shown in the lower panel of the figure, the non-monotonic dependence of WP observed in experiments is found in the present theoretical study as well. However, the position of the peak in the calculation is found to be at $X_{\text{TBA}} \approx 0.15$ whereas in experiment it is at $X_{\text{TBA}}=0.10$. Also the value of the peak in WP is greater than that reported in experiments. It is also clear from Fig. 3.4 and the subsequent figures that the MSA type correlations of asymmetric dipolar hard-sphere mixture^{21,58} are not that adequate to predict the experimental conductivity in water-TBA mixtures.

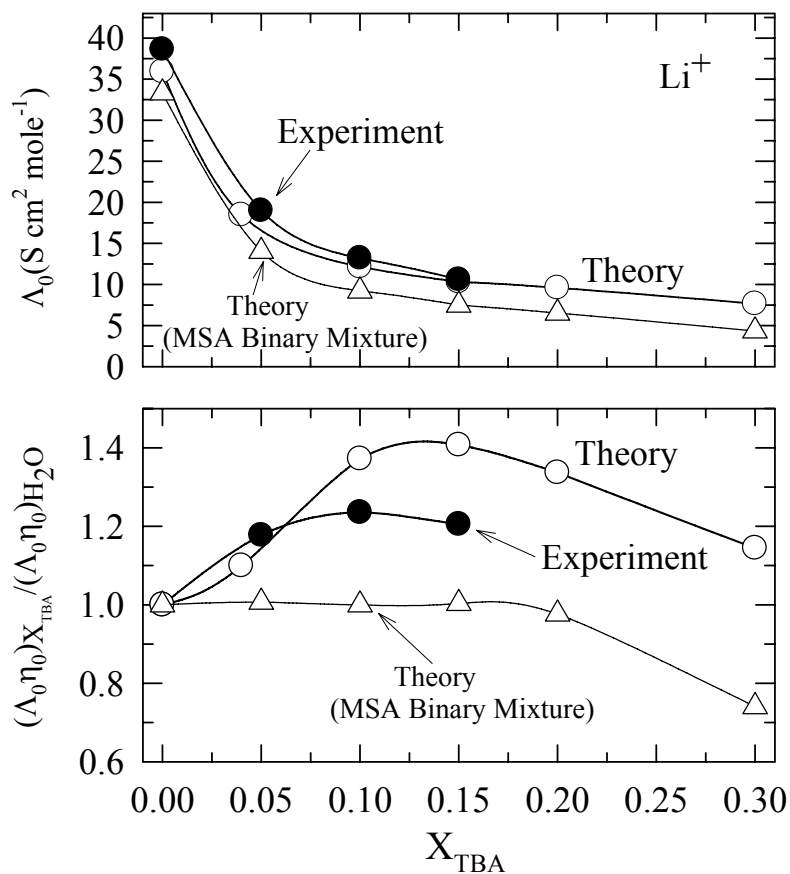


Figure 3.4: Upper panel: Limiting molar ionic conductivity of Li^+ ion in TBA-water mixture. Lower panel: Relative WP for Li^+ ion. Diameter of Li^+ ion used in the calculation is taken to be 1.18\AA .

Table 3.2: Solution parameters used in the calculation^(a)

	$X_{TBA}=0.00$	$X_{TBA}=0.04$	$X_{TBA}=0.10$	$X_{TBA}=0.15$	$X_{TBA}=0.20$	$X_{TBA}=0.30$
Viscosity (cP)	0.89	1.85	3.24	3.97	4.44	4.98
Density (gm/cc)	0.997	0.976	0.940	0.919	0.898	0.865

(a) From ref: Broadwater and Kay, J. Phys. Chem. **74**, 3802 (1970).

3.4.2 Na⁺ in Water-TBA

The limiting molar ionic conductivity (*upper panel*), and Walden product (*lower panel*) for Na⁺ ion in water-TBA mixture is shown in Fig. 3.5. Note that the theoretical value of limiting molar ionic conductivity is *quantitatively* agreeing with the experimental data.¹ The non-monotonic dependence of WP is captured by the present theory for this case also. Though the value of WP at all the composition is different, the WP ratio peaks at the alcohol mole-fraction very close to that found in experiments. Here again the predictions from the present theory are rather poorly described if one incorporates static correlations (solvent-solvent) from MSA model of binary dipolar mixture.

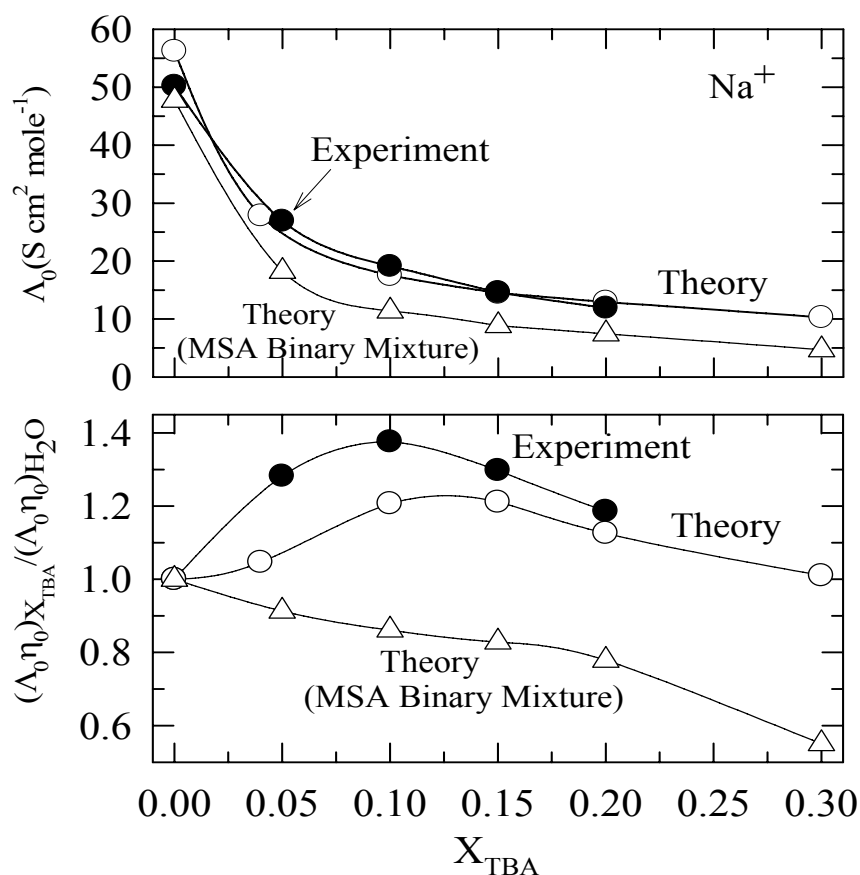


Figure 3.5: *Upper panel:* Limiting molar ionic conductivity of Na⁺ ion in TBA-water mixture. *Lower panel:* Relative WP for Na⁺ ion. Diameter of Na⁺ ion in the calculation is taken to be 1.94Å.

3.4.3 K^+ in Water-TBA

In Fig. 3.6 we show the calculated and experimental results for K^+ ion. The agreement between the theory and experiments for this ion is not as quantitative as found for other ions discussed above. The theoretical value of the limiting molar ionic conductivity of K^+ is smaller than the experimental ones at all the TBA mole fractions studied. But the basic trend is well captured by the present theory.

3.4.4 C_1 in Water-TBA

The limiting molar ionic conductivity, Λ_0 , for an organic ion, tetra-methyl-ammonium, C_1 , as a function of TBA molefraction is shown in Fig. 3.7. In this case also the predicted values of Λ_0 from the theory is smaller for all the compositions. But, the trend is similar to that of experiment.

3.4.5 C_4 in Water-TBA

The calculated results for a relatively large organic ion, tetra-butyl-ammonium, C_4 , at different composition of water-TBA mixture is shown in Fig. 3.8. The calculated value of Λ_0 for C_4 ion with slip boundary condition applied in calculating bare friction is larger than the experiments for TBA molefraction up to 0.10, the deviation becomes maximum for pure water. Note, however, that being larger in size the dielectric friction is negligible for C_4 ion in comparison to the bare friction (calculated from Stokes' law). The stick boundary condition is also examined considering the possibility that C_4 ion might interact with the medium more strongly due its propeller-type shape. Interestingly, at very low TBA mole-fractions ($X_{TBA} \leq 0.1$) calculations with stick boundary condition agree well with the experiments whereas predictions with slip boundary condition seem to describe well the experimental results at higher alcohol concentrations ($X_{TBA} \geq 0.1$). Since the dielectric friction is much less for ions with much larger ion-solvent size ratio, the dominance of the Stokes' friction in controlling the mobility of larger ions is expected. However, the apparent necessity of two different boundary conditions (in order to describe the limiting conductivity of C_4 ion) at extremely low and relatively high TBA concentrations is what requires further

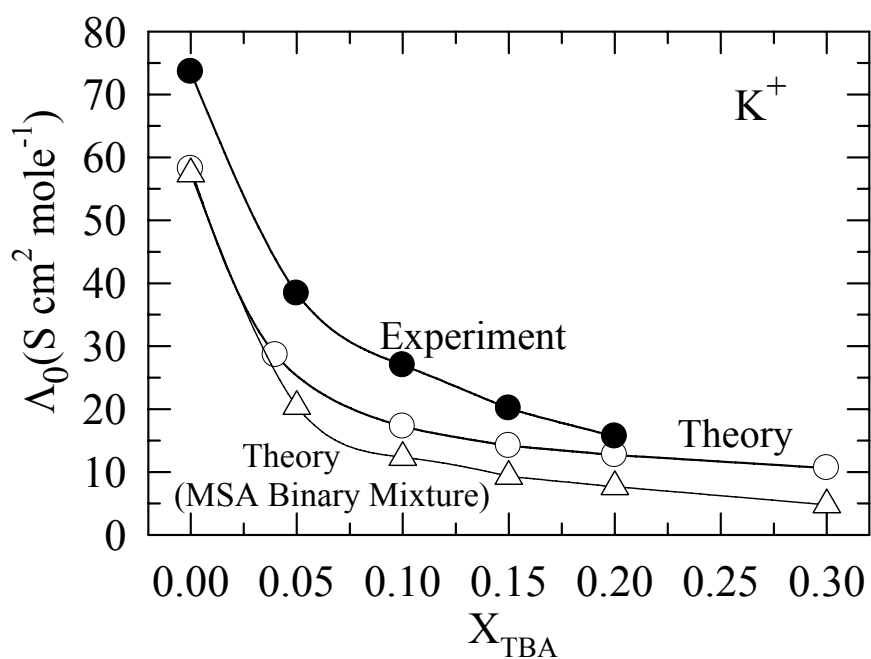


Figure 3.6: Limiting molar ionic conductivity of K^+ ion in TBA-water mixture. The diameter of K^+ ion in the calculation is taken to be 2.76\AA .

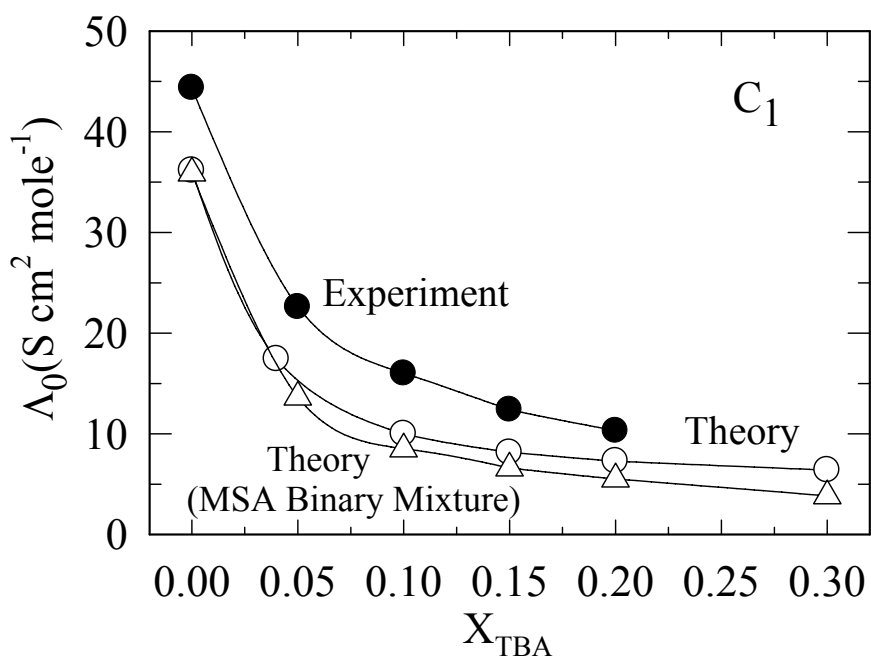


Figure 3.7: Limiting molar ionic conductivity of C_1 ion in TBA-water mixture. The diameter of C_1 ion in the calculation is taken to be 7.14\AA .

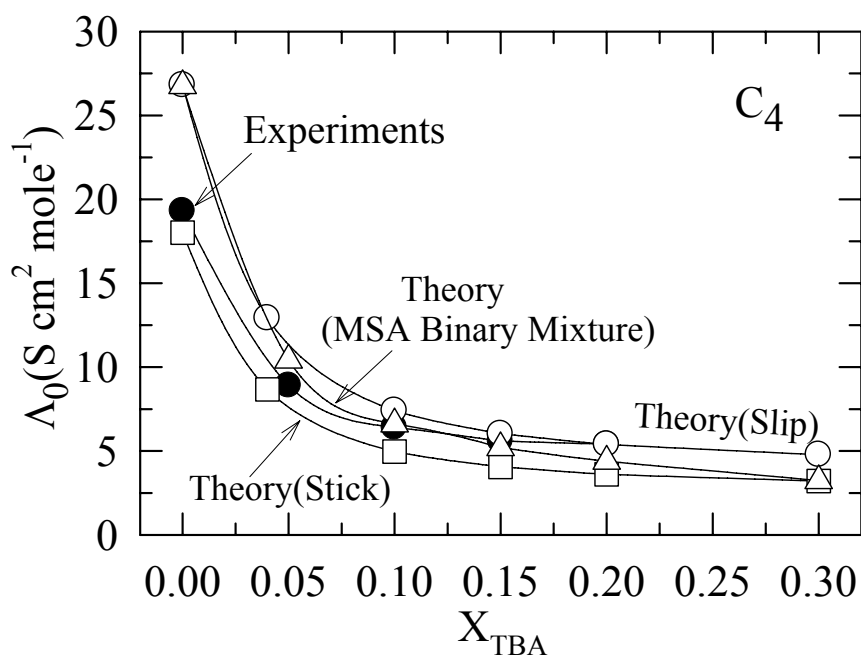


Figure 3.8: Limiting molar ionic conductivity of C_4 ion in TBA-water mixture. The diameter of C_4 ion in the calculation is taken to be 10.0\AA . Λ_0 calculated with bare friction using stick and slip boundary conditions are shown by *open circles* and *squares*, respectively. The predicted values of Λ_0 calculated with static correlations from MSA for ions in asymmetric binary dipolar mixture are shown by *open triangles*.

discussion. It may be recalled that several experimental and simulation studies have indicated strengthening of the three-dimensional H-bonding network of water upon addition of TBA.²⁻¹⁷ The strengthening effects in this regime have also been detected in a recent study where TBA mole-fraction induced large red-shift in the absorption spectrum of a dipolar solute probe has been observed.⁶⁶⁻⁶⁷ The stronger H-bonding network is then likely to exert more friction on the moving ion. This is akin to the enhancement of the local viscosity due to the presence of more structured solvent surrounding the ion. Now the tetrahedral water-like network structure progressively converts into a more alcohol-like zigzag chain structure upon further addition of TBA in the aqueous mixture. The structural transition is found to take place at TBA mole-fraction ~ 0.10 .¹⁻¹⁷ Since this alcohol mole-fraction induced transition reduces the stiffness in the solution structure, the bare friction becomes more close to that described by the slip boundary condition. Consequently, calculations with slip

boundary condition agree better to the experimental data at higher TBA mole fractions.

Since, the conductivity of large ions at infinite dilution is supposed to be *inversely* proportional to the solution viscosity (Stokes' law), the Walden product (WP) for C_4 However, WP for C_4 shows a linear increase with increasing TBA concentration (see Fig. 3.1). This means that the proportionality relation breaks down for large ions in water-TBA mixtures. One of the reasons for the observed linear increase of the WP for C_4 ion might be that the rate of increase of viscosity with TBA mole-fraction is greater than the rates of decrease of conductivity across the mixture compositions. This decoupling of ion mobility from the solution viscosity is a reminiscent of what has been observed for various super-cooled systems and therefore requires further study. Computer simulation studies of viscosity with more realistic model potentials could be particularly helpful to unravel the mechanism of the apparent decoupling.

3.5 Conclusion

We have used a microscopic theory to calculate the alcohol mole fraction dependent limiting ionic conductivity of singly charged cations in water-TBA mixtures where, as input to the calculations, solvent-solvent static correlations have been supplied from our own molecular dynamics (MD) simulation studies. The limiting ionic conductivities predicted by the present theory are found to be in good agreement with the relevant experimental data. The limiting molar ionic conductivity of a given ion decreases with increase of TBA molefraction because of two factors: (1) the solution viscosity increases hence bare friction and (2) the relaxation time increases and so the dielectric friction. The gradual decrease of limiting ionic conductivity with increasing TBA mole-fraction has been explained satisfactorily by the present theory even for smaller ions where contribution of Stokes' friction (that is the effect of viscosity) is less than the dielectric friction. Our analyses reveal that the non-monotonic alcohol mole fraction dependence for small ions originates from the static structural heterogeneity of water-TBA solution. The solvent-solvent static correlations adopted from MSA are unable to capture this microscopic heterogeneity present in real water-TBA mixture. Unlike the scenario in neat polar solvents, the limiting molar ionic

conductivity of relatively large tetra-butyl-ammonium ion, for which the magnitude of the dielectric friction is found to be negligible, cannot be understood from the Stokes-Einstein relation in these mixtures. Further studies, possibly molecular dynamics simulations with better model potentials that can reproduce the solution structure closest to the real systems, are therefore required to understand the ion conductivity in these kinds of binary polar mixtures.

References

1. T. L. Broadwater and R. L. Kay, *J. Phys. Chem.* **74**, 3802 (1970).
2. D. T. Bowron and J. L. Finney, *J. Phys. Chem. B.* **111**, 9838 (2007).
3. D. T. Bowron, J. L. Finney and A. K. Soper, *J. Phys. Chem. B.* **102**, 3551 (1998).
4. M. Nakada, O. Yamamuro, K. Maruyama and M. Misawa, *J. Phys. Soc. Jpn.* **76**, 054601 (2007).
5. V. Calandrini, A. Deriu, G. Onori, R. E. Lechner and J. Pieper, *J. Chem. Phys.* **120**, 4759 (2004).
6. (a) Y. Koga, *Chem. Phys. Lett.* **111**, 176 (1984); (b) Y. Koga, *Can. J. Chem.* **66**, 1187 (1988); (c) Y. Koga, *Can. J. Chem.* **66**, 3171 (1988).
7. (a) K. Iwasaaki and T. Fusiyaama, *J. Phys. Chem.* **81**, 1908 (1977); (b) K. Iwasaaki and T. Fusiyaama, *J. Phys. Chem.* **83**, 463 (1979).
8. K. Nakanishi, K. Ikari, S. Okazaki and H. Touhara, *J. Chem. Phys.* **80**, 1656 (1984).
9. H. Tanaka, K. Nakanishi and H. Touhara, *J. Chem. Phys.* **81**, 4065 (1984).
10. I. Omelyan, A. Kovalenko and F. Hirata, *J. Theo. Compu. Chem.* **2**, 193 (2003).
11. M. E. Lee and N. F. A. van der Vegt, *J. Chem. Phys.* **122**, 114509 (2005).
12. E. S. Ferrari, R. C. Burton, R. J. Davey and A. Gavezzotti, *J. Comput. Chem.* **27**, 1211 (2006).
13. A. Parera, F. Sokolic, L. Almasy and Y. Koga, *J. Chem. Phys.* **124**, 124515 (2006).
14. M. Kiselev and Ivlev, *J. Mol. Liq.* **110**, 193 (2004).
15. (a) P. G. Kusalik, A. P. Lyubartsev, D. L. Bergman, and Aatto Laaksonen, *J. Phys. Chem. B.* **104**, 9526 (2000); (b) P. G. Kusalik, A. P. Lyubartsev, D. L. Bergman, and Aatto Laaksonen, *J. Phys. Chem. B* **104**, 9533 (2000).
16. S. Paul and G. N. Patey, *J. Phys. Chem. B.* **110**, 10514 (2006).
17. H. K. Kashyap and R. Biswas *J. Chem. Phys.* 2009 (submitted).
18. F. Hofmeister *Arch. Exp. Pathol. Pharmacol.* **24**, 247 (1888).
19. W. Kunz, J. Henle and B. W. Ninham, *Curr. Opin. Colloid Interface* **9**, 19 (2004).
20. Y. Zhang and P. S. Cremer, *Curr. Opin. Chem. Bio.* **10**, 658 (2006).

21. H. K. Kashyap and R. Biswas, *J. Chem. Phys.* **127**, 184502 (2007).
22. H. K. Kashyap and R. Biswas, *J. Chem. Sci.* **119**, 391 (2007).
23. M. Born, *Z. Phys.* **1**, 45 (1920).
24. B. Bagchi and R. Biswas, *Adv. Chem. Phys.* **109**, 207 (1999) and references therein.
25. (a) B. Bagchi and A. Chandra, *Adv. Chem. Phys.* **80**, 1 (1991); (b) B. Bagchi, *Annu. Rev. Phys. Chem.* **40**, 115 (1989).
26. H. K. Kashyap, T. Pradhan and R. Biswas, *J. Chem. Phys.*, **125**, 174506 (2006).
27. R. M. Fuoss, *Proc. Natl. Acad. Sci.* **45**, 807 (1959).
28. (a) R. H. Boyd, *J. Chem. Phys.* **35**, 1281 (1961); (b) R. H. Boyd, **39**, 2376 (1963).
29. (a) R. Zwanzig, *J. Chem. Phys.* **38**, 1603 (1963); (b) R. Zwanzig, **52**, 3625 (1970).
30. (a) J. B. Hubbard and L. Onsager, *J. Chem. Phys.* **67**, 4850 (1977); (b) J. B. Hubbard, *J. Chem. Phys.* **68**, 1649 (1978).
31. J. B. Hubbard and P. G. Wolynes, in *The Chemical Physics of Solvation*, Ed. R. Dogonadze et al. (Elsevier, NY, 1988) Part C, Chap. 1, p. 33.
32. (a) J. B. Hubbard and R. F. Kayser, *J. Chem. Phys.* **74**, 3535 (1981); (b) J. B. Hubbard and R. F. Kayser, *J. Chem. Phys.* **76**, 3377 (1982).
33. Y. M. Kessler, R. S. Kumeev, I. I. Vaisman, R. B. Lyalina and R. H. Bratishko, *Ber. Bunsenges. Phys. Chem.* **93**, 770 (1989).
34. P. G. Wolynes, *J. Chem. Phys.* **68**, 473 (1978).
35. P. Colonomos and P. G. Wolynes, *J. Chem. Phys.* **71**, 2644 (1979).
36. P. G. Wolynes, *Annu. Rev. Phys. Chem.* **31**, 345 (1980).
37. B. Bagchi, *J. Chem. Phys.* **95**, 467 (1991).
38. R. Biswas and B. Bagchi, *J. Am. Chem. Soc.* **119**, 5946 (1997).
39. B. Bagchi and R. Biswas, *Adv. Chem. Phys.* **109**, 207 (1999) and references therein.
40. G. M. Roger, S. D. Vidal, O. Bernard and P. Turq, *J. Phys. Chem. B* **113**, 8670 (2009).
41. R. L. Kay and T. L. Broadwater, *J. Solution Chem.* **5**, 57 (1976).
42. M. Bester-Rogac, R. Neueder and J. Barthel, *J. Solution Chem.* **28**, 1071 (1999).

43. R. L. Kay and T. L. Broadwater, *Electrochim Acta* **16**, 667 (1971).
44. M. Goffredi and T. Shedlovsky, *J. Phys. Chem.* **71**, 2181 (1967).
45. A. Wypych-Stasiewicz, A. Szejgis, A. Chmielewska and A. Bard, *J. Mol. Liq.* **95**, 99 (2006).
46. (a) N. G. Foster and E. S. Amis, *Z. Phys. Chem.* **3**, 365, (1955); (b) J. L. Hawes and R. L. Kay, *J. Phys. Chem.* **69**, 2420 (1966); (c) A. J. Dill and O. Popovych, *J. Chem. Eng. Data* **14**, 156 (1969); (d) A. D'Aprano, M. Goffredi and R. Triolo, *Electrochim Acta* **21**, 139 (1976); (e) Y. H. Dicko and Y. Molenat, *J. Chim. Phys.* **75**, 174 (1978); (f) M. Tissier and G. Douheret, *J. Solution Chem.* **7**, 87 (1978); (g) J. Ananthaswamy, B. Sethuram and T. N. Rao, *Bull. Chem. Soc. Jpn.* **52**, 3076 (1979); (h) S. Zhang, H. Li, S. Dai, T. Wang and S. Han, *J. Chem. Eng. Data* **42**, 651 (1997); (i) A. Chatterjee and B. Das, *J. Chem. Eng. Data* **51**, 1352 (2006).
47. (a) J. E. Lind, Jr., R. M. Fuoss *J. Phys. Chem.* **65**, 999 (1961); (b) J. E. Lind, Jr., R. M. Fuoss *J. Phys. Chem.* **66**, 1727 (1962); (c) R. W. Kunze and R. M. Fuoss, *J. Phys. Chem.* **67**, 911 (1963); (d) R. W. Kunze and R. M. Fuoss, *J. Phys. Chem.* **67**, 914 (1963); (e) J. C. Justice and R. M. Fuoss, *J. Phys. Chem.* **67**, 1707 (1963); (f) T. L. Fabry and R. M. Fuoss, *J. Phys. Chem.* **68**, 971 (1964); (g) T. L. Fabry and R. M. Fuoss, *J. Phys. Chem.* **68**, 974 (1964); (h) C. F. Matina and R. M. Fuoss, *J. Phys. Chem.* **79**, 1604 (1975); (i) A. D'Aprano, F. Accascina and R. M. Fuoss, *J. Solution Chem.* **19**, 65 (1990).
48. (a) R. Bury and C. Treiner, *J. Chim. Phys.* **64**, 1410 (1968); (b) J. C. Justice, R. Bury and C. Treiner, *J. Chim. Phys.* **65**, 1708 (1968); (c) A. D'Aprano, J. Komiyama and R. M. Fuoss, *J. Solution Chem.* **5**, 279 (1976); (d) R. Bury and J. C. Justice, *J. Solution Chem.* **6**, 349 (1977); (e) S. K. Niazi, I. Jabeen and S. S. Shah, *J. Chem. Eng. Data* **38**, 285 (1993).
49. (a) D. S. Berns and R. M. Fuoss, *J. Am. Chem. Soc.* **82**, 5585 (1960); (b) B. Das and N. Saha, *J. Chem. Eng. Data* **45**, 2 (2000); (c) B. Das, N. Saha and D. K. Hazra, *J. Chem. Eng. Data* **45**, 353 (2000).
50. (a) J. Barthel, R. Neueder, M. Poxleitner, J. Seitz-Beywl and L. Werblan, *J. Electroanal. Chem.* **344**, 249 (1993); (b) A. Balkowska, A. Kowalska, M. Goral and L. Werblan, *J. Electroanal. Chem.* **354**, 11 (1993); (c) G. Moumouzias and G. Ritzoulis, *J. Solution Chem.* **25**, 1271 (1996); (d) G. Moumouzias and G. Ritzoulis, *J. Chem. Eng. Data* **41**, 326 (1996); (e) J.

- Barthel, R. Neueder, P. Rawytsch and H. Roch, *J. Electroanal. Chem.* **471**, 78 (1999).
51. K. Ibuki and M. Nakahara, *J. Chem. Phys.* **84**, 2776 (1986).
 52. K. Ibuki and M. Nakahara, *J. Chem. Phys.* **84**, 6979 (1986).
 53. A. Apelblat, *J. Phys. Chem. B* **112**, 7032 (2008).
 54. P. Wang and A. Anderko, *Ind. Eng. Chem. Res.* **42**, 3495 (2003).
 55. H. K. Kashyap and R. Biswas, *J. Phys. Chem. B*, 2009 (submitted).
 56. J. G. Kirkwood, *J. Chem. Phys.* **14**, 180 (1946).
 57. R. Kubo, *J. Math. Phys.* **4**, 174 (1963).
 58. D. Isbister and R. Bearman, *J. Mol. Phys.* **28**, 1297 (1974).
 59. D. Y. C. Chan, D. J. Mitchel and B. Ninham, *J. Chem. Phys.* **70**, 2946 (1979).
 60. M. S. Skaf, and B. M. Ladanyi, *J. Chem. Phys.* **102**, 6542 (1995).
 61. F. O. Raineri, H. Resat and H. L. Friedman, *J. Chem. Phys.* **96**, 3068 (1992).
 62. R. Biswas, S. Roy and B. Bagchi, *Phys. Rev. Lett.* **75**, 1098 (1995).
 63. R. Biswas and B. Bagchi, *J. Chem. Phys.* **106**, 5587 (1997).
 64. B. Bagchi and R. Biswas, *Acc. Chem. Res.* **31**, 181 (1998).
 65. S. Mashimo and N. Miura, *J. Chem. Phys.* **99**, 9874 (1993).
 66. T. Pradhan, P. Ghoshal and R. Biswas, *J. Phys. Chem. A.* **112**, 915 (2007).
 67. T. Pradhan, P. Ghoshal and R. Biswas, *J. Chem. Sci.* **120**, 275 (2008).

Chapter 4

Ion Solvation in Asymmetric Binary Dipolar Mixture

4.1 Introduction

Polarity of a medium is often found to have significant effects on the course and the outcome of a reaction in solution phase.¹⁻² Mixed dipolar solvents are good reaction media because one can tune polarity, solubility etc. by altering the composition of a mixture. The tuneable polarity of a binary mixture is the key for selective dissolution and precipitation of reactants and/or products of a solution phase chemical reaction. Polar binary mixtures are therefore better reaction media than neat solvents. Size disparity in the constituent solvent molecules can have profound effects on both the equilibrium and dynamical properties of a solution. An increase in size of one of the species is likely to inhibit its ability to solvate an ion due to packing constraints. Therefore, relatively smaller molecules will be preferred giving rise to what is widely known as *preferential solvation*. Interestingly, the inter-diffusion of these two types of molecules can make solvation considerably slower than that in a one-component solvent.³⁻⁵ Moreover, simulation studies have indicated that the slow exchange of one solvent species by the other in the adjacent solvent shells may not hold for mixtures with widely different effective volumes.⁶

Electrolyte solution in binary mixture is another important medium.⁷⁻⁸ Addition of electrolytes not only enhances the average polarity of the medium but also takes part in altering the reaction equilibrium by inducing salting in or salting out effects. Moreover, interaction between ions and a dissolved solute (reactive or non-reactive polar molecule) competes with the preferential solvation and hence modifies the average solvation structure around the dissolved solute. The competition becomes even more interesting for a binary polar mixture where the relatively bigger (in size) solvent molecule possesses a larger dipole moment. Such competition is likely to

affect the long-time dynamics of the solvent response. Naturally therefore, studies of structure and dynamics of the environment around an ionic or dipolar solute are essential for understanding the solvation processes and their effects on simple chemical events in such media.⁹⁻¹⁰

Several studies have already been carried out for determining the structure in binary polar mixtures.¹¹⁻¹³ For example, Adelman and Deutch¹² extended the Wertheim's solution for pure fluids¹¹ using the mean spherical approximation¹⁴ (MSA) into the binary polar mixture where solvent molecules of different species were characterized by equal hard sphere diameters ($R_1 = R_2$) with point dipoles of different magnitude at the centre ($\mu_1 \neq \mu_2$) of these hard spheres. Isbister and Bearman solved the MSA for completely asymmetric binary fluid mixture¹³ ($R_1 \neq R_2$ and $\mu_1 \neq \mu_2$). Subsequently, MSA was developed for electrolyte solution consisting of hard ions (charged hard spheres) in neat dipolar solvent and used to obtain the solvent structure around a dissolved ion.¹⁵ Recently, MSA has been used to study the polarization structure around an ion in binary polar mixture composed of solvent molecules of equal size but different dipole moments ($R_1 = R_2 \neq R$, R is the diameter of ion and $\mu_1 \neq \mu_2$).¹⁶ All these studies have contributed significantly to the understanding of solvation structure in terms of ion-solvent and solvent-solvent interactions. However, solvent polarization structure around an ion in a mixture of dipolar solvents with arbitrary size and dipole moments (that is, $R_1 \neq R_2 \neq R$ and $\mu_1 \neq \mu_2$) have not been studied yet. Such a study is very important because many thermodynamic properties of electrolyte solutions in binary polar mixtures depend on the partial polarization densities of the constituent solvents around the dissolved ions.

Here we use MSA in order to obtain analytical expressions for partial solvent polarization densities and Born free energies of solvation in an electrolyte solution of a completely asymmetric binary polar mixture. We restrict our study for symmetric uni-univalent electrolyte in the limit of infinite dilution. One of our goals here is to investigate the effects of relative size of the constituent solvents on Born free energy of solvation for a dissolved ion in model binary polar mixtures and partial solvent polarization densities around a dissolved ion. The calculation of partial solvent polarization densities is crucial since it provides a microscopic explanation for the

often observed non-ideal composition dependence of Born free energies of solvation in mixtures. Subsequently, the calculation scheme is applied to obtain the partial solvent polarization densities around a uni-positive rigid ion dissolved in room temperature binary mixtures of methanol-water, ethanol-water and tertiary butyl alcohol (TBA)-water and dimethyl sulfoxide (DMSO)-acetonitrile solutions. Note here that in the present theory the solvent components constituting the binary mixtures are characterized *only* by their molecular diameters and dipole moments. Specific interactions such as hydrogen bonding between solvent molecules of same species as well as between different species and hydrophobic interactions between alkyl groups of the alcohols have not been considered. Also, attempt has not been made in the present extension of the MSA to include any specific ion-solvent interaction that may be possible through the participation of lone pair of electrons on oxygen atom in water or alcohol molecules (for ion in alcohol-water mixtures) and in DMSO molecule (for ion in DMSO-acetonitrile mixtures). Therefore, these binary mixtures are much simplified versions of the real solutions and the neglect of these specific and complex interactions may lead to predictions very different from experimental results. Therefore, explicit potentials¹⁷⁻²⁰ that are generally used in simulation studies to represent the interactions more realistically in these systems have not been considered. This is because the present work focuses on, within the extended MSA framework, exploring the contributions to the non-ideality in the Born free energy of solvation originating purely from the ion-solvent and solvent-solvent size ratios as well as from the differing dipole moments.

Alcohol-water mixtures are known to exhibit anomalous thermodynamic properties at low alcohol concentrations.²¹⁻²² Extensive experimental²³⁻⁴⁴ and simulation⁴⁵⁻⁵⁵ studies have been carried out to investigate the liquid structure in alcohol-water mixtures. All these studies linked the deviation of a given property from its expected value with the modification of water structure in presence of alcohol, the deviation being the maximum for TBA. The solvation free energies can reflect the underlying solvent structure around these ions determined by a delicate balance of complex intermolecular interactions between the alcohol and water molecules. The calculated excess Born free energy of solvation in TBA-water indicate that at low TBA concentration, ions with size larger than or equal to that of a water molecule (for example, Cs^+ or Bu_4N^+) show a composition dependence very different from that for

smaller ions like Li^+ . This is in sharp contrast to the more ‘regular’ ion size dependence of excess Born free energy of solvation in methanol-water and ethanol-water mixtures.

The DMSO-acetonitrile is interesting because the larger component (DMSO) possesses higher dipole moment.^{2,56} This leads to a competition in packing around a dissolved ion in DMSO-acetonitrile mixture. Moreover, the molecular diameters of these solvents are similar^{2,56} and hence the nonideality in polarization structure (and hence in Born free energy of solvation) is expected to be weaker. In contrast, the dipole moment of water is slightly larger than the alcohols studied here but the size is considerably smaller. This assists water molecules to be preferably chosen in the first solvation shell and hence the nonideality is likely to be stronger. Naturally therefore, larger ions would be able to accommodate the larger solvent components leading to a more ‘homogeneous’ solvation structure. This, in turn, will render the nonideality weaker.

The organization of the rest of the chapter is as follows. Sec. 4.2 contains the details of the theoretical formulation. Numerical results along with discussion are presented in Sec. 4.3. Finally, we end this chapter with conclusion in section 4.4.

4.2 Theoretical Formulation

Recently, Morillo *et al.* have extended the MSA theory to study the solvent structure around a hard sphere ion dissolved in a binary dipolar mixture.¹⁶ These authors have modelled the binary mixture as a collection of dipolar hard spheres of equal size but with different dipole moments on different species and made use of the results of Adelman and Deutch¹² and those of Chan *et al.*¹⁵. In the present work we are studying solvent structure around an ion in a binary mixture of fluids made up of dipolar hard spheres with unequal radii and dipole moments. We have, therefore, used the MSA frameworks provided by Isbister and Bearman,¹³ Chan *et al.*¹⁴ and Blum *et al.*⁵⁷⁻⁶¹

4.2.1 Model Description

Let us now consider a solution of an electrolyte of equal-sized ions in a binary dipolar mixture. The dipolar solvent molecules are treated as hard spheres with point dipoles situated at the centre.¹⁵ The solvent dipoles are of two types characterized by different sizes and different dipole moments. Let R_i and R_j be the hard sphere diameters of the two types of solvent molecules with dipole moments μ_i and μ_j , respectively. The solvent number densities are ρ_i and ρ_j . Here, $R_i \neq R_j$ and $\mu_i \neq \mu_j$. The ions are hard spheres of equal diameters with embedded point charges. The electro-neutrality of such a solution is ensured by setting^{15-16,62-63}

$$\sum_{\alpha} \rho_{\alpha} z_{\alpha} = 0 \quad (4.1)$$

where ρ_{α} denotes the number density of ionic species α with charge z_{α} and diameter $R_{\alpha} = R$.

4.2.2 Interaction Potentials among Different Species

The interaction potentials between different species consists of a hard core repulsive term and ion-ion, ion-dipole and dipole-dipole components given by⁶²⁻⁶³

$$u_{\alpha\beta}(r) = z_{\alpha} z_{\beta} e^2 / r, \quad r > R_{\alpha\beta} = R \quad (4.2)$$

$$u_{\alpha j}(\mathbf{r}, \boldsymbol{\omega}_2) = -z_{\alpha} e \mu_j E_2 / r^2, \quad r > R_{\alpha j} = (R + R_j) / 2 \quad (4.3)$$

$$u_{i\beta}(\boldsymbol{\omega}_1, \mathbf{r}) = z_{\beta} e \mu_i E_1 / r^2, \quad r > R_{i\beta} = (R_i + R) / 2 \quad (4.4)$$

$$u_{ij}(\boldsymbol{\omega}_1, \mathbf{r}, \boldsymbol{\omega}_2) = -\mu_i \mu_j D_{12} / r^3, \quad r > R_{ij} = (R_i + R_j) / 2 \quad (4.5)$$

where α, β indices are for ions and i, j indices are for dipoles. $E_i = \hat{\boldsymbol{\mu}}(\boldsymbol{\omega}_i) \cdot \hat{\mathbf{r}}$ and $D_{12} = \hat{\boldsymbol{\mu}}(\boldsymbol{\omega}_1) \cdot \left(\mathbf{3} \hat{\mathbf{r}} \hat{\mathbf{r}} - \mathbf{I} \right) \cdot \hat{\boldsymbol{\mu}}(\boldsymbol{\omega}_2)$ describe the angle dependent parts of the interaction potentials. In above equations, e represents the elementary charge, \mathbf{I} denotes a 3×3 unit tensor, and $\hat{\mathbf{r}}$ is the unit vector from the molecule denoted by the first index

towards the one denoted by second index. The orientation of i^{th} type dipole is described by ω_1 .

4.2.3 Ornstein-Zernike (OZ) Relations for the System of Ions in Binary Mixture

The Ornstein-Zernike (OZ) relations for the correlation functions in an electrolyte solution of binary dipolar mixture are written as^{16,62-63}

$$h_{\alpha\beta}(r) = c_{\alpha\beta}(r) + \sum_{\gamma} \rho_{\gamma} \int d\mathbf{s} c_{\alpha\gamma}(|\mathbf{r}-\mathbf{s}|) h_{\gamma\beta}(s) + \sum_k \rho_k \int d\mathbf{s} \langle c_{\alpha k}(\mathbf{r}-\mathbf{s}) h_{k\beta}(\omega_3, \mathbf{s}) \rangle_{\omega_3} \quad (4.6)$$

$$h_{\alpha j}(\mathbf{r}, \omega_2) = c_{\alpha j}(\mathbf{r}, \omega_2) + \sum_{\gamma} \rho_{\gamma} \int d\mathbf{s} c_{\alpha\gamma}(|\mathbf{r}-\mathbf{s}|) h_{\gamma j}(\mathbf{s}, \omega_2) + \sum_k \rho_k \int d\mathbf{s} \langle c_{\alpha k}(\mathbf{r}-\mathbf{s}, \omega_3) h_{kj}(\omega_3, \mathbf{s}, \omega_2) \rangle_{\omega_3} \quad (4.7)$$

$$h_{i\beta}(\omega_1, \mathbf{r}) = c_{i\beta}(\omega_1, \mathbf{r}) + \sum_{\gamma} \rho_{\gamma} \int d\mathbf{s} c_{i\gamma}(\omega_1, \mathbf{r}-\mathbf{s}) h_{\gamma\beta}(s) + \sum_k \rho_k \int d\mathbf{s} \langle c_{ik}(\omega_1, \mathbf{r}-\mathbf{s}, \omega_3) h_{k\beta}(\omega_3, \mathbf{s}) \rangle_{\omega_3} \quad (4.8)$$

$$h_{ij}(\omega_1, \mathbf{r}, \omega_2) = c_{ij}(\omega_1, \mathbf{r}, \omega_2) + \sum_{\gamma} \rho_{\gamma} \int d\mathbf{s} c_{i\gamma}(\omega_1, \mathbf{r}-\mathbf{s}) h_{\gamma j}(\mathbf{s}, \omega_2) + \sum_k \rho_k \int d\mathbf{s} \langle c_{ik}(\omega_1, \mathbf{r}-\mathbf{s}, \omega_3) h_{kj}(\omega_3, \mathbf{s}, \omega_2) \rangle_{\omega_3} \quad (4.9)$$

where c and h denote the direct and total (or indirect) correlation functions, respectively. $\langle \rangle_{\omega} = 1/4\pi \int d\omega$, denoting angular convolution.

4.2.4 MSA Closure

The MSA closure conditions here are given by^{16,62}

$$h_{IJ}(\omega_1, \mathbf{r}, \omega_2) = -1, \quad r < R_{IJ}^c \quad (4.10)$$

$$c_{IJ}(\omega_1, \mathbf{r}, \omega_2) = -(k_B T)^{-1} u_{IJ}(\omega_1, \mathbf{r}, \omega_2), \quad r > R_{IJ}^c \quad (4.11)$$

where $I = \alpha, i; J = \beta, j$. Here upper case Latin indices run over both Greek and Latin indices. The arguments of the correlation functions should be adjusted depending on

the indices. For, if two Greek indices are present, the argument is only r . A Greek and a Latin index means arguments are \mathbf{r} and $\boldsymbol{\omega}$. The $\boldsymbol{\omega}$ can be $\boldsymbol{\omega}_1$ or $\boldsymbol{\omega}_2$ depending on whether Latin index is on first or second place. Two Latin indices carry the all arguments as in the above equations. $k_B T$ is the Boltzmann constant times the absolute temperature.

4.2.5 Multiplication Table for $1, E_i, D_{ij}$ and Δ_{ij}

The angular functions $1, E_i, D_{ij}$, and $\Delta_{ij} = \hat{\boldsymbol{\mu}}(\boldsymbol{\omega}_i) \cdot \hat{\boldsymbol{\mu}}(\boldsymbol{\omega}_j)$ form a closed set under the angular convolution $\langle A(\boldsymbol{\omega}_1, \boldsymbol{\omega}_3) B(\boldsymbol{\omega}_3, \boldsymbol{\omega}_2) \rangle_{\boldsymbol{\omega}_3}$. Multiplication tables for these quantities are taken from Ref. 15.

Table 4.1: Multiplication Table for the Angular Convolution $\langle A(\boldsymbol{\omega}_1, \boldsymbol{\omega}_3) B(\boldsymbol{\omega}_3, \boldsymbol{\omega}_2) \rangle_{\boldsymbol{\omega}_3}$

$A(\boldsymbol{\omega}_1, \boldsymbol{\omega}_3) \backslash B(\boldsymbol{\omega}_3, \boldsymbol{\omega}_2)$	1	Δ_{32}	D_{32}	E_3	E_2
1	1	0	0	0	E_2
Δ_{13}	0	$\Delta_{12}/3$	$D_{12}/3$	$E_1/3$	0
D_{13}	0	$D_{12}/3$	$(D_{12} + 2\Delta_{12})/3$	$2E_1/3$	0
E_3	0	$E_2/3$	$2E_2/3$	1/3	0
E_1	E_1	0	0	0	$(D_{12} + \Delta_{12})/3$

4.2.6 Ion-solvent and Solvent-solvent Correlation Functions in Electrolyte Solution of Binary Dipolar Mixture

Now the Ornstein-Zernike (OZ) relation can be used to obtain the MSA solution for the correlation functions in an electrolyte solution of binary dipolar mixture.^{15,61} Subsequently, the algebra described in Chan *et al.*¹⁵ leads to the following *ansatz*⁶²

$$f_{\alpha\beta}(r) = f_{\alpha\beta}^{HS}(r) + z_\alpha z_\beta f_{\alpha\beta}^C(r) \quad (4.12)$$

$$f_{aj}(\mathbf{r}, \boldsymbol{\omega}_2) = f_{aj}^{HS}(r) + z_\alpha f_{aj}^E(r) E_2 \quad (4.13)$$

$$f_{i\beta}(\boldsymbol{\omega}_1, \mathbf{r}) = f_{i\beta}^{HS}(r) - z_\beta f_{i\beta}^E(r) E_1 \quad (4.14)$$

$$f_{ij}(\boldsymbol{\omega}_1, \mathbf{r}, \boldsymbol{\omega}_2) = f_{ij}^{HS}(r) + f_{ij}^{\Delta}(r)\Delta_{12} + f_{ij}^D(r)D_{12} \quad (4.15)$$

where f^C represents the charge-charge correlations, f^E the charge-dipole correlations and, f^D and f^{Δ} the dipole-dipole correlations. The relevant angle independent closure conditions are^{15,62}

$$c_{\alpha\beta}^C(r) = -(k_B T)^{-1} e^2 / r, \quad r > R \quad (4.16)$$

$$c_{\alpha j}^E(r) = (k_B T)^{-1} e \mu_j / r^2, \quad r > R_{\alpha j} \quad (4.17)$$

$$c_{i\beta}^E(r) = (k_B T)^{-1} e \mu_i / r^2, \quad r > R_{i\beta} \quad (4.18)$$

$$c_{ij}^D(r) = (k_B T)^{-1} \mu_i \mu_j / r^3, \quad r > R_{i\beta} \quad (4.19)$$

where $k_B T$ represents the Boltzmann constant times the absolute temperature. Using the following definition of three dimensional Fourier transform

$$\tilde{f}(\boldsymbol{\omega}_1, \mathbf{k}, \boldsymbol{\omega}_2) = \int d\mathbf{r} e^{i\mathbf{k}\cdot\mathbf{r}} f(\boldsymbol{\omega}_1, \mathbf{r}, \boldsymbol{\omega}_2); \quad \tilde{f} = \tilde{h} \text{ or } \tilde{c} \quad (4.20)$$

we obtain the OZ equations in the Fourier space as⁶¹⁻⁶²

$$\tilde{h}_{\alpha\beta}(k) = \tilde{c}_{\alpha\beta}(k) + \sum_{\gamma} \rho_{\gamma} \tilde{c}_{\alpha\gamma}(k) \tilde{h}_{\gamma\beta}(k) + \sum_k \rho_k \langle \tilde{c}_{\alpha k}(\mathbf{k}, \boldsymbol{\omega}_3) \tilde{h}_{k\beta}(\boldsymbol{\omega}_3, \mathbf{k}) \rangle_{\boldsymbol{\omega}_3} \quad (4.21)$$

$$\tilde{h}_{\alpha j}(\mathbf{k}, \boldsymbol{\omega}_2) = \tilde{c}_{\alpha j}(\mathbf{k}, \boldsymbol{\omega}_2) + \sum_{\gamma} \rho_{\gamma} \tilde{c}_{\alpha\gamma}(k) \tilde{h}_{\gamma j}(\mathbf{k}, \boldsymbol{\omega}_2) + \sum_k \rho_k \langle \tilde{c}_{\alpha k}(\mathbf{k}, \boldsymbol{\omega}_3) \tilde{h}_{kj}(\boldsymbol{\omega}_3, \mathbf{k}, \boldsymbol{\omega}_2) \rangle_{\boldsymbol{\omega}_3} \quad (4.22)$$

$$\tilde{h}_{i\beta}(\boldsymbol{\omega}_1, \mathbf{k}) = \tilde{c}_{i\beta}(\boldsymbol{\omega}_1, \mathbf{k}) + \sum_{\gamma} \rho_{\gamma} \tilde{c}_{i\gamma}(\boldsymbol{\omega}_1, \mathbf{k}) \tilde{h}_{\gamma\beta}(k) + \sum_k \rho_k \langle \tilde{c}_{ik}(\boldsymbol{\omega}_1, \mathbf{k}, \boldsymbol{\omega}_3) \tilde{h}_{k\beta}(\boldsymbol{\omega}_3, \mathbf{k}) \rangle_{\boldsymbol{\omega}_3} \quad (4.23)$$

$$\tilde{h}_{ij}(\boldsymbol{\omega}_1, \mathbf{k}, \boldsymbol{\omega}_2) = \tilde{c}_{ij}(\boldsymbol{\omega}_1, \mathbf{k}, \boldsymbol{\omega}_2) + \sum_{\gamma} \rho_{\gamma} \tilde{c}_{i\gamma}(\boldsymbol{\omega}_1, \mathbf{k}) \tilde{h}_{\gamma j}(\mathbf{k}, \boldsymbol{\omega}_2) + \sum_k \rho_k \langle \tilde{c}_{ik}(\boldsymbol{\omega}_1, \mathbf{k}, \boldsymbol{\omega}_3) \tilde{h}_{kj}(\boldsymbol{\omega}_3, \mathbf{k}, \boldsymbol{\omega}_2) \rangle_{\boldsymbol{\omega}_3} \quad (4.24)$$

where,

$$\tilde{f}_{\alpha\beta}(k) = \tilde{f}_{\alpha\beta}^{HS}(k) + z_\alpha z_\beta \tilde{f}_{\alpha\beta}^C(k) \quad (4.25)$$

$$\tilde{f}_{\alpha j}(\mathbf{k}, \boldsymbol{\omega}_2) = \tilde{f}_{\alpha j}^{HS}(k) + z_\alpha \tilde{f}_{\alpha j}^E(k) \tilde{E}_2 \quad (4.26)$$

$$\tilde{f}_{i\beta}(\boldsymbol{\omega}_1, \mathbf{k}) = \tilde{f}_{i\beta}^{HS}(k) - z_\beta \tilde{f}_{i\beta}^E(k) \tilde{E}_1 \quad (4.27)$$

$$\tilde{f}_{ij}(\boldsymbol{\omega}_1, \mathbf{k}, \boldsymbol{\omega}_2) = \tilde{f}_{ij}^{HS}(k) + \tilde{f}_{ij}^\Delta(k) \Delta_{12} + \tilde{f}_{ij}^D(k) \tilde{D}_{12} \quad (4.28)$$

and

$$\tilde{E}_i = \hat{\boldsymbol{\mu}}(\boldsymbol{\omega}_i) \cdot \hat{\mathbf{k}}, \quad i = 1, 2 \quad (4.29)$$

$$\tilde{D}_{12} = \hat{\boldsymbol{\mu}}(\boldsymbol{\omega}_1) \cdot \left(\mathbf{3} \hat{\mathbf{k}} \hat{\mathbf{k}} - \mathbf{I} \right) \cdot \hat{\boldsymbol{\mu}}(\boldsymbol{\omega}_2) \quad (4.30)$$

Here each $\tilde{f}(k)$ is related to corresponding $f(r)$ by n^{th} order Hankel transform¹⁵⁻¹⁶ and the order of the transformation depends on the type of the correlation functions. Note that the last term in Eqs. (4.21)–(4.24) account for the angle averaged correlations between an ion and a dipole, and two dipoles of same and different types. Therefore, the summation runs over all solvent components present in the binary mixture. This term arises due to the difference in solvent size. Also, this term is absent in the works of Chan *et al.*¹⁵ since it deals with electrolyte solution in one component dipolar solvent. Further, these expressions reduces to those obtained by Morillo *et al.*¹⁶ for binary mixtures in the limit of equal solvent size ($R_i = R_j$) but different dipole moments ($\mu_i \neq \mu_j$). We will come back to this point when we present numerical results. However, the first two terms are similar to those in Chan *et al.*¹⁵ as these generalize the ion-ion, ion-dipole and dipole-dipole correlations with summation over all ionic species in electrolyte solution of binary dipolar mixtures.

If we define two *orthogonal* angular functions using Δ_{12} and \tilde{D}_{12} as^{15,62}

$$J_{12}^+ = \frac{1}{3}(\Delta_{12} + \tilde{D}_{12}) \quad (4.31)$$

$$J_{12}^- = \frac{1}{3}(2\Delta_{12} - \tilde{D}_{12}) \quad (4.32)$$

with coefficients

$$\tilde{f}_{ij}^+ = \tilde{f}_{ij}^\Delta + 2\tilde{f}_{ij}^D \quad (4.33)$$

$$\tilde{f}_{ij}^- = \tilde{f}_{ij}^\Delta - \tilde{f}_{ij}^D \quad (4.34)$$

and substitute in Eq. (4.28) we get

$$\tilde{f}_{ij}(\boldsymbol{\omega}_1, \mathbf{k}, \boldsymbol{\omega}_2) = \tilde{f}_{ij}^{HS}(k) + \tilde{f}_{ij}^+(k)J_{12}^+ + \tilde{f}_{ij}^-(k)J_{12}^- \quad (4.35)$$

Carrying out the angular convolution in Eqs (4.21)-(4.24) and using the charge neutrality condition, and setting^{16,62}

$$\rho_c = \sum_{\gamma} \rho_{\gamma} z_{\gamma}^2 \quad (4.36)$$

$$\rho_I = \sum_{\gamma} \rho_{\gamma} \quad (4.37)$$

we obtain the following coupled set of equations for the correlation functions due to hard sphere interaction:

$$\tilde{h}_{\alpha\beta}^{HS}(k) = \tilde{c}_{\alpha\beta}^{HS}(k) + \rho_I \tilde{c}_{\alpha\gamma}^{HS}(k) \tilde{h}_{\gamma\beta}^{HS}(k) + \sum_k \rho_k \tilde{c}_{\alpha k}^{HS}(k) \tilde{h}_{k\beta}^{HS}(k) \quad (4.38)$$

$$\tilde{h}_{\alpha j}^{HS}(k) = \tilde{c}_{\alpha j}^{HS}(k) + \rho_I \tilde{c}_{\alpha\gamma}^{HS}(k) \tilde{h}_{\gamma j}^{HS}(k) + \sum_k \rho_k \tilde{c}_{\alpha k}^{HS}(k) \tilde{h}_{kj}^{HS}(k) \quad (4.39)$$

$$\tilde{h}_{i\beta}^{HS}(k) = \tilde{c}_{i\beta}^{HS}(k) + \rho_I \tilde{c}_{i\gamma}^{HS}(k) \tilde{h}_{\gamma\beta}^{HS}(k) + \sum_k \rho_k \tilde{c}_{ik}^{HS}(k) \tilde{h}_{k\beta}^{HS}(k) \quad (4.40)$$

$$\tilde{h}_{ij}^{HS}(k) = \tilde{c}_{ij}^{HS}(k) + \rho_I \tilde{c}_{i\gamma}^{HS}(k) \tilde{h}_{\gamma j}^{HS}(k) + \sum_k \rho_k \tilde{c}_{ik}^{HS}(k) \tilde{h}_{kj}^{HS}(k) \quad (4.41)$$

These equations define a mixture of hard spheres with diameter $R_{\alpha} = R$ at number density ρ_I and diameter R_i at density ρ_i with Percus-Yevick (PY) closure^{14-16,62} Simultaneously, the correlations due to the electrostatic interactions between ions, ion-dipole and dipoles are described by the following set of coupled equations⁶²

$$\tilde{h}_{\alpha\beta}^C(k) = \tilde{c}_{\alpha\beta}^C(k) + \rho_c \tilde{c}_{\alpha\gamma}^C(k) \tilde{h}_{\gamma\beta}^C(k) - \frac{1}{3} \sum_k \rho_k \tilde{c}_{\alpha k}^E(k) \tilde{h}_{k\beta}^E(k) \quad (4.42)$$

$$\tilde{h}_{\alpha j}^E(k) = \tilde{c}_{\alpha j}^E(k) + \rho_c \tilde{c}_{\alpha\gamma}^C(k) \tilde{h}_{\gamma j}^E(k) + \frac{1}{3} \sum_k \rho_k \tilde{c}_{\alpha k}^E(k) \tilde{h}_{kj}^+(k) \quad (4.43)$$

$$\tilde{h}_{i\beta}^E(k) = \tilde{c}_{i\beta}^E(k) + \rho_c \tilde{c}_{i\gamma}^E(k) \tilde{h}_{\gamma\beta}^C(k) + \frac{1}{3} \sum_k \rho_k \tilde{c}_{ik}^+(k) \tilde{h}_{k\beta}^E(k) \quad (4.44)$$

$$\tilde{h}_{ij}^+(k) = \tilde{c}_{ij}^+(k) - \rho_c \tilde{c}_{i\gamma}^E(k) \tilde{h}_{\gamma j}^E(k) + \frac{1}{3} \sum_k \rho_k \tilde{c}_{ik}^+(k) \tilde{h}_{kj}^+(k) \quad (4.45)$$

Since the electrostatic Coulomb potential is longitudinal field and couples with J_{12}^+ function alone, the addition of ions therefore affects only the longitudinal response (h_{ij}^+).¹⁵ Hence, J_{12}^- function is decoupled from the rest and we obtain the following equation^{11-16,62}

$$\tilde{h}_{ij}^-(k) = \tilde{c}_{ij}^-(k) + \frac{1}{3} \sum_k \rho_k \tilde{c}_{ik}^-(k) \tilde{h}_{kj}^-(k) \quad (4.46)$$

4.2.7 Born Free Energy of Solvation of an Ion in a Binary Dipolar Mixture

The Born free energy is defined as “*the change in free energy due to electrostatic interactions for the transfer of one ion from vacuum into the solution*”.¹⁵ The Born free energy of solvation for an ion of charge $z_\alpha e$ can be obtained from Eqs. (4.42)-(4.45) with the condition $\rho_c = 0$. Since the functions $\tilde{f}_{\alpha\beta}^C(k)$, $\tilde{f}_{\alpha j}^E(k)$, $\tilde{f}_{i\beta}^E(k)$ and $\tilde{f}_{ij}^D(k)$, which describe electrostatic interactions, depend only upon $k = |\mathbf{k}|$ and therefore these quantities can be transformed back to r -space by using the following one-dimensional Fourier inverse transform

$$F(x) = \frac{1}{2\pi} \int_{-\infty}^{+\infty} dk e^{-ikx} \tilde{f}(k) \quad (4.47)$$

where F can be $F_{\alpha\beta}^C$, $F_{\alpha j}^E$, $F_{i\beta}^E$, F_{ij}^Δ or F_{ij}^D and \tilde{f} can be $\tilde{f}_{\alpha\beta}^C$, $\tilde{f}_{\alpha j}^E$, $\tilde{f}_{i\beta}^E$, \tilde{f}_{ij}^Δ or \tilde{f}_{ij}^D .

The relation between all f 's and F 's are given by^{15-16,62-63}

$$\begin{aligned}
F_{\alpha\beta}^C(x) &= 2\pi \int_x^\infty dr P_0(x/r) r f_{\alpha\beta}^C(r), & F_{\alpha\beta}^E(x) &= 2\pi \int_x^\infty dr P_1(x/r) r f_{\alpha\beta}^E(r), \\
F_{i\beta}^E(x) &= 2\pi \int_x^\infty dr P_1(x/r) r f_{i\beta}^E(r), & F_{ij}^\Delta(x) &= 2\pi \int_x^\infty dr P_0(x/r) r f_{ij}^\Delta(r), \\
F_{ij}^D(x) &= 2\pi \int_x^\infty dr P_2(x/r) r f_{ij}^D(r)
\end{aligned} \tag{4.48}$$

where $P_0(x) = 1$, $P_1(x) = x$, $P_2(x) = \frac{1}{2}(3x^2 - 1)$ are Legendre polynomials. In an equivalent way, one can write as

$$\begin{aligned}
2\pi r f_{\alpha\beta}^C(r) &= -\frac{d}{dr} F_{\alpha\beta}^C(r), & 2\pi r f_{\alpha\beta}^E(r) &= \left(\frac{1}{r} - \frac{d}{dr}\right) F_{\alpha\beta}^E(r), \\
2\pi r f_{i\beta}^E(r) &= \left(\frac{1}{r} - \frac{d}{dr}\right) F_{i\beta}^E(r), & 2\pi r f_{ij}^\Delta(r) &= -\frac{d}{dr} F_{ij}^\Delta(r), \\
\pi^2 f_{ij}^D(r) &= -r^2 \left(\frac{1}{r} \frac{d}{dr}\right)^2 \frac{1}{r} \int_0^r dx F_{ij}^D(x)
\end{aligned} \tag{4.49}$$

The Born energy of a single ion of charge $z_\alpha e$ dissolved in a dipolar mixture is given by^{16,62}

$$E_{Born} = \sum_k \rho_k \int d\mathbf{r} \langle u_{\alpha k}(\mathbf{r}, \boldsymbol{\omega}) g_{\alpha k}(\mathbf{r}, \boldsymbol{\omega}) \rangle_{\boldsymbol{\omega}} = -\frac{4\pi z_\alpha^2 e}{3} \sum_k \rho_k \mu_k \int_{R_{\alpha k}}^\infty dr h_{\alpha k}^E(r) \tag{4.50}$$

where the second equality follows because $h_{\alpha k}^E(r) = 0$ for $r < R_{\alpha k}$. We now need to

find $\int_{R_{\alpha k}}^\infty dr h_{\alpha k}^E(r)$ for evaluating E_{Born} . This is calculated from the ion-dipole correlation

function as follows^{15-16,62}

$$H_{\alpha j}^E(x) = 2\pi \int_x^\infty dr P_1(x/r) r h_{\alpha j}^E(r) = 2\pi x \int_{R_{\alpha j}}^\infty dr h_{\alpha j}^E(r) = x H_{\alpha j}^E, \quad \text{for } x \leq R_{\alpha j} \tag{4.51}$$

where $H1_{\alpha j}^E = 2\pi \int_{R_{\alpha j}}^{\infty} dr h_{\alpha j}^E(r)$ is a constant that needs to be determined. Equation (4.50) and the above discussion now provide the following expression of Born energy (E_{Born}) for an ion dissolved in binary mixture of dipolar solvents with unequal size and different dipole moments

$$E_{Born} = -\frac{2z_{\alpha}^2 e}{3} \sum_k \rho_k \mu_k H1_{\alpha k}^E = -\frac{2z_{\alpha}^2 e}{3} \sum_k \rho_k \mu_k H1_{k\alpha}^E \quad (4.52)$$

Now we need to calculate $H1_{k\alpha}^E (= H1_{\alpha k}^E)$. Baxter factorization^{61,62} gives for $x > S_{j\alpha} = (R_j - R_{\alpha})/2$

$$H_{j\alpha}^E(x) = -Q_{j\alpha}^E(x) + \frac{1}{3} \sum_k \rho_k \int_{S_{jk}}^{R_{jk}} dy Q_{jk}^+(y) H_{k\alpha}^E(x-y) \quad (4.53)$$

From Eq. (4.51) when $S_{j\alpha} < x \leq R_{j\alpha}$

$$x H1_{j\alpha}^E = -Q_{j\alpha}^E(x) + \frac{1}{3} \sum_k \rho_k H1_{k\alpha}^E \int_{S_{jk}}^{R_{jk}} dy Q_{jk}^+(y)(x-y) \quad (4.54)$$

where $Q_{jk}^+(x)$ depends solely on the dipolar mixture properties and is given by^{15,58,62-}

63

$$Q_{ij}^+(x) = 3 \left[\frac{1}{2} a_{ij} (x - R_{ij})(x - S_{ij}) + b_{ij} (x - R_{ij}) \right] \quad (4.55)$$

where the values of a_{ij} and b_{ij} are given in the Appendix at the end of present chapter.

Eq. (4.54) consists of two coupled simultaneous equations in $H1_{j\alpha}^E$ when $j = 1, 2$ and α is fixed (a given ionic species). Using Baxter's method we obtain the following expression for $C_{j\alpha}^E(x)$

$$C_{j\alpha}^E(x) = -Q_{j\alpha}^E(x) + \frac{1}{3} \sum_k \rho_k \int_{S_{kj}}^{R_{kj}} dy Q_{kj}^+(y) Q_{k\alpha}^E(x+y), \quad x \geq R_{j\alpha} \quad (4.56)$$

with closure relation

$$C_{j\alpha}^E(x) = 2\pi\epsilon\beta\mu_j, \quad x \geq R_{j\alpha} \quad (4.57)$$

Therefore, from Eqs. (4.56) and (4.57), we obtain

$$2\pi\epsilon\beta\mu_j = -Q_{j\alpha}^E(x) + \frac{1}{3} \sum_k \rho_k \int_{S_{kj}}^{R_{kj}} dy Q_{kj}^+(y) Q_{k\alpha}^E(x+y), \quad x \geq R_{j\alpha} \quad (4.58)$$

Eq. (4.58) contains two coupled simultaneous equations in $Q_{j\alpha}^E(x)$ when $j = 1, 2$ for a fixed α . By solving these two equations for $j = 1$ and 2 and applying the condition that $Q_{j\alpha}^E(x) = Q_{j\alpha}^E(x+y)$ for $x \geq R_{j\alpha}$ we obtain the following expressions for $Q_{j\alpha}^E(x)$

$$Q_{1\alpha}^E(x) = \frac{\left[2\pi\beta\epsilon\mu_1 - \frac{2\pi\beta\epsilon\mu_2}{-1 + I_{22}} I_{21} \right]}{\left[-1 + I_{11} \right] - \frac{I_{21}I_{12}}{[-1 + I_{22}]}}, \quad x \geq R_{1\alpha} \quad (4.59)$$

$$Q_{2\alpha}^E(x) = \frac{\left[2\pi\beta\epsilon\mu_2 - \frac{2\pi\beta\epsilon\mu_1}{-1 + I_{11}} I_{12} \right]}{\left[-1 + I_{22} \right] - \frac{I_{12}I_{21}}{[-1 + I_{11}]}}, \quad x \geq R_{2\alpha} \quad (4.60)$$

with

$$I_{ij} = \int_{S_{ij}}^{R_{ij}} \frac{1}{3} \rho_i Q_{ij}^+(y) dy = \rho_i \left[-\frac{1}{12} a_{ij} R_j^3 - \frac{1}{2} b_{ij} R_j^2 \right]; \quad i=1, 2 \quad (4.61)$$

Solution of Eq. (4.54) at $x = R_{j\alpha}$ provides the following expressions of $H1_{1\alpha}^E$ and $H1_{2\alpha}^E$ as,⁶²⁻⁶³

$$H1_{1\alpha}^E = \frac{-Q_{1\alpha}^E(R_{1\alpha})[R_{2\alpha} - R_{2\alpha}I_{22} + \tilde{I}_{22}] - Q_{2\alpha}^E(R_{2\alpha})[R_{1\alpha}\bar{I}_{12} - \tilde{I}_{12}]}{[R_{1\alpha} - R_{1\alpha}I_{11} + \tilde{I}_{11}][R_{2\alpha} - R_{2\alpha}I_{22} + \tilde{I}_{22}] - [R_{1\alpha}\bar{I}_{12} - \tilde{I}_{12}][R_{1\alpha}\bar{I}_{21} - \tilde{I}_{21}]} \quad (4.62)$$

$$H1_{2\alpha}^E = \frac{-Q_{2\alpha}^E(R_{2\alpha})[R_{1\alpha} - R_{1\alpha}I_{11} + \tilde{I}_{11}] - Q_{1\alpha}^E(R_{1\alpha})[R_{2\alpha}\bar{I}_{21} - \tilde{I}_{21}]}{[R_{1\alpha} - R_{1\alpha}I_{11} + \tilde{I}_{11}][R_{2\alpha} - R_{2\alpha}I_{22} + \tilde{I}_{22}] - [R_{1\alpha}\bar{I}_{12} - \tilde{I}_{12}][R_{1\alpha}\bar{I}_{21} - \tilde{I}_{21}]} \quad (4.63)$$

where,

$$\bar{I}_{ij} = \int_{S_{ij}}^{R_{ij}} \frac{1}{3} \rho_j Q_{ij}^+(y) dy = \rho_j \left[-\frac{1}{12} a_{ij} R_j^3 - \frac{1}{2} b_{ij} R_j^2 \right]; \quad i=1, 2 \quad (4.64)$$

$$\tilde{I}_{ij} = \int_{S_{ij}}^{R_{ij}} \frac{1}{3} \rho_i Q_{ij}^+(y) y dy = \rho_i \left[\frac{1}{12} b_{ij} R_j^3 - \frac{1}{24} R_i a_{ij} R_j^3 - \frac{1}{4} R_i b_{ij} R_j^2 \right]; \quad i=1, 2 \quad (4.65)$$

Substitution of $H1_{j\alpha}^E$ (from Eq. (4.62) and Eq. (4.63)) into Eq. (4.52) provides the required expression for E_{Born} . Born free energy (F_{Born}) of solvation is then calculated from the following relation¹⁵

$$F_{Born} = \int_0^e de(E_{Born}/e) \quad (4.66)$$

4.2.8 Solvent Partial Polarization Densities of an Ion at Infinite Dilution in a Binary Dipolar Mixture

In this section we give the expressions for partial polarization densities of constituent solvents around an ion with charge $z_\alpha e$ at infinite dilution. The total polarization density about an ion with charge $z_\alpha e$ is defined as^{15-16,62}

$$P_\alpha(r) = \sum_k P_{\alpha k}(r) = \frac{1}{4\pi} \sum_k \rho_k \mu_k \int d\omega g_{\alpha k}(r, \omega) (\hat{\mu}_k(\omega) \cdot \hat{r}) \quad (4.67)$$

where $P_{\alpha k}(r)$ is partial polarization density of k^{th} species. Since $h_{\alpha k}^E = h_{k\alpha}^E$ one can write the above equation as

$$\begin{aligned} P_\alpha(r) &= \frac{1}{3} \sum_k \rho_k \mu_k h_{\alpha k}^E(r) = \frac{1}{3} \sum_k \rho_k \mu_k h_{k\alpha}^E(r) \\ &= \frac{1}{3} \sum_k \rho_k \mu_k \left[\frac{1}{2\pi r} \left\{ \frac{1}{r} H_{k\alpha}^E(r) - \frac{d}{dr} H_{k\alpha}^E(r) \right\} \right] \end{aligned} \quad (4.68)$$

where $H_{k\alpha}^E(r)$ is given by^{15,61}

$$H_{j\alpha}^E(r) = r H_{j\alpha}^1, \quad r \leq R_{j\alpha} \quad (4.69)$$

$$H_{j\alpha}^E(r) = -Q_{j\alpha}^E(r) + \frac{1}{3} \sum_k \rho_k \int_{S_{jk}}^{R_{jk}} ds Q_{jk}^+(s) H_{k\alpha}^E(r-s), \quad r > R_{j\alpha} \quad (4.70)$$

Since $Q_{jk}^+(r)$ is known, $H_{j\alpha}^E(r)$ can easily be obtained numerically and hence $P_\alpha(r)$.

4.3 Results & Discussion

This section consists of three parts. In the first part we present numerical results for the Born free energy of solvation and excess Born free energy of solvation of a dissolved ion in a model binary polar mixture. Here we show the effects of relative size of the constituent solvent components on the nonideality of these quantities for a given ion. We then present numerical results for systems consisting of unipositive

ions in binary polar mixtures where diameters and dipole moments of the solvent components used in the calculations are those of water, methanol, ethanol, tertiary butanol, DMSO and acetonitrile. The calculated results for the mole fraction dependent partial solvent polarization densities around an ion in these mixtures are presented in the second part where the microscopic origin for the observed nonideality is discussed. In the third part we compare the results for Born free energy of solvation and excess Born free energy of solvation of a dissolved ion in alcohol-water and DMSO-acetonitrile mixtures with available experimental results. All the numerical results presented here are calculated at temperature $T=298.15$ K.

4.3.1 Born Free Energy of Solvation

4.3.1.1 Born Free Energy in Model Binary Mixtures

In Fig. 4.1 we show the Born free energy of solvation of an ion, F_{Born} , and excess Born free energy of solvation, ΔF_{Born} , as a function of mole fraction of the second component (x_2) whose dipole moment is larger than the other one. The parameters necessary for the calculation are given in Table 4.2. We have presented four sets of calculations for different solvent-solvent size ratios while the dipole moments (μ_1 and μ_2), ion diameter (R) and total packing fraction (ζ) are kept fixed. The *squares*, *inverted triangles*, *triangles* and *circles* indicate calculations at $R_2=0.5R_1$, $0.8R_1$, R_1 and $1.2R_1$, respectively. It is clear from the above figure (*upper panel*) that the Born free energy of solvation increases non-linearly as one increases the mole fraction of the component which possesses larger dipole moment. Born free energy of solvation calculated for $R_1=R_2$ matches *exactly* with available results of Morillo *et al.*¹⁶. This

Table 4.2: Parameters used in the calculation for model binary dipolar mixture^(a)

$\mu_1 (D)$	$\mu_2 (D)$	ζ	$R (\text{\AA})$	$R_1 (\text{\AA})$	$R_2 (\text{\AA})$
0.816	1.632	0.42	2.88	2.88	(i) $0.5R_1$ (ii) $0.8R_1$ (iii) $1.0R_1$ (iv) $1.2R_1$

(a) μ_1 and μ_2 are dipole-moment of solvent 1 and 2, respectively. ζ is packing fraction, R , R_1 and R_2 are diameters of ion, solvent components 1 and 2, respectively. D stands for Debye.

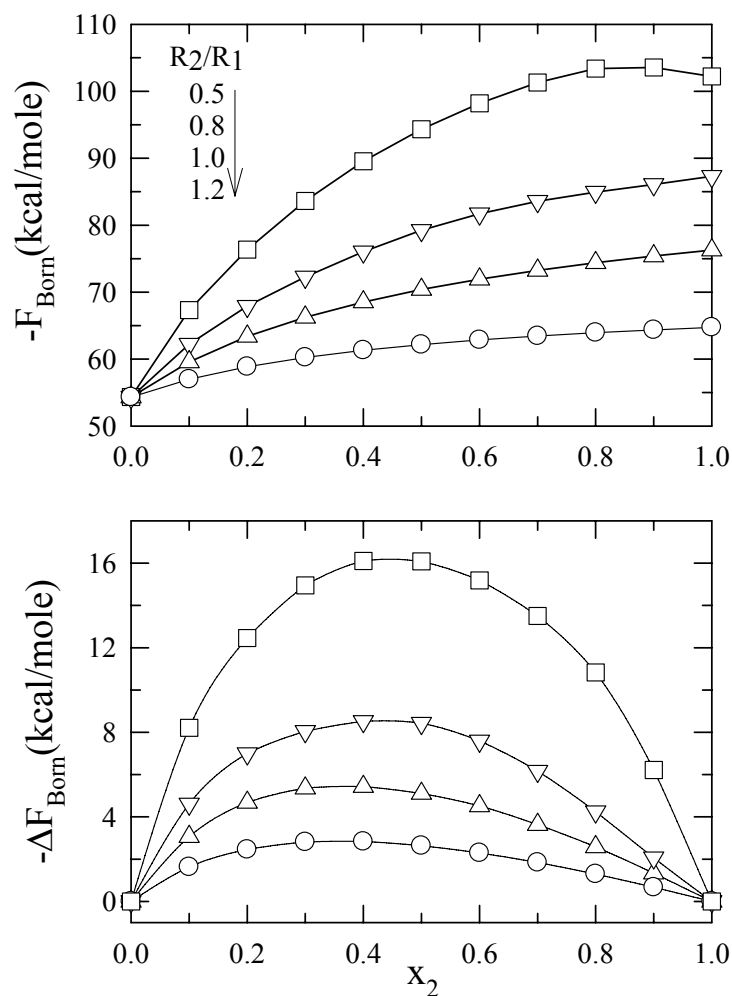


Figure 4.1: Born free energy of solvation, F_{Born} (*upper panel*) and excess Born free of solvation, ΔF_{Born} (*lower panel*) of a uni-positive, rigid ion as a function of mole fraction of second component (x_2) with higher dipole moment at different solvent-solvent size ratios (R_2/R_1). The *circles*, *triangles*, *inverted triangles* and *squares* are for solvent-solvent size ratio equal to 1.2, 1.0, 0.8 and 0.5, respectively. The line going through the points for each R_2/R_1 is a guide to the bare eye. The dipole moments of two solvent components (μ_1 and μ_2) and diameter of the ion (R) are kept fixed for all the solvent-solvent size ratios (Table 4.2).

indicates that the theory is correctly predicting the equal radii case. Note also that the reduction in size of the solvent component possessing larger dipole moment enhances the Born free energy of solvation. As a result, the nonlinearity is most pronounced for $R_2=0.5R_1$. The extent of non-linearity, which is a measure of nonideality, is better understood in terms of the excess Born free energy of solvation, ΔF_{Born} , calculated as follows:^{16, 64}

$$\begin{aligned}\Delta F_{Born}(x_2) &= F_{Born}(x_2) - F_{Born}(x_2 = 0) - x_2[F_{Born}(x_2 = 1) - F_{Born}(x_2 = 0)] \\ &= F_{Born}(x_2) - [(1 - x_2)F_{Born}(x_2 = 0) + x_2F_{Born}(x_2 = 1)]\end{aligned}\quad (4.71)$$

The second equality of Eq. (4.71) indicates that the excess Born free energy of solvation is the deviation in Born free energy of solvation for an ion at a given mole fraction (x_2) in a binary mixture from the *sum* of the mole fraction weighted Born free energies of solvation in the pure components. The excess Born free energy of solvation thus obtained is shown as a function of x_2 in the *lower panel* of Fig. 4.1. It is clear that the magnitude of nonideality increases as the size of the solvent having higher dipole moment is decreased. However, the peak positions of ΔF_{Born} on the mole fraction axis do not change substantially as one alters the solvent-solvent size ratio. This is because the ion size is kept fixed. All these observations indicate that the degree of nonideality in a completely asymmetric binary mixture depends not only on the relative dipole moments but also on the relative sizes of the constituent solvent species. The solvent size ratio dependence of nonideality in the excess Born free energy of solvation of an ion in a binary mixture is one of the main results of the present work.

4.3.1.2 Born Energy in Alcohol-Water Mixtures

We next apply the present scheme for calculating the Born free energy of solvation (F_{Born}) and excess Born free energy (ΔF_{Born}) of uni-positive ions in alcohol-water binary mixtures. We have studied methanol-water, ethanol-water and tertiary butanol (TBA)-water mixtures. The essential parameters^{2,56} used in the calculation are summarized in Table 4.3. The results obtained for Li^+ , Na^+ , Cs^+ and C_4 (quaternary tertiary butyl ammonium ion) in methanol-water mixture are shown in Fig. 4.2.

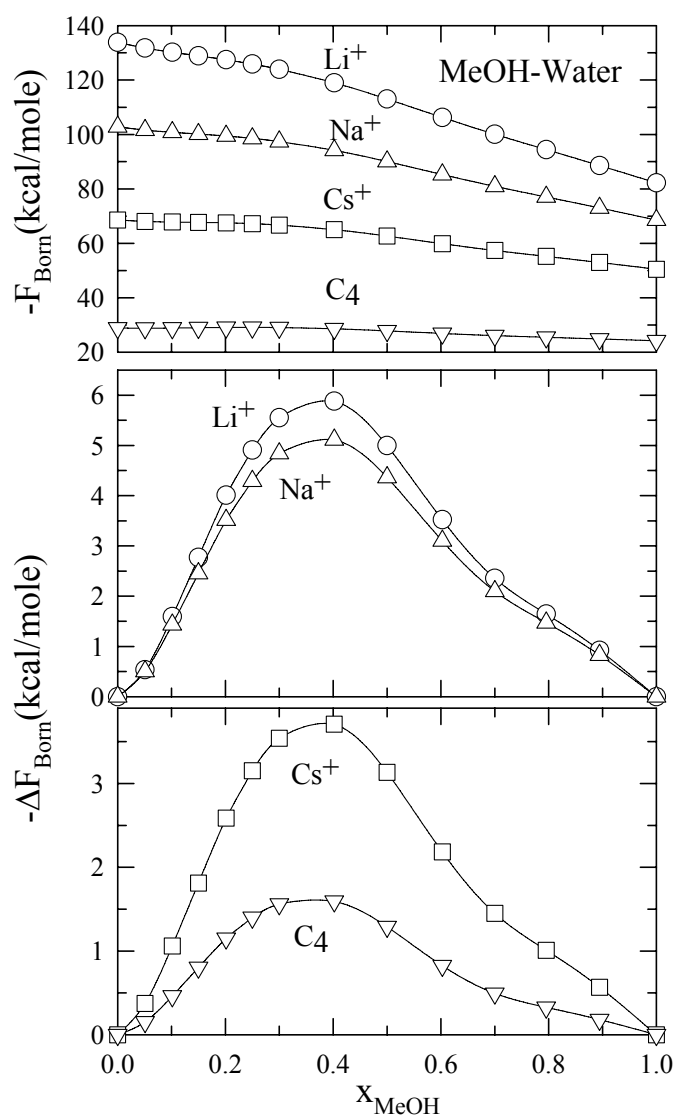


Figure 4.2: *Upper panel:* Comparison of Born free energy of solvation F_{Born} for Li^+ (circles), Na^+ (triangles), Cs^+ (squares) and C_4 (inverted triangles) ions as a function of mole fraction of methanol (x_{MeOH}) in methanol-water mixture. *Middle panel:* Comparison of excess Born free energy of solvation ΔF_{Born} for Li^+ (circles) and Na^+ (triangles) ions as a function of mole fraction of methanol (x_{MeOH}) in methanol-water mixture. *Lower panel:* Comparison of excess Born free energy of solvation ΔF_{Born} for Cs^+ (squares) and C_4 (inverted triangles) ions as a function of mole fraction of methanol (x_{MeOH}) in methanol-water mixture. Other representations remain the same as in the Figure 4.1.

Table 4.3: Solvent parameters used in the calculation for alcohol-water mixtures ^(a)

Solvent	Dipole moment (Debye)	Diameter (Å)
Water	1.85	2.80
Methanol	1.70	4.24
Ethanol	1.69	4.78
Tert-Butanol	1.66	5.58
Acetonitrile(ACN)	3.50	4.50
Dimethylsulfoxide(DMSO)	4.10	5.30

(a) Diameters of Li^+ , Na^+ , Cs^+ and C_4 ions are taken as 1.24, 1.96, 3.52 and 10 Å, respectively.

Several interesting features are to be noted from the upper panel of Fig. 4.2. First, F_{Born} for Li^+ at all methanol compositions is the largest of all the ions studied here.

This is also the prediction of earlier works in pure solvents¹⁵ and equal-sized dipolar mixtures.¹⁶ Also, F_{Born} calculated here for all ions in pure liquid (water or alcohol) matches exactly with those from Chan *et al.*¹⁵ Second, the nonideality in F_{Born} decreases as the size of the ion is increased. Note the peak ratio in ΔF_{Born} between Li^+ and $\text{C}_4 \sim 4$. This indicates that the larger solvent species is increasingly accommodated as the ion size is increased. In Fig. 4.3 we have shown the Born free energy of solvation (F_{Born}) and excess Born free energy (ΔF_{Born}) for Li^+ , Na^+ , Cs^+ and C_4 ions in ethanol-water mixture. The general features of F_{Born} very similar to methanol-water mixture except the extent of nonideality is more for Na^+ ion than for Li^+ at all the compositions. The situation becomes interesting for TBA-water mixtures, shown in Fig. 4.4. Here, the nonideality in F_{Born} for Li^+ to Na^+ shows a slope opposite to that found in aqueous methanol and ethanol solutions. The positive values of ΔF_{Born} for Li^+ to Na^+ in TBA-water mixture indicates that due to larger size TBA molecules cannot be packed around these smaller ions as efficiently as methanol or ethanol. This constraint is however partially lifted when the ion becomes larger. Consequently, ΔF_{Born} for Cs^+ and C_4 shows the similar mole fraction dependence as found in methanol-water and ethanol-water mixtures. This completes the non-ideal behavior on both sides of the ideal curve. It is interesting to note that even-though

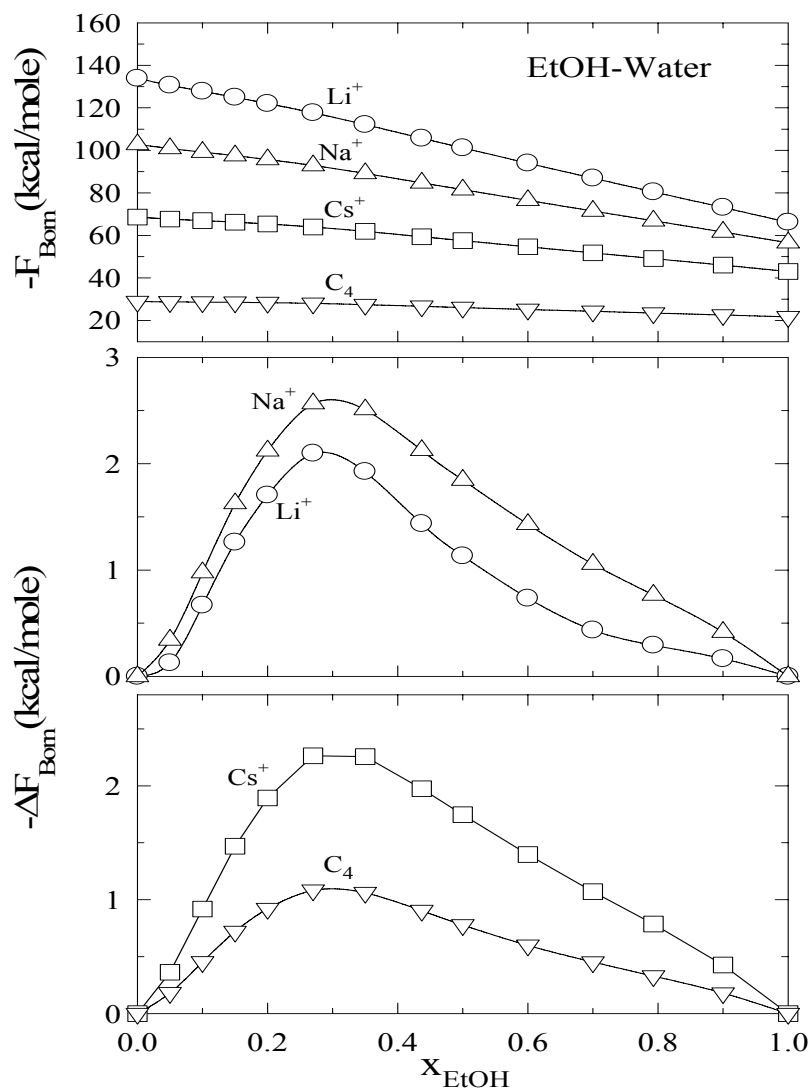


Figure 4.3: *Upper panel:* Comparison of Born free energy of solvation F_{Born} for Li^+ (circles), Na^+ (triangles), Cs^+ (squares) and C_4 (inverted triangles) ions as a function of mole fraction of ethanol (x_{EtOH}) in ethanol-water mixture. *Middle panel:* Comparison of excess Born free energy of solvation ΔF_{Born} for Li^+ (circles) and Na^+ (triangles) ions as a function of mole fraction of ethanol (x_{EtOH}) in ethanol-water mixture. *Bottom panel:* Comparison of excess Born free energy of solvation ΔF_{Born} for Cs^+ (squares) and C_4 (inverted triangles) ions as a function of mole fraction of ethanol (x_{EtOH}) in ethanol-water mixture.

TBA is larger in size than methanol, ΔF_{Born} for Cs^+ and C_4 is smaller in TBA-water mixture than that in methanol-water mixture. This is a manifestation of the role of ion-solvent size ratio in determining the extent of nonideality. As we would see later, the solvent structure in asymmetric binary polar mixture around larger ions is

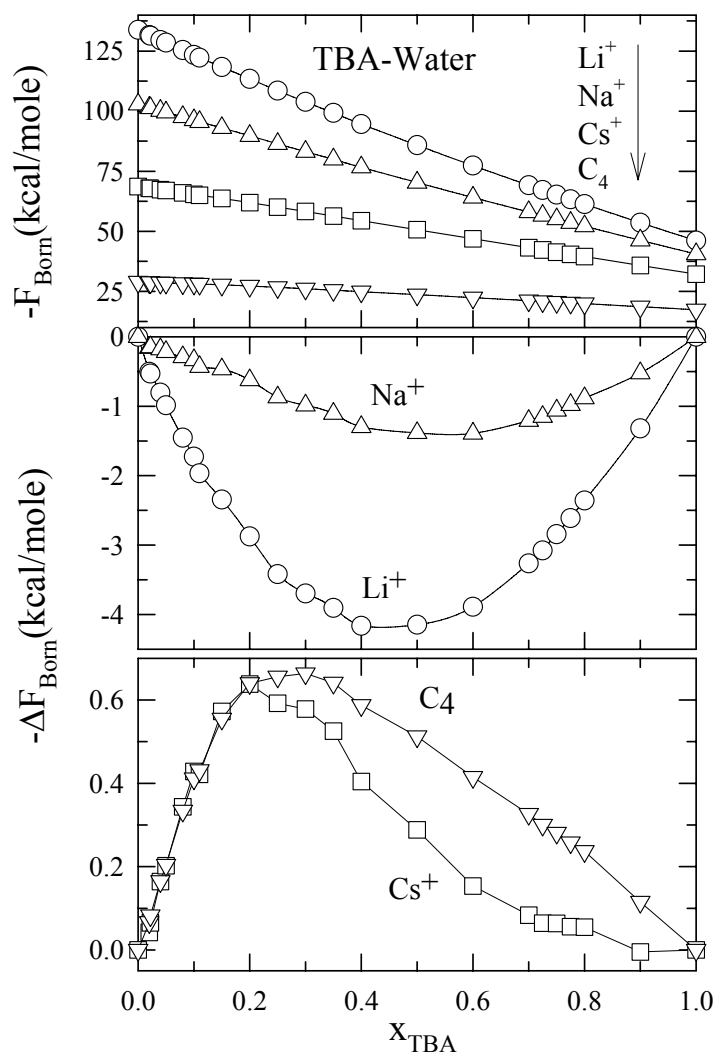


Figure 4.4: *Upper panel:* Comparison of Born free energy of solvation F_{Born} for Li^+ (circles), Na^+ (triangles), Cs^+ (squares) and C_4 (inverted triangles) ions as a function of mole fraction of tertiary butanol (x_{TBA}) in tertiary butanol-water (TBA-water) mixture. *Middle panel:* Comparison of excess Born free energy of solvation ΔF_{Born} for Li^+ (circles) and Na^+ (triangles) ions as a function of mole fraction of TBA (x_{TBA}) in TBA-water mixture. *Bottom panel:* Comparison of excess Born free energy of solvation ΔF_{Born} for Cs^+ (squares) and C_4 (inverted triangles) ions as a function of mole fraction of TBA (x_{TBA}) in TBA-water mixture.

relatively more ‘homogeneous’ than around smaller ions. Since dipole moments of these alcohols are almost the same², this result indicates the important roles being played by ion-solvent and solvent-solvent size ratios in governing the solvent structure around an ion in binary mixtures.

The solvent size ratio dependence of F_{Born} and ΔF_{Born} are shown in Fig. 4.5 where Born free energy of solvation and excess Born free energy of solvation are calculated for C_4 in aqueous methanol, ethanol and TBA solutions. As expected, the Born free energy of solvation (F_{Born} , *upper panel*) is the largest in aqueous methanol solutions at all compositions. Also, the peak in excess Born free energy (ΔF_{Born} , *lower panel*) is the highest in aqueous methanol solution. Note that the peak in ΔF_{Born} is shifting towards lower alcohol mole fraction as the chain length of the alcohol increases. It is believed that because the perturbation on water structure becomes stronger as the alkyl chain length increases, leading to an appreciable modification in water structure at lower alcohol concentration for TBA than for methanol.⁶⁵⁻⁶⁷ The fact that the solvent-solvent size ratio plays an important role in these complex mixtures is indeed manifested in Fig. 4.5. Moreover, these peaks are occurring between 0.3 – 0.2 mole fractions of alcohols studied here. In addition, the peak size depends on the size of the alcohol as well as that of the ion dissolved (see Fig. 4.2 also). All these observations are similar to what have been observed earlier when partial molal heat of solution for several crystalline salts was measured in alcohol-water mixtures.⁶⁵⁻⁶⁷ Studies of these systems using techniques such as sound velocity measurements,²³⁻²⁵ Fourier transform near-infrared spectroscopy,²⁶ light³⁴⁻³⁵ and x-ray scattering,³⁶⁻³⁷ neutron scattering and diffraction,^{29-32,38-41} dielectric relaxation,^{27,43} and computer simulation⁴⁵⁻⁵⁰ also revealed similar non-monotonic alcohol mole fraction dependence in the respective properties which was subsequently explained in terms of modification of the three dimensional hydrogen-bonded network structure of water by successive addition of alcohols. Since specific interaction such as hydrogen bonding between water and alcohol molecules are absent in the present theory, the emergence of these peaks and tuning of them with alcohol size is purely originating from the interactions between the ion and solvents of different types and also between solvent molecules of the same and different types. These interactions are essentially size mediated electrostatic attraction or repulsion giving rise to solvent structural rearrangement. Therefore, the size mediated structural rearrangement is an inherent property of an asymmetric binary mixture, the magnitude of which is accentuated or attenuated by the presence of specific interactions.

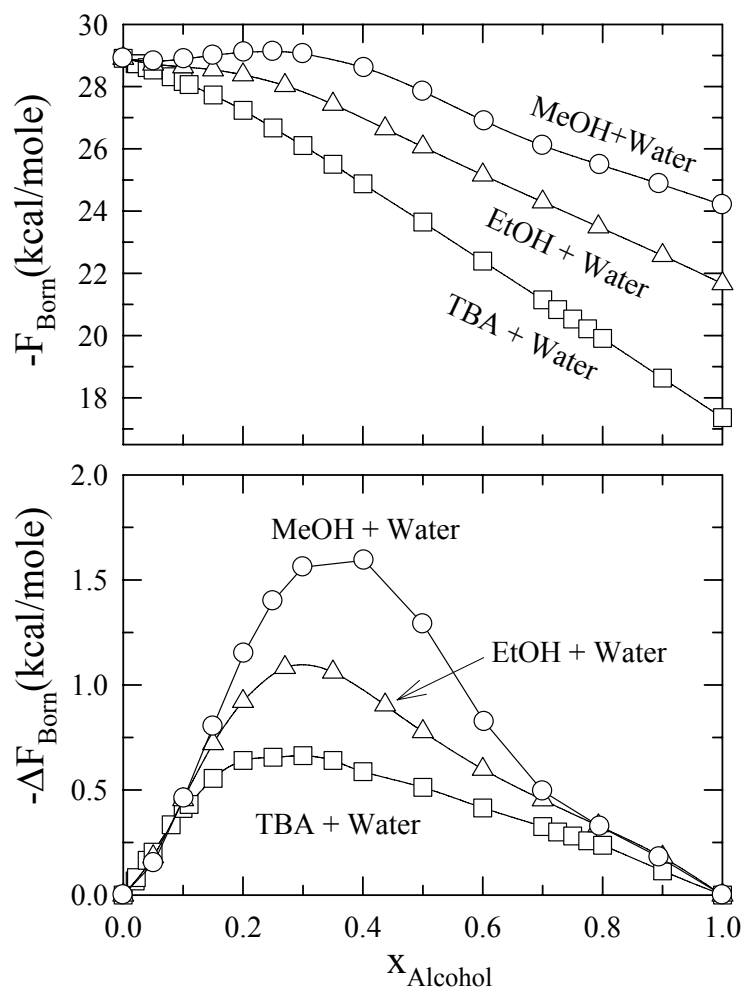


Figure 4.5: Comparison of Born free energy of solvation F_{Born} (upper panel) and excess Born free energy of solvation ΔF_{Born} (lower panel) for C_4 ion in methanol-water (circles), ethanol-water (triangles) and TBA-water mixture (squares). For further discussion, see text.

4.3.1.3 Born Energy in DMSO-Acetonitrile Mixtures

Fig. 4.6 shows the mole fraction dependence of Born free energy of solvation, F_{Born} and excess Born free energy of solvation, ΔF_{Born} in DMSO-acetonitrile mixture for two ions of very different diameters, Li^+ and C_4 . Also shown are the results for ethanol-water mixture in order to make a comparison between the two different kinds

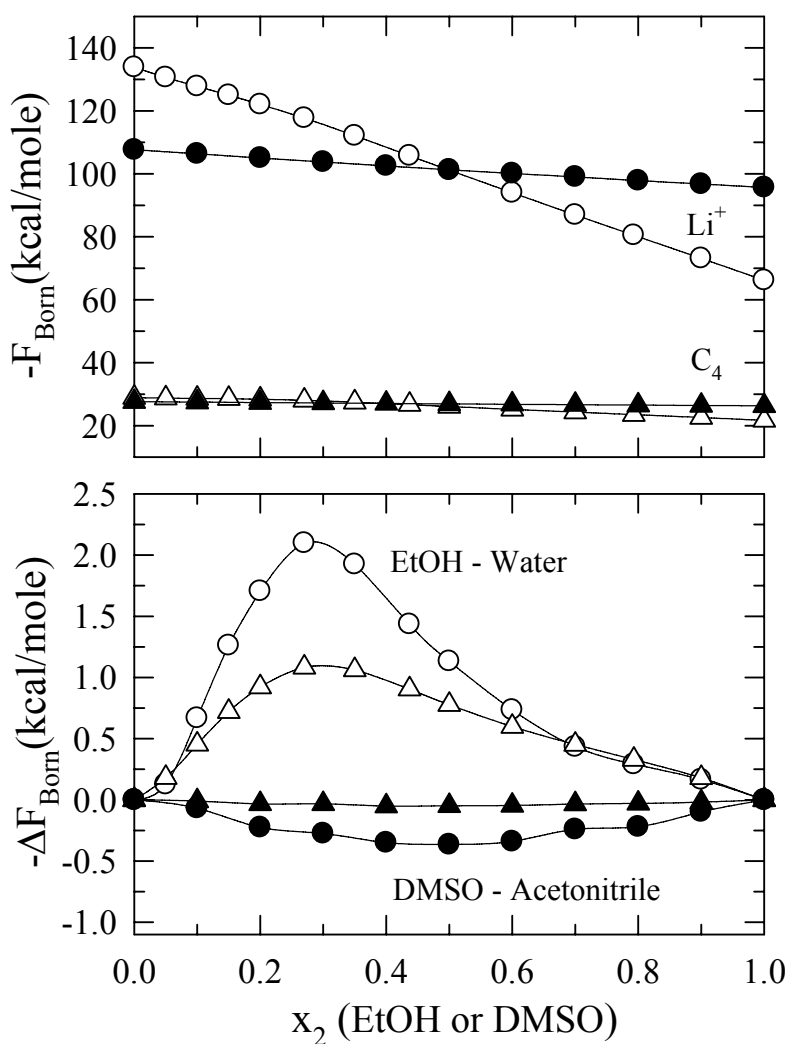


Figure 4.6: Born free energy solvation F_{Born} (upper panel) and excess Born free of solvation ΔF_{Born} (lower panel) for Li^+ (circles) and C_4 (triangles) ions as a function of mole fraction of second (larger) component (x_2) in DMSO-acetonitrile (solid symbols) and ethanol-water (open symbols) mixtures.

of mixture. The Born free energy of solvation, F_{Born} (upper panel) indicates different mole fraction dependence in ethanol-water and DMSO-acetonitrile mixtures. The insensitivity (or very weak dependence) of F_{Born} on DMSO mole fraction in DMSO-acetonitrile mixture (filled symbols) is a manifestation of competition between packing and electrostatic interactions. The dipole moment of DMSO is little larger than that of acetonitrile and hence ion-dipole interaction would favor DMSO more in number in the first solvation shell of an ion. However, packing constraint (repulsion) would disfavor DMSO as its size is slightly larger than acetonitrile. Therefore, a

delicate balance between these two interactions renders the mole fraction dependence of F_{Born} a very weak one. Note also that even in ethanol-water mixture (*open symbols*), the mole fraction dependence in F_{Born} for C_4 (*triangles*) is very weak. This indicates that C_4 being large in size can accommodate larger solvent molecules more favorably than smaller ions, resulting much less concentration fluctuations in the nearest neighbor solvent arrangements.⁶³

The *lower panel* of Fig. 4.6 shows the mole fraction dependence of the excess Born free energy of solvation, ΔF_{Born} for Li^+ and C_4 in DMSO-acetonitrile and ethanol-water mixtures. Note that the slope of ΔF_{Born} for DMSO-acetonitrile mixture is opposite to that found in ethanol-water mixtures. Similar results have also been found for smaller ions in TBA-water mixtures (see Fig. 4.4). The positive values of ΔF_{Born} clearly indicates that DMSO molecules around a small ion such as Li^+ is increasingly disfavored due to larger size. This is indeed a manifestation of dominance of repulsive interactions in determining the solvation structure around a solvated ion. Another important aspect of this figure (*lower panel*) is that the absolute magnitude of ΔF_{Born} is 4 times less for Li^+ in DMSO-acetonitrile mixture than that in ethanol-water solution. This indicates that the solvent size ratio indeed plays a crucial role in determining the extent of nonideality in binary mixtures. Also, the position of the extremum of DMSO-acetonitrile curve occurs at almost 50:50 composition whereas that for ethanol-water occurs at ~ 0.3 mole fraction of ethanol. This further proves that the solvent size ratio not only determines the extent of nonideality in Born free energy of solvation in binary mixtures, but determines also the location of the extremum on the mole fraction axis.⁶²⁻⁶³

4.3.2 Partial Polarization Densities

4.3.2.1 Partial Polarization Densities in Alcohol-Water Mixtures

Since the Born free energy of solvation (F_{Born}) is obtained from the partial solvent polarization densities (see Eqs. (4.50), (4.66) and (4.67)), one needs to look at these

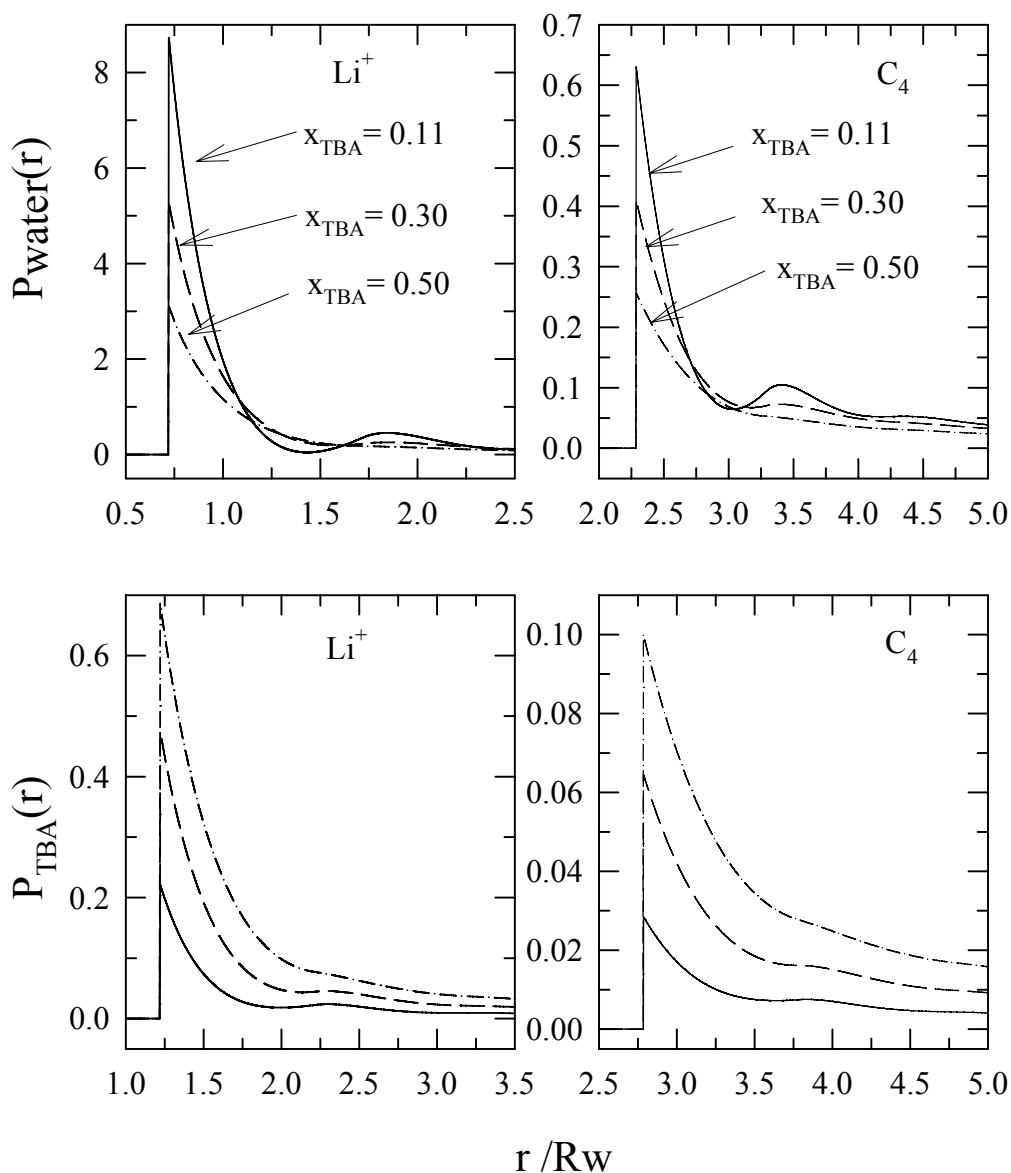


Figure 4.7: Partial polarization of water $P_{\text{water}}(r)$ and TBA $P_{\text{TBA}}(r)$ (both scaled by $\sqrt{k_B T / R_w^3}$) around Li^+ and C_4 ions as a function of distance r (scaled by water diameter R_w) from the centre of the ion at three different TBA mole fractions. In all the panels calculated data for TBA mole fractions 0.11, 0.30 and 0.50 are represented by *solid*, *dashed* and *dotted-dash* lines, respectively. For discussion, see text.

quantities for molecular level understanding of the non-ideality shown by F_{Born} in these alcohol-water mixtures. Here, we present the numerical results on the partial solvent polarization densities around Li^+ and C_4 in aqueous alcohol mixtures at three

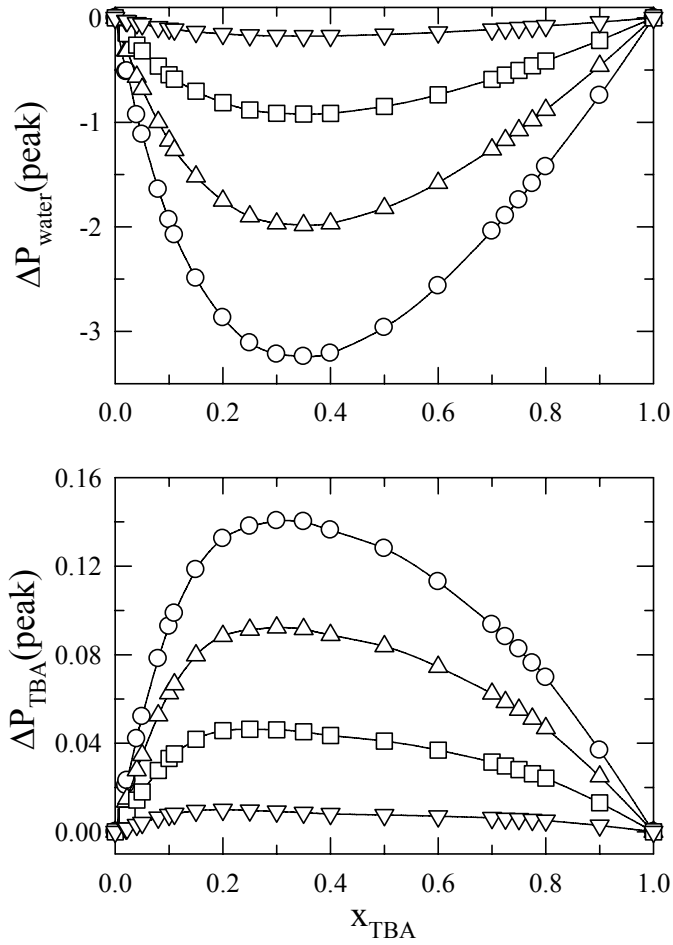


Figure 4.8: Excess partial polarization of water (*upper panel*) $\Delta P_{\text{water}}(\text{peak})$ and TBA $\Delta P_{\text{TBA}}(\text{peak})$ calculated from the peak values of respective partial polarizations for Li^+ (*circles*), Na^+ (*triangles*), Cs^+ (*squares*) and C_4 (*inverted triangles*) ions as a function of mole fraction of TBA (x_{TBA}) in TBA-water mixture. The following expression has been used to calculate $\Delta P_i(\text{peak})$ ($i=\text{water}$ or TBA): $\Delta P_i(\text{peak}, x_2) = P_i(\text{peak}, x_2) - P_i(\text{peak}, x_2 = 0) - x_2[P_i(\text{peak}, x_2 = 1) - P_i(\text{peak}, x_2 = 0)]$.

different compositions. Fig.4.7 shows the partial solvent polarization for Li^+ and C_4 dissolved in TBA-water mixture at three different TBA mole fractions. Note that the peak height in all cases is larger for smaller ions. This is consistent with the findings of Chan *et al.*¹⁵ in pure solvents. It is evident from this figure that the polarization density due to water around these ions is greater at all compositions than that due to TBA. Also, the water polarization density is decreased as the mole fraction of the

alcohol is gradually increased. Interestingly, even in 50:50 alcohol-water mixture, the peak in polarization density due to water is approximately 3 times larger than that due to TBA. This means that water is preferred over TBA molecules in the first solvation shells around these ions. This is the molecular origin of the non-ideality in Born energy of solvation, discussed already in connection with Figs. 4.2, 4.3 and 4.4. In fact, as shown in Fig. 4.8, the excess partial polarization densities ($\Delta P(\text{peak})$) calculated from the mole fraction dependent peak values in TBA-water mixtures also show non-ideality similar to what has been observed for the excess Born free energy of solvation (see Figs. 4.2, 4.3, 4.4 and 4.5). Also, $\Delta P(\text{peak})$ and ΔF_{Born} exhibit similar ion-size dependence.

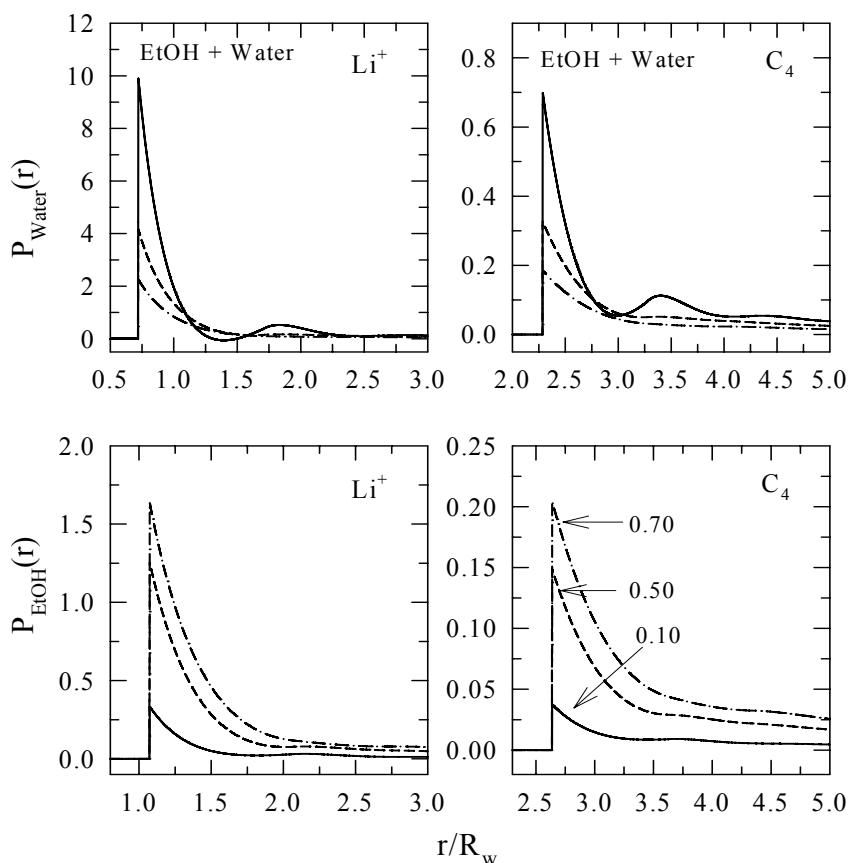


Figure 4.9: Partial polarization densities of water $P_{\text{water}}(r)$ and ethanol $P_{\text{EtOH}}(r)$ (both scaled by $\sqrt{k_B T / R_w^3}$) around Li^+ and C_4 ions as a function of distance r (scaled by water diameter R_w) from the centre of the ion at 0.10 (solid line), 0.50 (short dashed line) and 0.70 (dotted dashed line) mole fractions of ethanol in ethanol-water mixtures. For discussion, see text.

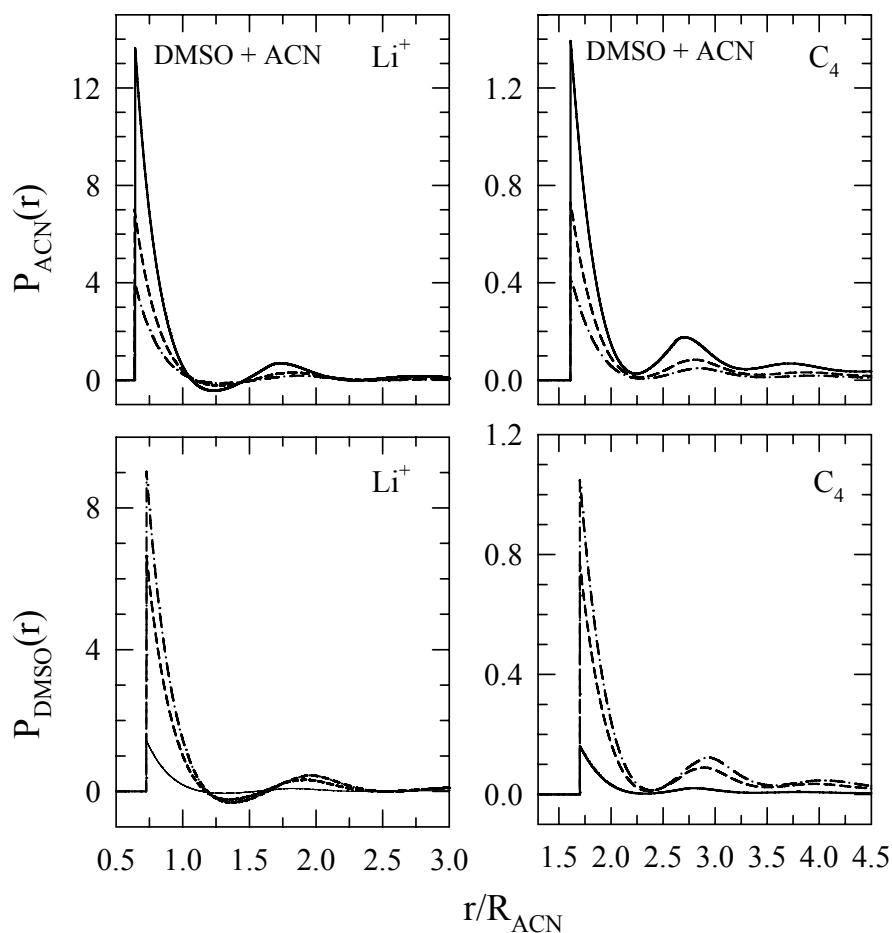


Figure 4.10: Partial polarization densities of acetonitrile $P_{ACN}(r)$ and dimethylsulfoxide $P_{DMSO}(r)$ (both scaled by $\sqrt{k_B T / R_{ACN}^3}$) around Li^+ and C_4 ions as a function of distance r (scaled by water diameter R_{ACN}) from the centre of the ion at 0.10 (*solid line*), 0.50 (*short dashed line*) and 0.70 (*dotted dashed line*) mole fractions of DMSO in DMSO-ACN mixtures.

Fig. 4.9 shows the partial solvent polarization densities in ethanol-water mixtures at 0.10, 0.50 and 0.70 mole fractions of ethanol. While the *upper* panels describe the partial polarization densities of water around Li^+ and C_4 , those of ethanol are shown in the *lower* panels. Note that at the lowest ethanol mole fraction (0.10), both the first and second solvation shells are clearly visible whereas the second solvation shell disappears with the increase in alcohol mole fraction in the mixture. As expected, the peak value of the water polarization density decreases with the increase in ethanol concentration and *vice-versa*.

4.3.2.2 Partial Polarization Densities in DMSO-Acetonitrile Mixtures

The results for DMSO-acetonitrile mixtures are shown in Fig. 4.10. The polarization peaks for both ACN and DMSO decrease as one increases the DMSO concentration (Fig. 4.11). In addition, the second solvation shell is well formed for most of the cases in this mixture. This is in contrast to what has been observed in alcohol-water mixtures. This is again due to the larger size of the solvent components constituting the binary mixtures.

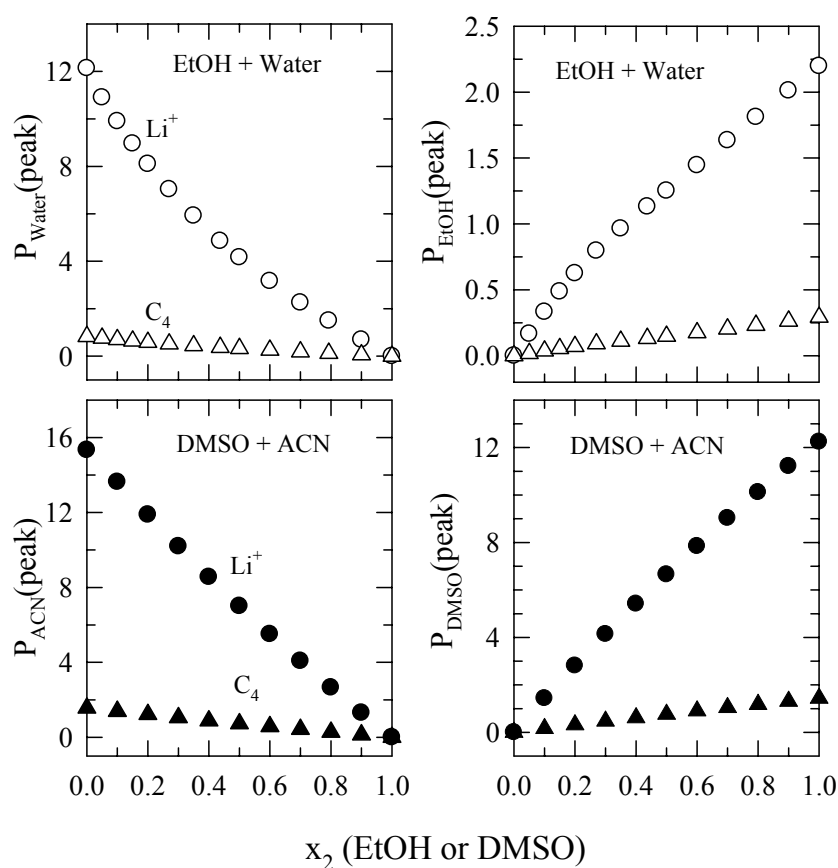


Figure 4.11: *Upper panels:* Comparison of peak values of partial polarization of water $P_{water}(peak)$ and ethanol $P_{EtOH}(peak)$ for Li^+ (open circles) and C_4 (open triangles) ions as a function of mole fraction x_2 of ethanol in ethanol-water mixture. *Lower panel:* Comparison of peak values partial polarization of acetonitrile $P_{ACN}(peak)$ and dimethylsulfoxide $P_{DMSO}(peak)$ for Li^+ (solid circles) and C_4 (solid triangles) ions as a function of mole fraction x_2 of DMSO in ACN-DMSO mixture.

We compare in Fig. 4.11 the mole fraction dependence of partial polarization peaks in associating (alcohol-water) and non-associating (DMSO-acetonitrile) solvent mixtures. The decrease or increase of partial solvent polarization peak is non-linear for ethanol-water mixtures, the extent of non-linearity being very weak for C_4 . As discussed earlier here and elsewhere,⁶²⁻⁶³ the nonlinearity is a manifestation of preferential solvation and hence this explains the microscopic origin of the strong nonideality observed for smaller ions in ethanol-water and other alcohol-water mixtures. In DMSO-acetonitrile mixture, however, the peaks of the partial solvent polarization densities decrease or increase *almost* linearly for both the ions showing a very weak preferential solvation. This is again due to the comparable sizes and dipole moments of DMSO and acetonitrile molecules.

4.3.3 Comparison with Experiments

As already discussed, the present theory treats the binary solvent components as dipoles embedded on hard spheres which is very different from the real situation. For example, alcohol-water solutions are known to exhibit anomalous behavior due to hydrophobic interaction and specific interaction (H-bonding) between the alcohol and water molecules. In such solutions where an intricate balance between hydrophobic hydration and H-bonding interaction dictates the solution property, the success of a simple theory like MSA in predicting the experimental behavior is somewhat fraught with danger. However, non-specific interactions such as size-mediated and coulomb (ion-dipole and dipole-dipole) interactions could still play a significant role in determining the solvent structure around an ion in these complex mixtures. Therefore, there is always a possibility that for some ion-solvent and solvent-solvent combinations, the non-specific interactions rather than the specific and hydrophobic interactions would dominate the preferential solvation. For those cases one would expect a qualitative agreement between the present theory and the relevant experimental results. We will now discuss several of those cases.

Fig. 4.12 depicts the comparison of nonideality in Born free energy of solvation in three different binary mixtures, namely, methanol-water, ethanol-water and DMSO-acetonitrile solutions. While the excess free energy of solvation obtained from

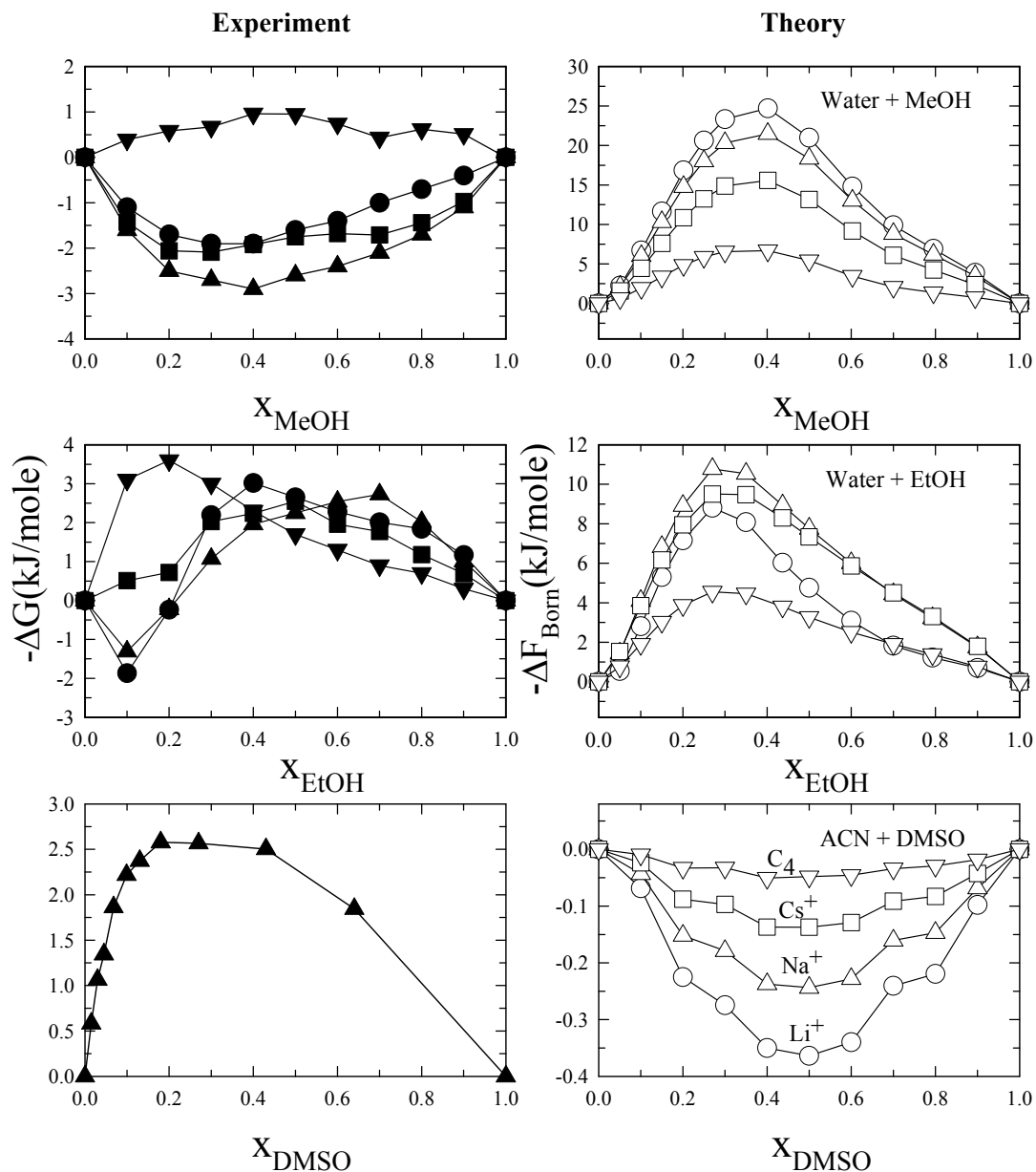


Figure 4.12: Comparison between the calculated excess Born free energy of solvation ($-\Delta F_{\text{Born}}$) and experimental excess free energy of solvation ($-\Delta G$) for Li^+ (circles), Na^+ (triangles), Cs^+ (squares) and C_4 (inverted triangles) ions in binary mixtures of methanol-water (upper panels), ethanol-water (middle panels) and DMSO-acetonitrile (bottom panel). These excess functions are shown as a function of mole fraction of one of the components in the mixture. The experimental data are represented by the *solid* symbols while the predictions from the extended MSA theory are shown by the *open* symbols.

experiments⁶⁸ for different ions in these solvent mixtures are shown in the left panels of Fig. 4.12, the theoretical results are presented in the right panels. We would like to mention here that one should not directly compare the experimental results with the theory as the present theory calculates only the electrostatic part of the free energy of solvation. It is also known that for alkali metal ions, the entropic contribution to the solvation free energy is negligible.⁶⁹ Several aspects are to be noted in this figure. First, for a large ion such as tetra-alkyl quaternary ammonium ion (C_4) in methanol-water mixture, the calculated excess Born free energy of solvation ($-\Delta F_{Born}$) shows a slope qualitatively similar to that in experimentally observed mole fraction dependent excess free energy of solvation ($-\Delta G$). For alkali metal ions, however, the slope is opposite to that found in experiments. This is probably because the solution structure in presence of a big organic ion is more homogeneous where the specific and hydrophobic interactions play a secondary role. Recent neutron diffraction studies of ternary mixtures composed of cyclohexene, TBA and water in 2:6:1 ratio suggest that the microscopic heterogeneity is much weaker in ternary solutions than in binary mixtures⁴⁰ and hence the solution is less biphasic where microclustering of water molecules is not supported. Similar modifications may also take place in methanol-water mixtures in presence of tetra-alkyl ammonium ion (C_4). Since the solvent structure around a dissolved ion in such cases is likely to be governed by the size mediated and electrostatic interactions, the MSA may be able to predict the qualitative behavior of the experimentally observed mole fraction dependence of free energy of solvation. However, the microscopic heterogeneity in solution structure is likely to remain unchanged in presence of smaller ions and hence the theory is in poor agreement with experiments in such cases. Even though the excess Born free energy of solvation for alkali metal ions such as Na^+ and Cs^+ in methanol-water solutions show nonideality in a direction opposite to that found in experiments, the experimentally observed ion size dependence is well captured by the present theory.

Next we discuss the mole fraction dependence of excess Born free energy of solvation ($-\Delta F_{Born}$) for these ions and compare them with the experimental excess free energy of solvation ($-\Delta G$) in ethanol-water mixtures. Interestingly, in water-ethanol mixtures (middle panels) the nonideality in $-\Delta F_{Born}$ for all the ions is qualitatively

similar to that found in experimentally obtained $-\Delta G$. From the arguments given for methanol-water solutions, $-\Delta F_{Born}$ for C_4 in ethanol-water mixture is expected to show qualitative agreement with the corresponding experimental $-\Delta G$. However, the reasons for the qualitative agreement between theory and experiments for alkali metal ions (Li^+ , Na^+ and Cs^+) are not obvious to us. It might be that since $-\Delta F_{Born}$ in the present theory is dictated by a combination of ion-size, solvent-solvent size ratio, dipole moments and solution density (obtained from experiments), the calculation explores the right parameter space which leads to such a qualitative agreement with experiment. It could also be that such an agreement is fortuitous if one keeps in mind the complexity of the interactions involved in these systems and also the simplified model that the present theory is using to study them. Therefore, one should use sophisticated theories such as those proposed by Hirata and co-workers⁴⁹⁻⁵⁰ in order to explore how subtle differences in the hydrophobic and H-bonding interactions and their effects on microscopic solution structure lead to a different behavior of excess free energy of solvation for alkali metal ions in methanol-water and ethanol-water solutions. Similar comparisons for TBA-water systems could not be made as the experimental data at all TBA mole fractions are not available. However, for larger ions such as Cs^+ and C_4 , the available data on free energy of solvation is showing the same qualitative trend as predicted by the present theory.

Let us now focus our attention on similar studies in a non-associating binary liquid mixture where both the solvent components are polar yet not involved in H-bonding interaction either between molecules of same species or between different species. We have chosen DMSO-acetonitrile mixture as an example of the above type. In addition, the molecular diameter and dipole moment of DMSO are slightly larger (4.1 D and 5.3 Å) than those of acetonitrile (3.5 D and 4.5 Å). Therefore, a competition between the size mediated and electrostatic interactions would lead to a non-ideality much less pronounced compared to the systems composed of molecules with dissymmetric size and dipole moments. This is indeed the scenario as shown by the calculated $-\Delta F_{Born}$ in the bottom panel of Fig. 4.12. However, the predicted non-ideality is not only growing in a direction opposite to that found in experiments^{68(b)} (data available only for Na^+) but differs in magnitude also. This is probably due to the specific ion-solvent interaction between the dissolved ion and DMSO molecule (through the lone pair of

electrons). Effects of such specific ion-solvent interactions have also been found while studying ion mobility in DMSO-acetonitrile mixtures. Such ion-solvent specific interaction may drastically alter the solution structure around a dissolved ion which cannot be accounted for by the extended MSA approach. This is definitely a limitation of the present theory.

4.4 Conclusion

In this work we have found that the excess Born free energy of solvation depends both on the ion size and size disparity between solvent molecules in a binary mixture. This is in addition to the contribution arising out of difference in dipole moments. Note here that ion solvation in an asymmetric dipolar mixture has already been studied by several authors.^{5,64} In these studies,^{5,64} however, the MSA was not solved by consistently incorporating the ion size. Instead, solvent intra and intermolecular correlations were obtained from the solutions of dipolar MSA. Systematic incorporation of ion size is crucial because the polarization structure at the surface of the ion is very different from that at two or three molecular diameter away. The present work therefore reveals that not only the size of the solvent molecules but also the size of the ion plays an important role in determining the extent of nonideality.

When the present theory is applied to binary mixtures with solvent parameters representing water and several mono-hydroxyl alcohols, the excess Born free energy of solvation shows a non-monotonic mole fraction dependence. The peak in the excess Born free energy of solvation has been found to decrease with the increase in the size of the alcohol molecule. Also, the peaks are occurring at lower mole fraction of alcohol as the alcohol size becomes larger. These results are surprisingly similar to what have been found earlier in several experimental studies. In the present work the non-monotonic alcohol mole fraction dependence of the excess Born free energy of solvation arises due to a novel interplay among size-mediated electrostatic interactions between ion, alcohol and water molecules, and between alcohol-alcohol, alcohol-water and water-water molecules. The calculated microscopic partial polarization densities around a dissolved ion indicate the molecular origin of the preferential solvation and explain the nonideality in excess Born free energy of solvation in terms of intra and inter-molecular correlations. These results also indicate

that for a system of equal size and dipole moments, the nonideality will be either very weak or non-existent in the absence of any specific interactions. Dimethyl sulfoxide (DMSO) and acetonitrile molecules are both very close in size and dipole moments and our studies with DMSO-acetonitrile mixtures indeed show a very weak nonideality.⁶³ However, experimental data on mobility for small alkali ions in DMSO-acetonitrile mixtures⁷⁰ indicate the presence of a donor-acceptor bond between ion and a DMSO molecule, probably through the interaction of the ion with the lone-pair of electrons on the oxygen atom of a DMSO molecule. Therefore, the experimental data with small alkali ions in this mixture are expected to show a stronger nonideality than predicted by the present theory. Formation of donor-acceptor type ion-solvent complex is unfavorable with large symmetrical organic ions due to steric reasons and hence the theoretical predictions for these ions would be closer to experimental results.

It is to be noted here that since the present work is based upon the mean spherical approximation (MSA), the effects of shape of the molecules and specific interactions among them have not been incorporated. Therefore, the correlations derived from the present work are qualitative in nature. Needless to say, a full non-linear treatment with a systematic incorporation of the shape and specific interaction effects will lead to a quantitative description of solution structure in binary dipolar mixtures. Integral equation theory coupled with RISM approach by Hirata and co-workers⁵⁰⁻⁵¹ has been found to be successful in describing qualitatively many of the experimental data in water-alcohol systems discussed here. However, this approach is non-trivial and numerically involved. The present approach, on the other hand, is based on the simple MSA framework, which is simple and analytically tractable, yet capable of describing *qualitatively* the nonideality in alcohol-water mixtures in terms of microscopic solvent structure.

Appendix

The values of $b_{ij} \equiv [b]$ can be obtained by the following equation

$$[b] = [R][B] \left\{ I - \frac{1}{6} [\rho][R^3][B] \right\}^{-1} \quad (\text{A1})$$

and $a_{ij} \equiv [a]$ is given by

$$[a] = 2 \left\{ I + \frac{1}{2} [b][R^2][\rho] \right\} \left\{ I - \frac{1}{6} [B][R^3][\rho] \right\}^{-1} [B] \quad (\text{A2})$$

where,

$$[\rho]_{ij} = \rho_i \delta_{ij}, [R^n]_{ij} = R_i^n \delta_{ij} \text{ and } [B]_{ij} = 2\pi\kappa_{ij} \quad (\text{A3})$$

where $\kappa_{ij} = \int_{R_{ij}}^{\infty} \frac{h_{ij}^D(r)}{r} dr = \kappa_{ji}$ are obtained by solving the following set of equations^{13,58}

$$\begin{aligned} 3y_{11} &= \Phi_{11}(2\rho_1\kappa_{11}, 2\rho_2\kappa_{12}^2/\kappa_{11}) - \Phi_{11}(-\rho_1\kappa_{11}, -\rho_2\kappa_{12}^2/\kappa_{11}) \\ 3y_{22} &= \Phi_{22}(2\rho_1\kappa_{12}^2/\kappa_{22}, 2\rho_2\kappa_{22}) - \Phi_{22}(-\rho_1\kappa_{12}^2/\kappa_{22}, -\rho_2\kappa_{22}) \\ 3y_{12} &= \frac{\kappa_{12}}{\kappa_{11}} \left\{ \Phi_{12}(2\rho_1\kappa_{11}, 2\rho_2\kappa_{22}) - \Phi_{12}(-\rho_1\kappa_{11}, -\rho_2\kappa_{22}) \right\} \end{aligned} \quad (\text{A4})$$

$$\text{where } 3y_{ij} = \frac{4\pi}{3} \beta\rho_i\mu_i\mu_j$$

$\Phi_{ij}(\rho_i, \rho_j)$ is given by

$$\Phi_{ij} = \rho_i \frac{\partial \beta\mu_i}{\partial \rho_j} \quad (\text{A5})$$

μ_i is the chemical potential of i^{th} species in the mixture which is given by

$$\begin{aligned} \beta\mu_i(\rho_1, \rho_2) &= \ln(\rho_i \Lambda_i^3) - \ln(1 - \zeta) + \frac{\pi}{6} R_i^3 \beta p + \frac{3R_i^2}{(1 - \zeta)} (\eta_1 R_1 + \eta_2 R_2) \\ &+ \frac{9R_i^2}{2(1 - \zeta)^2} (\eta_1 R_1^2 + \eta_2 R_2^2)^2 + \frac{3R_i}{(1 - \zeta)} (\eta_1 R_1^2 + \eta_2 R_2^2) \end{aligned} \quad (\text{A6})$$

where $\zeta = \zeta_1 + \zeta_2$, $\zeta_i = (\pi/6)\rho_i R_i^3$, and $\eta_i = (\pi/6)\rho_i$. In Eq. (A6), p is the compressibility pressure which is given by,

$$\begin{aligned} \beta p &= (\rho_1 + \rho_2)(1 + \zeta + \zeta^2)(1 - \zeta)^{-3} - \frac{18}{\pi} \eta_1 \eta_2 (R_2 - R_1)^2 \\ &\quad \{ (R_1 + R_2) + R_1 R_2 (\eta_1 R_1^2 + \eta_2 R_2^2) \} (1 - \zeta)^{-3} \end{aligned} \quad (\text{A7})$$

References

1. G. R. Fleming and P. G. Wolynes, *Phys. Today* **43**, 36 (1990).
2. B. Bagchi and R. Biswas, *Adv. Chem. Phys.* **109**, 207 (1999).
3. R. Gupta and A. Chandra, *J. Chem. Phys.* **127**, 024503 (2007).
4. (a) S. Chowdhuri and A. Chandra, *J. Chem. Phys.* **123**, 234501 (2005); (b) S. Chowdhuri and A. Chandra, *J. Chem. Phys.* **119**, 4360, (2003).
5. A. Chandra, *Chem. Phys. Lett.* **235**, 133 (1995).
6. T. J. F. Day and G. N. Patey, *J. Chem. Phys.* **110**, 10937 (1999).
7. C. Chapman and M. Maroncelli, *J. Phys. Chem.* **95**, 9095 (1991).
8. D. Huppert, V. Ittah and E. M. Kosower, *Chem. Phys. Lett.* **159**, 267 (1989).
9. D. Laage and J. T. Hynes, *Proc. Natl. Acad. Sci.* **104**, 11167 (2007).
10. K. Kwak, S. Park and M. D. Fayer, *Proc. Natl. Aca. Sci. USA* **104**, 14221 (2007).
11. M. S. Wertheim, *J. Chem. Phys.* **55**, 4291 (1971).
12. S. A. Adelman and J. M. Deutch, *J. Chem. Phys.* **59**, 3971 (1973).
13. D. Isbister and R. Bearman, *J. Mol. Phys.* **28**, 1297 (1974).
14. C. G. Gray and K. E. Gubbins, *Theory of Molecular Liquids* (Clarendon, Oxford, 1984).
15. D. Y. C. Chan, D. J. Mitchel and B. Ninham, *J. Chem. Phys.* **70**, 2946 (1979).
16. M. Morillo, C. Denk, F. S. Burgos and A. Sanchez, *J. Chem. Phys.* **113**, 2360 (2000).
17. G. N. Patey and L. Carnie, *J. Chem. Phys.* **78**, 5183 (1983).
18. B. Montgomery and P. J. Rossky, *J. Chem. Phys.* **77**, 1451 (1982).
19. H. Tanaka, K. Nakanishi, H. Touhara, *J. Chem. Phys.* **81**, 4065 (1984).
20. L. L. Blum, F. Vericat and L. Degreve, *Physica A.* **265**, 396 (1999).
21. F. Franks and D. J. G. Ives, *Q. Rev. Chem. Soc.* **20**, 1 (1966).
22. M. D. Zeidler, In *Water, a Comprehensive Treatise*, edited by F. Franks, (Plenum, New York, 1973), **2**, 529 (1973).
23. M. Brai and U. Kaatze, *J. Phys. Chem.* **90**, 8946 (1992).
24. U. Kaatze, M. Brai, F. -D. Scholle and R. Pottel, *J. Mol. Liq.* **44**, 197 (1990).
25. (a) U. Kaatze, R. Pottel and P. Schmidt, *J. Phys. Chem.* **92**, 3669 (1988); (b) U. Kaatze, R. Pottel and P. Schmidt, *J. Phys. Chem.* **93**, 5623 (1989); (c) U. Kaatze, K. Menzel and R. Pottel, *J. Phys. Chem.* **95**, 324 (1991).

26. D. Wojkow and M. A. Czarnecki, *J. Phys. Chem. A* **109**, 8218 (2005).
27. S. S. N. Murthy, *J. Phys. Chem. A* **103**, 7927 (1999).
28. (a) K. Iwasaki and T. Fujiyama, *J. Phys. Chem.* **83**, 463 (1979); (b) K. Iwasaki and T. Fujiyama, *J. Phys. Chem.* **81**, 1908 (1977).
29. S. Dixit, J. Crain, W. C. K. Poon, J. L. Finney and A. K. Soper, *Nature* **416**, 829 (2002).
30. A. K. Soper and J. L. Finney, *Phys. Rev. Lett.* **71**, 4346 (1993).
31. D. T. Bowron, A. K. Soper and J. L. Finney, *J. Chem. Phys.* **114**, 6203 (2001).
32. J. Turner and A. K. Soper, *J. Chem. Phys.* **101**, 6116 (1994).
33. M. D'Angelo, G. Onori and A. Santucci, *J. Chem. Phys.* **100**, 3107 (1994).
34. K. Egashira and N. Nishi, *J. Phys. Chem. B* **102**, 4054 (1998).
35. K. Yoshida and T. Yamaguchi, *Z. Naturforsch. A* **56**, 529 (2001).
36. K. Nishikawa, Y. Kodera and T. Iijima, *J. Phys. Chem.* **91**, 3694 (1987).
37. Y. Koga, *Chem. Phys. Lett.* **111**, 176 (1984).
38. J. L. Finney, D. T. Bowron and A. K. Soper, *J. Phys. Condens. Matter* **12** A123 (2000).
39. D. T. Bowron, J. L. Finney and A. K. Soper, *J. Phys. Chem. B* **102**, 3551 (1998).
40. D. T. Bowron and S. D. Moreno, *J. Phys. Chem. B* **109**, 16210 (2005).
41. D. T. Bowron and S. D. Moreno, *J. Chem. Phys.* **117**, 3753 (2002).
42. G. W. Euliss and C. M. Sorensen, *J. Chem. Phys.* **80**, 4767 (1984).
43. T. Sato and R. Buchner, *J. Chem. Phys.* **119**, 10789 (2003).
44. T. Pradhan, P. Ghoshal and R. Biswas, *J. Phys. Chem. A* **112**, 915 (2007).
45. H. Tanaka and K. Gubbins, *J. Chem. Phys.* **97**, 2626 (1992).
46. M. Ferrario, M. Haughney, I. R. McDonald and M. L. Klein, *J. Chem. Phys.* **93**, 5156 (1990).
47. G. Palinkas, E. Hawlicka and K. Heinzinger, *Chem. Phys.* **158**, 65 (1991).
48. A. Wakisaka, S. Komatsu and Y. Usui, *J. Mol. Liq.* **90**, 175 (2001).
49. K. Nakanishi, K. Ikari, S. Okazaki and H. Touhara, *J. Chem. Phys.* **80**, 1656 (1984).
50. K. Yoshida, T. Yamaguchi, A. Kovalenko and F. Hirata, *J. Phys. Chem. B* **106**, 5042 (2002).
51. I. Omelyan, A. Kovalenko and F. Hirata, *J. Theo. Comp. Chem.* **2**, 193 (2003).

52. A. Laaksonen, P. G. Kusalik and I. M. Svishchev, *J. Phys. Chem. A* **101**, 5910 (1997).
53. H. K. Kashyap and Ranjit Biswas (unpublished results).
54. S. K. Allison, J. P. Fox, R. Hargreaves and S. P. Bates, *Phys. Rev. B* **71**, 024201 (2005).
55. L. Dougan, S. P. Bates, R. Hargreaves, J. P. Fox, J. Crain, J. L. Finney, V. Reat and A. K. Soper, *J. Chem. Phys.* **121**, 6456 (2004).
56. J. T. Edward, *J. Chem. Edu.* **47**, 261(1970).
57. L. Blum, *J. Chem. Phys.* **61**, 2129 (1974).
58. P. T. Cummings and L. Blum, *J. Chem. Phys.* **85**, 6658(1986).
59. L. Blum and D. Q. Wei, *J. Chem. Phys.* **87**, 555(1987).
60. D. Wei and L. Blum, *J. Chem. Phys.* **87**, 2999 (1987).
61. R. J. Baxter, *J. Chem. Phys.* **52**, 4559 (1970).
62. H. K. Kashyap and Ranjit Biswas, *J. Chem. Phys.* **127**, 184502 (2007).
63. H. K. Kashyap and Ranjit Biswas, *J. Chem. Sci.* **119**, 391 (2007).
64. A. Chandra and B. Bagchi, *J. Chem. Phys.* **94**, 8367 (1991).
65. E. M. Arnett and D. R. McKlevey, *J. Am. Chem. Soc.* **88**, 5031 (1966).
66. E. M. Arnett and D. R. McKlevey, *J. Am. Chem. Soc.* **87**, 1393 (1965).
67. E. M. Arnett, W. G. Bentrude, J. J. Burke and P. M. Duggleby, *J. Am. Chem. Soc.* **87**, 1541 (1965).
68. (a) C. Kalidas, G. Hefter and Y. Marcus, *Chem. Rev.* **100**, 819 (2000); (b) B. G. Cox, A. J. Parker and W. E. Waghorne, *J. Phys. Chem.* **78**, 1731 (1974).
69. D. M. Heyes, *The Liquid State: Applications of Molecular Simulations*, Wiley Series in Theoretical Chemistry (Wiley, New York, 1998).
70. V. K. Syal, S. Chauhan and M. S. Chauhan, *Indian J. Chem.* **29A**, 693 (1990).

Chapter 5

Dipolar Solvation Dynamics in Dipolar Room Temperature Ionic Liquids

5.1 Introduction

The presence of Coulomb interactions have rendered ionic liquids several unique solvent properties, such as, low vapour pressure, considerable polarity, wide liquid range, enhanced thermal stability and miscibility with other solvents.¹⁻² These properties have made RTILs better and environment-friendly reaction media in chemical industry for synthesis, separation, catalysis and a host of other applications. That is why RTILs are now called as ‘*Green Solvents*’. Since chemical reactions usually involve charge transfer and/or redistribution, the stabilization of various intermediates and products is intimately connected to the time scale at which the surrounding solvent molecules reorganize. Understanding the time scale of solvent reorganization in such reaction media may therefore be crucially important for designing a solvent for carrying out a specific reaction for a desired product. The last few years have witnessed intense activity towards understanding the solvation dynamics of photo-excited dyes in room temperature ionic liquids (RTIL).³⁻³⁹

Solvation dynamics experiments provide the solvent reorganization time scale via monitoring the time dependent shift in the fluorescence emission spectrum of a laser-excited dye molecule.⁴⁰⁻⁴² The time dependent progress of solvation is expressed in terms of solvation response function,⁴⁰⁻⁴² $S(t) = [\nu(t) - \nu(\infty)] / [\nu(0) - \nu(\infty)]$, where $\nu(t)$ denotes some measure of the time dependent frequency (usually, peak or the first moment) of the fluorescence emission spectrum of the laser excited dye dissolved in that medium. $\nu(0)$ is the emission frequency of the time zero spectrum (at a time when the vibrational relaxation in the excited probe molecule is complete but the solvent relaxation has not begun yet) and $\nu(\infty)$ represents the emission frequency

after the solvent relaxation is complete. For solvents with fast dynamics, $\nu(\infty)$ is expected to be the same as that obtained from the steady state emission spectrum of the same dye molecule in that solvent.⁴⁰ Note that $S(t)$ is normalized such that it decays from unity at $t = 0$ to zero at $t = \infty$, and a time integration of $S(t)$ produces the average solvation time, $\langle\tau_s\rangle$.

Recently, solvation dynamics in a number of RTILs have been investigated and the results from these studies can be summarized as follows:^{3-16, 22-25}

- (i) For imidazolium and pyrrolidinium ionic liquids, $S(t)$ shows biphasic decay where a fast component with time constant in the range of 100 – 700 fs accounts for approximately 20% of the total decay followed by a much slower component with time constant spanning over a few picoseconds to several nanoseconds.
- (ii) While the fast component originates from the inertial motion of the ions, the structural relaxation in RTIL is responsible for the slow component.
- (iii) The slow component can be fitted either to a stretched exponential or to a bi-exponential functions of time.
- (iv) For phosphonium and several ammonium ionic liquids, the biphasic decay is absent where a stretched exponential with one time constant could sufficiently describe the full decay dynamics.
- (v) For a given RTIL, the average solvation time, $\langle\tau_s\rangle$, shows a considerable probe dependence.

ven-though the above results are quite general, there exist several issues pertaining to the solvation dynamics in ionic liquids which are currently under debate and discussion. For example, fluorescence upconversion measurements in two imidazolium ionic liquids²⁵ have indicated a smaller (~10%) fast component with a much slower time constant (600 – 900 fs) than those reported in earlier studies. These studies²⁵ have further suggested that several factors such as the internal conformational dynamics of the probe molecule and its distribution between polar and non-polar environments in the RTIL could enhance the initial fast decay of the solvent

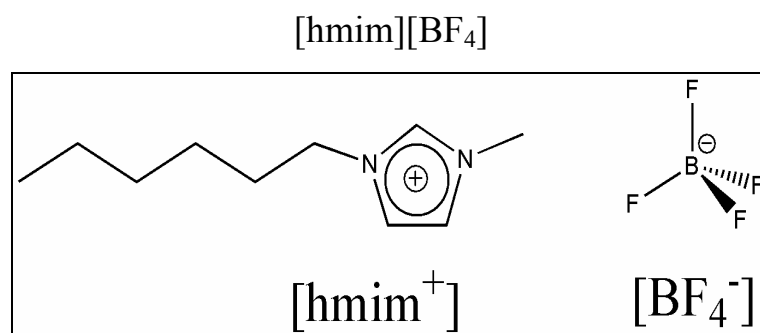
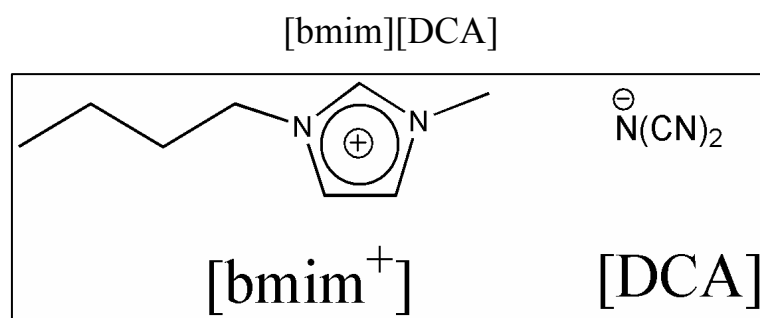
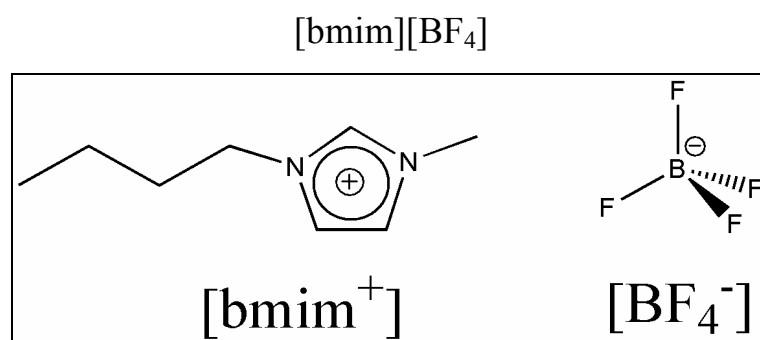
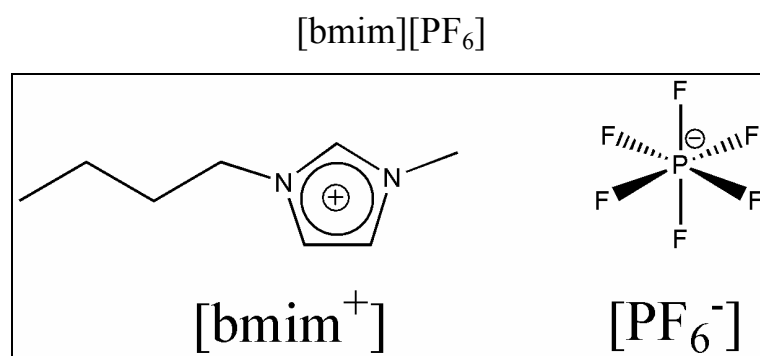


Figure 5.1: Room Temperature Ionic Liquids studied here.

response function as well as shorten the fast time constant. Interestingly, simulation studies of solvation dynamics in imidazolium ionic liquids predict larger amplitude of the fast component (30-75%) with a much shorter time constant (70 – 200 fs) than what have been observed in experiments.^{27-29, 33-36} Recently, solvation dynamics in ethylammonium nitrate have been calculated using the dielectric relaxation data of the solvent and a good agreement between the calculated results and experiments found.²³ However, recent continuum model calculations for several imidazolium ionic liquids indicate *disagreement* between theory (continuum model) and experiments.¹⁰ Note, however, that these attempts neither included the ion-ion and ion-solute static correlations nor could use the high resolution dielectric relaxation data for imidazolium liquids which are made available only recently.⁴³ One therefore wonders whether, just like observed earlier for dipolar solvents,⁴⁰⁻⁴² the success of such simple models for RTILs is also determined critically by the complete measurement of the dielectric relaxation and systematic inclusion of the relevant static correlations. Moreover, recent optical heterodyne-detected Raman-induced Kerr effect spectroscopic (OHD-RIKES) studies with several RTILs have revealed the presence of low frequency ($\sim 20 - 150 \text{ cm}^{-1}$) intermolecular librational modes.⁴⁴⁻⁴⁸ It would therefore be also interesting to investigate whether and to what extent these librational modes couple to the solvation dynamics and influences the initial part of the polar solvation energy relaxation in ionic liquids. This question becomes relevant as the low frequency intermolecular solvent modes have been found earlier to strongly influence the solvation dynamics and ionic mobility in amides and substituted amides.⁴⁹⁻⁵⁰

In this chapter, we investigate the solvation dynamics of three different probe molecules in several imidazolium ionic liquids for which the dielectric relaxation have been measured most recently by Stoppa *et al.*⁴³. These ionic liquids, shown in Fig. 5.1, are 1-N-butyl-3-N-methylimidazolium tetrafluoroborate, [bmim][BF₄], and its hexafluorophosphate, [bmim][PF₆], and dicyanamide, [bmim][DCA], and 1-N-hexyl-3-N-methylimidazolium tetrafluoroborate, [hmim][BF₄]. The most important aspect of this dielectric relaxation study⁴³ is that these data cover the dielectric dispersion due to intermolecular librations at terahertz (THz) frequencies in ionic liquids. Subsequently, the complete dielectric relaxation data for these RTILs have been used as input in an extended molecular hydrodynamic theory (EMHT) developed earlier for studying solvation dynamics and ionic mobility in polar

liquids.⁴¹⁻⁴² The solute parameters (such as dipole moment, diameter etc.) used in the calculation are those of the following probe molecules: coumarin 153 (C153), 4-aminophthalimide (4-AP) and trans-4-dimethylamino-4'-cyanostilbene (DCS). In addition, we have approximated the solvation process of a laser-excited probe molecule in RTIL as that in an effective dipolar medium,⁵¹ dipole moment of which is determined by the experimentally measured static dielectric constant.⁴³ The static correlations (solute-solvent and solvent-solvent) are then assumed to be given by the mean spherical approximation (MSA) theory with corrections both at the short and the long wavelength limits.⁵² Note, however, that the inaccurate description of the static correlations at molecular length scales by the MSA theory may not vitiate the qualitative understanding of solvation dynamics in these liquids as the polar solvation energy relaxation has been found to be dominated by the collective response of the system.⁴¹ Subsequently, we have investigated the effects of cation libration⁴⁴⁻⁴⁸ on solvation energy relaxation in imidazolium ionic liquids by sequentially switching off the fast components in the experimentally measured⁴³ dielectric relaxation data.

The main results of the chapter are as follows. For all the ionic liquids studied here, the calculated decay of the solvation response function ($S(t)$) is found to be biphasic with the slower component being non-exponential with time. It is also noticed that multi-exponential functions cannot adequately describe the calculated $S(t)$. The time constants associated with the calculated decay of $S(t)$ are found to be in the range of sub-picosecond and a few hundreds of picosecond, with β (stretching exponent) values (0.4 – 0.5) close to those observed in experiments. In addition, the theoretically predicted time constants are in semi-quantitative agreement with those in experiments and simulation studies. The average solvation times ($\langle\tau_s\rangle$) are, however, found to be smaller by a factor of ~ 2 than those in experiments, indicating that a slower mechanism in addition to those captured in the dielectric relaxation studies might be present in the system which has not been incorporated in the present study. The freezing of the translational motion of the effective solvent dipoles does not lead to any further slowing down of the dynamics as the translational motion in these high viscous solvents is already severely restricted. The theoretical results presented here also do not reveal any probe dependence as the parameters used in the calculation for describing the different probes vary slightly from each other. The present study also

reports dipolar solvation dynamics in two other room temperature ionic liquids, [bmim][DCA] and [hmim][BF₄], which should be tested against experiments.

The remaining part of the chapter is arranged as follows: In section 5.2 we give an overview of the theoretical formulation and discuss about the computational details. In section 5.3 we present the numerical results and compare with experimental data wherever possible. We study the probe dependence of solvation dynamics in these ionic liquids in section 5.4. The chapter then ends with concluding remarks in section 5.5.

5.2 Computational Details

The same EMHT^{41-42,53-54} described in chapter 2 has been used for studying the solvation dynamics for a dipolar solute in the aforementioned RTILs. In the EMHT the time dependent solvation energy for a dipolar solute is obtained from the density functional theory.⁴¹⁻⁴² Although the use of the density functional theory for ionic liquids may be inappropriate and should therefore be debated, the presence of dipolar interactions (in addition to the ionic interactions) in these liquids may allow one to follow the same approach as devised for normal dipolar solvents.⁴¹⁻⁴² Consequently, the time dependent fluctuating solvation energy for a dipolar solute (due to dipole-dipole interaction) in such an effectively dipolar medium becomes^{41,51}

$$\Delta E_{sol}(\mathbf{r}, \mathbf{\Omega}, t) = -k_B T \int d\mathbf{r}' d\mathbf{\Omega}' c_{sd}(\mathbf{r}, \mathbf{\Omega}; \mathbf{r}', \mathbf{\Omega}') \delta\rho_d(\mathbf{r}', \mathbf{\Omega}, t), \quad (5.1)$$

where $\Delta E_{sol}(\mathbf{r}, \mathbf{\Omega}, t)$ is the fluctuating solvation energy of a dipolar solute located at position \mathbf{r} with orientation $\mathbf{\Omega}$ at a time t . $c_{sd}(\mathbf{r}, \mathbf{\Omega}; \mathbf{r}', \mathbf{\Omega}')$ denotes the direct correlation function between the solute dipole and an effective solvent dipole at positions \mathbf{r} and \mathbf{r}' with orientations $\mathbf{\Omega}$ and $\mathbf{\Omega}'$, respectively. Then, a tedious but straightforward algebra leads to the following expression for the normalized solvation response function^{51,5}

$$S(t) = \frac{\int_0^{\infty} dk k^2 \left\{ |c_{sd}^{10}(k)|^2 \left[1 - \frac{1}{\varepsilon_L(k)} \right] L^{-1} [z + \Sigma_{10}(k, z)]^{-1} + 2 |c_{sd}^{11}(k)|^2 [\varepsilon_T(k) - 1] L^{-1} [z + \Sigma_{11}(k, z)]^{-1} \right\}}{\int_0^{\infty} dk k^2 \left\{ |c_{sd}^{10}(k)|^2 \left[1 - \frac{1}{\varepsilon_L(k)} \right] + 2 |c_{sd}^{11}(k)|^2 [\varepsilon_T(k) - 1] \right\}} \quad (5.2)$$

In the above equation (Eq. 5.2) $c_{sd}^{10}(k)$ and $c_{sd}^{11}(k)$ represent the longitudinal and transverse components of the wavenumber (k) dependent direct correlation function between the dipolar solute and an effective solvent dipole and has been calculated using mean spherical approximation (MSA) theory.⁵² $\varepsilon_L(k)$ and $\varepsilon_T(k)$ are the longitudinal and the transverse components of wavenumber dependent dielectric constant. These functions have been calculated by using the MSA model for a pure solvent with proper corrections at both $k \rightarrow 0$ and $k \rightarrow \infty$ limits $\Sigma_{10}(k, z)$ and $\Sigma_{11}(k, z)$ are the longitudinal ($l=1, m=0$) and transverse ($l=1, m=1$) components of the wavenumber and frequency (z) dependent generalized rate of solvent orientational polarization density relaxation, ($\Sigma_{lm}(k, z)$).^{41,53-54}

The expressions involved for the calculation of wavenumber and frequency dependent generalized rate of solvent polarization relaxation, $\Sigma_{lm}(k, z)$, are given in chapter 2 (section 2.3.1). It contains two dissipative kernels – the rotational kernel ($\Gamma_R(k, z)$) and the translational kernel ($\Gamma_T(k, z)$).^{41,53-54} The translational dissipative kernel, $\Gamma_T(k, z)$, has been calculated by using the isotropic dynamic structure factor of the effective dipolar medium while the rotational kernel $\Gamma_R(k, z)$ at $k \rightarrow 0$ limit is directly related to the experimentally determined frequency dependent dielectric function, $\varepsilon(z)$ of RTILs, measured recently by Stoppa *et al.* These authors⁴³ have performed dielectric relaxation experiment over the frequency range of 0.1 GHz – 3 THz. The measured dielectric relaxation data have been expressed as follows⁴³

$$\varepsilon(z) = \varepsilon_{\infty} + \frac{S_1}{[1 + (z\tau_1)^{1-\alpha_1}]^{\beta_1}} + \frac{S_2}{[1 + z\tau_2]} + \frac{S_3}{[1 + z\tau_3]} + \frac{S_4\Omega_4^2}{[\Omega_4^2 + z^2 + z\Gamma_4]} \quad (5.3)$$

Table 5.1: Dielectric relaxation parameters (from Ref. 43) used in the calculation of Solvation dynamics in RTILs

	[bmim][PF ₆]	[bmim][BF ₄]	[bmim][DCA]	[hmim][BF ₄]
ϵ_0	11.8	12.2	11.3	10.1
S_1	7.4	8.94	6.42	6.32
τ_1 (ps)	1406	1140	63.0	1322
α_1	0	0	0.33	0
β_1	0.37	0.21	1	0.27
S_2	0.45	0.37	0.75	0.18
τ_2 (ps)	38.8	73.1	2.09	42.6
S_3	0.81	1.15	0.94	1.46
τ_3 (ps)	1.26	0.389	0.240	0.331
S_4	1.38	0.70	1.04	0.69
$\nu_4 = \Omega_4 / 2\pi$ (THz)	2.77	2.85	3.68	2.4
$\gamma_4 = \Gamma_4 / 2\pi$ (THz)	7.77	4.85	6.37	2.47
ϵ_∞	2.10	1.06	2.13	1.47

Table 5.2: Solute and solvent parameters used in the calculation of solvation dynamics in RTILs at 298 K

RTIL	Diameter (Å)	Dipole-moment (Debye) ^(e)	Density (g/cc)	Viscosity (Poise)
[bmim][PF ₆] ^(a)	7.78	4.4	1.37	3.10
[bmim][BF ₄]	7.20	3.8	1.21	1.54
[bmim][DCA]	7.48	3.8	1.06	0.33
[hmim][BF ₄]	7.72	3.9	1.15	2.40
DCS ^(b)	7.8	20	-	-
C153 ^(c)	7.8	14	-	-
4-AP ^(d)	6.2	13.6	-	-

(a) The value of the dipole moment for [bmim⁺] shown here (obtained from static dielectric constant) is very close to value reported in the following work: H. Jin, B. O'Hare, J. Dong, S. Arzhantsev, G. A. Baker, J. F. Wishart, A. J. Benesi and M. Maroncelli, *J. Phys. Chem. B* **112**, 81 (2008).

(b) From the work: S. Arzhantsev, K. A. Zachariasse and M. Maroncelli, *J. Phys. Chem. A* **110**, 3454 (2006).

(c) From Ref. 40

(d) From the work: D. E. Wetzler, C. Chesta, R. Fernandez-Prini and P. F. Aramendia, *J. Phys. Chem. A* **106**, 2390 (2002).

(e) The values of the dipole moment of the solutes (C153, DCS and 4-AP) are those in the excited state.

where ε_∞ is the limiting value of $\varepsilon(z)$ at high frequency, τ_j the relaxation time for the S_j dispersion. The parameters α_1 and β_1 determine the shape of a relaxation spectrum. Ω_4 and Γ_4 denote respectively the resonance frequency and the damping constant for the contribution at the THz frequency that has been described using the damped harmonic oscillator model.⁴³ The dielectric relaxation fit parameters obtained by Stoppa *et al.*⁴³ are given in Table 5.1. Note that these data indicate that fastest modes present in the RTILs such as librations and intermolecular vibrations are responsible for dispersion amplitudes, S_2 , S_3 and S_4 . Therefore, availability of the full dielectric relaxation data allows us to investigate the effects of librational motion on solvation dynamics in room temperature ionic liquids which has not been done before.

The other solute (probe) and solvent parameters necessary for the calculation are summarized in Table 5.2, where solvent densities and viscosities are taken from experiments,¹ dipole moments calculated from the experimentally measured dielectric constants and diameters from the van der Waal's space filling model.

5.3 Results & Discussion

In this section we present numerical results on dipolar solvation dynamics of the following systems: (i) DCS in [bmim][PF₆], (ii) DCS in [bmim][BF₄], (iii) C153 in [bmim][PF₆] and (iv) 4-AP in [bmim][PF₆]. For all these probe – RTIL systems, the theoretical results have been compared with the available experimental data wherever possible. Dipolar solvation dynamics have been predicted for two other systems also, DCS in [bmim][DCA] and DCS in [hmim][BF₄], for which experimental results are not available yet. The solvation response function, $S(t)$, calculated by using the Eq. 5.2 then fitted to the following function

$$S(t) = a_1 \exp[-t/\tau_1] + a_2 \exp[-(t/\tau_2)^\beta] \quad (5.4)$$

where a_1 and a_2 are the amplitudes of the biphasic components constituting the total decay of normalized $S(t)$ so that $a_1 + a_2 = 1$. Analytical integration of Eq. 5.4 then

leads to the following expression for the average solvation time,

$$\langle \tau_s \rangle = a_1 \tau_1 + \frac{a_2 \tau_2}{\beta} \sqrt{1/\beta}.$$

5.3.1 DCS in [bmim][PF₆]

In Fig. 5.2 we show the decay of the solvation response function for DCS in [bmim][PF₆] calculated by using Eq. 5.2 (*solid lines*) and compare with the experimental results (*open circles*) of Arzhantsev and coworkers.⁸ It is evident from Fig. 5.2 that, as observed in experiments,⁸ the calculated decay of the solvation response function is indeed biphasic with two distinctly different time constants. In the same figure we also show the results of our investigation regarding the contributions of the librational and intermolecular vibrational modes to the solvation dynamics in ionic liquids. It is clear from this figure that calculation by considering all four of the experimentally measured dielectric dispersions in this solvent leads to the fastest decay (curve 4) of the solvation response function, whereas incorporation of only the slowest dispersion results a decay much slower (curve 1) than what has been observed in experiments.⁸ Systematic inclusion of two other dispersions in addition to the slowest one then makes the decay sequentially faster (curves 2 and 3) and closer to the experiments. This observation, therefore, indicates that, like in amide and substituted amides,⁴⁹⁻⁵⁰ the libration modes couple to the solvation dynamics in [bmim][PF₆], and the fast component of the polar solvation energy relaxation originates from such coupling.

As the calculated solvation response function is very sensitive to the quality of the dielectric relaxation data, the present theory provides an opportunity to investigate the effects of uncertainty associated with the estimates of various dispersion amplitudes⁴³ obtained through fit to the experimental dielectric relaxation data. The results of one such calculation for [bmim][PF₆] is also presented in the same figure (dashed line) where only the first three dispersions are considered along with $S_4 = 0.68$ and $\varepsilon_\infty = 2.1 + 0.7 = 2.8$. In the *inset* we show the decay of the solvation response function up to 5 ps where the calculated initial fast component of the solvation energy relaxation appears to agree quantitatively with that in experiments.⁸ The parameters required to fit the calculated decays by using Eq. 5.4 are summarized in Table 5.3 and an

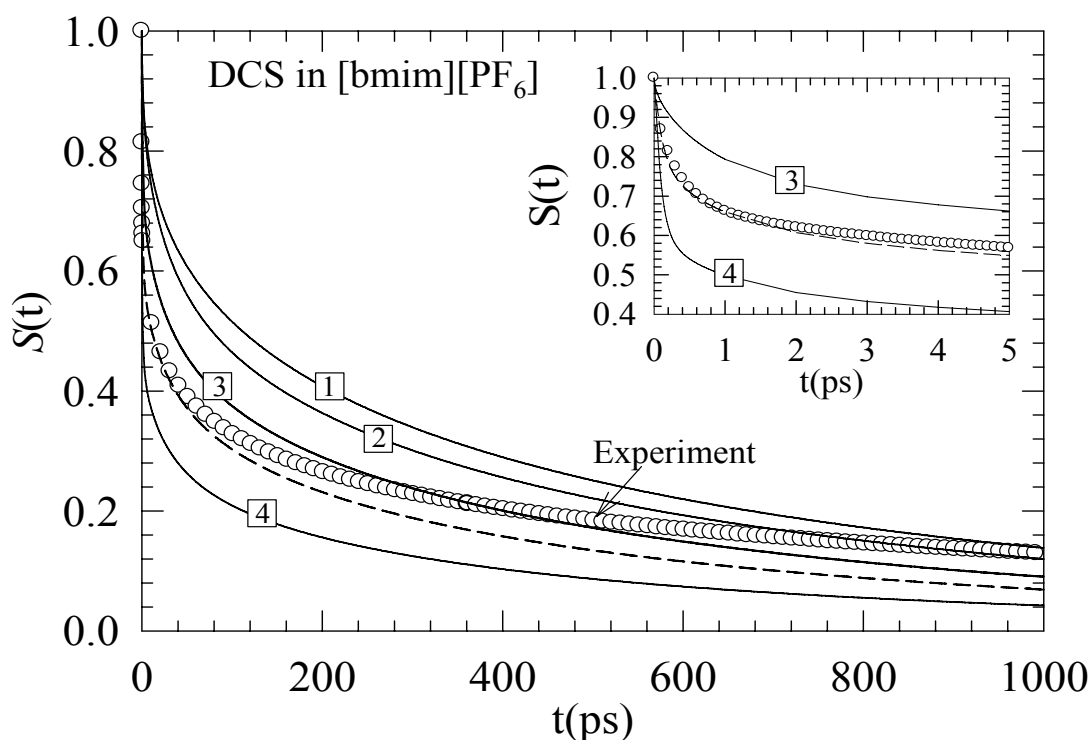


Figure 5.2: Comparison between the predicted decay (solid lines) of the solvation response function, $S(t)$ and that obtained from experiments (circles) for DCS in [bmim][PF₆]. The tags on the calculated curves represent the following: (i) ‘4’ - calculation with all the four dispersion steps reported by the experimental dielectric relaxation data by Stoppa *et al.*⁴³, (ii) ‘3’ - calculation with the first three dispersion steps (the fastest step, S_4 is switched off), (iii) ‘2’ - calculation with first two dispersion steps (S_3 and S_4 are switched off) and (iv) ‘1’ - calculation with only the slowest (S_1) dispersion. The *short dashed* line represents the theoretical prediction when the magnitude of fastest relaxation step (S_4) in dielectric relaxation (DR) data is tuned such that $S_4=0.68$ and $\varepsilon_\infty = 2.8$. *Inset:* Curves ‘3’, ‘4’ and the one obtained with the tuned DR data are presented in a smaller time window in order to show the comparison with experimental results at early times. For decay fit parameters see Table 5.3.

inspection to these data reveal that modification of ε_∞ and leaving out of the fastest dispersion leads not only the fast and slow time constants (τ_1 and τ_2 , respectively) but the stretching exponent (β) also to a good agreement with those obtained from experimental studies.⁸ However, the calculated τ_1 is moderately faster (212 fs) with slightly larger amplitude (24%) than those in experiments (330 fs and 19%).⁸ These

parameters along with ~30% larger β value (0.41 versus 0.31) give rise to average solvation time ($\langle\tau_s\rangle$) 300 ps, a value approximately 3 times less than that (1000 ps) in experiments.⁸ This disagreement is not unexpected given the fact that no attempt has been made in the present calculation to include the structural heterogeneity of the medium. Note also that the calculated τ_1 is agreeing well with that found in recent simulation studies of solvation dynamics in this ionic liquid.²⁷

Another feature to be noted in the theoretical study of solvation dynamics of DCS in [bmim][PF₆] is that calculations with any number of dispersions leads to non-exponential and biphasic decay of the solvation response function with time constants lying between ~100 – 900 fs and ~100-300 ps with β values in the range of 0.38 – 0.41. Interestingly, an initial fast time scale of 600 – 900 fs with ~10 % amplitude, which are comparable to those reported in a recent fluorescence up-conversion study of C153 in two other imidazolium based ionic liquids,²⁵ is obtained only after switching off the two higher frequency librational contributions in [bmim][PF₆]. Even though this switching off leads to higher values for β , the calculated values are still at least 1.5 times smaller than those reported in the above up-conversion experiments.²⁵ It is, however, to be recognized here that the side chains attached to the imidazolium unit and the counter ions are different in the ionic liquids used in the up-conversion study²⁵ and hence in the absence of complete dielectric relaxation data the present calculation cannot suggest anything about the degree of correctness of the up-conversion data in these ionic liquids.²⁵

5.3.2 DCS in [bmim][BF₄]

In Fig.5.3 we show the numerical results on solvation dynamics of DCS in another RTIL, [bmim][BF₄] and compared with the relevant experimental data.⁸ While the solid lines represent the theoretically predicted solvation response functions obtained after sequential addition of dielectric dispersion steps, the circles represent the experimental results of Arzhantsev and coworkers.⁸ As observed in [bmim][PF₆], the calculated solvation response function with any number of dispersions exhibits biphasic decay, even though the time constants become increasingly slower as the fast components in the dielectric relaxation data are switched off systematically (see Table

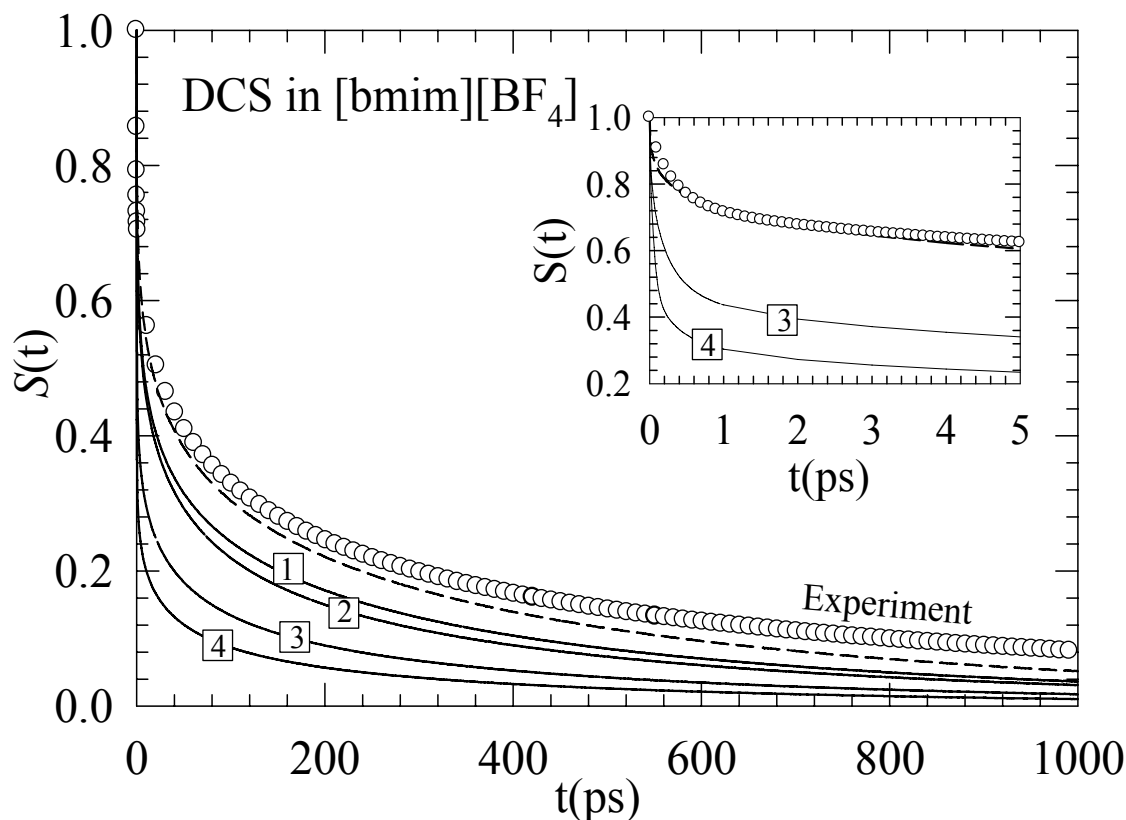


Figure 5.3: Comparison between the predicted decay (*solid lines*) of the solvation response function, $S(t)$ and that obtained from experiments (*circles*) for DCS in [bmim][BF₄]. The tags on the calculated curves represent the same protocol of the calculations as described in Fig. 5.2. The dashed line represents the calculation by considering only the slowest step (S_1) of the DR data but with a tuning to make $\varepsilon_1 = \varepsilon_\infty = 4.66$. Here again the *inset* shows the comparison between the theory and experiments at early times. The representations remain the same as in Fig. 5.2. The decay fit parameters are summarized in Table 5.3.

5.3). Note in Fig. 5.3 that, unlike in [bmim][PF₆], solvation dynamics in [bmim][BF₄] appears not to couple to the fast modes of the solvent. Moreover, use of only the slowest dispersion step in the dielectric relaxation data does not make the decay of the solvation response function as slow as that observed in experiments. The fit parameters summarized in Table 5.3 indicate that calculation even with only the slowest dispersion gives rise to the fast and slow time constants respectively four times and twice as small as those found in experiments, although the calculated

amplitudes are comparable. On the other hand, the total magnitude of spectral shift measured in the time resolved experiments⁸ does not indicate missing of any component faster than what has been detected. Then, the observed discrepancy between the theory and experiments could be due to either the enhanced heterogeneity in [bmim][BF₄], or, a small over-estimation of the dispersion amplitudes in the dielectric relaxation data of [bmim][BF₄].⁴³ Interestingly, the β_1 values reported by the dielectric relaxation experiments⁴³ seem to suggest that [bmim][BF₄] is more heterogeneous than [bmim][PF₆], which is, however, opposite to the trend found in solvation dynamics experiments in these two liquids.⁸

Subsequently, we have performed a test calculation by using *only* the slowest dispersion with its amplitude decreased by 1.4, leaving the relaxation time unchanged. That is, $\varepsilon_0(12.2) \rightarrow \varepsilon_1(4.66)$ with the Cole-Davidson relaxation time, $\tau_{CD} = 1140$ ps and the shape parameter, $\beta_1 = 0.21$.⁴³ The solvation response function thus calculated is shown by the dashed line in Fig. 5.3, which is agreeing semi-quantitatively with the experiments.⁶ In order to show the agreement at the initial time, we compare the results in a smaller time-window (upto 5 ps) in the *inset*. These results and the fit parameters given in Table 5.3 therefore suggests that a little tuning in the dielectric dispersion data is probably warranted for the agreement between theory and experiments on solvation dynamics in [[bmim][BF₄]. We of course mention that the observed decoupling of the calculated solvation dynamics from the librational and intermolecular vibrational modes in ionic liquids may originate from the fact that the present theory completely neglects the structural heterogeneity that characterizes these media. Therefore, the observed agreement upon tuning the dielectric relaxation data may not reveal the totally correct mechanism of the solvation dynamics in these room temperature ionic liquids.

5.3.3 C153 in [bmim][PF₆]

Next we present the results on solvation dynamics for C153 probe in [bmim][PF₆]. The calculated decays of the solvation response function with this probe in this ionic liquid is shown in Fig. 5.4 and compared with the relevant experimental results.⁶ It is evident from the figure that the experimental decay⁶ is much slower than the theory

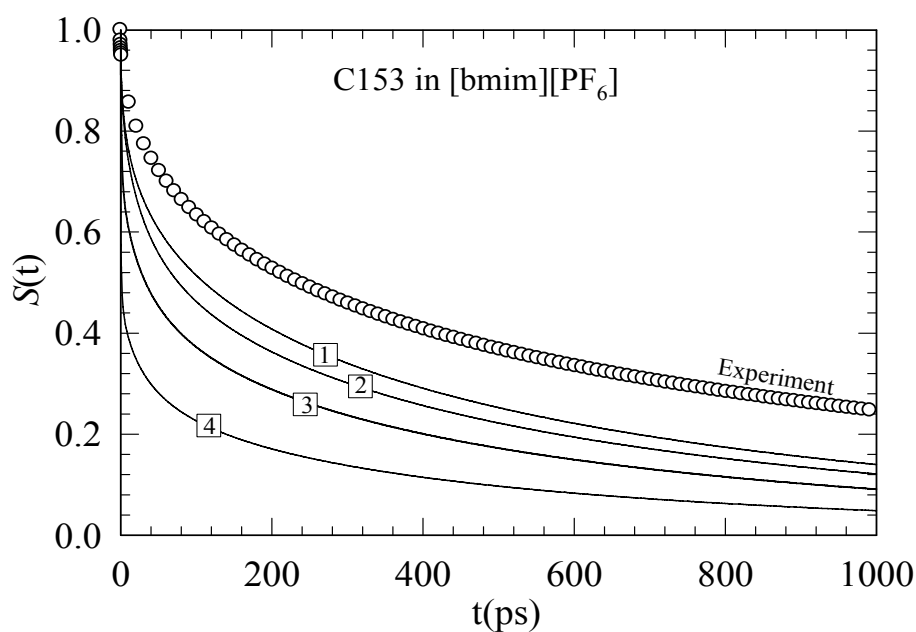


Figure 5.4: Comparison between the calculated and experimentally obtained decays of the solvation response function for C153 in [bmim][PF₆]. The representations remain the same in Fig. 5.2. Note here that a substantial fraction of the early dynamics has been missed in the experiment. Fit parameters are provided in Table 5.3.

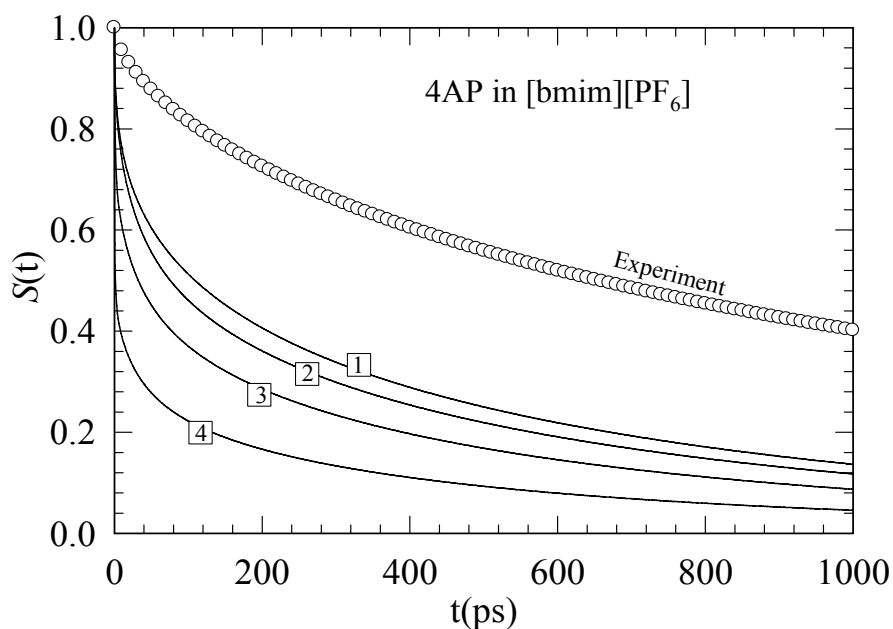


Figure 5.5: Solvation dynamics of 4-AP in [bmim][PF₆]. The representations remain the same as in Fig. 5.2. Note that ~60% of the total decay has been missed in the experiment. The fit parameters are given in Table 5.3. For discussion, see text.

even when the calculation is performed using only the slowest dispersion. Experimental studies with C153 have indicated that ~30% of the initial fast dynamics is missed due to the limited time resolution employed in the experiments.⁶ It is seen that when experiments are able to capture the complete solvation dynamics,⁸ a fast time constant of ~300 fs with ~20% amplitude is obtained and the rest is carried by a component with a time constant of 100-150 ps. The present calculation also reveals similar time scales in this ionic liquid, *albeit* with a little tuning in the dielectric relaxation data. Also, simulation studies²⁷ of C153 in [bmim][PF₆] suggests the presence of a fast component of amplitude ~10-20% with a time constant of ~200 fs. Furthermore, consideration of only the collective ($k\sigma \rightarrow 0$) mode of the solvent polarization relaxation obtained after using the tuned (as described in Fig. 5.3) dielectric relaxation data⁴³ can generate the biphasic decay with two time constants, one in the range of ~200 fs and the other ~50 ps, and a β value of 0.33 (see Table 5.3). Therefore, the existence of a fast component of amplitude ~10-20% with time constant in the range of 200 – 300 fs associated with the solvation dynamics of dipolar probes in imidazolium ionic liquids is well supported by the present calculations.

5.3.4 4-AP in [bmim][PF₆]

The calculated decays of the solvation response function for 4-AP probe in [bmim][PF₆] is shown in Fig. 5.5 and compared with the relevant experimental results.⁵ The fit parameters are given in Table 5.3. It is clear from the figure that like for C153 the experimental decay⁵ is much slower than the theory even when the calculation is performed using only the slowest dispersion. The calculated decay is biphasic for all the dispersion steps in DR data whereas the experiment data is best fitted with only a single stretched exponential. The time zero analysis shows that the missing component for 4-AP is ~60% which is larger than that for C153. However, the above studies indicate that one would expect an additional fast component when experiment is performed with better resolution⁸.

5.3.5 DCS in [bmim][DCA]

The calculated decays of solvation response function for DCS probe in a relatively low viscous ionic liquid, [bmim][DCA], is shown in Fig. 5.6 and the decay fit parameters are summarized in Table 5.3. Note that there is no experimental data available for this system for comparison. The calculated dynamics in [bmim][DCA] is predicted to be 4-5 times faster than its hexafluorophosphate analogue. However, the solvation dynamics in [bmim][BF₄] is found to be comparable with that in [bmim][DCA]. It is to be noted that [bmim][DCA] is different from the other three ionic liquids in the sense that it possesses the lowest density, smallest viscosity and fastest rotational relaxation times, along with a non-zero value for α_1 and the highest value for β_1 . Therefore, the time scale of solvation dynamics in [bmim][DCA] is expected to be different and this is also reflected in the present calculation. However, the calculated average solvation times in these RTILs do not scale linearly with the solvent viscosity which probably a manifestation of the strong structural heterogeneity that exists in these ionic liquids. Another interesting point that emerges from the predicted solvation dynamics in all these four ionic liquid is that the value of β (the stretching exponent in Eq. 5.4) becomes successively smaller as the fast components in the dielectric relaxation data are sequentially incorporated in the calculation (Table 5.3). This is in corroboration with the observations of Arzhantsev and coworkers⁸ who found that complete detection of faster dynamics led to the reduction in β values obtained earlier⁶ with broader time resolution.

5.3.6 DCS in [hmim][BF₄]

The predicted decay of solvation dynamic of solvation response function for DCS probe in [hmim][BF₄] is shown in Fig. 5.7. There is no experimental data available yet for this system also. Here also the calculated decay is biphasic for all the dispersion steps. Note that solvation dynamics in this ionic liquid is 2 times slower than that in [bmim][DCA].

5.4 Probe Dependence of Solvation Dynamics in RTILs

Next we turn our attention to the probe dependence of solvation dynamics in ionic liquids. Experimental studies of solvation dynamics in [bmim][PF₆] with different probe molecules such as DCS, C153 and 4-AP have revealed that the average

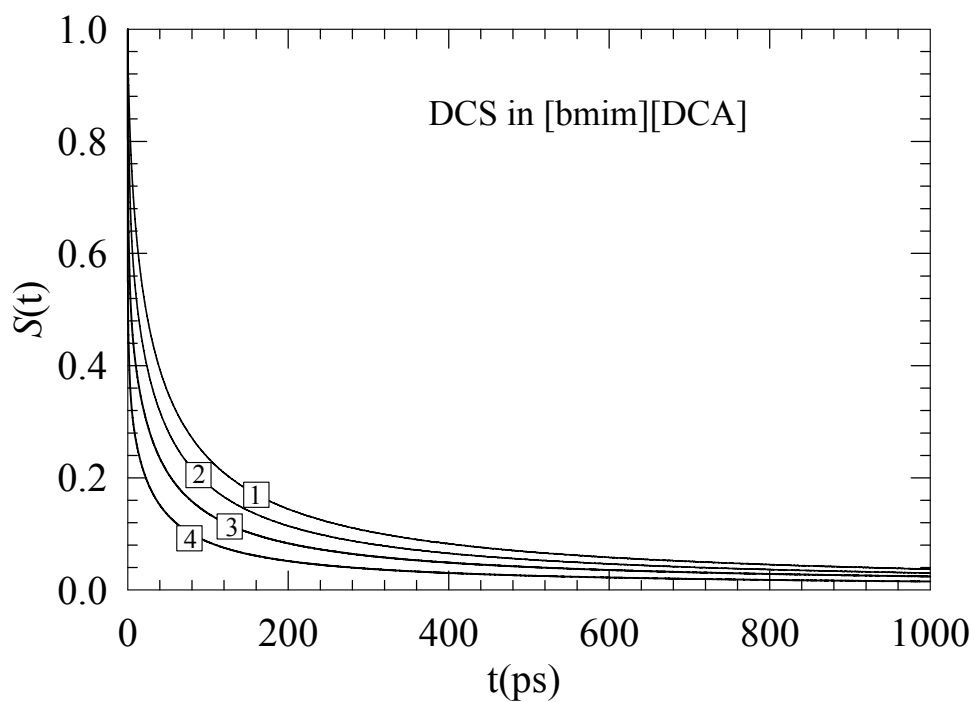


Figure 5.6: The decay of the solvation response function, $S(t)$, for DCS in [bmim][DCA]. Representations remain the same as in Fig. 5.2.

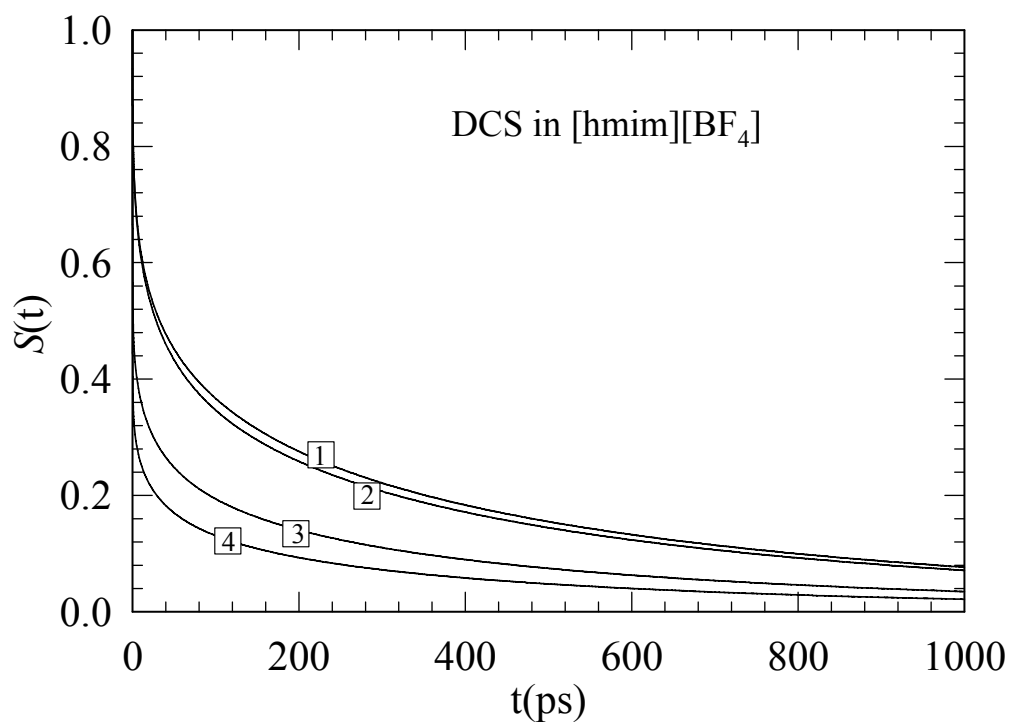


Figure 5.7: The decay of the solvation response function, $S(t)$, for DCS in [hmim][BF₄]. Representations remain the same as in Fig. 5.2.

Table 5.3: Fit parameters required to describe the calculated and experimental $S(t)$

System	Type of Study	a_1	τ_1 (ps)	a_2	τ_2 (ps)	β	$\langle \tau_s \rangle$ (ns)
DCS in [bmim][PF ₆]	Theory						
	1	0.09	0.78	0.91	308	0.52	0.51
	2	0.07	0.90	0.93	224	0.47	0.47
	3	0.21	0.82	0.79	197	0.46	0.4
	4	0.40	0.13	0.60	87	0.38	0.2
	Tuned DR data with 4 dispersion steps	0.24	0.21	0.76	126	0.41	0.3
	4 dispersion steps but only $k\sigma \rightarrow 0$ mode	0.31	0.19	0.69	32	0.33	0.13
Experiment (Ref. 8)	0.19	0.33	0.81	140	0.31	1.0	
DCS in [bmim][BF ₄]	Theory						
	1	0.17	0.09	0.83	56	0.38	0.18
	2	0.15	0.08	0.85	43	0.37	0.16
	3	0.35	0.13	0.65	23	0.33	0.1
	4	0.51	0.07	0.49	16	0.31	0.06
	Tuned DR data with the slowest dispersion step	0.15	0.10	0.85	92	0.41	0.23
	Experiment (Ref. 8)	0.19	0.32	0.81	130	0.41	0.34
C153 in [bmim][PF ₆]	Theory						
	1	0.10	0.79	0.90	310	0.52	0.52
	2	0.07	0.94	0.93	224	0.46	0.49
	3	0.21	0.83	0.79	195	0.46	0.37
	4	0.39	0.13	0.61	101	0.39	0.22
	Experiment (Ref. 6)	-	-	1.00	500	0.49	1.0
4AP in [bmim][PF ₆]	Theory						
	1	0.11	0.81	0.89	312	0.52	0.52
	2	0.07	0.91	0.93	225	0.47	0.47
	3	0.22	0.81	0.78	193	0.46	0.35
	4	0.39	0.13	0.61	96	0.39	0.20
	Experiment (Ref. 5)	-	-	1.00	1150	0.65	1.6
DCS in [bmim][DCA]	Theory						
	1	0.33	24.6	0.67	81	0.45	0.14
	2	0.27	11.6	0.73	49	0.41	0.11
	3	0.15	0.61	0.85	20	0.35	0.08
	4	0.31	0.08	0.69	11	0.32	0.05
DCS in [hmim][BF ₄]	Theory						
	1	0.13	0.22	0.87	142	0.45	0.30
	2	0.11	0.19	0.89	119	0.43	0.29
	3	0.44	0.18	0.56	88	0.42	0.15
	4	0.58	0.09	0.42	66	0.39	0.1

solvation time varies by approximately a factor of 2 among these probes, a result obtained from experimental data where a significant portion of the early dynamics has been missed.⁶ The present theory does not predict such a probe dependence for [bmim][PF₆] as the average solvation times calculated with a given number of dispersion steps (see Table 5.3) remain largely *insensitive* to the identity of these probes. As the amplitudes and time constants associated with the biphasic decay of the calculated solvation response function are not too different due to small variations in the probe parameters (Table 5.2), the average solvation time exhibits almost complete independence from the nature of the probe used in this study. Similar probe dependence has also been predicted for solvation dynamics in dipolar solvents at ambient condition because of the dominance of the collective ($k\sigma \rightarrow 0$) mode of the solvent polarization relaxation.⁴¹

5.5 Conclusion

Solvation dynamics of different dipolar probes in four imidazolium cation based ionic liquids have been studied using a molecular hydrodynamic theory where the most recent dielectric relaxation data⁴³ have been used as input. The present theory models these ionic liquids as effective dipolar media whose dipole moments are obtained from the experimentally measured static dielectric constants. While the static probe-solvent and solvent-solvent correlations required for the calculation have been obtained from the MSA with corrections at both the short and long wavelength limits, the present theory does not include the structural heterogeneity that originates from the relatively longer-ranged ion-ion interactions in these liquids. The solution heterogeneity is also reflected in several studies^{38-39,48,56} that report formation of polar and non-polar regions through tail aggregation. In heterogeneous systems, the molecular correlation is known to extend over longer range⁵⁷ (beyond a couple of molecular diameters) which, in turn, makes the structural relaxation sluggish. The use of dipolar MSA in such systems would always underestimate the static correlations because such simple models are useful for homogeneous liquids. Since ion-solvent and solvent-solvent static correlations are important inputs in the present theory, any underestimation of these correlations would make the polar solvation energy relaxation faster than what should be in the presence of proper enhanced correlations. This is probably one of the reasons that the theoretically predicted solvation response

functions are uniformly faster than those observed in experiments. Nonetheless, it is interesting to see that even with a simplified model, the present theory can predict the experimentally observed biphasic dynamics where the calculated time scales are in semi-quantitative agreement with those from experiments and simulation studies. The reason for this success of this effective medium calculation is probably due to the dominance of the long wavelength ($k\sigma \rightarrow 0$) polarization fluctuation and the use of the complete experimental dielectric relaxation data. The success of the present molecular theory in predicting solvation dynamics and ionic mobility in polar solvents have also been traced earlier to the above factors. Hence, we believe and also predicted already by Petrich and coworkers²⁷ that the use of complete dielectric relaxation data can lead to the understanding of the essential features of the polar solvation dynamics in ionic liquids. We have also presented theoretical results on solvation dynamics in two ionic liquids for which experimental data are not available yet. These predictions should be tested against experiments.

We would like to mention here that the discrepancy between theory and experiment can also come from the inaccuracy⁵⁸ in the dielectric data of Stoppa *et al.*⁴³ For instance, when a Cole-Davidson relaxation is used for the slowest mode, one obtains an unexpected increase of static permittivity with temperature.⁵⁸ If a Cole-Cole relaxation is used, the expected decrease of static permittivity with increasing temperature is found. Therefore, the use of these models in fitting the dielectric relaxation data of these liquids requires further work as the experimental accuracy below 1 GHz is too limited (here the dominating conductivity contribution swamps the "dielectric" signal).⁵⁸

The present calculations also show that the solvent fast modes such as libration and intermolecular vibrations may or may not couple completely to the polar solvation dynamics in the room temperature ionic liquids studied here. We would also like to mention here that the present theory will not be able to predict the solvation dynamics in ionic liquids where the frequency dependent dielectric function, $\varepsilon(z)$ would be close to $\varepsilon(\infty)$ for all frequencies. In such systems, the solvation dynamics would be closer to non-polar solvation dynamics where the translational motions, rather than the ion rotations, would account for the relaxation time scales.⁵⁹⁻⁶⁰ One therefore

requires two different theories, where the different interactions would be consistently incorporated while properly calculating the static correlations in order to investigate the solvation dynamics in these inherently heterogeneous systems. That would definitely be a challenging task.

References and Notes

1. R. D. Rogers and K. R. Seddon, *Ionic Liquids: Industrial Application for Green Chemistry*, American Chemical Society Symposium Series 818, American Chemical Society: Washington, DC, 2002.
2. P. Wasserscheid and T. Welton, *Ionic Liquids in synthesis*; Wiley-VCH: New York, 2003.
3. R. Karamkar and A. Samanta, *J. Phys. Chem. A* **106**, 4447 (2002).
4. R. Karamkar and A. Samanta, *J. Phys. Chem. A* **106**, 6670 (2002).
5. J. A. Ingram, R. S. Moog, N. Ito, R. Biswas and M. Maroncelli, *J. Phys. Chem. B* **107**, 5926 (2003).
6. N. Ito, S. Arzhantsev and M. Maroncelli, *Chem. Phys. Lett.*, **396**, 83 (2004).
7. H. Jin, B. O'Hare, J. Dong, S. Arzhantsev, G. A. Baker, J. F. Wishart, A. J. Benesi and M. Maroncelli, *J. Phys. Chem. B* **112**, 81 (2008).
8. S. Arzhantsev, H. Jin, G. A. Baker and M. Maroncelli, *J. Phys. Chem. B* **111**, 4978 (2007).
9. H. Jin, X. Li and M. Maroncelli, *J. Phys. Chem. B* **111**, 13473 (2007).
10. H. Jin, G. A. Baker, S. Arzhantsev, J. Dong and M. Maroncelli, *J. Phys. Chem. B* **111**, 7291 (2007).
11. A. Paul and A. Samanta, *J. Phys. Chem. B* **111**, 4724 (2007).
12. A. Paul and A. Samanta, *J. Phys. Chem. B* **111**, 1957 (2007).
13. A. Samanta, *J. Phys. Chem. B* **110**, 13704 (2006).
14. P. K. Mandal and A. Samanta, *J. Phys. Chem. B* **109**, 15172 (2005).
15. P. K. Mandal, M. Sarkar and A. Samanta, *J. Phys. Chem. B* **108**, 9048 (2004).
16. R. Karamkar and A. Samanta, *J. Phys. Chem. A* **107**, 7340 (2003).
17. D. Chakrabarty, A. Chakraborty, D. Seth and N. Sarkar, *J. Phys. Chem. A* **109**, 1764 (2005).
18. A. Chakraborty, D. Seth, D. Chakrabarty, P. Setua and N. Sarkar, *J. Phys. Chem. A* **109**, 11110 (2005).
19. D. Chakrabarty, P. Hazra, A. Chakraborty, D. Seth and N. Sarkar, *Chem. Phys. Lett.* **381**, 697 (2003).
20. A. Adhikari, K. Sahu, S. Dey, S. Ghose, U. Mandal and K. Bhattacharyya, *J. Phys. Chem. B* **111**, 12809 (2007).
21. A. Adhikari, S. Dey, D. Das, U. Mandal, S. Ghose and K. Bhattacharyya, *J.*

- Phys. Chem. B **112**, 6350 (2008).
22. P. K. Chowdhury, M. Halder, L. Sanders, T. Calhoun, J. L. Anderson, D. W. Armstrong, X. Song and J. W. Petrich, J. Phys. Chem. B **108**, 10245 (2004).
23. M. Halder, L. S. Headley, P. Mukherjee, X. Song and J. W. Petrich, J. Phys. Chem. A **110**, 8623(2006).
24. P. Mukherjee, J. A. Crank, M. Halder, D. W. Armstrong and J. W. Petrich, J. Phys. Chem. A **110**, 10725 (2006).
25. B. Lang, G. Angulo and E. Vauthey, J. Phys. Chem. A **110**, 7028 (2006).
26. N. Ito and R. Richert, J. Phys. Chem. B **111**, 5016 (2007).
27. M. N. Kobrak, J. Chem. Phys. **125**, 064502 (2006).
28. M. N. Kobrak and V. Znamenskiy, Chem. Phys. Lett. **395**, 127 (2004).
29. M. N. Kobrak, J. Chem. Phys. **127**, 184507 (2007).
30. C. Pinilla, M. G. Del Popolo, R. M. Lynden-Bell, and J. Kohanoff, J. Phys. Chem. B **109**, 17922 (2005).
31. M. G. Del Popolo, R. M. Lynden-Bell, and J. Kohanoff, J. Phys. Chem. B **109**, 5895 (2005).
32. M. G. Del Popolo, J. Kohanoff, R. M. Lynden-Bell and C. Pinilla, Acc. Chem. Res. **40**, 1156 (2007).
33. Y. Shim, D. Jeong, S. Manjari, M. Y. Choi and H. J. Kim, Acc. Chem. Res. **40**, 1130 (2007).
34. Y. Shim, J. Duan, M. Y. Choi and H. J. Kim, J. Chem. Phys. **119**, 6411 (2003).
35. Y. Shim, Choi, M. Y. Choi and H. J. Kim, J. Chem. Phys. **122**, 044511 (2005).
36. D. Jeong, M. Y. Choi, Y. J. Jung and H. J. Kim, J. Chem. Phys. **128**, 174504 (2008).
37. B. L. Bhargava and S. Balasubramanian, J. Chem. Phys. **123**, 144505 (2005).
38. G. Raabe and J. Kohler, J. Chem. Phys. **128**, 154509 (2008).
39. T. I. Morrow and E. J. Maginn, J. Phys. Chem. B **106**, 12807 (2002).
40. M. L. Horng, J. Gardecki, A. Papazyan and M. Maroncelli, J. Phys. Chem. **99**, 17311 (1995).
41. B. Bagchi and R. Biswas, Adv. Chem. Phys. **109**, 207 (1999).
42. B. Bagchi and A. Chandra, Adv. Chem. Phys. **80**, 1 (1991).
43. A. Stoppa, J. Hunger, R. Buchner, G. Hefter, A. Thoman and H. Helm, J. Phys. Chem. B **112**, 4854 (2008).
44. G. Giraud, C. M. Gordon, I. R. Dunkin and K. Wynne, J. Chem. Phys. **119**, 464

- (2003).
45. H. Shirota, A. M. Funston, J. F. Wishart and E. W. Jr. Castner, *J. Chem. Phys.* **122**, 184512 (2005).
 46. H. Shirota and E. W. Castner Jr., *J. Phys. Chem. A* **109**, 9388 (2005).
 47. H. Shirota and E. W. Castner Jr., *J. Phys. Chem. B* **109**, 21576 (2005).
 48. B. -R. Hyun, S. V. Dzyuba, R. A. Bartsch and E. L. Quitevis, *J. Phys. Chem. A* **106**, 7579 (2002).
 49. H. K. Kashyap, T. Pradhan and R. Biswas, *J. Chem. Phys.* **125**, 174506 (2006).
 50. B. Bagchi and R. Biswas, *J. Phys. Chem.* **100**, 1238 (1996).
 51. H. K. Kashyap and R. Biswas, *J. Phys. Chem. B* **112**, 12431 (2008).
 52. C. G. Grey and K. E. Gubbins, *Theory of Molecular Fluids*, Vol. I, Oxford University: Oxford, 1984.
 53. S. Roy and B. Bagchi, *J. Chem. Phys.* **98**, 1310 (1993).
 54. S. Roy and B. Bagchi, *J. Chem. Phys.* **99**, 9938 (1993).
 55. Eq. 5.2 is obtained by using the following expression for the normalized solvation energy correlation function: $S_E(t) = \frac{\langle \Delta E_{sol}(t) \Delta E_{sol}(0) \rangle}{\langle |\Delta E_{sol}(0)|^2 \rangle}$. Note that while $S_E(t)$ is an equilibrium correlation function, $S(t)$ constructed from the frequency of time resolved fluorescence emission spectra is a non-equilibrium correlation function. Within the linear response regime, $S(t)$ is assumed to be the equivalent of $S_E(t)$. See the relevant discussions in Refs. 41 and 42.
 56. Y. Wang and G. A. Voth, *J. Am. Chem. Soc.* **127**, 12192 (2005).
 57. J. P. Hensen and I. R. McDonald, *Theory of Simple Liquids*, Academic Press: San Diego, CA, 1986.
 58. R. Buchner, Private communication.
 59. E. Bart, A. Meltsin and D. Huppert, *J. Phys. Chem.* **98**, 3295 (1994).
 60. E. Bart, A. Meltsin and D. Huppert, *J. Phys. Chem.* **98**, 10819 (1994).

Chapter 6

Solvation Dynamics in Room Temperature Ionic Liquids: Role of Dipole-dipole and Dipole-ion Interactions

6.1 Introduction

In the previous chapter, we used a molecular hydrodynamic theory to study the solvation dynamics of a dipolar solute probe in a few imidazolium ionic liquids where, along with the solute-solvent and solvent-solvent static correlations, the most recent dielectric relaxation data¹ were used as inputs. The ionic liquid was modelled as an effective dipolar medium and the calculated decay was found to be biphasic with a strongly non-exponential slow component. Even-though the consideration of dipole-dipole interactions alone in the above work could successfully predict the biphasic dynamics observed experimentally for several imidazolium ionic liquids, all the calculated time constants were found to be uniformly smaller than the experimental² ones. Also, the non-exponential component accompanied a stretching exponent (β) whose value ranged between 0.3 – 0.5.² Note these β values are much smaller than what was found in solvation dynamics studies of fused inorganic salts at elevated temperatures.³⁻⁴ The emergence of the stretching exponent was attributed to the microscopic heterogeneity in RTILs due to domain formation via the interactions among the alkyl groups attached to the cations.⁵⁻¹¹ Consequently, the calculated

average solvation times ($\langle \tau_s \rangle = \int_0^{\infty} dt S(t)$) were much smaller than the experimental

values. This definitely indicates that the solvation dynamics in these ionic liquids is not completely controlled by the rate of the orientational polarization density relaxation as envisaged in our earlier work (chapter 5) but a slower relaxation channel is also operative through which a certain fraction of solvation energy relaxes. It is therefore natural to link the ion density relaxation, arising due to dipole-ion

interaction between solute dipole and solvent charge, to the relatively slower decay of the experimentally measured solvation response function.

In addition, when a dye molecule of relatively shorter excited state life time such as DCS (life time ~ 1.5 ns) was used,² a dynamic Stokes shift of ~ 4000 cm^{-1} was detected which is twice than that observed with probes such as C153 and 4-AP¹²⁻¹³ (life time ~ 6 ns). This immediately leads to the following questions:

- (a) What is the source of such a large dynamical Stokes shift in these weakly polar ionic liquids whose average dielectric constants (ϵ_0) lie in the range of 10–15 ?
- (b) What is the correct magnitude of dynamical Stokes shift for a given ionic liquid that originates *purely* from the time dependent rearrangement of solvent molecules around an excited dipolar solute ?

In time resolved experiments¹²⁻¹⁷ $\nu(0) - \nu(\infty)$, also known as dynamic Stokes' shift ($\Delta\nu'$), represents the total amount of spectral shift induced by the solvent rearrangement, magnitude of which is determined by the difference between the interactions of the excited solute with the initial ($t = 0$) and final ($t = \infty$) solvent configurations. The solvation response function describes how the normalized $\Delta\nu'$ decays from unity to zero as $\nu(t)$ approaches $\nu(\infty)$ with time. It is then expected that while the nature of the solute-solvent interaction determines the magnitude of $\Delta\nu'$, the coupling of solute-solvent interaction with the inherent solvent dynamics dictates the time evolution of the Stokes' shift. In many room temperature ionic liquids (RTIL) where at least one of the constituent ions possesses permanent dipole moment, the solute-solvent interactions will have two major components. For a dipolar solute, these are dipolar solute – dipolar ion (dipole-dipole) and dipolar solute-ion (dipole-ion) interactions. Solute-solute interactions are usually ignored because in experiments solutes are used as 'probes' at very low concentrations ($\sim 10^{-5} - 10^{-7}$ mol/lit).^{2,17-18} Conventional time-resolved measurements, however, cannot separate out these contributions. Since the solvent reorganization energy is an important input for the calculation of electron transfer rate using the Marcus theory, this becomes a relevant issue in understanding electron transfer reaction¹⁹ in this class of liquids.

Therefore, the detail investigation of different roles played by these interactions in determining the solvation time scales as well as $\Delta\nu'$ in these liquids is crucial.

Recently, conductivity data for several dipolar ionic liquids have been analyzed by using the much celebrated Nernst-Einstein equation and provides useful information regarding the degree of dissociation of these molten salts in liquid state at room temperature.²⁰⁻²² This motivates us to model dipolar ionic liquid as an electrolyte solution in a solvent of appropriate average polarity (ϵ_0). The dipolar ionic liquids that have been considered are 1-N-butyl-3-N-methylimidazolium tetrafluoroborate, [bmim][BF₄], and its hexafluorophosphate, [bmim][PF₆], and dicyanamide, [bmim][DCA], and 1-N-hexyl-3-N-methylimidazolium tetrafluoroborate, [hmim][BF₄]. The choice of these liquids stems from the fact that nearly accurate dielectric relaxation data over a broad frequency range for these liquids are recently made available¹. In addition, complete measurement of solvation dynamics of several of these liquids have been performed in recent times which facilitates a direct comparison with the predictions from the present theory.²

As before, we use the classical density functional theory²³⁻²⁴ (DFT) to obtain the expression for the total time dependent solvation energy for a solute due to ions and dipoles that surrounds it in solution. This treatment leads to the total time dependent solvation energy as a sum of contributions coming from the dipole-dipole and dipole-ion interactions. Subsequently, an expression for the total solvation energy auto-correlation function is derived assuming that the fluctuating time scales of dipole and ion polarization densities are completely decoupled from each other. This is true for electrolyte solutions in *fast* solvents where the relaxation of dipolar part is completely decoupled from that of ionic contribution. We use the mean spherical approximation (MSA) model to calculate the wavenumber (k) dependent solute-solvent static correlations whereas the wavenumber dependent solute-ion static correlations have been approximated by its mean field value. The solvent-solvent dipolar static correlations are also obtained from the MSA model after correcting both at $k \rightarrow 0$ and $k \rightarrow \infty$ limits. The ion-ion static correlations have been obtained from the works of Attard *et al.* While the solvent orientational dynamic structure factor has been calculated from the dielectric relaxation data as done previously for pure dipolar

solvents,²³⁻²⁶ the ion dynamic structure factor has been obtained by considering only the diffusive dynamics. Note here that consideration of the full dynamics that includes the inertial translational motion of the ions did not induce any change in the calculated time scales for these highly viscous liquids.

In this chapter, we describe a molecular theory that includes both dipole-dipole and dipole-ion interactions which provides a more general framework for studying solvation dynamics in imidazolium and phosphonium ionic liquids. The above dipolar RTILs are again considered in this work in order to study the effects of dipole-ion interaction. The phosphonium ionic liquids we study here are trihexyl(tetradecyl)phosphonium chloride, $[\text{P}(\text{C}_6)_3\text{C}_{14}][\text{Cl}]$, bromide, $[\text{P}(\text{C}_6)_3\text{C}_{14}][\text{Br}]$ and tetrafluoroborate $[\text{P}(\text{C}_6)_3\text{C}_{14}][\text{BF}_4]$. We treat these phosphonium ionic liquids as ‘non-dipolar’ ones since none of the ions constituting these liquids possesses permanent dipole moment. This distinguishes these liquids from the ‘dipolar’ imidazolium RTILs considered in this study in which at least one of the ions contains permanent dipole moment. This distinction may not be strictly correct as the alkylphosphonium cations can possess non-zero dipole moment due to the asymmetry in its structure.¹⁸ Unfortunately, nothing is known at this moment about the magnitude of the dipole moment characterizing these asymmetric ions as there is no study on this aspect of these phosphonium ionic liquids. It may, however, be logical to consider that asymmetry-induced dipole moment of the alkylphosphonium cation would be small compared to those in imidazolium ions, and, as a result, these phosphonium ionic liquids might be much less polar than the imidazolium ones. Treating the phosphonium liquids as ‘non-dipolar’ ones is based purely on this consideration and therefore the present study rather *loosely* classifies the imidazolium and phosphonium liquids into dipolar and non-dipolar categories. Suitable quantum chemical calculations and other relevant study should be carried out for phosphonium liquids in order to make a rigorous comparison of the polarity aspects with those of imidazolium ones so that the justifiability of categorizing these liquids into two different groups can be checked more rigorously. It may, however, be justifiable to say that dynamically this means while the orientational relaxation would govern the dynamics of one class of liquids (imidazolium ones), it would play much less important role for the other ones (phosphonium liquids). In addition to the classification (polar and non-dipolar ones) in such a manner, another advantage of studying these liquids emanates

from the possibility of checking the predictive power of the present theoretical formulation by comparing the calculations directly with the experiments as dynamic Stokes' shift have been measured for most of these liquids.^{2,18} Also, this would help testing the validity of the dynamic continuum model theories²⁷⁻²⁸ more rigorously.

The rest of the chapter is organized as follows. We describe the molecular theory in the next section where computational details are also discussed. The relevant part of the derivation is given in Appendix III. Numerical results are presented in section 6.3 where comparisons with relevant experimental data are also made. We then conclude the chapter in section 6.4.

6.2 The Molecular Theory

The microscopic theory presented here is a generalization of the molecular hydrodynamic theory developed earlier²³⁻²⁴ for studying solvation dynamics in conventional polar solvents and is based on the following simple model. The dipolar RTILs are assumed to be electrolyte solutions²⁹ of polar solvents where the dipolar interactions among the ions possessing permanent dipole moments produce the effective average dielectric constants³⁰ (ϵ_0). The non-dipolar RTILs are then the $\epsilon_0 = n_D^2$ (n_D being the refractive index) limit of this model. Note that such a limit ensures very large inverse Debye screening length (κ) and makes the interaction length scale much shorter than that expected on the basis of longer-ranged charge-charge interaction.³¹ As we shall see later, this has an important consequence on the solvation times scales in non-dipolar ionic liquids. For both types of liquids, electrolytes are characterized by effective ionic concentrations which could be determined from the ratios of the experimentally measured ionic conductivities and diffusivities.²⁰⁻²¹ Therefore, these ionic liquids consist of cations, anions and ion-pairs. A solute dissolved in such a medium then interacts with all these species and both the Stokes' shift and the solvation energy (of the solute) derive contributions from each of these different types of interactions.

6.2.1 Total Solvation Response Function, $S_E(t)$

With the above model we now briefly discuss the derivation of the expression for the time dependent solvation energy of a dipolar solute dissolved in a dipolar RTIL. For such a solute-RTIL combination, the main contributors are the dipole-dipole interaction between the solute and dipolar ionic species, and the dipole-ion interaction between the solute and the constituent ions. For dipolar ionic liquids, the interaction contribution between the solute and ion-pair (IP) is not treated separately because the concentration of ion-pair is much smaller than the dipolar and ionic species constituting the ionic liquid.²⁰⁻²¹ However, the effects of solute-IP interaction are indirectly incorporated via experimental dielectric relaxation data as inputs to the subsequent calculations. As done earlier,^{23-24,32-33} the position (\mathbf{r}), orientation ($\mathbf{\Omega}$) and time (t) dependent total solvation energy for a mobile dipolar solute is obtained by using the density functional theory (see Appendix III),

$$\begin{aligned}\Delta E_{total}(\mathbf{r}, \mathbf{\Omega}, t) &= -k_B T \rho_s(\mathbf{r}, \mathbf{\Omega}, t) \left[\int d\mathbf{r}' d\mathbf{\Omega}' c_{sd}(\mathbf{r}, \mathbf{\Omega}; \mathbf{r}', \mathbf{\Omega}') \delta\rho_d(\mathbf{r}', \mathbf{\Omega}'; t) + \sum_{\alpha=1}^2 \int d\mathbf{r}' c_{s\alpha}(\mathbf{r}, \mathbf{\Omega}; \mathbf{r}') \delta n_{\alpha}(\mathbf{r}', t) \right] \\ &= \Delta E_{sd}(\mathbf{r}, \mathbf{\Omega}, t) + \Delta E_{si}(\mathbf{r}, \mathbf{\Omega}, t)\end{aligned}\quad (6.1)$$

where $\rho_s(\mathbf{r}, \mathbf{\Omega}, t)$ is the position (\mathbf{r}), orientation ($\mathbf{\Omega}$) and time (t) dependent number density of the dissolved solute. In the above equation while $c_{sd}(\mathbf{r}, \mathbf{\Omega}; \mathbf{r}', \mathbf{\Omega}')$ denotes the direct correlation function (DCF) between a dipolar solute at position \mathbf{r} with orientation $\mathbf{\Omega}$ and a dipolar ion at \mathbf{r}' with $\mathbf{\Omega}'$, $c_{s\alpha}(\mathbf{r}, \mathbf{\Omega}; \mathbf{r}')$ represents that between a dipolar solute placed at \mathbf{r} with orientation $\mathbf{\Omega}$ and a charged species (ion) located at \mathbf{r}' . α denotes the type of ions (cation and anion) that are interacting with the solute. The fluctuations in dipolar density ($\delta\rho_d$) and ion density (δn_{α}) from the respective equilibrium bulk values are then defined as follows: $\delta\rho_d(\mathbf{r}, \mathbf{\Omega}) = \rho_d(\mathbf{r}, \mathbf{\Omega}) - \rho_d^0 / 4\pi$ and $\delta n_{\alpha}(\mathbf{r}) = n_{\alpha}(\mathbf{r}) - n_{\alpha}^0$. Note that the time dependence in the fluctuating total solvation energy, $\Delta E_{total}(\mathbf{r}, \mathbf{\Omega}, t)$, is introduced through the temporal modulation of the dipolar and ion density fluctuations,²³ $\delta\rho_d(\mathbf{r}, \mathbf{\Omega}, t)$ and $\delta n_{\alpha}(\mathbf{r}, t)$. Since the linear response approximation allows one to consider the fluctuation in densities either from the initial ($t = 0$) or final ($t = \infty$) state, the time dependent fluctuating total solvation energy $\Delta E_{total}(\mathbf{r}, \mathbf{\Omega}, t)$ may be expressed as Eq. 6.1. It is to be mentioned here that the

solute-solvent and solvent-solvent direct correlation functions are assumed to remain unchanged with time even-though $\delta\rho_d(\mathbf{r},\mathbf{\Omega},t)$ and $\delta n_\alpha(\mathbf{r},t)$ evolves with time.²³ This is equivalent to the approximation that the presence of the solute and its excitation induces a very weak perturbation to the liquid structure and hence both the statics and dynamics of the solution can be assumed to be that of the pure solvent (linear response). Therefore, within the mean field approximation, Eq. 6.1 is exact to the first order of the density fluctuation.²³ Note that the fluctuating solvation energy, $\Delta E_{total}(\mathbf{r},\mathbf{\Omega},t)$ consists of two separate fluctuating contributions: one due to the dipole-dipole interaction, $\Delta E_{sd}(\mathbf{r},\mathbf{\Omega},t)$ and other due to the dipole-ion interaction, $\Delta E_{si}(\mathbf{r},\mathbf{\Omega},t)$. This decomposition of total solvation energy is a direct consequence of assumption that the total solvation energy can be expressed as a sum of dipole-dipole and ion-dipole interaction contributions. An evidence of sort in favour of such simple summation can be found in dynamic Stokes' shift measurements of electrolyte solutions where the 'ionic' part was found to add to the 'pure' dipolar solvent component.³⁴

The expression for the fluctuating total solvation energy (fluctuation from the equilibrium value) auto-correlation function can then be written as follows,

$$\begin{aligned}
\langle \Delta E_{total}(t)\Delta E_{total}(t') \rangle &= \langle \Delta E_{sd}(t)\Delta E_{sd}(t') \rangle + \langle \Delta E_{sd}(t)\Delta E_{si}(t') \rangle \\
&\quad + \langle \Delta E_{si}(t)\Delta E_{sd}(t') \rangle + \langle \Delta E_{si}(t)\Delta E_{si}(t') \rangle \\
&= \langle \Delta E_{sd}(t)\Delta E_{sd}(t') \rangle + \langle \Delta E_{si}(t)\Delta E_{si}(t') \rangle \quad (6.2)
\end{aligned}$$

where the position and orientation dependencies of the variables are not shown explicitly in order to avoid crowding. The second equality in Eq. 6.2 follows from the approximation that the fluctuation of dipole density ($\delta\rho_d$) is much faster than that of ion density (δn_α) and hence the fluctuating dipole-dipole and ion-dipole contributions get uncorrelated from each other in the following manner:

$$\langle \Delta E_{sd}(t)\Delta E_{si}(t') \rangle = \langle \Delta E_{sd}(t) \rangle \langle \Delta E_{si}(t') \rangle \quad \text{and}$$

$\langle \Delta E_{si}(t)\Delta E_{sd}(t') \rangle = \langle \Delta E_{si}(t) \rangle \langle \Delta E_{sd}(t') \rangle$. Now each of the $\langle \Delta E_{sx} \rangle$ (x being d or i) terms become zero as it represents averaging of a randomly fluctuating (from

equilibrium value) quantity. As a result, both the cross-correlation terms, $\langle \Delta E_{sd}(t)\Delta E_{si}(t') \rangle$ and $\langle \Delta E_{si}(t)\Delta E_{sd}(t') \rangle$, vanish and the total solvation energy auto-correlation function simply becomes a sum of dipole-dipole and dipole-ion contributions. However, a note of caution here is that such a clear separation between the dipole-dipole and ion-dipole contributions may not exist in real systems and they may, in fact, be even strongly correlated. Fortunately, dynamic Stokes' shift measurements in electrolyte solutions³⁴ of several 'fast' polar solvents have indicated a considerable degree of decoupling between the ion dynamics and dipolar solvent dynamics where the observed separation is explained in terms of adiabatic adjustment of the faster dipolar solvent molecules to the fluctuations due to ion locations. Such a mechanism of decoupling between the dipole-dipole and ion-dipole contributions can be equally applicable here as the ionic liquids are modelled as electrolyte solutions in the present work.

The time dependence of the solvation energy relaxation is then followed in terms of the normalized solvation energy auto-correlation function (see Appendix III),

$$S_E(t) = \frac{\langle |\Delta E_{sd}(0)|^2 \rangle S_{sd}(t)}{\langle |\Delta E_{sd}(0)|^2 \rangle + \langle |\Delta E_{si}(0)|^2 \rangle} + \frac{\langle |\Delta E_{si}(0)|^2 \rangle S_{si}(t)}{\langle |\Delta E_{sd}(0)|^2 \rangle + \langle |\Delta E_{si}(0)|^2 \rangle} \quad (6.3)$$

where $S_{sx}(t)$ terms ($x = d$ or i) denote the normalized solvation energy auto-correlation functions due to solute-medium dipolar interaction ($S_{sd}(t)$) and solute-ion (dipole-ion) interaction ($S_{si}(t)$). Note that in Eq. (6.3) the individual normalized solvation energy auto-correlation functions contribute with a certain weight (as indicated by the prefactors) to the total normalized solvation energy auto-correlation function, $S_E(t)$. This means that $S_E(t)$ can decay via two separate channels where, even though the channel which is inherently fast would dominate the total decay, the average rate of the decay would be determined by the slowest of these two. In the limit of linear solvent response, $S_E(t)$ becomes equivalent to the experimentally measured spectral or solvation response function, $S(t)$. Hereafter, both these

quantities ($S_E(t)$ and $S(t)$) will be described as solvation response function in order to keep the subsequent discussion simple.

6.2.2 Solvation Response Function due to Solute Dipole and Solvent Dipole Interaction, $S_{sd}(t)$

Since the normalized solvation energy auto-correlation function due to the dipole-dipole interaction ($S_{sd}(t)$) has already been calculated in chapter 5 and discussed in detail elsewhere,³⁰ we write down only the relevant expression here,

$$S_{sd}(t) = \frac{\langle \Delta E_{sd}(t) \Delta E_{sd}(0) \rangle}{\langle |\Delta E_{sd}(0)|^2 \rangle} = \frac{P \int_0^\infty dk k^2 S_{solute}^{10}(k, t) |c_{sd}^{10}(k)|^2 S_{solvent}^{10}(k, t) + 2P \int_0^\infty dk k^2 S_{solute}^{11}(k, t) |c_{sd}^{11}(k)|^2 S_{solvent}^{11}(k, t)}{P \int_0^\infty dk k^2 S_{solute}^{10}(k) |c_{sd}^{10}(k)|^2 S_{solvent}^{10}(k) + 2P \int_0^\infty dk k^2 S_{solute}^{11}(k) |c_{sd}^{11}(k)|^2 S_{solvent}^{11}(k)} \quad (6.4)$$

where P denotes the prefactor, $2\rho_d^0 \left(\frac{k_B T}{2\pi} \right)^2$. In the above equation $c_{sd}^{lm}(k)$ represents the Fourier transform of the (l, m) component of the static correlation function between the solute and dipolar ionic liquid species, and $S_{solvent}^{lm}(k, t)$ is the same component of the orientational dynamic structure factor of the dipolar ionic liquid. $c_{sd}^{lm}(k)$ has been obtained by using the mean spherical approximation (MSA) theory for binary dipolar mixtures with one of the component (dipolar solute) at limiting concentration.^{35(a,b)} $S_{solvent}^{lm}(k, t)$ for these liquids has been calculated exactly in the same manner as that followed for common polar solvents described in chapter 2 and 5. This requires, as inputs, the orientational static structure factor, translational diffusion coefficient and the frequency dependent dielectric function of the dipolar RTIL. The use of experimental dielectric relaxation data¹ that span relaxation times ranging from a couple of hundred femtosecond to nanoseconds and also bear the signature of liquid heterogeneity, ensures the biphasic decay of solvation response functions in these dipolar ionic liquids. In the present calculation, the orientational static structure factor for the dipolar RTILs are obtained from the MSA model^{35(a)} with proper corrections at both $k \rightarrow 0$ and $k \rightarrow \infty$ limits. $S_{solute}^{lm}(k, t)$ denotes the (l, m)

component of solute self-dynamic structure factor which is assumed to be given by²⁴

$$S_{solute}^{lm}(k, t) = \frac{1}{4\pi} \exp\left[-\left(l(l+1)D_R^s + k^2 D_T^s\right)t\right].$$

The rotational (D_R^s) and translational (D_T^s) diffusion coefficients of the solute (assumed as spherical body) are obtained from liquid viscosity using the *stick* and *slip* boundary conditions, respectively. Interestingly, earlier studies of the effects of solute motion revealed that solute motions can significantly accelerate the rate of its own solvation in viscous polar liquids.³³ In ionic liquids, where the viscosity is even larger and slow structural relaxation plays a more important role, both the motions of the solute – particularly the rotational one – can have significant effects.

Note that the denominator of the above equation is the square of the excess solvation energy due to solute-solvent dipolar interactions evaluated at time zero ($\Delta E_{sd}(t=0)$) when the dipolar species have not started rearranging yet in response to a changed dipolar field. This excess solvation energy decays with time to zero at $t = \infty$ when the dipolar rearrangement becomes complete. Therefore, in the present theory, the square root of the denominator of Eq. (6.4) provides an estimate for the magnitude of the solvent induced dynamic Stokes shift that originates *only* from the dipolar interaction between the solute and dipolar ionic species. The dipole-dipole contribution to the total dynamical fluorescence Stokes shift is then $\sqrt{\langle |\Delta E_{sd}(0)|^2 \rangle}$.

6.2.3 Solvation Response Function due to Solute Dipole and Solvent

Charge (Ion) Interaction, $S_{si}(t)$

Following Eq. (6.1) the expression for the normalized dipole-ion solvation energy auto-correlation function can be written as²⁹

$$S_{si}(t) = \frac{\langle \Delta E_{si}(t) \Delta E_{si}(0) \rangle}{\langle |\Delta E_{si}(0)|^2 \rangle} = \frac{2 \left(\frac{k_B T}{2\pi} \right)^2 \sum_{\alpha, \beta} \sqrt{n_\alpha^0 n_\beta^0} \int_0^\infty dk k^2 S_{solute}^{10}(k, t) c_{s\alpha}^{10}(k) c_{s\beta}^{10}(-k) S_{\alpha\beta}^{ion}(k, t)}{2 \left(\frac{k_B T}{2\pi} \right)^2 \sum_{\alpha, \beta} \sqrt{n_\alpha^0 n_\beta^0} \int_0^\infty dk k^2 S_{solute}^{10}(k) c_{s\alpha}^{10}(k) c_{s\beta}^{10}(-k) S_{\alpha\beta}^{ion}(k)}$$

(6.5)

The derivation of Eq. (6.5) is discussed in Appendix III. $S_{\alpha\beta}^{ion}(k, t)$ is the partial isotropic ion dynamic structure factors and is assumed to be given by³⁶

$$S_{\alpha\beta}^{ion}(k, t) = S_{\alpha\beta}^{ion}(k) \exp[-D_\alpha k^2 t / S_{\alpha\alpha}(k)] = S_{\alpha\beta}^{ion}(k, t) \exp[-t/\tau_\alpha(k)] \quad (6.6)$$

where D_α , the diffusion coefficient of an ion of type α has been taken from experiments.^{22,37} For liquids where experimental data are not available, Stokes-Einstein relation with slip boundary condition is used to obtain D_α . $\tau_\alpha(k) = S_{\alpha\alpha}(k)/D_\alpha k^2$, denotes the wavenumber dependent relaxation time constant for the ion dynamic structure factor which controls the relaxation behaviour at a given wavenumber k . $S_{\alpha\alpha}(k)$ has been approximated by the Percus-Yevick (P-Y) solution of binary hard-sphere mixture.^{35(c)} We have assumed each of the ions as singly charged hard spheres with equal radii and used the expressions derived elsewhere³⁸⁻³⁹ for the calculation of ion static structure factor, $S_{\alpha\beta}^{ion}(k)$. The longitudinal component of the wavenumber dependent direct correlation function between the dipolar solute and ions, $c_{s\alpha}^{10}(k)$, is again calculated in the homogeneous limit and is taken as,²³⁻²⁴

$$c_{s\alpha}^{10}(k) = -\sqrt{\frac{4\pi}{3}} \left(\frac{4\pi i \mu_1 q_\alpha}{k_B T \epsilon_0 k} \right) \frac{\sin(kr_c)}{kr_c}, \text{ where } \mu_1 \text{ is the excited state dipole-moment of}$$

the dipolar solute, q_α the charge of α^{th} type ion, r_c the distance of the closest approach between the solute dipole and the ionic species. Note that the above calculation schemes for the ion-dipole and ion-ion static correlations do not consider at all the static heterogeneity that characterizes these systems. As a result, the signature of the medium heterogeneity is expected to be completely missing in the subsequent calculation of the ion-dipole interaction contribution to the total solvation energy relaxation. It should, however, be kept in mind that since $\tau_\alpha(k)$ depends on $S_{\alpha\alpha}(k)/k^2$, each contributing wavenumber to $S_{si}(t)$ would be associated with a different relaxation time. One therefore expects a distribution of time constant in the ion-dipole part of the solvation energy relaxation even if one does not consider explicitly the medium heterogeneity. However, description of $S_{\alpha\alpha}(k)$ via P-Y approximation weakens the distribution (due to the missing of the heterogeneity-

induced broadening of the static structure factor) and divides $\tau_a(k)$ ‘roughly’ into two groups - one large at collective wavelengths ($k\sigma \rightarrow 0$ limit) and the other small at nearest neighbour distances ($k\sigma \rightarrow 2\pi$ limit). This leads to the relaxation of $S_{st}(t)$ with *effectively* two different time constants. This will be discussed further when we present numerical results in section 6.3. We now just note that solvation energy due to solute-ion interaction (Eq. 6.5) decays with time constants mainly due to the relaxation of ion dynamic structure factor where translational motion of the ions induces the spectral shift. Therefore, the ion-solute contribution to the dynamical Stokes’ shift is given by $\sqrt{\langle |\Delta E_{st}(0)|^2 \rangle}$ which can be calculated easily from the denominator of Eq. 6.5.

6.3 Results & Discussion

6.3.1 Imidazolium Ionic Liquids: Stokes’ Shift and Dynamics

Let us first present the theoretical estimates of the total dynamical fluorescence Stokes’ shift ($\Delta\nu'$) for dipolar solute probes, DCS, C153 and 4-AP in [bmim][BF₄], [bmim][PF₆], [bmim][DCA], and [hmim][BF₄]. Table 6.1 summarizes the estimated total dynamical Stokes shifts, the separated out dipole-dipole and dipole-ion interaction contributions and the measured dynamic Stokes’ shifts in these dipolar RTILs. A comparison with experimental shifts² (last column, Table 6.1) immediately reveals that calculated shifts for C153 and 4-AP in [bmim][PF₆] are in quantitative agreement with experiments, whereas the calculated shifts for DCS are almost half of what have been measured in experiments. Besides this general observation, one also notices the following. For each of the solute + imidazolium ionic liquid combinations, the predicted $\Delta\nu'$ with solute’s excited state dipole moment (μ_1) from the AM1/CI calculations (~ 14 D)¹⁷ varies in a small range of ~ 2000 - 2300 cm⁻¹. Interestingly, the experimental shifts for C153 and 4-AP also show the similar variation.¹²⁻¹³ This small variation in dynamic Stokes’ shift for these solutes (DCS, C153 and 4-AP) in a given solvent is a reflection of some differences in their sizes and dipole moments. For example, a shift ($\Delta\nu'$) of ~ 2100 cm⁻¹ for DCS and C153 in [bmim][PF₆] can be attributed to their equal diameters ($\sigma_{DCS} = \sigma_{C153} = 7.8 \text{ \AA}$), whereas a relative

Table 6.1: Dynamic Stokes' shift ($\Delta\nu^t$) for several dipolar solutes in imidazolium ionic liquids at 298 K: Comparison between theory and experiments

System	μ_1 (Debye) ^(a)	Dipole-dipole contribution, $\Delta\nu_{sd}^t$ (cm^{-1})	Dipole-ion contribution, $\Delta\nu_{si}^t$ (cm^{-1})	Total ($\Delta\nu^t = \Delta\nu_{sd}^t$ + $\Delta\nu_{si}^t$) (cm^{-1})	Expt. (cm^{-1})
DCS in [bmim][PF ₆]	14.5	896	1262	2158	4240
DCS in [bmim][BF ₄]	14.5	760	1281	2041	4080
C153 in [bmim][PF ₆]	14.0	861	1219	2080	2000 ^(b)
4AP in [bmim][PF ₆]	13.6	1024	1305	2329	2300 ^(b)
DCS in [bmim][DCA]	14.5	855	1372	2227	-
DCS in [hmim][BF ₄]	14.5	784	1436	2220	-
DCS in [bmim][PF ₆]	20 ^(c)	1242	1740	2982	4240
DCS in [bmim][BF ₄]	20	915	1767	2682	4080
DCS in [bmim][DCA]	20	1047	1892	2939	-
DCS in [hmim][BF ₄]	20	1034	1980	3014	-
DCS in [bmim][PF ₆]	28 ^(d)	1736	2438	4174	4240
DCS in [bmim][BF ₄]	28	1629	2473	4102	4080
DCS in [bmim][DCA]	28	1658	2649	4307	-
DCS in [hmim][BF ₄]	28	1527	2771	4298	-

(a) Excited state dipole-moment of solute used in the calculation.

(b) Obtained in experiments via the 'time-zero' estimate (Maroncelli and coworkers, Chem. Phys. Lett. **396**, 83 (2004)).

(c) Estimated from the emission spectra using the Lippert-Mataga relation (Maroncelli and coworkers, J. Phys. Chem. A **110**, 3454 (2006)).

(d) See text.

decrease of ~25% in diameter ($\sigma_{4AP} = 6.2A^0$) for 4-AP increases $\Delta\nu^t$ in the same solvent by another ~200 cm^{-1} . Note that for all these solutes, the difference in dipole moments remains within ~3-7% only (see Table 6.1). The solute size and dipole-moment dependencies of $\Delta\nu^t$ enters into the present calculation through the solute-dipole and solute-ion static correlations ($c_{sd}^{lm}(k)$ and $c_{s\alpha}^{10}(k)$). Only a 10% increase in

shift for 4-AP relative to that for DCS and C153 therefore indicates a weak solute dependence of the spectral shift in these liquids and is a signature of solvent reorganization being dominated by the relatively longer-ranged dipole-dipole and ion-dipole interactions.²³

The simple representation of a solute by its dipole moment and volume suffices for C153 or 4-AP in these complex liquids because the short-ranged solute-solvent non-polar type interaction effects are masked by the overwhelming contributions from the longer-ranged interaction. Also, for these solutes the underlying vibronic structure of the emission spectrum remains largely insensitive to the solvent polarity.¹⁷ For DCS, however, more extended representation of the solute seems to be necessary as the minimalist description of the solute cannot explain the reasons for the factor of 2 difference between the shifts measured with it, and with C153 and 4-AP. Note that for all the solutes considered here, the dipole-dipole contribution to the shift ranges roughly between $700 - 1000 \text{ cm}^{-1}$ which is, on an average, $\sim 40\%$ of the total shifts calculated for these liquids. Interestingly, this magnitude of the dipole-dipole contribution is approximately in the same range of shift measured with C153 in a few moderately polar solvents (dichloromethane, 1-chlorobutane and tetrahydrofuran) whose dielectric constants are similar to these ionic liquids.¹⁷ The dipole-ion interaction, on the other hand, constitutes almost 60% to the total calculated shifts in these dipolar RTILs. This is an important finding of this work as we shall see later that the presence of the dipole-ion contribution in the measured shift leads to the apparent break-down of the existing theories of polar solvation dynamics for these ionic liquids.

The disagreement between the predicted and measured Stokes' shift for DCS in these liquids deserve further attention as an accurate prediction of solvent-induced Stokes' shift is critical for a proper understanding of the solvent control of electron transfer reactions in these media.⁴⁰ We further find that the present theory cannot reproduce the experimentally measured shifts for DCS in these liquids even if the calculations consider 20 D as μ_1 , a value estimated from the solution phase fluorescence emission spectra of DCS⁴¹. A nearly 40% increase in μ_1 over the AM1/CI value does increase the shift further by $\sim 600-800 \text{ cm}^{-1}$ but the calculated total shifts are still less by ~ 1000

cm^{-1} than the measured values ($\sim 4000 \text{ cm}^{-1}$). A more recent study, however, suggests that μ_1 of DCS is $\sim 22 \text{ D}$ ⁴² which is significantly larger than the AM1/CI predictions. Such a large value for μ_1 of DCS is therefore explains partially the greater Stokes' shift for DCS than the other two solutes. Curiously, a quantitative agreement between the calculated and measured shifts for DCS in these liquids can be obtained if one uses 28 D as μ_1 (see the last four rows of Table 6.1). Relevant quantum chemical calculations indeed predicted such a large value for μ_1 (and even larger ones⁴³⁻⁴⁵) where fluorescence emission in DCS was thought to occur from a twisted intramolecular charge transfer (TICT) state. Recent analyses of solvatochromic data of DCS via the Independent State (IS) model did produce $\mu_1 \approx 29 \text{ D}$ but simultaneously predicted an unrealistically low ground state dipole moment ($\mu_0 \approx 2 \text{ D}$).⁴¹ Subsequent line-shape analyses suggested a strong solvent polarity dependence of the vibronic structure of DCS which, in turn, makes the interpretation of the measured dynamic Stokes' shift more complex. The above agreement between theory and experiment with $\mu_1 = 28 \text{ D}$ probably suggests that if the solvent-induced modifications in vibronic structure of DCS in these complex liquids is effectively accounted for via a suitable value of μ_1 , then the present theory can successfully predict the observed shift for this solute also. Such an agreement, however, reflects merely a factor of 2 increase in μ_1 over the AM1/CI value, and does not imply that the excited state dipole moment of DCS is indeed as large as $\sim 28 \text{ D}$. What all it suggests that the dynamic Stokes' shift measured with DCS in these liquids and also in common polar solvents⁴¹ might not be due to the solvent rearrangement alone.

Next we present in Fig. 6.1 the predicted decays of the solvation response function from Eq. (6.3) (large dashed line) for DCS in [bmim][PF₆] where the corresponding time-resolved data² are also shown (circles) in the same figure for comparison. Note the agreement between the calculated $S_{sd}(t)$ and experimental results at short times (lower panel). It is evident from Fig. 6.1 that the decay of the calculated total solvent response function is much slower than that measured in experiments. The individual decays due to the two separate mechanisms, the dipole-dipole (solute-dipolar ion) and dipole-ion (solute-ion) interactions are also presented in the same figure. Interestingly, the individual decays seem to suggest that while the dipole-dipole interaction drives

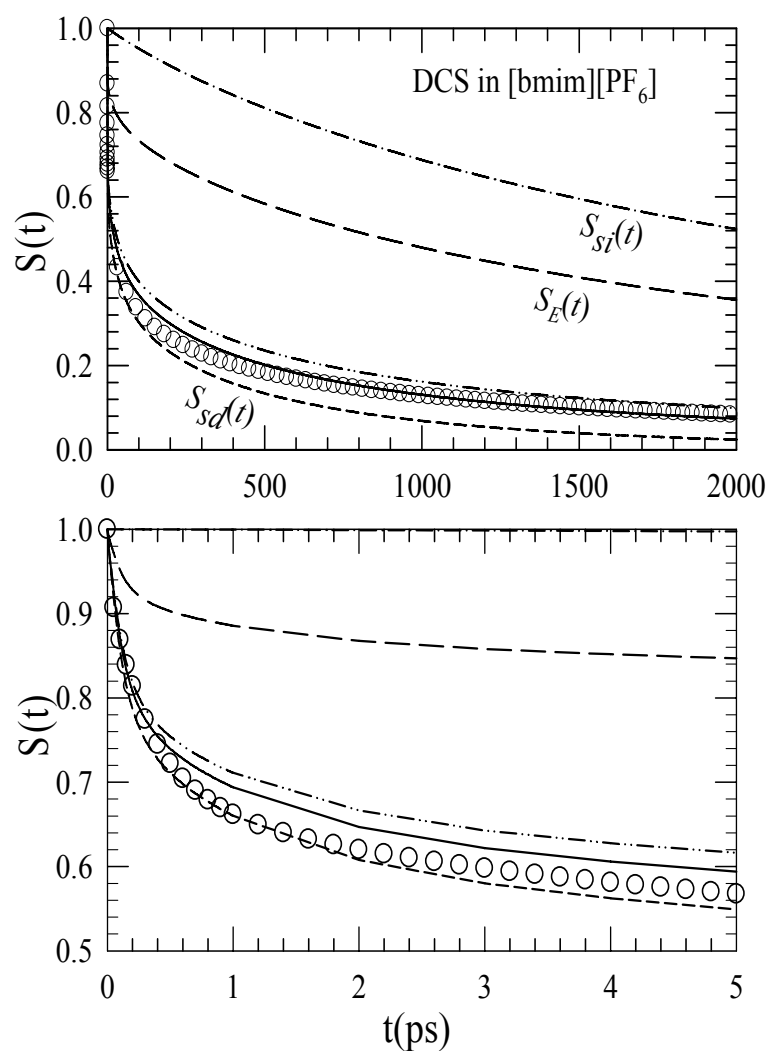


Figure 6.1: Upper panel: Comparison of predicted decay of solvation response function, $S(t)$, for DCS in [bmim][BF₄] with experimental data (open circles). The short dashed, dotted dashed and long dashed lines represent solvation response function, $S_{sd}(t)$, $S_{si}(t)$ and $S_E(t)$, respectively. The numerically synthesized solvation response function given by $S(t) = 0.90S_{sd}(t) + 0.10S_{si}(t)$ is shown by solid line. Lower Panel: The short-time dynamics of the solvation response functions are shown in shorter time window for clarity. Parameters necessary for the calculation of the solvation response functions are discussed in Tables 6.1 & 6.2.

the solvation energy relaxation at the early times, the same at the longer times are carried out by the dipole-ion interaction. In addition, the dipole-dipole interaction allows solvation energy to relax at a rate more than an order of magnitude faster than that by the dipole-ion interaction alone. Parameters obtained from numerical fits of the calculated and measured decays to the following general form, $S(t) = a_1 \exp[-t/\tau_1] + a_2 \exp[-(t/\tau_2)^\beta]$, are summarized in Table 6.2 in order to facilitate a more detail comparison. The huge difference in the calculated decay time-scales (0.3 ns for the dipole-dipole part versus 4 ns for the dipole-ion part) validates the assumption that dipolar dynamics is decoupled from the ion dynamics in these dipolar ionic liquids. In fact, these results also provide a microscopic explanation for the separation of the “pure solvent dynamics” from the “ion dynamics” observed earlier for electrolyte solutions of “fast” solvents.³⁴ Note that in the present theory the separation of time scales originates from the difference in relaxation rates between the orientational dynamic structure factor and the ion dynamic structure factor of these liquids.

The experimental average solvation time for the above system being in the nanosecond range and approximately three times larger than that calculated from the dipole-dipole interaction ($S_{sd}(t)$) decay indicates that ion structural relaxation does contribute to the solvation energy relaxation in this dipolar RTIL. However, as the corresponding decay curves in Fig. 6.1 indicate, the ion structural relaxation contributes only after a large part of the solvation energy relaxes via the faster relaxation of the orientational dynamic structure factor. The solvent translational modes are also found to accelerate the polar solvation energy relaxation in the dipolar RTILs but the effects are negligible due to very high liquid viscosity.^{20-21, 46-50} The slow relaxation of the dipole-ion interaction energy takes over in the long time after the dipolar part of the solvation response function has decayed to almost e^{-1} . The slowing down of the long-time decay of the solvent response function via the ion translation is a generic feature not only for the dipolar RTILs but also for electrolyte solutions of polar solvents where solute-ion interaction contributes appreciably to the total shift and to the long time dynamics of energy relaxation. For example, a slow component of ~15-20% is found at long time in the spectral dynamics of electrolyte solutions in presence of 1.0 M salt concentration.³⁴

Table 6.2: Solvation dynamics of dipolar solutes in imidazolium ionic liquids at temperature 298 K: Comparison between theory and experiments^{(a), (b)}

Solvation Response Function	a_1	τ_1 (ps)	a_2	τ_2 (ps)	β	$\langle\tau_s\rangle$ (ns)
DCS in [bmim][PF ₆]						
$S_{si}(t)$	0.27	846	0.73	5281	1	4.08
$S_{sd}(t)$	0.24	0.21	0.76	126	0.41	0.3
$S_E(t)$	0.14	0.46	0.86	2484	0.58	3.33
$0.90S_{sd}(t)+0.10S_{si}(t)$	0.22	0.23	0.78	219	0.38	0.66
$0.85S_{sd}(t)+0.15S_{si}(t)$	0.21	0.23	0.79	289	0.37	0.96
Experiment	0.19 ± 0.03	0.33 ± 0.08	0.81 ± 0.13	140 ± 28	0.31 ± 0.05	1.0 ± 0.20
DCS in [bmim][BF ₄]						
$S_{si}(t)$	0.40	595	0.60	3601	1	2.40
$S_{sd}(t)$	0.15	0.10	0.85	92	0.41	0.23
$S_E(t)$	0.08	0.24	0.92	1294	0.57	1.94
$0.90S_{sd}(t)+0.10S_{si}(t)$	0.14	0.12	0.86	147	0.40	0.42
Experiment	0.19 ± 0.03	0.32 ± 0.08	0.81 ± 0.13	130 ± 26	0.41 ± 0.05	0.34 ± 0.07
C153 in [bmim][PF ₆]						
$S_{si}(t)$	0.27	846	0.73	5281	1	4.08
$S_{sd}(t)$	0.30	0.26	0.70	158	0.46	0.26
$S_E(t)$	0.14	0.47	0.86	2508	0.59	3.32
$0.85S_{sd}(t)+0.15S_{si}(t)$	0.21	0.24	0.79	293	0.37	0.97
Experiment	-	-	1.00	500	0.49 ± 0.1	1.0 ± 0.20
4AP in [bmim][PF ₆]						
$S_{si}(t)$	0.30	863	0.70	4885	1	3.68
$S_{sd}(t)$	0.30	0.29	0.70	183	0.48	0.28
$S_E(t)$	0.15	0.46	0.85	2050	0.58	2.75
$0.85S_{sd}(t)+0.15S_{si}(t)$	0.22	0.25	0.78	329	0.40	0.85
Experiment	-	-	1.00	1150	0.65 ± 0.1	1.6 ± 0.30
DCS in [bmim][DCA]						
$S_{si}(t)$	0.66	286	0.34	1880	1	0.83
$S_{sd}(t)$	0.31	0.08	0.69	11	0.32	0.05
$S_E(t)$	0.11	0.06	0.89	405	0.54	0.63
$0.85S_{sd}(t)+0.15S_{si}(t)$	0.27	0.08	0.73	38	0.31	0.22
DCS in [hmim][BF ₄]						
$S_{si}(t)$	0.29	1209	0.71	7437	1	5.63
$S_{sd}(t)$	0.58	0.09	0.42	66	0.39	0.1
$S_E(t)$	0.15	0.12	0.85	4362	0.66	4.98
$0.85S_{sd}(t)+0.15S_{si}(t)$	0.45	0.09	0.55	273	0.28	1.93

(a) The liquid viscosity is 3.1P for [bmim][PF₆], 1.54P for [bmim][BF₄], 0.33P for [bmim][DCA] and 2.4P for [hmim][BF₄]. Here ‘P’ stands for Poise.

(b) The diameter of various species used in the calculations: $\sigma_{DCS} = 7.8\text{\AA}$, $\sigma_{C153} = 7.8\text{\AA}$, $\sigma_{4-AP} = 6.2\text{\AA}$, $\sigma_{[bmim]^+} = 6.8\text{\AA}$, $\sigma_{[hmim]^+} = 7.2\text{\AA}$, $\sigma_{PF_6^-} = 5.4\text{\AA}$, $\sigma_{BF_4^-} = 4.6\text{\AA}$ and $\sigma_{DCA^-} = 5.0\text{\AA}$. (Ref. 2)

In view of the above experimental observations for electrolyte solution and its closeness to the model that has been used to describe the dipolar RTILs in the present work, we have performed a numerical experiment to explore how much of the solute-ion (dipole-ion) interaction induced dynamics, $S_{si}(t)$, contributes to the experimental decay of the solvation response function measured with DCS in [bmim][PF₆]. As the relevant decays shown in Fig. 6.1 and the corresponding fit parameters summarized in Table 6.2 indicate, agreement to experimental results becomes almost quantitative when $S_{si}(t)$ contributes ~10-15% of the total decay. The close similarity in contribution of the ‘ion dynamics’ to the total decay of the solvent response function between the dipolar RTILs and electrolyte solutions strongly suggest that the dipole-ion contribution is linked to the more specific ion-solvent exchange dynamics where the formation or breakage of the solvent structure in the immediate vicinity of the solute is involved. This is essentially the preferential solvation of the dissolved dipolar solute by the dispersed ions in a dipolar medium. As we shall see later, the time scale for the solvation by the ions is indeed originating from the nearest-neighbor interactions as the dynamics in non-dipolar ionic liquids is dominated by this interaction length scale ($k\sigma \rightarrow 2\pi$) only. The domination of the nearest-neighbor length scale in the dipole-ion part of the solvation energy relaxation also makes the solution static heterogeneity effects more important as ion translation is coupled strongly to the detail of the local solvent structure.⁵¹ A complete neglect of the static heterogeneity has therefore led to the bi-exponential rather than a stretched exponential decay of $S_{si}(t)$ (see Table 6.1).⁵² Moreover, the presence of this slow component in the decay dynamics of dipolar RTIL and its absolute dominance in non-dipolar ionic liquids render the continuum model based dynamical theories²⁷⁻²⁸ insufficient for these liquids.

We next present our calculations for DCS in [bmim][BF₄] in Fig. 6.2 where the experimental data² are also shown for comparison. Here again the calculated $S_{sd}(t)$ agrees very well with the experimental decay at short times (lower panel). As evident from Fig. 6.2 and the corresponding fit parameters in Table 6.2, a separation of time scales between ion and dipolar dynamics also exists for [bmim][BF₄] where the ion dynamics, as expected, contributes fractionally to the total decay of the

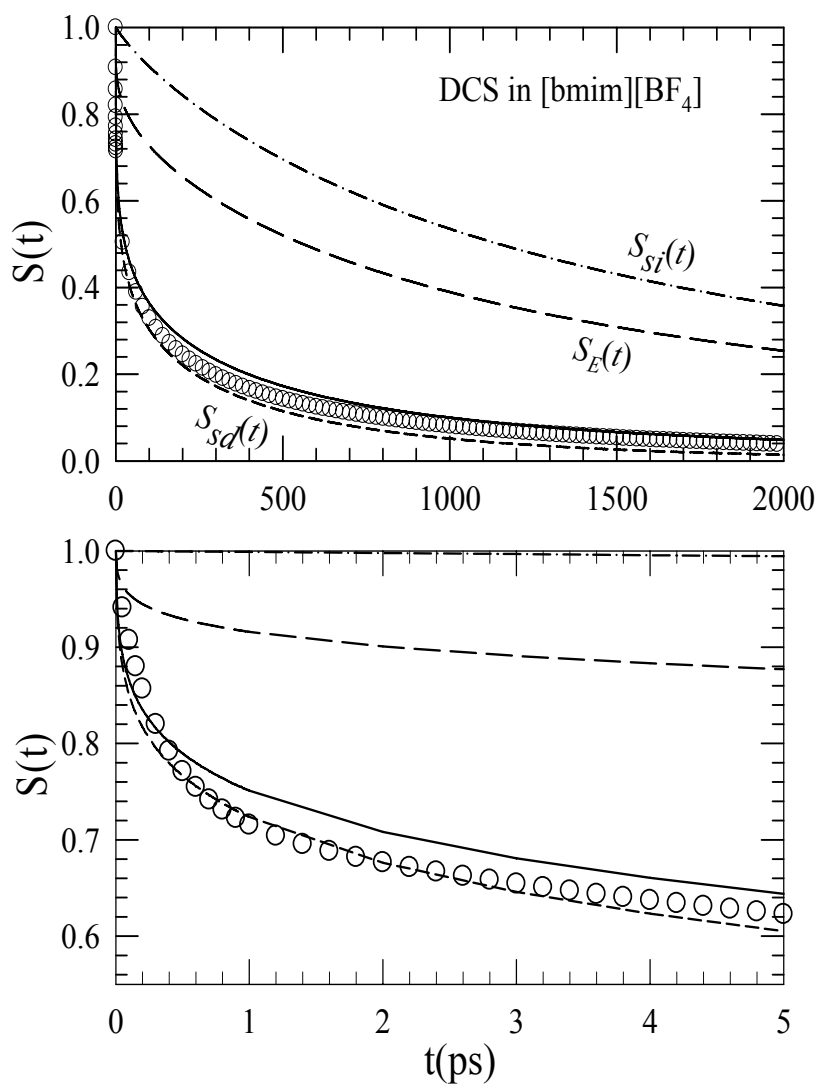


Figure 6.2: Upper panel: Comparison of predicted decay of solvation response function, $S(t)$, for DCS in [bmim][BF₄] with experimental data (open circles). The short dashed, dotted dashed and long dashed lines represent solvation response function, $S_{sd}(t)$, $S_{si}(t)$ and $S_E(t)$, respectively. The numerically synthesized solvation response function given by $S(t) = 0.90S_{sd}(t) + 0.10S_{si}(t)$ is shown by solid line. Lower Panel: The short-time dynamics of the solvation response functions are shown in shorter time window for clarity. Parameters necessary for the calculation of the solvation response functions are discussed in Tables 6.1 & 6.2.

solvation response function in this liquid. In fact, a 10% contribution from $S_{si}(t)$ to the calculated total solvent response function for this liquid not only leads the calculated average solvation time to compare well with the experimental value but also brings the amplitudes, time constants and the stretching exponent (β) in very good agreement with those from experiments. The fit parameters summarized in Table 6.2 also reveals that when C153 or 4-AP is used as solute probe in [bmim][PF₆], the predicted solvation times and stretching exponents are nearly the same as found for DCS. Although a direct comparison with the relevant experimental data cannot be made due to incomplete detection^{12-13, 53-55} of the total dynamics with C153 and 4-AP, the calculated results do not indicate any probe dependence of the average solvation times for a given solvent. In addition, the present calculations predict a much larger (~25-50%) ultra-fast component with a time constant less than 100 fs for both [bmim][DCA] and [hmim][BF₄] (see Table 6.2). Such a rapid response in the calculated solvation energy relaxation of [bmim][DCA] originates from the faster dielectric relaxation times (see Table 5.1 in chapter 5). In fact, if the solvent librational modes are believed to couple to solvation energy relaxation (via the dipole-dipole part) then the present calculations suggests a sub-picosecond response is only expected because of the presence of a libration frequency in the ~2-4 THz range and a dielectric relaxation time of nearly a picosecond or a quarter of it in these liquids. This is the reason that for all the (solute + imidazolium liquid) combinations the relaxation of the calculated $S_{sd}(t)$ is characterized by a fast relaxation time that ranges between 80–300 femtosecond. Since all the dielectric relaxation times are the fastest in [bmim][DCA] among the ionic liquids studied here, the dipole-dipole part of the solvation energy decays at a much faster rate producing the smallest average solvation time in this liquid. For [hmim][BF₄], although the slowest dielectric relaxation time is in the nanosecond, similar participation of the shortest dielectric relaxation time and the libration mode produces the sub-hundred femtosecond component in the $S_{sd}(t)$. It may be further interesting to note that the calculated average solvation time for [bmim][DCA] is ~200 ps which is comparable to what has been measured for decanol with C153 at room temperature.¹⁷ Experiments on solvation dynamics in these two dipolar RTILs are therefore suggested so that the presence of such an ultrafast component is verified and the contribution from the dipole-ion interaction estimated.

Table 6.3: Dynamic Stokes' shift of C153 in Phosphonium Ionic Liquids at 343 K: Comparison between theory and experiments^(a)

Ionic Liquids	Dipole-ion contribution, $\Delta\nu_{si}^t$ (cm ⁻¹)	Dipole-dipole contribution, $\Delta\nu_{sd}^t$ (cm ⁻¹)	Total ($\Delta\nu_{sd}^t + \Delta\nu_{si}^t$) (cm ⁻¹)	Expt. (cm ⁻¹)
[P _{14,666}][Br]	1214	371	1585	1590
[P _{14,666}][Cl]	1231	370	1601	1500
[P _{14,666}][BF ₄]	928	381	1309	1370

(a) These shifts are calculated with μ_1 for C153 as shown in Table 6.2.

6.3.2 Phosphonium Ionic Liquids: Stokes' Shift and Dynamics

We next extend the present theory to calculate the dynamical Stokes' shift for C153 at 343 K in the three phosphonium ionic liquids we have already mentioned in the Introduction. For simpler representation, we abbreviate the singly charged trihexyl(tetradecyl)phosphonium cation by $[P_{14,666}^+]$. The calculated dipole-ion contribution to the total shift for each of the phosphonium ionic liquids is presented in Table 6.3 where experimental results¹⁸ are also shown. A comparison between the calculated and measured shifts reveals that the dipole-ion interaction accounts for ~75% of the measured Stokes' shifts for these ionic liquids. This is somewhat surprising because in the absence of any dipole-dipole interactions Stokes' shifts in these liquids are expected to be determined only by the dipole-ion (solute-ion) interaction. One wonders then what could be the source for the remaining 25% of the observed shift which amounts to approximately 400 cm⁻¹ in these non-dipolar ionic liquids. What follows next is a brief discussion on the possible mechanisms which can account for the missing shift in these non-dipolar ionic liquids.

Since a significant fraction of these liquid molecules does not contribute to the ionic conduction,²⁰ there is a possibility that the undissociated fractions remain as ion-pairs. Subsequent quantum chemical calculations²¹ indicate that the formation of ion-pairs is energetically favored (approximately by -80 kcal/mol) in these ionic liquids where the electrostatic attraction between oppositely charged ions has been found to be the major contributor. The degree of ion-association is found to be larger in ionic liquids

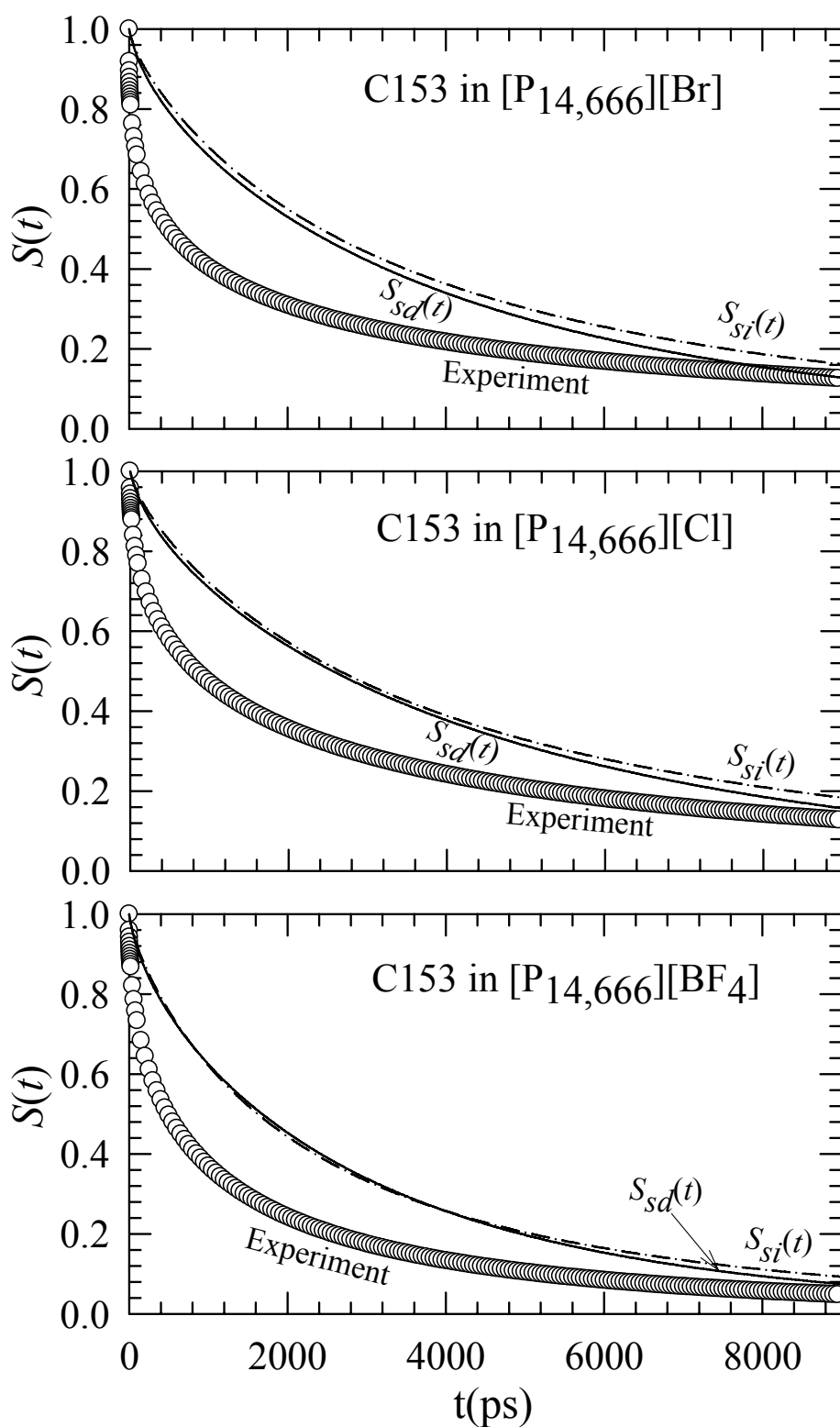


Figure 6.3: Solvation Dynamics for C153 in three phosphonium ionic liquids at 343 K. The solid and dot-dashed lines represent $S_{sd}(t)$ and $S_{si}(t)$, respectively. Circles represent the experimental decays.

where ions are asymmetric in shape. Moreover, for a few non-dipolar ammonium ionic liquids the effective concentration of undissociated molecules has been estimated to be $\sim 30\%$ of their molar concentrations.²¹ In the absence of similar studies for phosphonium ionic liquids and considering the general results obtained from the conductivity measurements and quantum chemical calculations for a variety of ionic liquids, the ion-pair (IP) concentration for the phosphonium ionic liquids studied here can be expected in the same order. These ion-pairs then interact with the dissolved dipolar solute via dipole-dipole interactions and contribute to both the dynamical Stokes' shift and the solvation energy relaxation. In addition, these ion-pairs, via dipole-dipole interaction among themselves, can generate an effective dipolar environment. If the average dielectric constant of such an environment is assumed to be ~ 5 , then the subsequent calculations find the solute-IP (dipole-dipole) interaction contribution is $\sim 400 \text{ cm}^{-1}$ (see Table 6.3) which is $\sim 25\%$ of the experimentally observed shift with C153 in these phosphonium ionic liquids. This brings the total calculated Stokes' shifts in much closer to the experimental data. The present calculation therefore indicates that in addition to the dominant solute-ion interaction, a small but non-negligible contribution may also arise from the dipolar interaction between the solute and ion-pairs that are present in these ionic liquids due to incomplete dissociation.

Next we present the calculated results on solvation dynamics of C153 in these phosphonium ionic liquids and compare with the relevant experimental data. The calculated individual solvent response functions due to the dipole-ion (solute-ion) and dipole-dipole (solute-IP) interactions for each of the phosphonium ionic liquids are shown in Fig. 6.3. In the absence of any dielectric relaxation data for these phosphonium liquids, we calculate the dipole-dipole term, $S_{sd}^{ip}(t)$, in the diffusive limit where both the rotational and translational diffusion coefficients of the constituent ion-pairs are obtained from the liquid viscosity³⁷ at that temperature. Note that the difference in decay rates between these two individual solvent response functions is not as dramatic as found in imidazolium ionic liquids because here the time scales for both $S_{si}(t)$ and $S_{sd}^{ip}(t)$ are completely determined by the liquid viscosity alone. As already stated, a complete neglect of liquid heterogeneity in the present theory has led to the bi-exponential decay of the calculated solvent response

Table 6.4: Solvation dynamics of C153 in phosphonium ionic liquids at 343 K:Comparison between theory and experiments^{(a), (b)}

Solvent Response Function	a_1	τ_1 (ps)	a_2	τ_2 (ps)	β	$\langle\tau_s\rangle$ (ns)
C153 in [P _{14,666}][Br]						
S _{si} (t)	0.38	1289	0.62	6774	1	4.69
S _{sd} (t) (ion pair)	0.25	708	0.75	5081	1	3.99
S _E (t)	0.37	1275	0.63	6634	1	4.65
Experiment	1	1310±70	-	-	0.38±0.05	5.05±0.43
C153 in [P _{14,666}][Cl]						
S _{si} (t)	0.37	1359	0.63	7402	1	5.17
S _{sd} (t) (ion pair)	0.24	765	0.76	5714	1	4.53
S _E (t)	0.36	1344	0.64	7262	1	5.13
Experiment	1	1860±90	-	-	0.46±0.05	4.49±0.30
C153 in [P _{14,666}][BF ₄]						
S _{si} (t)	0.46	1047	0.54	5139	1	3.26
S _{sd} (t) (ion pair)	0.26	581	0.74	3876	1	3.02
S _E (t)	0.44	1023	0.56	4948	1	3.22
Experiment	1	1010±50	-	-	0.51±0.05	1.98±0.11

(a) The viscosities are 1.16, 1.33 and 0.87P, respectively, for phosphonium ionic liquids containing Br⁻, Cl⁻ and BF₄⁻ as anions.

(b) The size of the cation is taken to be 10.68Å with $\sigma_{Br^-} = 4.5\text{\AA}$, $\sigma_{Cl^-} = 4.18\text{\AA}$, and $\sigma_{BF_4^-} = 4.6\text{\AA}$. (Ref. 18).

functions in these liquids.⁵² Parameters required to fit these calculated decays are summarized in Table 6.4 where experimental fit parameters are also tabulated. The most interesting aspect of these parameters (Table 6.4) is that one of the calculated time constants is ~ 1 ns which is very similar to the experimental solvation time constants (τ_{solv}) for these alkylphosphonium liquids. This close similarity between theory and experiments suggest that solvent structural relaxation via ion-translation is

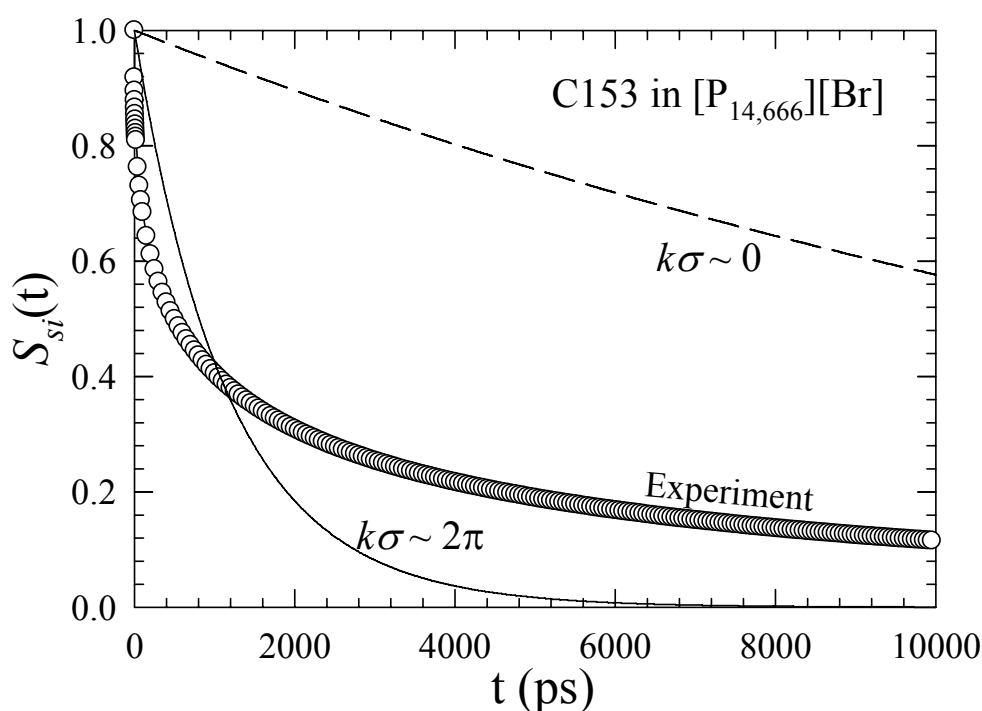


Figure 6.4: The origin of the one-nanosecond solvation time constant in solvation energy relaxation in phosphonium ionic liquids at 343 K. Solvation response functions for C153 in $[P_{14,666}][Br]$ are calculated after considering the structural relaxation at collective ($k\sigma \sim 0$) solvent mode (dashed line) and nearest neighbor ($k\sigma \sim 2\pi$) solvent modes (solid line). The calculate decays for both the wavenumbers are found to fit to single exponentials with time constant 18.2ns and 1.2ns, respectively, for $k\sigma \sim 0$ and $k\sigma \sim 2\pi$ modes.

indeed the principal mechanism for the solvation energy relaxation in these non-dipolar ionic liquids.

In order to explore further the origin of the single exponential decay of the experimental solvent response functions with time constant approximately in the nanosecond regime, we have calculated solvation energy relaxations in these liquids corresponding only to the collective ($k\sigma \rightarrow 0$) and the nearest-neighbor ($k\sigma \rightarrow 2\pi$) solvent modes. Fig. 6.4 is a representative of such calculations where the predicted decays for C153 in $[P_{14,666}^+][Br^-]$ corresponding to these modes are shown along with the relevant experimental data.¹⁸ Fig. 6.4 clearly demonstrates that the experimental

solvation time constant of ~ 1 ns in these ionic liquids originates from the structural relaxation involving the nearest neighbor ($k\sigma \rightarrow 2\pi$) mode only. The quadratic wavenumber dependence of the exponential relaxation of the ion dynamic structure factor (see Eq. (6.6)) is responsible for the extreme slow dynamics at these collective solvent modes. The slower relaxation corresponding to $k\sigma \rightarrow 0$ has not been detected in Stokes' shift measurements because either the shift due to this mode was undetectably small or simply the collective solvent modes are irrelevant for the dipole-ion interaction induced solvation energy relaxation. A simple calculation using $\epsilon_0 \approx 2$ shows that the Debye screening length for these liquids is $\sim 1\text{\AA}$. Even-though such a small value of Debye screening length is unphysical for these molecular liquids, it suggests that the solvation energy relaxation in these liquids couples only to the rearrangement of the local solvent structure, and the Stokes' shift remains insensitive to the events occurring beyond probably the first couple of solvation shells. Consequently, the relaxation of the isotropic solvent dynamic structure factor sets the solvation time scale in these phosphonium ionic liquids where the orientational relaxation plays a much less important role. This is counter-intuitive because one expects that charge fluctuations in these liquids are highly coupled and that correlated dynamics extending over many solvation shells play a role in solvation.⁵⁶ Due to the lack of any permanent dipole moment on the ions and hence non-existence of significant medium dielectric constant, much larger inverse Debye screening length probably compels the phosphonium ionic liquids to behave as if the ionic system is governed by relatively much less longer-ranged interactions.⁵⁷ A signature of such an effect has recently been observed while studying temperature dependence of spectral shifts in electrolyte solutions of non-aqueous solvents of varying polarity.⁵⁸ This is therefore in sharp contrast to the solvation mechanism of a dipolar solute in dipolar solvents where collective solvent polarization density relaxation governs the time scale of the polar solvent response. It is only in this sense that solvation dynamics in these non-dipolar ionic liquids may be termed as non-polar solvation dynamics.⁵⁹

As several simulation and experimental studies⁵⁻¹¹ reveal domain formation via aggregation of alkyl chains in ionic liquids that contain alkylated ions, dipolar solutes can be partitioned into these domains and contribute to the over-all Stokes' shift

dynamics. However, the contribution due to non-polar interactions between the solute and the aggregated domains is expected to be very small since experimental dynamical Stokes' shift for C153 has been found to be zero in several alkanes⁶⁰ and $\sim 200 \text{ cm}^{-1}$ in supercritical ethane⁶¹ with $\pm 100 \text{ cm}^{-1}$ uncertainty in those measurements. If the assumption that the solute's vibronic structure is independent of solvation environment still holds, then these results suggest that the contribution to the Stokes' shift due to non-polar interaction would be at most 200 cm^{-1} , which is nearly half of what is not accounted for by the dipole-ion interactions alone in these phosphonium ionic liquids. Interestingly, experimental study of non-polar solvation dynamics of dimethyl-s-tetrazine in n-butylbenzene, extending over a viscosity range of 5-orders of magnitude, not only reports a total shift in the range of $\sim 100\text{-}200 \text{ cm}^{-1}$ ($\pm 10 \text{ cm}^{-1}$), but finds also that the structural component of the shift relaxes non-exponentially with $\beta \approx 0.5$ and a time constant proportional to medium viscosity.⁶² The use of the correlation between the viscosity and relaxation time constructed in this work produces solvation time constants (τ_{solv}) for these phosphonium ionic liquids very similar to those found in experiments. Based on the knowledge of non-polar solvation dynamics gained earlier, if the solvation in butyl benzene is assumed to be mainly carried out by the relaxation of the isotropic part of the solvent structure factor, then this striking similarity between the calculated and measured time constants may indicate that solute-domain non-polar interaction may also contribute to the total dynamical Stokes' shift.

6.3.3 Continuum Model and Present Theory

Let us examine (i) why did the dynamic continuum model of Rips, Klafter and Jortner (RKJ)²⁸ fail for these liquids and (ii) can the dipolar part of the separated out dynamics of these dipolar imidazolium ionic liquids be understood by the above RKJ theory? RKJ theory, which does not consider the molecularity of the solvent particles, provides the following expression for normalized solvation response function²⁷⁻²⁸

$$S_{sd}^{RKJ}(t) = \frac{L^{-1}\{(\chi(z) - \chi(0))/z\}}{\chi(\infty) - \chi(0)}, \quad (6.7)$$

where L^{-1} stands for inverse Laplace transform. $\chi(z)$ is calculated from the frequency dependent dielectric function, $\varepsilon(z)$, as follows²⁷⁻²⁸

$$\chi(z) = \frac{\varepsilon(z) - 1}{\varepsilon(z) + (1/2)\varepsilon_u}, \quad (6.8)$$

where ε_u is a cavity dielectric constant and is expressed by $(\varepsilon_u - 1)/(\varepsilon_u + 2) = \alpha a^3$, α being the cavity polarizability and a is the solute radius. Note here that the same $\varepsilon(z)$ which has been used to calculate the dipolar part of the solvation energy relaxation ($S_{sd}(t)$) in the present theory is also required to compute the normalized solvation response from the RKJ theory. However, RKJ theory, being a continuum model based theory, considers only the collective part of the orientational polarization density relaxation of the dipolar solvent. Also, it does not consider the contribution of the solvent translational modes to the solvation energy relaxation. Therefore, the consideration of only the collective ($k\sigma \rightarrow 0$) solvent mode and freezing of the solvent translation (by simply putting $D_T = 0$) in $S_{sd}(t)$ of the present theory will be appropriate for comparison with the RKJ predictions. Since the present theory suggests that the early time dynamics in these liquids is arising from the orientational polarization density relaxation and since the RKJ theory provided a sound qualitative understanding of dipolar solvation dynamics in conventional polar solvents, a direct comparison between these two predictions should help decode the relationship between the frequency dependent dielectric function of these liquids and the rate of solvation energy relaxation in them. In our calculation we have used tuned dielectric relaxation data (see chapter 5) where we have taken $\varepsilon(\infty)$ as that of experiment¹ for the calculation of $\chi(\infty)$. We have assumed non-polarizable solute cavity so that $\alpha = 0$.

In Fig. 6.5 we compare the results obtained from the RKJ theory for DCS in [bmim][PF₆] and [bmim][BF₄] with the predicted decays of $S_{sd}(t)$. Since the RKJ theory considers only the collective solvent polarization ($k\sigma \rightarrow 0$) mode to calculate the normalized solvent response, we have removed the contributions from the solvent finite wavenumber modes in our calculations of $S_{sd}(t)$. It is clear from Fig. 6.5 that

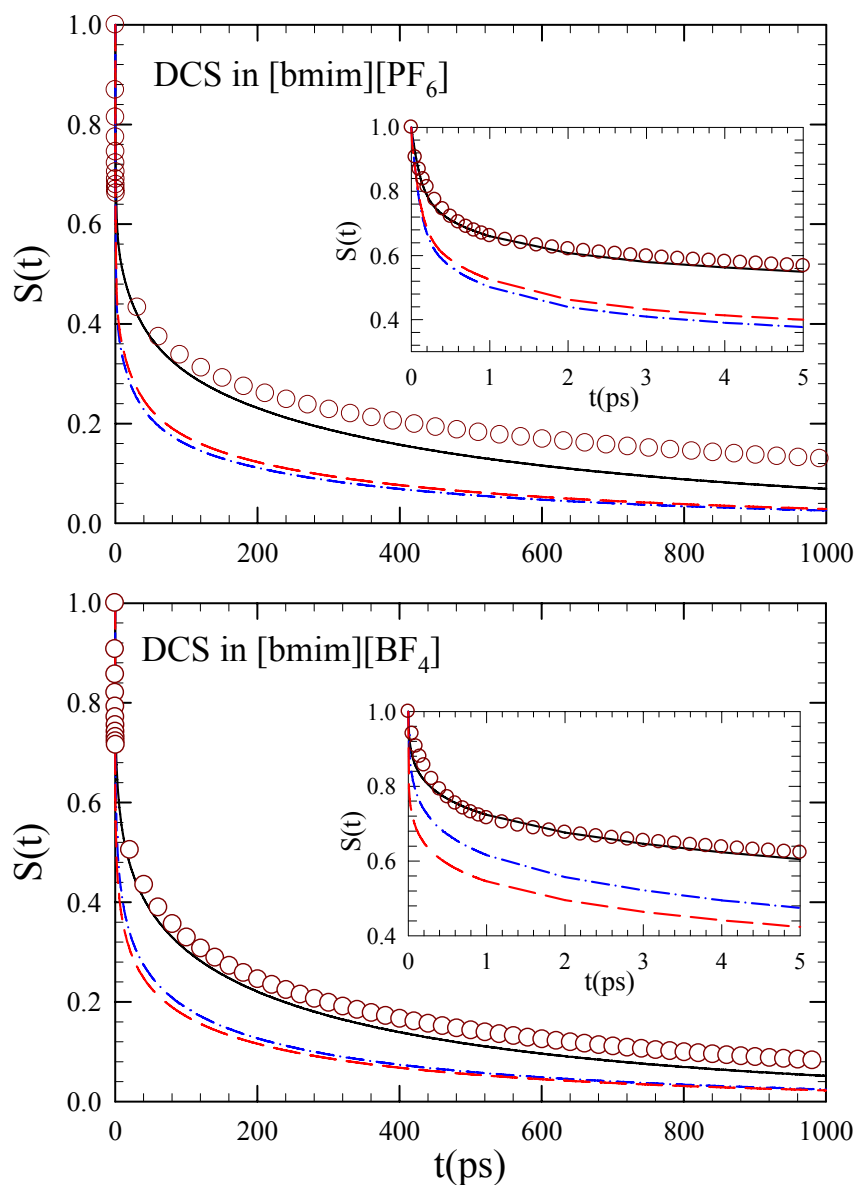


Figure 6.5: Validity test of the dynamic continuum model for solvation energy relaxations of DCS in imidazolium ionic liquids. Solvation response functions calculated from the dynamic continuum model are represented by dashed lines (red) for [bmim][PF₆] (upper panel) and [bmim][BF₄] (lower panel). The experimental results are shown by circles. Predictions from the present theory for these liquids by considering only the $k\sigma \rightarrow 0$ mode of the solvent polarization relaxation are shown by the dot-dashed (blue) lines. Solid lines in these two panels represent the calculations of $S_{sd}(t)$ after incorporating contributions from all solvent modes. Here the short-time dynamics displayed in the inset are for clear view. Note the close agreement between the continuum model predictions and the present theory at the proper limiting condition.

$S_{sd}(t)$ so calculated agree well with the RKJ predictions for both the liquids. These results also demonstrate that the RKJ theory can provide similar level of understanding as in common polar solvents if only the dipolar part of the total energy relaxation in these liquids is considered. As expected, inclusion of finite wavenumber contributions slows down the dynamics, particularly at long-time due to the participation of solvent structure at this stage. This is also shown in Fig. 6.5. Note the slowing down of the dynamics due to solvent structure at finite wavenumbers in common polar solvents has already been explained in terms of Onsager's inverse snow-ball picture.²⁴ Interestingly, the accessibility to a much slower dipole-ion interaction mechanism as a separate channel not only nullifies the accelerating effects of solvent translation on generalized rate of orientational polarization relaxation, but also restores the Onsager's inverse snow-ball picture via reversing the role of ion-translations through the relaxation of ion dynamic structure factor. Therefore, the RKJ theory, being insensitive to the dipole-ion interaction induced contributions, predicts a faster dynamics than what is observed in experiments for these ionic liquids. This is the reason for the apparent break-down of the RKJ theory and other theories of polar solvation dynamics while explaining the Stokes' shift dynamics in these liquids.

6.4 Conclusion

The molecular theory presented here demonstrates that dynamic Stokes' shifts measured with dipolar solute probes in several dipolar RTILs can be divided into two parts— the solute-dipolar ion (dipole-dipole) and the solute-ion (dipole-ion) interaction contributions. The dipolar RTILs considered in this study are those imidazolium ionic liquids for which dielectric relaxation data over a very broad frequency range is available. The solutes used are C153, 4-AP and DCS which were used in several experiments for dynamic Stokes' shift measurements. The calculated total shifts are in very good agreement with the measured values in these dipolar RTILs and the dipole-ion interaction contribution is found to account for ~60% of the measured shift. For phosphonium ionic liquids, where the interaction between the dipolar solute and constituent ions (non-dipolar) is expected to dominate, the solute-ion interaction contributes nearly 75% to the experimentally observed shift. The present theory also predicts that the interactions of the solute with the ion-pairs and non-polar domains may together make a non-negligible contribution to the shift measured in

phosphonium ionic liquids. The non-polar interaction contribution is much less important for shifts in imidazolium ionic liquids because of the additional presence of dipole-dipole interaction. Also, the use of experimental dielectric relaxation data in the calculation partially accounts for the solute-IP contribution to the dynamic Stokes' shift in these dipolar RTILs. The unusually large shift ($\sim 4000 \text{ cm}^{-1}$) measured with DCS in these liquids can be reproduced in the present theory as a pure solvent-induced dynamic Stokes' shift by using only an excited state dipole moment of DCS almost twice of that predicted by the AM1/CI calculations. A strong solvent dependence of vibronic structure is suggested to be responsible for the large Stokes' shift measured with DCS in these liquids.

A comparison with the calculated solvent response functions for imidazolium ionic liquids with those measured in experiments suggests that while the coupling of the collective solvent libration and fast dipolar rotations to the solvation energy relaxation gives rise to the initial sub-picosecond dynamics observed in these dipolar RTILs, slow relaxation of isotropic ion dynamic structure factor via ion translation produces the long time decay with time constant in the nanosecond range. The present theory reveals a strong link between the rapid initial solvent response and the fast orientational relaxation of these low polar ionic liquids which is reminiscent of what has been found in many theoretical studies of solvation dynamics in conventional polar solvents. This origin of the fast solvent response is therefore opposite to the argument^{2,63-70} that the collective ion translation is responsible for the sub-picosecond solvent response in these liquids. The dynamics of solvation in dipolar RTILs is found to be dominated by the orientational polarization relaxation of the environment created by the dipolar ions ('dipolar dynamics') where the ion translational motion ('ion dynamics') accounts for $\sim 10\text{-}15\%$ of the total dynamics. The dominance of the orientational relaxation in the dipolar dynamics and that of the structural relaxation in the ion dynamics lead to the natural separation of time scales between these two and enable one to describe the Stokes' shift dynamics in dipolar RTILs in terms of preferential solvation. The presence of the slow component is found to be responsible for failure of the existing theories of polar solvation dynamics in these ionic liquids. Further analyses, however, reveal that dynamic continuum model theory can be used to describe the separated out dipolar dynamics if only the collective modes ($k\sigma \rightarrow 0$)

of the solvent polarization fluctuations are considered in the calculation of the solvation response function.

In phosphonium ionic liquids, where solute-solvent dipolar interaction is much less important due to the absence of permanent dipole moment in the constituent ions, the ion-solute (ion-dipole) interaction contributes $\sim 75\%$ to the measured shift and governs the solvation dynamics. The absence of ‘dipolar dynamics’ therefore explains both single stretched exponential decay of the solvent response functions measured in these non-dipolar ionic liquids and the absence of sub-picosecond component in them. In addition, an absolute dominance of the ion-dipole interaction contribution in the solvation response is the principal reason for dramatically larger average solvation times for phosphonium ionic liquids than those for imidazolium counterparts of comparable viscosities.

We would like to further elaborate on the mechanism of sub-picosecond solvent response in the imidazolium ionic liquids as the present work seems to provide an explanation alternative to that suggested by several simulation and experimental results. Note here that the present work calculates the solvation energy relaxation due to solute-solvent dipolar interaction in imidazolium ionic liquids by using the experimentally determined frequency dependent dielectric function, $\varepsilon(z)$. Experimental measurements have indicated that $\varepsilon(z)$ for these ionic liquids are characterized by four distinct relaxations, two of which are undoubtedly diffusive in nature (the slowest ones). The other two relaxations in the tera-Hertz (~ 0.6 THz and ~ 3 THz) are thought to originate from the libration (rocking back-and-forth or up-and-down) of the cations. Further measurements of intermolecular dynamics by using in tandem the optical Kerr effect (OKE) and dielectric relaxation spectroscopic techniques, have clearly revealed that these high frequency relaxations are associated with the restricted angular motion of the dipolar moiety as both OKE and DR spectroscopies are predominantly sensitive to the rotational motions and only weakly sensitive to translations through the collision-induced response.⁷¹ This is because the time dependent change in the dipole moment auto-correlation function ($\frac{d}{d\tau}[\langle\mu(\tau)\mu(0)\rangle]$) is what is relevant to the DR measurements whereas the same

(time derivative) of the anisotropic part of the collective polarizability tensor $(\frac{d}{d\tau}[\langle \Pi_{xy}(\tau)\Pi_{xy}(0) \rangle])$ gives rise to the OKE signal.⁷¹ Naturally therefore, when a measured $\varepsilon(z)$ with all its dispersion steps is used to calculate the time dependent change in solvation energy, it is primarily the time scale of the orientational polarization density relaxation of the dipolar environment what is reflected in the calculated dynamics. As a result, the present semi-molecular theory interprets the experimentally observed sub-picosecond response in imidazolium ionic liquids as originating from the collective orientational response of the liquid. This is in general agreement with simulation predictions that early time dynamics arises from the cooperative motions of many particles together but differs greatly in the identity of the collective motion (rotation rather than translation) that renders ultrafast response in these ionic liquids.

Further support for the predicted dominance of the solvent reorientation may be obtained from the following facts. Our earlier study reveals that even if the high frequency contributions (~ 0.6 THz and ~ 3 THz) in $\varepsilon(z)$ are completely neglected and only the slowest dispersions are retained, the calculated dipolar dynamics in these liquids (except the [bmim][DCA]) can still be characterized by a sub-picosecond component with an amplitude of $\sim 10 - 15\%$. The participation of the high frequency modes then simply enhances the calculated rate of the solvation energy relaxation. Attention may now be focused to the Table AIII.1 (Appendix III) where a few characteristics from the dynamic Stokes' shift measurements in imidazolium and phosphonium ionic liquids have been compiled. Had the collective inertial ion translations been primarily responsible for generating the sub-picosecond response, it (the sub-picosecond) would have also been detected in phosphonium ionic liquids, particularly in [P_{14,666}][BF₄] where the anion, [BF₄⁻], is also common to [bmim][BF₄]. The fact that the average solvation times in comparatively much less viscous phosphonium ionic liquids are at least five times larger and dynamic Stokes shift $\sim 30\%$ lesser (compared to that for C153 which is ~ 2000 cm⁻¹) than those for imidazolium ionic liquids only stresses the role played by the solute-solvent dipolar interactions in governing both the magnitude of the shift and its dynamics in these two

types of ionic liquids. As expected, inclusion of the inertial translational dynamics in the calculation by using the following expression for ion dynamic structure factor⁷²

$$S_{\alpha\beta}^{ion}(k;t) = S_{\alpha\beta}^{ion}(k) \exp\left\{-\frac{k^2 k_B T}{m_\alpha \zeta_\alpha^{ion}} \left[t + \frac{1}{\zeta_\alpha^{ion}} (e^{-t\zeta_\alpha^{ion}} - 1)\right]\right\}, \quad (6.9)$$

(ζ_α^{ion} is the translational friction on the α^{th} type ion with mass m_α) did not produce results that might have led to conclusion any different from what has already been drawn regarding the origin of the observed sub-picosecond solvent response. Further computer simulations studies, particularly for phosphonium ionic liquids, along the line of what have been done with several imidazolium ionic liquids⁷³⁻⁷⁴ are therefore required to uncover the reasons for the observed difference in solvation energy relaxations in these two types of ionic liquids.

Even-though the present theory successfully explained in molecular terms the measured Stokes shift and its dynamics in imidazolium and phosphonium ionic liquids, the theory did so without incorporating the microscopic heterogeneity present in these complex liquids. This is definitely a shortcoming of the present theory that requires further improvement. Since alkyl chains are attached to the cations in these liquids are relatively long and hence possess some degree of flexibility, the chain may rearrange itself when the dipolar cation moiety reorients or either of the ions translate in response to the changed dipole moment of the solute. This would lead to a coupling of motions which may play some role in evolving the spectral dynamics in these liquids. The effects of coupled motion of the alkyl chain and ion on solvation energy relaxation may therefore be investigated in detail as coupled motion of protein side chain and water molecules has been found to play an important role in hydration dynamics near biologically active surfaces.⁷⁵ One notices that neglect of liquid heterogeneity did not severely affect the results for dipolar RTILs due to the use of experimental dielectric relaxation data. For phosphonium ionic liquids, although the theory can correctly predict a time constant close to that found in experiments, misrepresentation of the liquid structure by its homogeneous analogue leads to incorrect prediction of bi-exponential decay of solvation response functions in these liquids. Given the complexity of these liquids, it is indeed surprising that such a

simple formalism, which relies upon the MSA model or its suitable variants for structural inputs and dielectric relaxation data for medium dynamics, can describe so successfully not only the dynamical Stokes' shift and solvation response in both dipolar and non-dipolar ionic liquids but explains also in molecular terms the reasons for failure of the existing theories of polar solvation dynamics in these media.

References and Notes

1. A. Stoppa, J. Hunger, R. Buchner, G. Hefter, A. Thoman and H. Helm, *J. Phys. Chem. B* **112**, 4854 (2008).
2. S. Arzhantsev, H. Jin, G. A. Baker and M. Maroncelli, *J. Phys. Chem. B* **111**, 4978 (2007).
3. E. Bart, A. Meltsin and D. Huppert, *J. Phys. Chem.* **98**, 3295 (1994).
4. E. Bart, A. Meltsin and D. Huppert, *J. Phys. Chem.* **98**, 10819 (1994).
5. Y. Wang and G. A. Voth, *J. Am. Chem. Soc.* **127**, 12192 (2005).
6. A. Triolo, O. Russina and H. Bleif and E. D. Cola, *J. Phys. Chem. B* **111**, 4641 (2007).
7. P. K. Mandal, M Sarkar and A. Samanta, *J. Phys. Chem. B* **108**, 9048 (2004).
8. H. Jin, X. Li and M. Maroncelli, *J. Phys. Chem. B* **111**, 13473 (2007).
9. A. Adhikari, K. Sahu, S. Dey, S. Ghose, U. Mandal and K. Bhattacharyya, *J. Phys. Chem. B* **111**, 12809 (2007).
10. Z. Hu and C. J. Margulis, *Proc. Natl. Acad. Sci. U. S. A.* **103**, 831 (2006).
11. A. Triolo, O. Russina, B. Fazio, G. B. Appetecchi, M. Carewska and S. Passerini, *J. Chem. Phys.* **130**, 164521 (2009).
12. S. Arzhantsev, N. Ito and M. Maroncelli, *Chem. Phys. Lett.* **381**, 278 (2003).
13. N. Ito, S. Arzhantsev and M. Maroncelli, *Chem. Phys. Lett.* **396**, 83 (2004).
14. M. Maroncelli, J. MacInnis and G. R. Fleming, *Science* **243**, 1674 (1989).
15. D. Huppert and E. M. Kosower, *Annu. Rev. Phys. Chem.* **37**, 127 (1986).
16. P. F. Barbara and W. Jarzeba, *Acc. Chem. Res.* **21**, 195 (1988).
17. M. L. Horng, J. Gardecki, A. Papazyan and M. Maroncelli, *J. Phys. Chem.* **99**, 17311 (1995).
18. N. Ito, S. Arzhantsev, M. Heitz and M. Maroncelli, *J. Phys. Chem. B* **108**, 5771 (2004).
19. B. Bagchi and N. Gayathri *Adv. Chem. Phys.* **107**, 1 (1999).
20. (a) K. J. Fraser, E. I. Izgorodina, M. Forsyth, J. L. Scott and D. R. MacFarlane, *Chem. Commun.* **37**, 3817 (2007); (b) H. Tokuda, S. Tsuzuki, M. A. B. H. Susan, K. Hayamizu and M. Watanabe, *J. Phys. Chem. B* **110**, 19593 (2006).
21. H. Tokuda, S. Tsuzuki, K. Hayamizu, M. Watanabe, *J. Phys. Chem. B* **109**, 16474 (2005).
22. H. Jin, B. O'Hare, J. Dong, S. Arzhantsev, G. A. Baker, J. F. Wishart, A. J.

- Benesi and M. Maroncelli, *J. Phys. Chem. B* **112**, 81 (2008).
23. B. Bagchi and R. Biswas, *Adv. Chem. Phys.* **109**, 207 (1999).
24. B. Bagchi and A. Chandra, *Adv. Chem. Phys.* **80**, 1 (1991).
25. (a) S. Roy and B. Bagchi, *J. Chem. Phys.* **99**, 9938 (1993); (b) S. Roy and B. Bagchi, *J. Chem. Phys.* **98**, 1310 (1993).
26. (a) N. Nandi, S. Roy and B. Bagchi, *J. Chem. Phys.* **102**, 1390 (1995); (b) B. Bagchi and R. Biswas, *J. Phys. Chem.* **100**, 1238 (1996).
27. P. G. Wolynes, *J. Chem. Phys.* **86**, 5133 (1987).
28. I. Rips, J. Klafter and J. Jortner, *J. Chem. Phys.* **88**, 3246 (1988).
29. H. K. Kashyap and R. Biswas, *J. Phys. Chem. B* 2009 (in press).
30. H. K. Kashyap and R. Biswas, *J. Phys. Chem. B* **112**, 12431 (2008).
31. D. A. McQuarrie, *Statistical Mechanics*; University Science Books: CA, 2003.
32. H. K. Kashyap and R. Biswas, *J. Chem. Phys.* **125**, 174506 (2006).
33. (a) R. Biswas and B. Bagchi, *J. Phys. Chem. B* **100**, 4261 (1996); (b) R. Biswas, N. Nandi and B. Bagchi, *J. Phys. Chem. B* **101**, 2968 (1997).
34. C. F. Chapman and M. Maroncelli, *J. Phys. Chem.* **95**, 9095 (1991).
35. (a) C. G. Grey and K. E. Gubbins, *Theory of Molecular Fluids*, Vol. I, Oxford University: Oxford, 1984; (b) D. Isbister and R. Bearman, *J. Mol. Phys.* **28**, 1297 (1974); (c) J. L. Labowitz, *Phys. Rev.* **133**, A895 (1964).
36. J. P. Hansen and I. R. McDonald, *Theory of Simple Liquids*, Academic, London, 1986.
37. H. Jin, G. A. Baker, S. Arzhantsev, J. Dong and M. Maroncelli, *J. Phys. Chem. B* **111**, 7291 (2007).
38. P. Attard, *Phys. Rev. E* **48**, 3604 (1993).
39. A. Chandra and B. Bagchi, *J. Chem. Phys.* **110**, 10024 (1999).
40. (a) R. M. Lynden-Bell, *J. Phys. Chem. B* **111**, 10800 (2007); (b) I. Streeter, R. M. Lynden-Bell and R. G. Compton, *J. Phys. Chem. C* **112**, 14538 (2008).
41. S. Arzhantsev, K. A. Zachariasse and M. Maroncelli, *J. Phys. Chem. B* **110**, 3454 (2006).
42. C. Swalina, S. Arzhantsev, H. Li and M. Maroncelli, *J. Phys. Chem. B* **112**, 14959 (2008).
43. R. Lapouyade, A. Kuhn, J.-F. Letard and W. Rettig, *Chem. Phys. Lett.* **208**, 48 (1993).
44. Y. Amatatsu, *Theor. Chem. Acc.* **103**, 445 (2000).

45. Y. Amatatsu, Chem. Phys. **274**, 87 (2001).
46. T. Nishida, Y. Tashiro and M. Yamamoto, J. Fluorine Chem. **120**, 135 (2003).
47. Y. A. Sanmamed, D. Gonzalez-Salagado, J. Troncoso, C. A. Cerdeirina and L. Romani, Fluid Phase Equilib. **252**, 96 (2007).
48. M. E. Van Valkenburg, R. L. Vaughn, M. Williams and J. S. Wilkes, Thermochim. Acta **425**, 181 (2005).
49. J. G. Huddleston, A. E. Visser, W. M. Richert, H. D. Willauer, G. A. Broker and R. D. Rogers, Green Chem. **3**, 156 (2001).
50. S. V. Dzyuba and R. A. Bartsch, ChemPhysChem **3**, 161 (2002).
51. B. Bagchi and R. Biswas, Acc. Chem. Res. **31**, 181 (1998).
52. We have noticed that reasonable fits for the calculated $S_{si}(t)$ can be obtained by using any of the following equations (i) $S_{si}^{fit}(t) = \exp[-(t/\tau)^\beta]$, (ii) $S_{si}^{fit}(t) = a_1 \exp[-(t/\tau_1)] + (1 - a_1) \exp[-(t/\tau_2)^\beta]$, and (iii) $S_{si}^{fit}(t) = a_1 \exp[-(t/\tau_1)^\beta] + (1 - a_1) \exp[-(t/\tau_2)^\beta]$ by varying the value of the stretching exponent (β) roughly between 0.7 – 0.8. The quality of fits obtained by using these forms are not too different from that obtained by using a bi-exponential form, $S_{si}^{fit}(t) = a_1 \exp[-(t/\tau_1)] + (1 - a_1) \exp[-(t/\tau_2)]$. As the static heterogeneity of these liquids has not been incorporated in the calculations of $S_{si}(t)$ and also as the fitted values of β (~0.7 – 0.8) are not much away from unity, the bi-exponential form rather than those with the stretching exponents are chosen. See Fig. AIII.1 in Appendix III for further information.
53. R. Karamkar and A. Samanta, J. Phys. Chem. A **106**, 4447 (2002).
54. R. Karamkar and A. Samanta, J. Phys. Chem. A **106**, 6670 (2002).
55. J. A. Ingram, R. S. Moog, N. Ito, R. Biswas and M. Maroncelli, J. Phys. Chem. B **107**, 5926 (2003).
56. Mark Maroncelli (*private communication*).
57. This may arise from the $(\epsilon_0)^{1/2}$ dependence of the inverse Debye screening length (κ) appearing in the electrical potential (ψ) at a distance r from an ion: $\psi(r) = \frac{z_i q}{\epsilon_0} \cdot \frac{e^{-\kappa r}}{r}$, where z_i is the valence of the i^{th} type ion and q is the

unit of electric charge ($q = \frac{F}{N_A}$, F being the Faraday and N_A the Avogadro

number). The inverse Debye screening length is determined from the number density of ions of type i (n_i) present in the medium as follows:

$$\kappa = \left(\frac{4\pi q^2}{\epsilon_0 k_B T} \sum_i n_i z_i^2 \right)^{1/2}. \text{ Therefore, } \kappa \text{ becomes large for a small value of}$$

ϵ_0 which compels ψ to fall off with r at a much faster rate than what should have been in a medium of relatively larger polarity. This might lead a ‘purely’ (no permanent dipole moment on the ions) ionic system to behave as that governed by a much shorter-ranged interaction. (See for equations and discussion: S. Glasstone, In *An Introduction to Electrochemistry*; Litton Educational Publishing, 1942).

58. T. Pradhan, H. A. R. Gazi and R. Biswas, *J. Chem. Phys.* **131**, 054507 (2009).
59. B. Bagchi, *J. Chem. Phys.* **100**, 6658 (1994).
60. L. Reynolds, J. Gardecki, S. J. Frankland, M. L. Horng and M. Maroncelli, *J. Phys. Chem.* **100**, 10337 (1996).
61. R. Biswas, J. E. Lewis and M. Maroncelli, *Chem. Phys. Lett.* **310**, 485 (1999).
62. J. T. Fourkas, A. Benigno and M. Berg, *J. Chem. Phys.* **99**, 8552 (1993).
63. B. L. Bhargava and S. Balasubramanian, *J. Chem. Phys.* **123**, 144505 (2005).
64. Y. Shim, J. Duan, M. Y. Choi and H. J. Kim, *J. Chem. Phys.* **119**, 6411 (2003).
65. Y. Shim, Choi, M. Y. Choi and H. J. Kim, *J. Chem. Phys.* **122**, 044511 (2005).
66. Y. Shim, Choi, M. Y. Choi and H. J. Kim, *J. Chem. Phys.* **122**, 044510 (2005).
67. M. N. Kobrak, *J. Chem. Phys.* **125**, 064502 (2006).
68. M. N. Kobrak and V. Znamenskiy, *Chem. Phys. Lett.* **395**, 127 (2004).
69. C. J. Margulis, *Mol. Phys.* **102**, 829 (2004).
70. Z. Hu and C. J. Margulis, *J. Phys. Chem. B* **110**, 11025 (2006).
71. D. A. Turton, J. Hunger, A. Stoppa, G. Hefter, A. Thoman, M. Walther, R. Buchner and K. Wynne, *J. Am. Chem. Soc.* **131**, 11140 (2009).
72. S. Chandrasekhar, *Rev. Mod. Phys.* **14**, 180 (1943).
73. Y. Shim, H. J. Kim, *J. Phys. Chem. B* **112**, 11028 (2008).
74. (a) C. Schroder, M. Haberler and O. Steinhauser, *J. Chem. Phys.* **128**, 134501

(2008); (b) C. Schroder and O. Steinhauser, *J. Chem. Phys.* **131**, 114504 (2009).

75. T. Li, A. A. Hassanali, Y.-T. Kao, D. Zhong and S. Singer, *J. Am. Chem. Soc.* **129**, 3376 (2007).

Chapter 7

Molecular Dynamics Simulation Studies of Water-Tert Butyl Alcohol (TBA) Mixtures: Equilibrium and Dynamical Properties

7.1 Introduction

It is already mentioned in chapters 3 and 4 that alcohol-water mixtures exhibit anomalous properties at low alcohol concentration.¹⁻³⁰ The observed anomalies in many of thermodynamic and transport properties of these mixtures, starting from excess partial molar enthalpies,¹ heat capacities,¹⁻² concentration fluctuations³ and its temperature dependence, non-monotonic molefraction dependence of Walden's rule for ions¹⁶ etc, are often linked to the structure of these solutions. Also, other properties such as mean molar volume, self-diffusion coefficient, compressibility, and the excess entropy are significantly smaller than the values expected from an ideal mixture of the pure liquids. Neutron diffraction^{9,11,14} and X-ray scattering^{1,5-6} experiments of water-TBA mixture indicate that the hydrophobic interaction between alkyl groups of TBA drives the self association of TBA molecules when present at low molefractions in aqueous solution. The self-association of TBA molecules renders an enhanced structure of the mixture causing significant amount of loss of entropy.² And, as we move from water-rich region towards TBA-rich region, the tetrahedral (water like) structure gradually transforms to zigzag alcohol like structure.

Several Monte Carlo^{7,9,11,14,18} (MC) and Molecular Dynamics^{19-21,25-30} (MD) simulations were performed earlier to investigate the structure and dynamics of alcohol-water mixtures. Nakanishi *et al.* performed MC¹⁸ and subsequently MD¹⁹⁻²⁰ simulation studies for very small concentration of TBA in the mixture of water-TBA. In their simulation studies, self association of TBA molecules was observed, however hydrogen bonding between TBA molecules was not found. Noto and coworkers²¹ carried out *ab initio* quantum chemical calculations in order to investigate the

hydration structure around TBA molecule and compared with those around trimethylamine-N-oxide (TMAO). Their results indicated that water is more tightly coordinated by TMAO molecule than TBA. Similar comparison was made by Paul and Patey³⁰ to explain the region behind association of TBA in water when present in low molefraction. Note that TMAO does not show this kind of aggregation. The stronger interaction of hydrophilic group of TMAO with water than that of TBA was found to be principle reason behind this. Bowron *et al.* performed MC simulation using empirical potential structure refinement (EPSR) method to extract the structure functions at different compositions of the water-TBA mixtures.^{9,11,14} Later on, Kusalik and coworkers modified the potential parameters of Noto *et al.* model of TBA and carried out fully flexible all atom MD simulations in concentrated aqueous solution.²⁹ Hirata and coworkers²²⁻²⁴ extensively studied the TBA-water mixture by using the reference interaction site model (RISM) integral equation theory where association of polar molecules is considered through an appropriate closure description. These authors used the extended simple point charge (SPC/E) model for water and the optimized potential for liquid simulation (OPLS) force field for TBA.²² These studies indicated that at low TBA concentration the TBA molecules have been found to form cluster through hydrophobic interactions among the methyl groups, whereas the TBA-hydroxyl groups are involved in hydrogen bonding with water molecules surrounding the cluster. However, the agreement between the calculated partial radial distribution functions and those from neutron diffraction experiments and molecular dynamics simulations was found to be qualitative, even though realistic potentials with proper closure functions were used.²³

Even-though the above simulation studies revealed interesting structural aspects of water-TBA mixtures, the TBA concentration range considered was rather narrow. The only simulation work we find which covered the whole composition range of water-TBA mixture is that of Lee and Vegt.²⁵ However, their studies were focussed only on thermodynamic and structural properties. In this chapter we shall present the simulation results for the mixtures of flexible 3-site SPC water³¹ and 15-site all atoms TBA.²⁹ These models for water and TBA have been successfully used for pure as well as mixtures of TBA and water with low molefractions of TBA.²⁹ One of our goals in this work is to check the ability of the models for reproducing the real solution structure for the whole composition range of the TBA water mixtures.

The rest of the chapter is arranged as follows: In section 7.2 we shall give details of the MD simulations and the simulated results are presented and discussed in Sec. 7.3. Finally, this chapter ends with conclusion in section 7.4.

7.2 Models and Simulation Details

Molecular dynamics simulations for the mixture of flexible 3-site SPC³¹ and 15-site all atom TBA,²⁹ covering the whole composition range, have been performed with the MDynaMix³² simulation program at 300 K with 256 total number of molecules at all the molefractions considered. The general form of the force field in the program is given by

$$\begin{aligned}
 U = & \sum_{\text{Bonds}} k_b (b - b_{eq})^2 + \sum_{\text{Angles}} k_\theta (\theta - \theta_{eq})^2 + \sum_{\text{Dihedrals}} k_\phi (1 + \text{Cos}(n\phi - \delta)) \\
 & + \sum_{\text{Non-bonded}} 4\varepsilon_{ij} \left[\left(\frac{\sigma_{ij}}{r_{ij}} \right)^{12} - \left(\frac{\sigma_{ij}}{r_{ij}} \right)^6 \right] + \sum_{\text{Non-bonded}} \frac{q_i q_j}{r_{ij}}
 \end{aligned} \tag{7.1}$$

where b , θ and ϕ are bond length, bond angle and torsion angles. k_b , k_θ and k_ϕ are the force constants for bond distortion, angle distortion and torsional rotation, respectively. q is atomic charge; ε and σ are the Lennard-Jones parameters. r_{ij} is the distance between two atomic centers. The off-diagonal Lennard-Jones parameters σ_{ij} and ε_{ij} are obtained by using the Lorentz-Berthelot combination rules: $\varepsilon_{ij} = (\varepsilon_i \varepsilon_j)^{1/2}$ and $\sigma_{ij} = (\sigma_i + \sigma_j)/2$. In addition, the O-H stretching mode is made anharmonic via the Morse potential^{29,31-32} for both water and TBA molecules. The form of Morse potential is given as: $U_{\text{Morse}} = D\{1 - \exp[-\rho(b - b_0)]\}^2$. The potential parameters for the models used here are given in Tables 7.1 and 7.2.

At each mole fractions, the initial configuration has been started from a face-centred cubic (FCC) lattice in a cubic box with traditional periodic boundary condition and minimum image convention. At each mole-fraction, the volume of the simple cubic box was estimated from the experimental¹⁶ density. Ewald^{33,34} summation technique has been used for the treatment of long-range electrostatic interactions. The cut off

Table 7.1: Potential parameters and molecular topology for flexible 3-site SPC H₂O^(a)

Non-bonded interaction parameters			
Atomic site	ϵ (kJ/mol)	σ (Å)	q(e)
O	0.6506	3.1656	-0.8476
H	0.0	0.0	+0.4238

(a) $r_{eq}(\text{O-H})=1.00$ Å and $\theta_{eq}(\text{H-O-H})=109.47^\circ$. Other bonded potential parameters can be found in the article by Toukan and Rahman (Phys. Rev. B **31**, 2643 (1985)).

Table 7.2: Potential parameters and molecular topology for flexible 15-site TBA

Non-bonded interaction parameters			
Atomic site	ϵ (kJ/mol)	σ (Å)	q (e)
O	0.67	3.00	-0.5723
C(central-carbon)	0.1674	3.80	+0.3885
C(methyl-carbon)	0.1674	3.80	-0.3510
H(methyl)	0.1674	2.40	+0.1010
H(hydroxyl)	0.0	0.0	+0.3278
Bonded interaction parameters			
Bond	k_b (kJ/mol/Å)	b_{eq} (Å)	Comment
O-H	2284	0.9292	Morse ^(a)
O-C _c	1580	1.4164	
C _c -C _m	923	1.5240	
C _m -H _m	1294	1.111	
Angle	k_θ (kJ/mol/deg)	θ_{eq} (deg)	
H-O- C _c	195.4	111.28	
O-C _c -C _m	314.0	111.28	
C _m -C _c -C _m	222.3	108.745	
C _c -C _m - H _m	143.1	111.445	
H _m -C _m - H _m	147.3	108.754	
Dihedral angle	k_ϕ (kJ/mol)	δ	n
H-O- C _c -C _m	0.58	0.0	3
O-C _c -C _m -H _m	0.83	0.0	3
C _m -C _c -C _m --H _m	0.83	0.0	3

(a) $D=376.35$ kJ/mol, $\rho=2.44$ Å⁻¹.

Ref: Kusalik *et al.*, J. Phys. Chem. B **104**, 9526, (2000).

radius for the Lennard-Jones (LJ) potential and the real-space part of the electrostatic interaction are set equal to the half of the box length. Nose-Hoover³⁵ thermostat with coupling constant of 30 fs has been used to maintain the system temperature at 300 K. The multiple time-steps algorithm³⁶ is adopted in the leapfrog Verlet integration scheme with long and short time steps of 1fs and 0.1fs, respectively. A neighbour list has been used for calculating the LJ potential, and the real space portion of the Ewald sum updated after every 10 fs. Each simulation has been equilibrated for 200ps before a production run of 800 ps. The equilibrium trajectories were saved after each 10 fs for further analyses. The stored trajectories were then analysed to calculate various equilibrium and dynamical quantities by using TRANAL³² utility of the package and home-made subroutines.

7.3 Results & Discussion

We have calculated a number of experimentally measurable properties from the equilibrium trajectories saved. Single molecule properties reported here are averaged over both the number of molecules and the simulation trajectories while the collective properties are averaged over the simulation trajectories only. This section is divided into two parts. In the first part we shall present the equilibrium/static properties of the simulated system and compare with experiments wherever possible. The dynamical properties of the simulated system shall be presented and compared with available experiments in the next part.

7.3.1 Equilibrium Properties

7.3.1.1 Potential Energies

In Table 7.3 we give potential energies for intra- and inter species pair of molecules for different mole fraction of TBA and a summary of all the potential energies is given in Table 7.4. Note that the potential energies given in Table 7.3 for pair of molecular types are divided by the number of water molecules, N_{water} , for H₂O-H₂O, by number of TBA molecules, N_{TBA} , for TBA-TBA and by $\min(N_{\text{water}}, N_{\text{TBA}})$ for H₂O-TBA. It is can be seen from Table 7.4 that for water-water the dominant electrostatic contribution in the interaction energy is consistently attractive whereas LJ contribution is repulsive at all the composition studied. For water-TBA, both the

Table 7.3: Intermolecular Potential Energies in H₂O-TBA mixtures^(a)

X _{TBA}	Inter-molecular Potential Energies (kJ/mol)					
	H ₂ O-H ₂ O		H ₂ O-TBA		TBA-TBA	
	<U _{Electrostatic} >	<U _{LJ} >	<U _{Electrostatic} >	<U _{LJ} >	<U _{Electrostatic} >	<U _{LJ} >
0.00	-57.24	9.47(-0.19)	-	-	-	-
0.04	-57.64	9.56(-0.15)	-57.46	-25.19(-2.01)	-0.99	-4.48(-0.27)
0.10	-54.08	9.56(-0.09)	-33.03	-14.32(-1.18)	-2.89	-12.04(-0.42)
0.15	-52.66	9.47(-0.06)	-34.63	-10.44(-0.85)	-2.28	-14.97(-0.49)
0.20	-51.34	9.28(-0.05)	-30.87	-8.76(-0.53)	0.36	-16.28(-0.53)
0.25	-51.29	9.21(-0.04)	-26.63	-6.87(-0.47)	0.33	-17.79(-0.51)
0.30	-49.43	9.04(-0.03)	-25.51	-6.09(-0.37)	-1.32	-18.44(-0.52)
	-45.92	8.67(-0.02)	-21.89	-4.31(-0.22)	-4.91	-19.99(-0.48)
0.50	-42.62	8.26(-0.01)	-17.84	-3.09(-0.14)	-4.51	-21.13(-0.47)
0.60	-40.27	7.85(-0.01)	-19.65	-3.10(-0.12)	-6.04	-22.05(-0.40)
0.70	-36.22	7.19(-0.01)	-23.70	-2.99(-0.11)	-6.09	-22.85(-0.38)
0.80	-29.21	5.93(0.00)	-30.79	-2.86(-0.11)	-5.25	-23.49(-0.34)
0.90	-17.92	3.72(0.00)	-42.38	-2.07(-0.10)	-5.41	-24.06(-0.32)
1.00	-	-	-	-	-6.32	-24.68(-0.30)

(a) The quantity in bracket for LJ interactions is cut-off correction energy in LJ interaction.

Table 7.4: Summary of the interaction potential energies in H₂O-TBA mixtures^(a)

X _{TBA}	<U _{Non-bonded/ N_{Total}} > (kJ/mol)	<U _{Bonded/ N_{Total}} > (kJ/mol)	<U _{Inter/ N_{Total}} > (kJ/mol)	<U _{Total/ N_{Total}} > (kJ/mol)
0.00	-48.40	6.89	-48.40	-41.51
0.04	-66.01	8.50	-47.89	-57.51
0.10	-92.49	10.96	-47.18	-81.53
0.15	-115.24	13.05	-46.35	-102.19
0.20	-137.85	15.13	-45.39	-122.71
0.25	-160.59	17.24	-44.57	-143.35
0.30	-181.58	19.18	-43.81	-162.40
0.40	-226.89	23.39	-41.99	-203.50
0.50	-272.28	27.57	-40.25	-244.72
0.60	-315.96	31.63	-38.60	-284.33
0.70	-361.21	35.79	-36.72	-325.42
0.80	-404.88	39.86	-35.08	-365.02
0.90	-450.18	44.08	-33.26	-406.09
1.00	-495.99	48.49	-31.60	-447.50

(a) As we increase the TBA concentration from water-rich to TBA-rich region the non-bonded 1-4 intramolecular potential energy, present only in TBA, varies from -481.10 to -481.17 kJ/mol due to Coulomb interactions and from 17.06 to 17.08 kJ/mol due to LJ interactions

electrostatic and LJ contributions are attractive, and for TBA-TBA LJ is attractive for all the composition whereas electrostatic part has mixed effects. At $X_{\text{TBA}}=0.04$ the cross-interaction (water-TBA) to the total energy is largest in magnitude, showing a strong attractive interaction between unlike molecules. This energy decreases as we increase TBA mole fraction up-to equimolar solution and then start decreasing with further increase of TBA concentration. The general feature of Table 7.4 is that the magnitude of intermolecular potential energy decreases while that of total increases as we increase the TBA concentration. This is because a large amount of non-bonded intramolecular contribution to the potential energies comes from electrostatic 1-4 interactions present in TBA molecules.

7.3.1.2 Site-site Radial Distribution Functions

The relative density of one type of atom, β , from another type, α , as a function of distance, r , is described by site-site radial distribution function (RDF), $g_{\alpha\beta}(r)$. RDFs are calculated from normalized histograms of the distances between the various atom pairs. We show RDFs for $O_{\text{W}}-H_{\text{W}}$, $O_{\text{W}}-O_{\text{W}}$, $O_{\text{W}}-H_{\text{TBA}}$, $O_{\text{TBA}}-H_{\text{W}}$, $O_{\text{TBA}}-O_{\text{TBA}}$ and $O_{\text{TBA}}-H_{\text{TBA}}$, in Fig. 7.1 while the RDFs for $CC_{\text{TBA}}-O_{\text{W}}$, $CC_{\text{TBA}}-O_{\text{TBA}}$, $CC_{\text{TBA}}-CC_{\text{TBA}}$ and $CC_{\text{TBA}}-CM_{\text{TBA}}$ have been depicted in Fig. 7.2. The results are shown only for 5 compositions of water-TBA mixtures for clarity. Here, O_{W} refers to the water oxygen, H_{W} to the water hydrogen, H_{TBA} to the TBA hydroxyl hydrogen, O_{TBA} to the TBA oxygen, and CC_{TBA} and CM_{TBA} to central carbon and methyl carbon of TBA, respectively. RDFs for $O_{\text{W}}-H_{\text{W}}$ and $O_{\text{W}}-O_{\text{W}}$ shown in Fig. 7.1a and 7.1b, respectively, indicate that in TBA-rich composition the water molecules have tendency to associate through hydrogen bonding thereby forming clusters. However, the positions of the first peaks for these RDFs are weakly sensitive to the alcohol mole-fractions. Simultaneously, water and TBA molecules are distributed in such a way that hydrogen bonding between water-TBA and TBA-TBA also increases. In this regime H_2O dimers, chains and single free water molecules (without forming hydrogen bond network among themselves) in solution coexist as a mixture. This feature might be an indication of micro-heterogeneities present in the TBA-rich region of the mixture. Several MD simulation studies and small angle neutron scattering (SANS) experiments have also reported this kind of feature in water-TBA as well as in other alcohol-water binary mixtures.^{4,7,11,25,37-39} Note that our simulation results overestimate

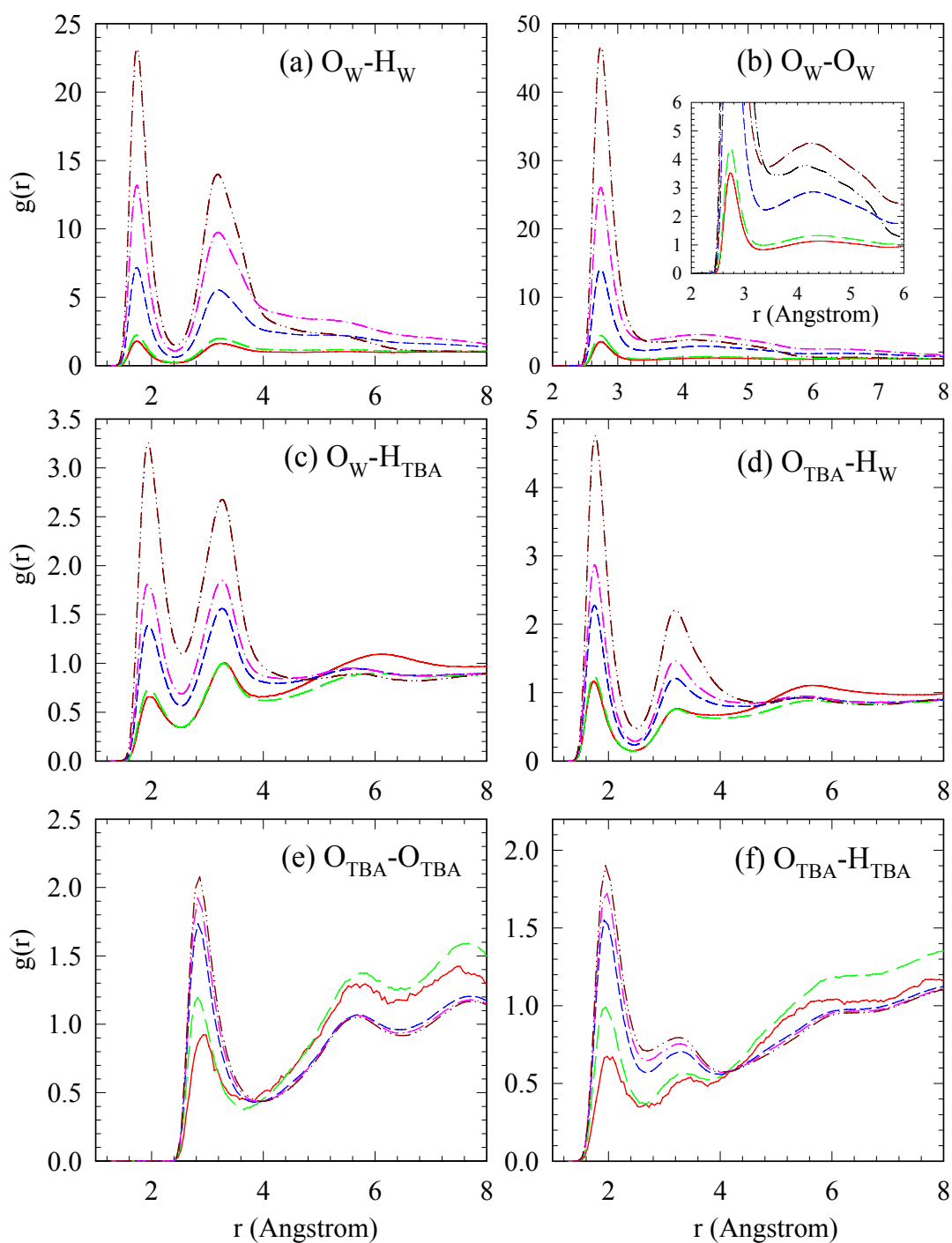


Figure 7.1: Radial distribution function, $g(r)$, for various atomic pairs as a function of separation, r , at different molefractions of TBA. For labelling of various sites see text. The inset shown in the panel for O_W-O_W is the same plot at different scale for clear view of second solvation shell. In all the panels, the *solid* (red), *long-dashed* (green), *short-dashed* (blue), *dotted-dashed* (pink) and *double dotted-dashed* (dark red) are the RDFs at $X_{TBA} = 0.04, 0.10, 0.50, 0.70$ and 0.90 , respectively.

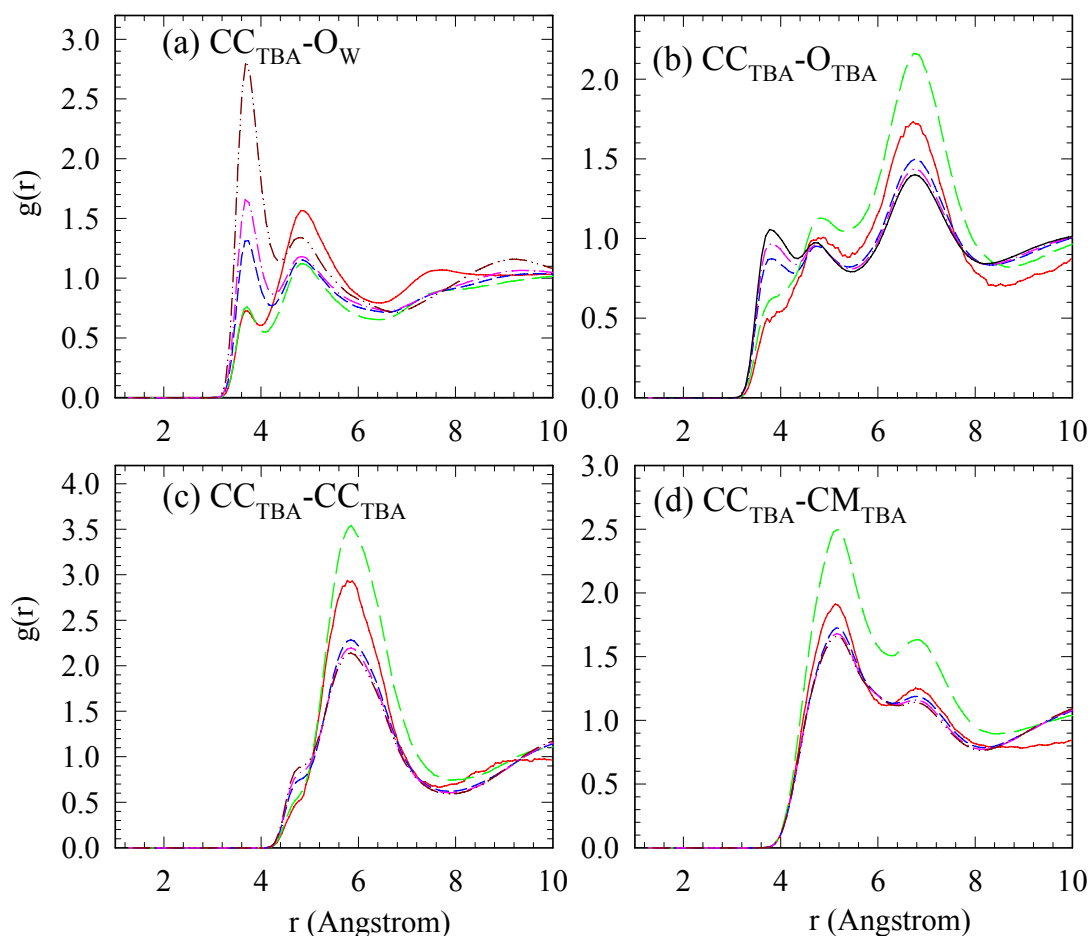


Figure 7.2: Radial distribution function, $g(r)$, for various atomic pairs as a function of separation, r , at different molefractions of TBA. For labelling of various sites see text. Notations used here for different molefractions of TBA are those used in Fig. 7.1.

the degree of water-water association in TBA-water mixtures. The simple empirical potentials for pure water and TBA, and the use of combining rules for cross interactions might be inaccurate to describe the proper association of water-water in such complex systems. Fig. 7.1c and 7.1d show that water is strong hydrogen bond donor to TBA than TBA to water at all the compositions. The first maximum in Fig. 7.1e and 7.1f for $O_{TBA}-O_{TBA}$ and $O_{TBA}-H_{TBA}$ RDFs decrease with decreasing TBA concentration. This indicates that TBA structure gradually disappears as it becomes more dilute. Also, Fig. 7.1f for $O_{TBA}-H_{TBA}$ RDF suggests that there is a significant

amount of hydrogen bonding among TBA molecules at $X_{\text{TBA}}=0.04$, in agreement with Bowron¹⁴ *et al.* This feature is completely absent in the work of Lee²⁵ *et al.*

Fig. 7.2a suggests that the swollen structure of water around TBA (smaller first peak and larger and broader second peak) becomes tighter when the TBA content in the mixture is more (increase in the first peak and decrease in the second peak). The most pronounced peaks in RDFs shown in Fig. 7.2b, 7.2c and 7.2d increase first and then start decreasing with increasing TBA concentration. This could be an indicative of strengthening of water structure up-to 0.10 molefraction ($\sim X_{\text{TBA}}=0.10$) of TBA and the breaking of structure with further increase of TBA.

7.3.1.3 Orientational Distribution Functions

The orientational ordering of the effective linear dipoles of molecules is in general given by the dipolar symmetry projections $h^{110}(r)$ and $h^{112}(r)$ of the pair correlation function, $h(1,2)$, where 1 and 2 denote the locations of molecule 1 and 2, respectively. For a mixture, $h^{11l}(r)$ where $l = 0,2$ are determined by the weighted sums of the dipolar symmetry projections of pair distributions for species i and j , $h_{ij}^{11l}(r)$, as⁴⁰

$$h^{11l}(r) = \sum_{i,j} \frac{x_i x_j \mu_i \mu_j}{\mu^2} h_{ij}^{11l}(r); \quad \mu^2 = \sum_i x_i \mu_i^2 \quad (7.2)$$

where x_i and μ_i are molefraction and the dipole-moment of species i , respectively.

The dipolar symmetry coefficients $h_{ij}^{11l}(r)$ for a pair of molecules of species i and j are calculated assuming water and TBA as linear molecules and are given by⁴⁰⁻⁴²

$$h_{ij}^{110} = 3 \langle h_{ij}(1,2) \Delta(1,2) \rangle_{\Omega_1 \Omega_2} = \frac{3}{(4\pi)^2} \int h_{ij}(1,2) (\hat{u}_1 \cdot \hat{u}_2) d\Omega_1 d\Omega_2 \quad (7.3)$$

$$h_{ij}^{112} = \frac{3}{2} \langle h_{ij}(1,2) D(1,2) \rangle_{\Omega_1 \Omega_2} = \frac{3}{2(4\pi)^2} \int h_{ij}(1,2) [3(\hat{u}_1 \cdot \hat{r})(\hat{u}_2 \cdot \hat{r}) - (\hat{u}_1 \cdot \hat{u}_2)] d\Omega_1 d\Omega_2 \quad (7.4)$$

where \hat{u}_1 and \hat{u}_2 are the unit vectors along the dipole moment of the molecule 1 and 2 respectively, \hat{r} is the unit vector along the intermolecular separation between the centre of masses of the two molecules and, Ω_1 and Ω_2 are the solid angles.

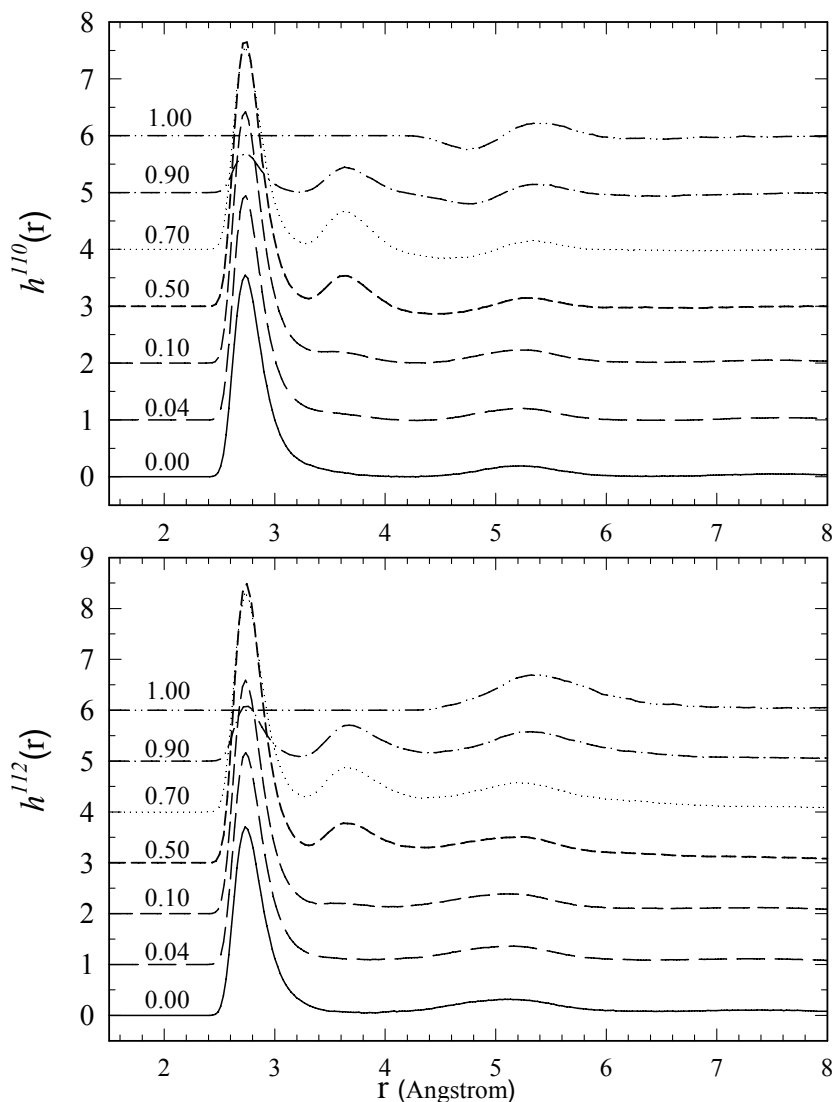


Figure 7.3: Dipolar symmetry projections $h^{110}(r)$ (upper panel) and $h^{112}(r)$ (lower panel) as a function of separation, r . The number tagged on each curve represents the molefraction of TBA. The successive curves are offset 1 unit along the y-axis.

In Fig. 7.3 we have shown $h^{110}(r)$ (upper panel) and $h^{112}(r)$ (lower panel) as a function of separation r calculated from simulations. In pure water the function $h^{110}(r)$ has peaks at positions ~ 2.8 and ~ 5.2 Å while this function has a minimum and a maximum at ~ 4.7 and ~ 5.4 Å. The peak position at ~ 2.8 Å is consistently found in the mixture of TBA-water at all molefraction, whereas the peak at ~ 5.2 Å is shifted

gradually to $\sim 5.4 \text{ \AA}$ with increasing mole fraction of alcohol. Also, an intermediate peak at approximately 3.7 \AA , which is absent in pure water and alcohol, is emerging with increasing TBA concentration. The projection $h^{112}(r)$ has also two prominent peaks at positions ~ 2.8 and $\sim 5.1 \text{ \AA}$ in pure water where there is only one prominent peak at $\sim 5.2 \text{ \AA}$ has been found in the case of pure TBA. Other features of projection $h^{112}(r)$ for the mixture are very similar to that of $h^{110}(r)$.

7.3.1.4 Dielectric Constant

Once the orientational correlation functions are obtained, the static dielectric constant (ϵ_0) of the mixture can be calculated by using the famous Kirkwood formula⁴⁰⁻⁴²

$$\frac{(\epsilon_0 - 1)(2\epsilon_0 + 1)}{9\epsilon_0 y} = 1 + \frac{4\pi\rho}{3} \int_0^\infty r^2 h^{110}(r) dr \quad (7.5)$$

where $y = \frac{4\pi\beta\rho\mu^2}{9}$ is called polarity parameter and ρ is the total number density.

The value of ϵ_0 can also be calculated from the fluctuation of the collective dipole moment of the system defined as, $\mathbf{M} = \sum \boldsymbol{\mu}$, $\boldsymbol{\mu}$ being molecular dipole moment, using following equation⁴⁰⁻⁴²

$$\epsilon_0 = 1 + \frac{4\pi}{3Vk_B T} [\langle \mathbf{M}^2 \rangle - \langle \mathbf{M} \rangle^2] \quad (7.6)$$

with V as the average volume of the simulation system, k_B as the Boltzmann constant. In Fig. 7.4 the calculated dielectric constants for TBA-water mixtures using Eqs 7.5, and 7.6 are shown by *open circles* and *triangles*, respectively. Also shown are the experimental data (*filled circles*) for static dielectric constant reported in the works of Broadwater and Kay.¹⁶ The average value of ϵ_0 and the error bars were calculated using block method by dividing the collected trajectories into slightly

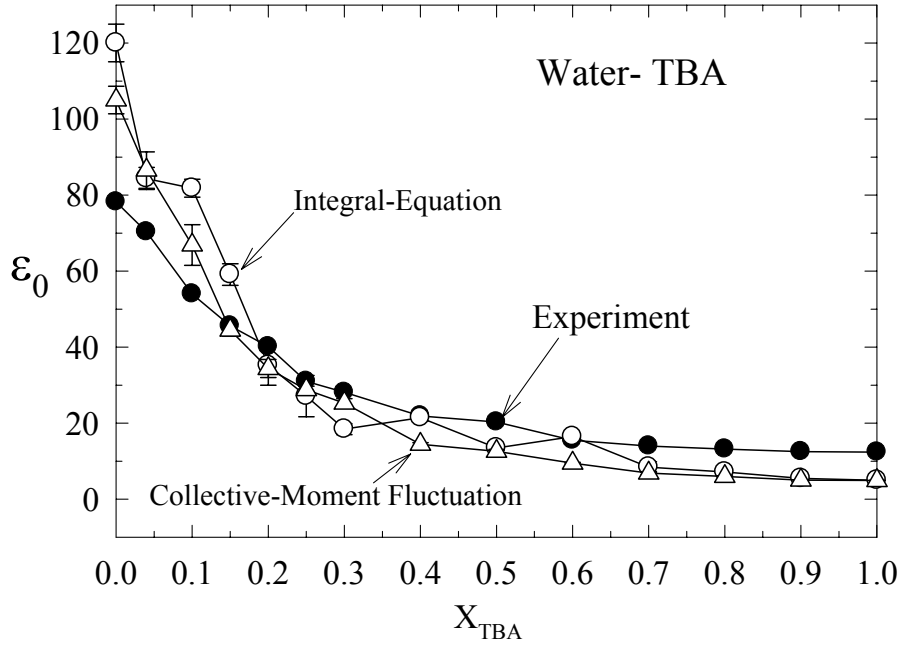


Figure 7.4: Comparison between calculated static dielectric constants using Eq. 7.5 (connected open circles) and Eq. 7.6 (connected open triangles), and experimental data (filled circles). The error bars have been estimated using block method.

overlapping (0 to 500ps, 100 to 600ps etc) blocks of 500ps time span. The calculated values of static dielectric constant are in good agreement with experimental data.

7.3.2 Dynamical Properties

7.3.2.1 Velocity Autocorrelation Function

In a binary mixture of species 1 and 2, the normalized velocity autocorrelation function (VACF) for i^{th} ($i=1, 2$) species particle is defined as

$$f_v^i(t) = \frac{\langle \vec{v}(t_0 + t) \cdot \vec{v}(t_0) \rangle_{N_i, t_0}}{\langle \vec{v}(t_0)^2 \rangle_{N_i, t_0}} \quad (7.7)$$

where $\vec{v}(t)$ is velocity at time t and $\langle \rangle$ describes the average over both the number of i^{th} species particles N_i and initial time t_0 . The calculated VACF for both water and TBA molecules as a function of time at different mole fractions are shown in Fig.

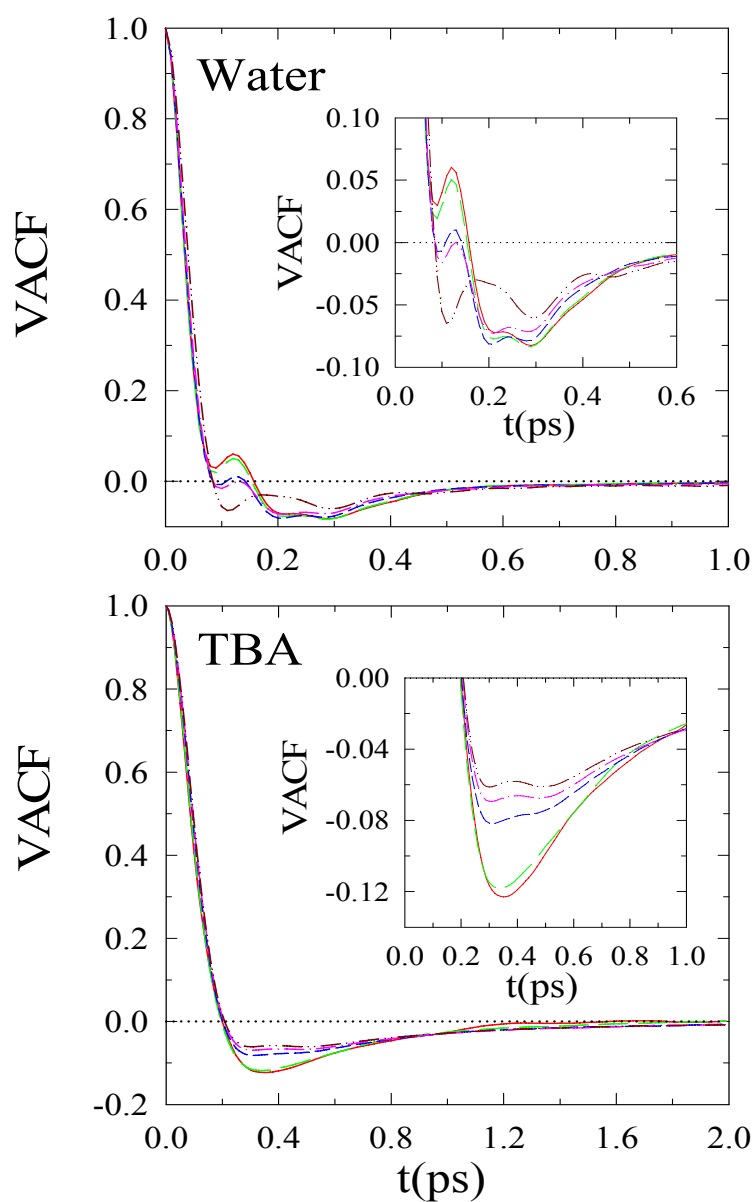


Figure 7.5: Velocity autocorrelation function (VACF) for water (*upper panel*) and TBA (*lower panel*) molecules as a function of time t at different molefractions of TBA. VACFs at $X_{\text{TBA}}=0.04, 0.10, 0.50, 0.70$ and 0.90 are shown by *solid (red), long-dashed (green), short-dashed (blue), dotted-dashed (pink) and double dotted-dashed (dark red)* lines, respectively. The insets shown in both the panels are for clear view.

7.5. In the *upper panel* we have shown VACFs for water while the decay profile of VACFs for TBA molecule has been shown in the *lower panel*. Typical backscattering behaviour is found for both types of solvent molecules at all the composition studied here. This is a well-known signature of closely packed structure of the surrounding near neighbours. The position of the local minimum at short time in VACF for water is gradually shifting towards right with more negative value of VACF with increasing TBA molfraction. This suggests that for short time (0.075-0.15ps) the degree of backscattering in the translational motion of water molecules increases with increasing TBA molefraction while this feature is completely reversed for longer times(0.15-0.5ps). A significant amount of negative portion in the VACF of TBA reveals that there is moderate cage formation around TBA molecules and the strength of the caging effect increases with decreasing TBA concentration.

7.3.2.2 Mean Square Displacement

The average mean square displacement (MSD) of i^{th} ($i=1, 2$) species particle is given by $\langle [\vec{r}(t+t_0) - \vec{r}(t_0)]^2 \rangle_{N_i, t_0}$ where $\vec{r}(t)$ is the position at time t , and $\langle \rangle$ denotes the average over both the number of i^{th} species particles N_i and initial time t_0 . The calculated MSD for both water and TBA molecules as a function of time at different mole fractions are depicted in Fig. 7.6. The square root of MSD, so-called root mean square displacement (RMSD), is a measure of effective distance travelled by the particle. Let's take an example of $X_{\text{TBA}}=0.10$ shown by *long-dashed line* of the Fig. 7.6 for both water and TBA. After 100ps the average distance travelled by a water molecule is about 10Å while it remains 8Å for TBA after same time. Therefore, the mobility of water molecule is more than that of TBA at this mole fraction. For water, MSD curve shows that the mobility of water decreases up-to 70% of TBA and then increases. While, for TBA it decreases first up-to ~15% and after then start increasing as we increase the TBA concentration. This behaviour can be clearly seen in diffusion coefficient of each molecule which has been calculated from the slope of the MSD curve (for time t sufficiently large) as a function of TBA mole fraction.

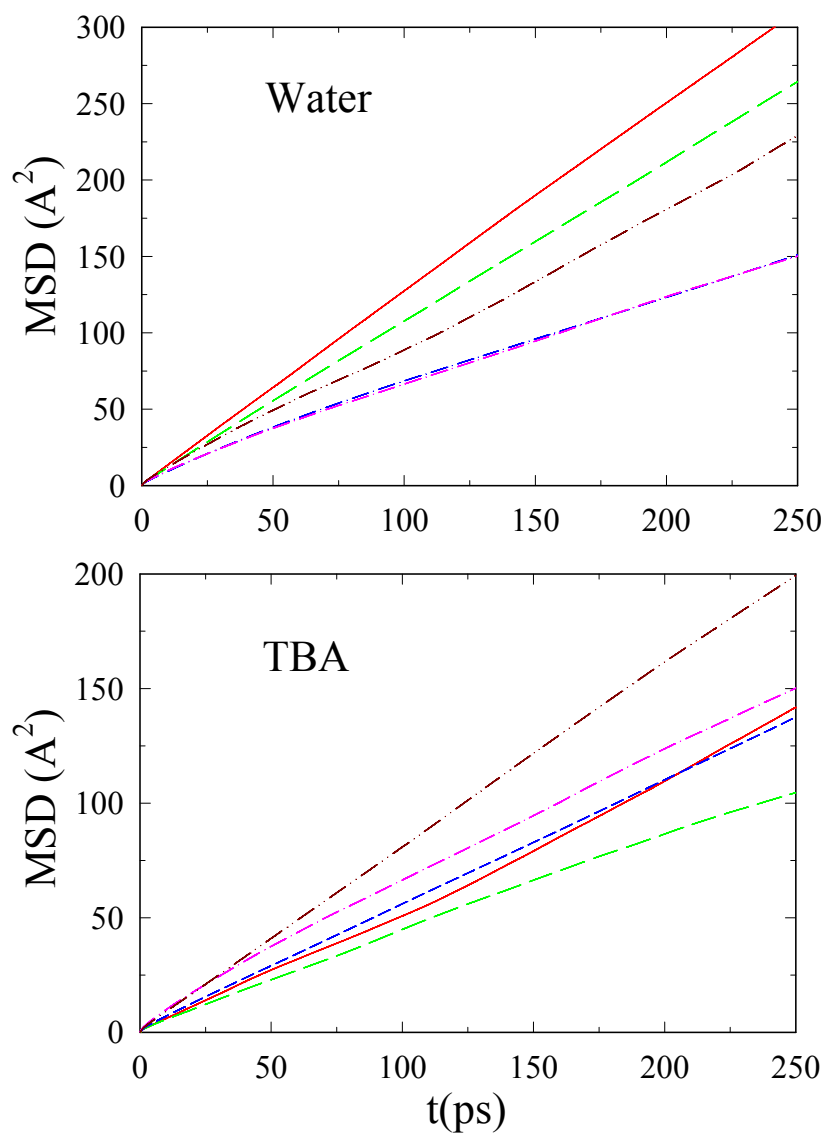


Figure 7.6: Mean square displacement (MSD) for water (*upper panel*) and TBA (*lower panel*) molecules as function of time, t , at different molefractions of TBA. Notation remains the same as that in Figure 7.5.

7.3.2.3 Self Diffusion Coefficient

The translational self-diffusion coefficient D_i of i^{th} species particle can be determined by Green-Kubo relation through the integral of VACF over a sufficiently long time as

$$D_i = \frac{k_B T}{m_i} \int_0^{\infty} f_v^i(t) dt, \quad (i=1 \text{ or } 2) \quad (7.8)$$

where m_i is mass of the i^{th} species particle. The translational self-diffusion coefficient D_i can also be determined from the slope of the mean square displacement (MSD) as

$$D_i = \lim_{t \rightarrow \infty} \frac{\langle [\vec{r}(t) - \vec{r}(0)]^2 \rangle_{N_i}}{6t}, \quad (i=1 \text{ or } 2) \quad (7.9)$$

The calculated self-diffusion coefficients for water (*upper panel*) and TBA (*lower panel*) molecules from VACF (*connected open circles*) and MSD (*connected open triangles*) roots have been shown in Fig. 7.7. The integration limits in Eq. (7.8) have been taken from 0 to 50ps for both water and TBA at all the molfractions. We have taken the slope of MSD in Eq. (7.9) from time t equal to 25 to 250ps in all the cases. These data were also compared with PGSE NMR experiments done in two different groups by Kipkemboi *et al.*⁴³ (*filled circles*) and by Price⁴⁴ and co-workers (*filled squares*). In the both the experiments below $X_{\text{TBA}}=0.20$ the self-diffusion coefficients of both water and TBA decrease rapidly with increasing TBA molfraction. Above $X_{\text{TBA}}=0.20$ the diffusion coefficients of both the components remain nearly invariant with the composition of the mixture. Apart from the magnitude, from Fig. 7.7 it is clear that the basic trend of diffusion coefficients of water is well captured up to $X_{\text{TBA}}=0.70$, and simulation predicts a significant increase of water diffusion coefficient for $X_{\text{TBA}} > 0.70$. The diffusion coefficient of TBA is poorly predicted by the simulation except at water-rich region.

7.3.2.4 Mutual Diffusion Coefficient

In binary liquid mixtures, mutual diffusion describes the ability of one species diffusing into the other. This is different from self-diffusion which is a measure of

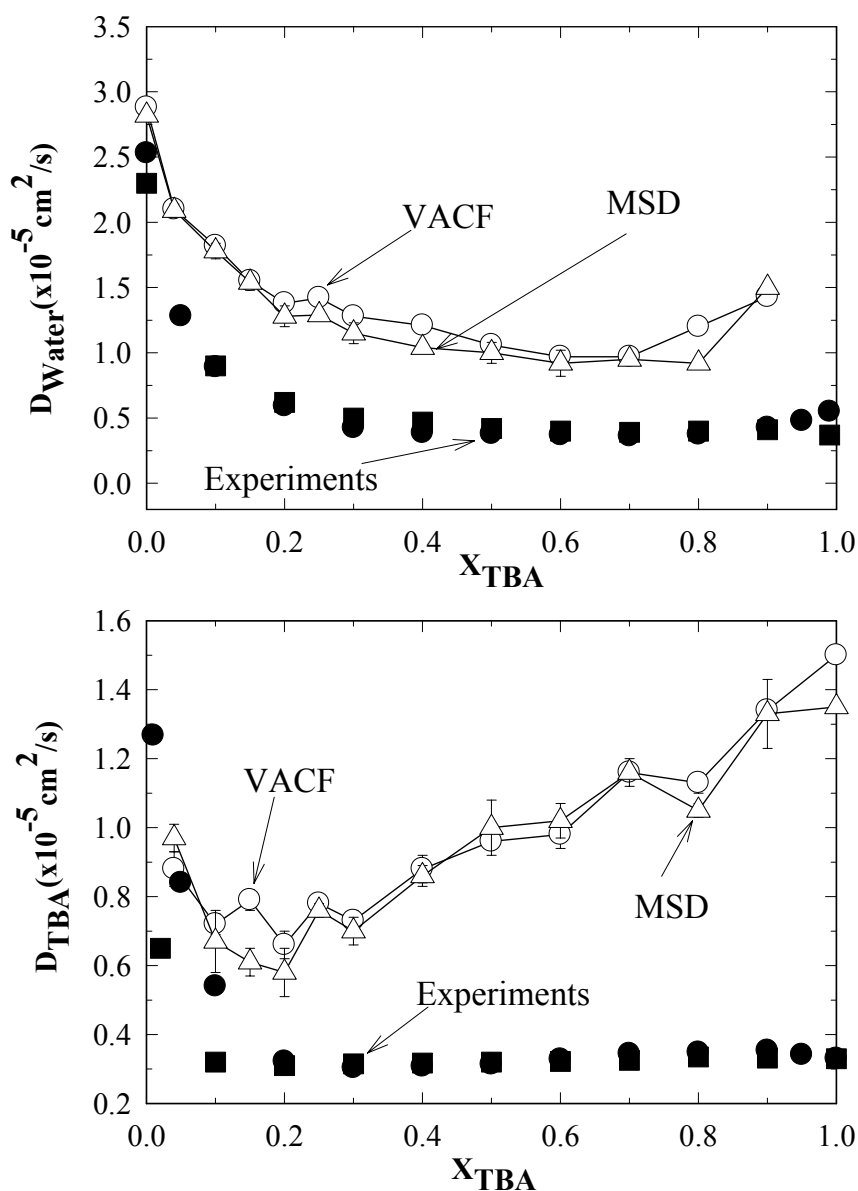


Figure 7.7: Self-diffusion coefficients of water (*upper panel*) and TBA (*lower panel*) molecules as functions of composition of water-TBA mixtures: The self-diffusion coefficients calculated from VACF and MSD are shown by the *connected open circles* and *connected open triangles*. Also shown are the data spin-echo-NMR experiments for the diffusion coefficients from Refs. 43 (*filled circles*) and 44 (*solid squares*).

mobility of each component in the absence of any external force. Therefore, mutual diffusion is associated with the collective motion of many particles together in the mixture and arises due to the gradient of the composition (or chemical potential). Mutual diffusion can be expressed in terms of velocity correlation functions of the collective motion of the system or in terms of mean square displacement of the centre

of mass of the particles of either of the two components. The mutual diffusion coefficient D_{12} ($= D_{21}$) in a binary mixture of species 1 and 2 is defined by Green-Kubo relation as⁴⁵⁻⁴⁸

$$D_{12} = \frac{Q}{3Nx_1x_2} \int_0^{\infty} \langle \vec{J}_{12}(t) \cdot \vec{J}_{12}(0) \rangle dt \quad (7.10)$$

where relative velocity $\vec{J}_{12}(t)$ is defined as

$$\vec{J}_{12}(t) = x_2 \sum_{k=1}^{N_1} \vec{v}_k(t) - x_1 \sum_{l=1}^{N_2} \vec{v}_l(t) \quad (7.11)$$

and N is the total number of particles, x_1 and x_2 are mole fractions of species 1 and 2, respectively. $\vec{v}_k(t)$ is the velocity of k^{th} particle of species 1 at time t and $\vec{v}_l(t)$ the velocity of l^{th} particle of species 2 at time t . The thermodynamic factor Q can be expressed as

$$Q = [1 + x_1x_2\rho(G_{11} + G_{22} - 2G_{12})]^{-1} \quad (7.12)$$

with

$$G_{ij} = 4\pi \int_0^{\infty} r^2 [g_{ij}(r) - 1] dr \quad (7.13)$$

where ρ is the number density and $g_{ij}(r)$ is the radial distribution function for pair of species ij .

By putting the value of $\vec{J}_{12}(t)$ from Eq. (7.11) into Eq. (7.10) and following the straight forward algebra we get

$$D_{12} = Q(x_2D_1 + x_1D_2 + x_1x_2D^d) \quad (7.14)$$

where D_1 and D_2 are self-diffusion coefficient of species 1 and 2, respectively. The distinct diffusion coefficient D^d arising due to all the dynamic cross correlation functions is given by

$$D^d = \frac{1}{3Nx_1^2} \int_0^\infty \left\langle \sum_{k=1}^{N_1} \sum_{k' \neq k}^{N_1} \vec{v}_k(t) \cdot \vec{v}_{k'}(0) \right\rangle dt + \frac{1}{3Nx_2^2} \int_0^\infty \left\langle \sum_{l=1}^{N_2} \sum_{l' \neq l}^{N_2} \vec{v}_l(t) \cdot \vec{v}_{l'}(0) \right\rangle dt - \frac{2}{3Nx_1x_2} \int_0^\infty \left\langle \sum_{k=1}^{N_1} \sum_{l=1}^{N_2} \vec{v}_k(t) \cdot \vec{v}_l(0) \right\rangle dt \quad (7.15)$$

Here, $\langle \rangle$ denotes the time average. The physical significance of distinct diffusion coefficient is as follows: when $D^d = 0$ the mixture is ideal, meaning that correlations between intra and inter species molecules are balanced. A negative (or positive) value of distinct diffusion coefficient is an indicator of associative (or dissociative) nature of the mixture. When D^d is positive then the mutual diffusivity will be greater than its ideal value and if it is negative, the mutual diffusivity will be less than the ideal value (weighted sum of self-diffusion coefficients).

The mutual diffusion coefficient D_{12} has been calculated from the integration of relative velocity correlation function (RVCF) with integration limit 0 to 50ps. In Fig. 7.8 shown are simulated (*open circles*) and experimental⁴⁹⁻⁵¹ (*filled circles*) mutual diffusion coefficients. Note that agreement between simulation and experimental data is semi-quantitative for water-rich region while comparison could not be made beyond 15% concentration of TBA due to lack of experimental results. Also note that the statistical error in the simulated mutual diffusivity. Here error bars in this case have been calculated by block method. The statistical error in mutual diffusivity is of great concern and could be reduced up to some extent by averaging over more simulation runs. In the above calculations, the value of thermodynamic factor Q has been calculated using Eq. 7.12 where $g_{ij}(r)$ has been determined using the centre-of mass of each molecule. The numerical error in the integration of radial distribution functions is also of serious concern and therefore several other proposed methods (e.g. by using activity coefficient and vapour pressure data) for calculating Q could also be used. The typical behaviour of RVCF as a function of time is shown in Fig. 7.9 at

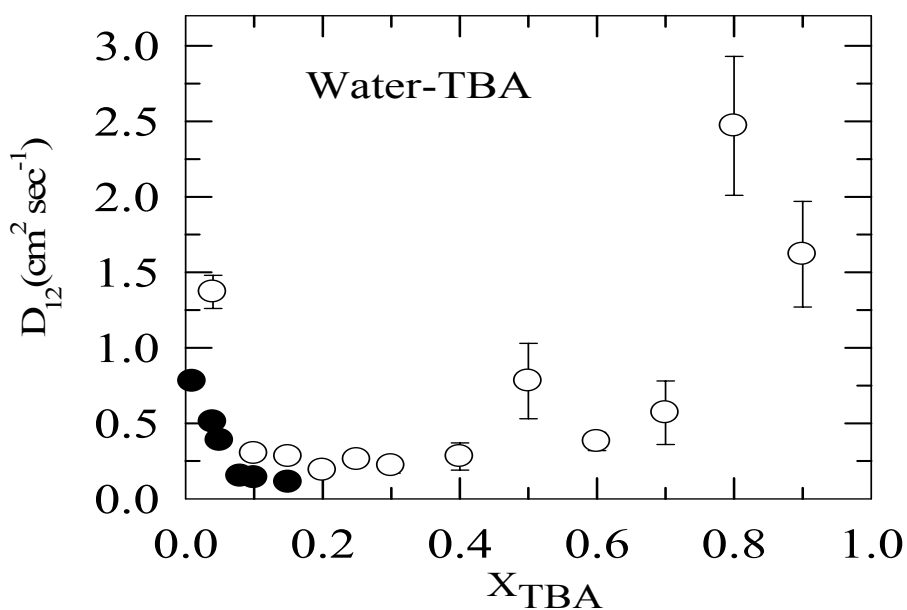


Figure 7.8: Mutual diffusion coefficient in water-TBA mixture as function of TBA mole fraction. The simulated results have been shown by the *open circles* while available experimental data for a few mole fractions are shown by the *filled circles*.

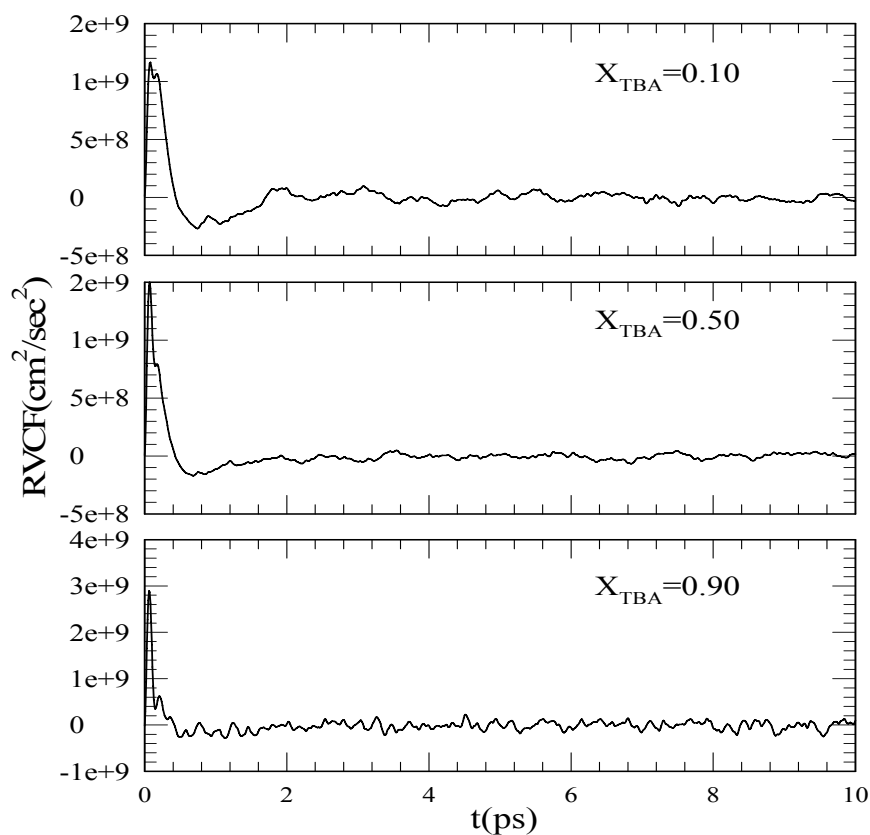


Figure 7.9: Relative velocity correlation function (RVCF) as a function of time, t , at $X_{\text{TBA}} = 0.10$ (top panel), 0.50 (middle panel) and 0.90 (bottom panel).

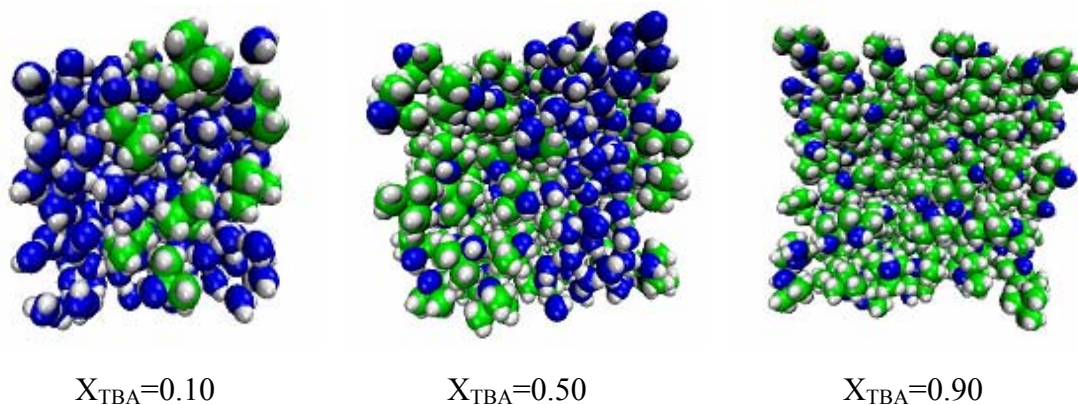


Figure 7.10: Snapshots of the simulated box for $X_{TBA}=0.10$, 0.50 and 0.90 . Oxygens are shown as blue, carbons as green and hydrogens as white spheres.

three different mole fractions of TBA. Since RVCFs are collective quantities unlike VACF, which is averaged over number of particles also, they show larger fluctuations.

7.4 Summary and Conclusion

Let us summarise first the main results of this chapter. We have performed molecular dynamics simulation for fully flexible alcohol-water mixtures over whole composition range and compared the equilibrium and dynamical properties with existing experimental results. The simulated results indicate that these models for water and TBA molecules are able to capture many physical properties of their mixture at least in semi-quantitative level. For TBA concentration less than 15%, the hydrophobic interaction between alkyl groups of TBA molecules makes it strong structure maker. The enhanced water structure induced by hydrophobic interactions is gradually broken down beyond 15-20 % of TBA and simultaneously the contribution to inter and intra species hydrogen-bonding strength increases. Also, at concentrated TBA regime the water dimers and chains are formed, showing very pronounced peaks in corresponding radial distribution functions. Along with these dimers and chains a few *free* water molecules are found in the simulation. The simulated dielectric constant of the mixture is semi-quantitatively agreeing with the experimental data. Self-diffusion coefficient of water is qualitatively matching with PGSE experiment at all

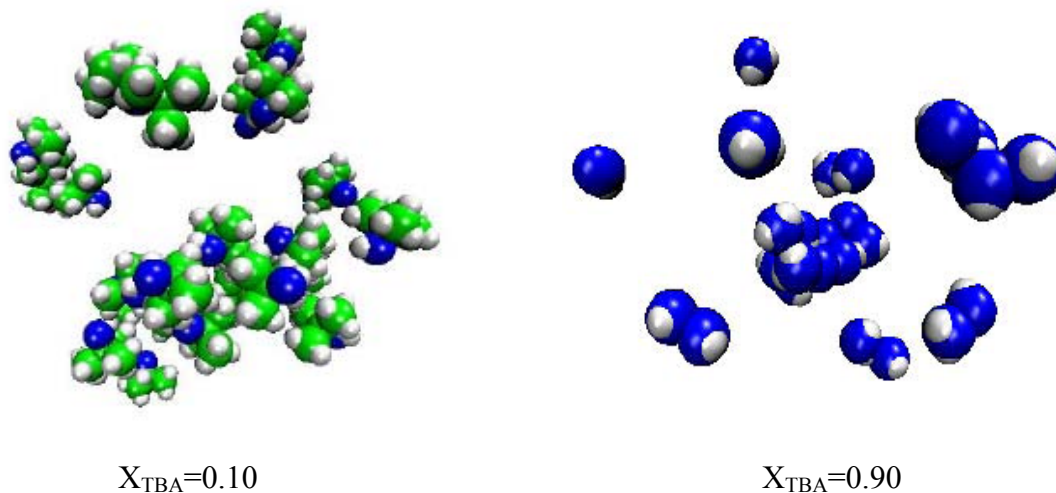


Figure 7.11: Snapshots of the simulated box for $X_{TBA}=0.10$ where water molecules have been removed for clarity and for $X_{TBA}=0.90$ where TBA molecules have been removed to enhance the visibility of water dimers, and chains.

molefractions while self-diffusion coefficient for TBA is poorly predicted by the simulation. Mutual diffusion coefficient in the mixture is also found to be in good agreement with the available experimental data in water-rich region. Further studies are required to understand why the present simulations fail to predict the self-diffusion coefficients any better. Particularly, one needs to understand whether the model potentials used in the present study is sufficient enough to create the structure as observed in real solutions.

References

1. (a) Y. Koga, Chem. Phys. Lett. **111**, 176 (1984); (b) Y. Koga, Can. J. Chem. **66**, 1187 (1988); (c) Y. Koga, Can. J. Chem. **66**, 3171 (1988).
2. Y. Koga, W. W. Y. Siu and T. Y. H. Wang, J. Phys. Chem. **94**, 7700 (1990).
3. (a) K. Iwasaaki and T. Fusiyaama, J. Phys. Chem. **81**, 1908 (1977); (b) K. Iwasaaki and T. Fusiyaama, J. Phys. Chem. **83**, 463 (1979).
4. G. W. Euliss and C. M. Sorensen, J. Chem. Phys. **80**, 4767 (1984).
5. K. Nishikawa, Y. Kodera, and T. Iijima, J. Phys. Chem. **91**, 3694 (1987).
6. K. Nishikawa, J. Phys. Chem. **97**, 10824 (1993).
7. S. Dixit, J. Crain, W. C. K. Poon, J. L. Finney and A. K. Soper, Nature **416**, 829 (2002).
8. D. T. Bowron, J. L. Finney and A. K. Soper, Mol. Phys. **93**, 531 (1998).
9. D. T. Bowron, J. L. Finney and A. K. Soper, J. Phys. Chem. B. **102**, 3551 (1998).
10. D. T. Bowron, A. K. Soper and J. L. Finney, J. Chem. Phys. **114**, 6203 (2001).
11. D. T. Bowron and S. D. Moreno, J. Chem. Phys. **117**, 3753 (2002).
12. D. T. Bowron and S. D. Moreno, J. Phys.: Condens. Matter **15**, S121 (2003).
13. D. T. Bowron and S. D. Moreno, J. Phys. Chem. B **109**, 16210 (2005).
14. D. T. Bowron and J. L. Finney, J. Phys. Chem. B **111**, 9838 (2007).
15. (a) T. Pradhan, P. Ghoshal and R. Biswas, J. Phys. Chem. A **112**, 915 (2007); (b) T. Pradhan, P. Ghoshal and R. Biswas, J. Chem. Sci. **120**, 275 (2008).
16. T. L. Broadwater and R. L. Kay, J. Phys. Chem. **74**, 3802 (1970).
17. V. Calandrini, A. Deriu, G. Onori, R. E. Lechner and J. Pieper, J. Chem. Phys. **120**, 4759 (2004).
18. K. Nakanishi, K. Ikari, S. Okazaki and H. Touhara, J. Chem. Phys. **80**, 1656 (1984).
19. H. Tanaka, K. Nakanishi and H. Touhara, J. Chem. Phys. **81**, 4065 (1984).
20. H. Tanaka and K. Nakanishi, Fluid Phase Equilib. **83**, 77 (1993).
21. R. Noto, V. Martorana, A. Emanuele and S. L. Fornili, J. Chem. Soc., Faraday Trans. **91**, 3803 (1995).
22. K. Yoshida, T. Yamaguchi, A. Kovalenko and F. Hirata, J. Phys. Chem. B **106**, 5042 (2002).

23. K. Yoshida, T. Yamaguchi, A. Kovalenko and F. Hirata, *J. Phys. Chem. B* **106**, 5042 (2002).
24. I. Omelyan, A. Kovalenko and F. Hirata, *J. Theo. Compu. Chem.* **2**, 193 (2003).
25. M. E. Lee and N. F. A. van der Vegt, *J. Chem. Phys.* **122**, 114509 (2005).
26. E. S. Ferrari, R. C. Burton, R. J. Davey and A. Gavezzotti, *J. Comput. Chem.* **27**, 1211 (2006).
27. A. Parera, F. Sokolic, L. Almasy and Y. Koga, *J. Chem. Phys.* **124**, 124515 (2006).
28. M. Kiselev and Ivlev, *J. Mol. Liq.* **110**, 193 (2004).
29. (a) P. G. Kusalik, A. P. Lyubartsev, D. L. Bergman, and Aatto Laaksonen, *J. Phys. Chem. B* **104**, 9526 (2000); (b) P. G. Kusalik, A. P. Lyubartsev, D. L. Bergman, and Aatto Laaksonen, *J. Phys. Chem. B* **104**, 9533 (2000).
30. S. Paul and G. N. Patey, *J. Phys. Chem. B* **110**, 10514 (2006).
31. K. Toukan and A. Rahman, *Phys. Rev. B* **31**, 2643 (1985).
32. A. P. Lyubartsev and Aatto Laaksonen, *Comp. Phys. Commun.* **128**, 565 (2000).
33. M. P. Allen, D. J. Tildesley, *Computer Simulations of Liquids* (Clarendon Press, Oxford, 1987).
34. B. Smith, D. Frenkel, *Understanding Molecular Simulation* (Academic Press, San Diego, 1996).
35. S. Nose, *Mol. Phys.* **52**, 255 (1984).
36. M. Tukerman, B. Berne, G. Martyna, *J. Chem. Phys.* **97**, 1990 (1992).
37. A. Laaksonen, P. G. Kusalik and I. M. Svishchev, *J. Phys. Chem. A* **101**, 5910 (1997).
38. S. K. Allison, J. P. Fox, R. Hargreaves and S. P. Bates, *Phys. Rev. B* **71**, 024201 (2005).
39. L. Dougan, S. P. Bates, R. Hargreaves, J. P. Fox, J. Crain, J. L. Finney, V. Reat and A. K. Soper, *J. Chem. Phys.* **121**, 6456 (2004).
40. M. S. Skaf, and B. M. Ladanyi, *J. Chem. Phys.* **102**, 6542 (1995).
41. C. G. Gray and K. E. Gubbins, *Theory of Molecular Fluids* (Clarendon, Oxford, 1984), Vol. I.
42. J. P. Hansen and I. R. McDonald, *Theory of Simple Liquids* (Academic Press, 1976)

43. P. K. Kipkemboi and A. J. Easteal, *Bull. Chem. Soc. Jpn.* **67**, 2956(1994).
44. W. S. Price, H. Ide and Y. Arata, *J. Phys. Chem. A* **107**, 4784 (2003).
45. C. R. Kamala, K. G. Ayappa and S. Yashonath, *Phys. Rev. E* **65**, 061202 (2002).
46. Z. Zhou, B. D. Todd, K. P. Travis and R. J. Sadus, *J. Chem. Phys.* **123**, 054505 (2005).
47. L. Zhang, Y. Liu, and Q. Wang, *J. Chem. Phys.* **123**, 144701 (2005).
48. L. Zhang, Y. Liu, Q. Wang and L. Zhang, *J. Chem. Phys.* **123**, 144701 (2005).
49. K. R. Harris and H. N. Lam, *J. Chem. Soc. Faraday Trans.* **91**, 4071 (1995).
50. K. R. Harris and P. J. Newitt, *J. Phys. Chem. A* **103**, 6508 (1999).
51. N. Ito, T. Kato and T. Fujiyama, *Bull. Chem. Soc. Jpn.* **54**, 2573 (1981).

Chapter 8

Concluding Remarks and Future Problems

Since concluding remarks are already given in each chapter, we refrain from adding a whole new chapter for Conclusion alone. Rather, we take this opportunity to briefly outline the main results of the works that have embodied the present Thesis and mention some related and interesting problems for future study.

It may be evident from the results presented in previous chapters that the theme of this Thesis revolves around generating an understanding of the interaction effects of various kinds (for example, solute-solvent, ion-solvent, ion-ion, solvent-solvent etc.) on simple chemical events in complex liquids and solution mixtures. Since both technologically relevant and biologically important chemical reactions occur mostly in complex liquid environments, study of events in solution phase assumes even more importance. The complexity in pure solvents may some time originate from specific interactions, such as, H-bonding interactions in water and amide systems. It has indeed been suggested that collective vibrations of network constructed via intermolecular H-bonding in such systems is relevant for many biologically relevant activity. One of the goals of the present study has been to explore the role of such collective low frequency modes in formamide on something very simple – ion diffusion and solvation energy relaxation. Results presented in chapter 2 do indicate that the complexity in solvent-solvent interactions affects these solute events occurring in this medium. In fact, the relevant results suggest that without the participation of these collective modes, the calculated results would be far away from being in good agreement with the experimental data.

As solute-solvent and solvent-solvent interactions can be probed by monitoring diffusion of a species in a given medium, ion transport and particle diffusion have been studied in binary mixtures. Inter- and intra-species interactions in water-TBA mixtures renders heterogeneity in solution structure which affect these diffusive processes enormously. It is this heterogeneity in solution structure that has been found

in the calculations (presented in chapter 3) to regulate the non-monotonic alcohol mole fraction dependence of limiting ionic conductivity of alkali metal ions in water-TBA mixtures. The importance of heterogeneous structure is further realized when static correlations obtained by employing the MSA for model binary polar mixtures (developed in chapter 4) are found to be insufficient as input in the theory for the calculation of ionic conductivity. Even-though the MSA theory based analytical scheme developed in chapter 4 for studying the role of solvent size and dipole moment disparity is insufficient for treating the real complex mixtures, it has clearly indicated that ‘preferential solvation’ in binary mixtures is rather generic in nature, extent of which is accentuated (attenuated) in presence (absence) of specific ion-solvent and solvent-solvent interactions.

The situation becomes even more complex when electrostatic interaction, in addition to dipolar and non-polar interactions also exist in a liquid solvent. Several room temperature ionic liquids, particularly imidazolium ionic liquids are examples of this category. In such solvents, measured Stokes’ shifts (dynamic) have been found to be as large as in strongly dipolar liquids and also an ultrafast component in the time evolution of fluorescence spectrum of a dissolved dipolar probe. Results reported in chapters 5 and 6 reveal that large Stokes shift in these otherwise less polar systems originates from the interaction of the dipolar solute with the dipolar moiety of the ions constituting the liquid (dipole-dipole interaction) and with the ions (ion-dipole interaction). It is also shown that while the presence of the solute-solvent dipolar interaction may be responsible for the ultrafast solvent response at early times in these liquids, the ion-solute (ion-dipole) interaction gives rise to a slow decay of the solvation response function which, in turn, renders the continuum model based theories inapplicable. As already discussed, the collective orientational response of the dipolar environment has been suggested to be the origin for early time response in these liquids which is different from the explanations proposed by many simulation studies. Even-though the present theoretical approach generates some debate about the validity of the model (ionic liquids modelled as electrolyte solutions) used, the works reported here (chapters 5 and 6) explain very satisfactorily the solvation dynamics measurements in both imidazolium (dipolar) and phosphonium (non-dipolar) ionic liquids. It is interesting to note that except the present theory, no other study (simulation or theory) is known to describe systematically the difference found

in dynamic Stokes' shift measurements involving imidazolium and phosphonium ionic liquids.

The results presented in chapters 2 – 6 in this Thesis are obtained via theory that required significant computational endeavour. It was then only logical to expand the computational aspect to another domain – simulation studies - in order to study the real systems with all its complexities. Aqueous mixtures of TBA are chosen for such simulation study where generation of static solvent structure as accurate as possible has been another motivation. It has been found in chapter 3 that accurate description of static solvent structure is crucially important for understanding the alcohol mole-fraction dependence of limiting ionic conductivity in water-TBA mixtures. Another motivation of studying this mixture is to explore the ability of the model potentials to describe the experimentally observed composition dependence of the self and mutual diffusion coefficients of water and TBA molecules. Simulation results presented in chapter 7 indicate a partial success in this direction. Further studies are required to generate better understanding of this mixture and other related polar mixtures which would help a molecular description of non-reactive dynamical events in mixtures of complex solvents.

8.1 Future Problems

8.1.1 Electrolyte Concentration Dependence of Molar Ionic

Conductivity in Mixed Solvents

In chapters 2 & 3 we have already discussed about a microscopy theory of limiting ionic conductivity of ions when dissolved in infinite dilution in pure and mixed solvents. The success of the present theory encourages its obvious generalization to concentrated electrolyte solutions where experimental results are also available.¹ Though such a theory in pure solvents has already been established,² studies in mixture of solvents are still lacking. In concentrated electrolyte solutions one would expect a crucial role of ion-ion interaction and effects of preferential solvation on the ionic conductivity.

8.1.2 Ionic Conductivity of Multivalent Ions in Pure Solvents

Limiting ionic conductivity of multivalent ions is another area where no microscopic theory is found to explain the existing experimental data.³⁻⁴ Like the monovalent ions, the Walden product for multivalent also show a non-monotonic dependence with the inverse of the crystallographic radii.⁴ The validity of the extended molecular hydrodynamic theory presented in chapter 2 for multivalent ions could, however, be questioned because of the following reasons. The EMHT theory is based on *linear response* assumption i. e. the perturbation produced by the electric field of the ionic solute is assumed be so small that solvent structure and dynamics do not change. However, the linear response may break down for multivalent ions and the nonlinear effects will play a crucial role in determining the ionic conductivity. Therefore, a molecular theory which accounts for the non-linearity in both structure and dynamics of pure solvents is certainly would be necessary for studying ion conductivity of multivalent ions in pure polar solvents.

8.1.3 Solvation and Rotational Dynamics in Electrolyte Solutions of Mixed Solvents

Electrolyte solutions of mixed polar solvents are good reaction medium as reactant-medium interaction can be modified by changing either the mole-fraction of one of the solvent component or by increasing the salt concentration. Simple fluorescence Stokes' shift studies of a dipolar solute in such 'ternary' solutions can provide useful information on the competition between ion-solute interaction and ion-solvent preferential solvation. Time-resolved studies may further reveal the effects of these interactions on solvation and rotational dynamics of a solute in such mixtures. Experimental results for these systems are now beginning to emerge.⁵ Hence, theoretical or simulation study would be extremely useful to understand the experimental results of these multi-component mixtures.

8.1.4 Solvation and Rotational Dynamics in (Amide + Salt) Mixtures

It has been long-known that acetamide, upon mixing with sodium or potassium thiocyanate, becomes molten at room temperature. This mixture also super-cools and

the extent of supercooling depends on the identity and valence of the mixed ions.⁶ A large number of physico-chemical studies of such mixtures have been carried out but there exists hardly any dynamical studies of these mixtures. One should investigate these non-aqueous electrolyte mixtures in order to reveal the effects interactions on simply dynamical events in such systems and also to find out how dynamically similar these systems are to ionic liquids.

8.1.5 Electron Transfer Reactions in Room Temperature Ionic

Liquids

In a very recent computer simulation study, the solvent modification of the rate of an electron transfer reaction (ETR) in a room temperature ionic liquid is found to be very similar to that in acetonitrile.⁷ This is surprising because the average solvation rates in these two types of liquids are quite different. However, there exists a similarity in the time scale of the ultrafast solvation response in these two liquids. If the origin of the ultrafast solvation response in the ionic liquid considered in the simulation is the same as that in acetonitrile (that is, arising from the solvent orientational polarization relaxation), then such a similarity of solvent-induced modification of rate between these two types of solvents are only expected. This should be explored further in order to establish the relation between ETR and solvation dynamics in ionic liquids in one hand and to find out the reason for such similarity in rate modification between ionic liquid and common dipolar solvents on the other.

8.1.6 Solvation Dynamics in Common Dipolar Solvents Using DCS as

Probe

Recent dynamic Stokes' shift measurements in common dipolar solvents with trans-4-dimethylamino-4'-cyanostilbene (DCS) have found Stokes' shifts in common dipolar solvents are uniformly larger and dynamics somewhat faster than observed with another solvatochromic probe, coumarin 153 (C153). This has also been the finding for room temperature ionic liquids. Recent calculations of Stokes' shift in ionic liquids (discussed in chapter 6) indicate the whole of the observed shift for DCS may not originate purely from the solvent rearrangement. Interestingly, a very large value

of excited state dipole moment of DCS is required in the calculations to generate shifts as large as found in experiments involving ionic liquids. However, such a large value of the excited state dipole moment for DCS is not supported by the quantum mechanical calculations and a change in vibronic structure is suggested to be responsible for the observed large shift. It would therefore be interesting to calculate both Stokes' shift and solvation dynamics for several dipolar solvents with both DCS and C153 as probes and find out the correlation between the observed *larger* shift and *faster* dynamics.

The problems discussed above are just a few representative ones, study of which may provide useful information on interactions and their effects on various events occurring in various complex media. Since for these systems either experimental results are already available or would be made available soon, simultaneous theoretical and simulation studies would bring out comprehensive understanding of these systems. This is important not only from the basic scientific point of view but also from the industrial aspects as many of these systems possess great potential for use in chemical industry and technology development. This has been certainly one of the goals of the work described in the present Thesis which is probably partially satisfied. Therefore, a lot more is to be done.

References

1. T. L. Broadwater and R. L. Kay, *J. Phys. Chem.* **74**, 3802 (1970).
2. A. Chandra and B. Bagchi, *J. Chem. Phys.* **110**, 10024 (1999).
3. T. L. Broadwater and D. F. Evans, *J. Sol. Chem.* **3**, 757 (1974).
4. D. F. Evans, T. Tominaga, J. B. Hubbard and P. G. Wolynes, *J. Phys. Chem.* **83**, 2669 (1979) and the references therein.
5. H. A. R. Gazi, H. K. Kashyap and R. Biswas, *J. Chem. Phys.* (in preparation).
6. B. Guchhait, H. A. R. Gazi, H. K. Kashyap and R. Biswas, *J. Chem. Phys.* (in preparation).
7. Y. Shim and H. J. Kim *J. Phys. Chem. B* **113**, 12964 (2009).

Appendix I

The Generalized Rate of Orientational Polarization Density

Relaxation, $\sum_{lm}(k, z)$

The generalized rate of orientational polarization density relaxation, $\sum_{lm}(k, z)$, is an outcome in the solution of coupled hydrodynamic equations for number and momentum densities. The origin of $\sum_{lm}(k, z)$ is as follows: In general, for a *dense* molecular liquids the *slow-conserved* variables are number density, $\rho_d(\mathbf{r}, \mathbf{\Omega}, t)$, and the translational and angular momentum densities, $\mathbf{g}_T(\mathbf{r}, \mathbf{\Omega}, t)$ and $\mathbf{g}_R(\mathbf{r}, \mathbf{\Omega}, t)$, respectively. The extended hydrodynamic equations for these conserved variables are given by^{1,2}

$$\frac{\partial \rho_d(\mathbf{r}, \mathbf{\Omega}, t)}{\partial t} + \frac{1}{M} \nabla_T \cdot \mathbf{g}_T(\mathbf{r}, \mathbf{\Omega}, t) + \frac{1}{I} \nabla_R \cdot \mathbf{g}_R(\mathbf{r}, \mathbf{\Omega}, t) = 0 \quad (\text{AI.1})$$

where I represents the average moment of inertia of solvent molecule of mass M ,

and

$$\frac{\partial \mathbf{g}_i(\mathbf{r}, \mathbf{\Omega}, t)}{\partial t} = -\rho_d(\mathbf{r}, \mathbf{\Omega}, t) \nabla_i \frac{\delta \Delta F[\rho_d(t)]}{\delta \rho_d(\mathbf{r}, \mathbf{\Omega}, t)} - \int_0^t dt' \int d\mathbf{r}' d\mathbf{\Omega}' \Gamma_i(\mathbf{r}-\mathbf{r}', t-t') \delta(\mathbf{\Omega}-\mathbf{\Omega}') \mathbf{g}_i(\mathbf{r}', \mathbf{\Omega}', t) + f_i(\mathbf{r}, \mathbf{\Omega}, t) \quad (\text{AI.2})$$

where i stands for either translation (T) or rotation (R). $\Delta F[\rho_d(t)]$ is the excess free energy functional of pure solvent (without solute). Equation AI.1 is continuity equation for number density, $\rho_d(\mathbf{r}, \mathbf{\Omega}, t)$, of the solvent. Note here that the memory kernel $\Gamma_i(\mathbf{r}-\mathbf{r}', t-t') \delta(\mathbf{\Omega}-\mathbf{\Omega}')$ describes the dissipative dynamics in a non-Markovian system where the forces and torques acting on a solvent molecule are correlated only *space* and *time* but not in *orientation*. This approximation¹ has been found to be sufficiently valid in the study of polar solvation dynamics which basically probes only the orientational relaxation of rank $l=1$. $f_i(\mathbf{r}, \mathbf{\Omega}, t)$ are the random force and the random torque acting on a particle at time t . The dissipative memory kernels are

related to the random force and random torque auto correlation functions through second fluctuation dissipation theorem.¹

Now, Eqs. (AI.1) and (AI.2) are solved by using Fourier and Laplace transformation in space and time, respectively. In the inverse space the above coupled equations consist of fluctuating number density $\delta\rho_d(\mathbf{k}, \boldsymbol{\Omega}, t)$ and direct correlation function $c(k, \boldsymbol{\Omega}, \boldsymbol{\Omega}')$ of the solvent. Then, these functions are expanded in spherical harmonics as¹

$$\delta\rho_d(\mathbf{k}, \boldsymbol{\Omega}, t) = \sum_{l,m} a_{lm}(\mathbf{k}, t) Y_{lm}(\boldsymbol{\Omega}) \quad (\text{AI.3})$$

$$c(k, \boldsymbol{\Omega}, \boldsymbol{\Omega}') = \sum_{l,m} c(llm, k) Y_{lm}(\boldsymbol{\Omega}) Y_{lm}(\boldsymbol{\Omega}') \quad (\text{AI.4})$$

Here, k is chosen to be parallel to the z -axis of laboratory fixed frame. The use of above expansion in hydrodynamic equations gives an equation in terms of expansion coefficients $a_{lm}(\mathbf{k}, t)$ and $c(llm, k)$. It is to be noted that the evolution of density relaxation takes place through $a_{lm}(\mathbf{k}, t)$. Therefore, the solution of the coupled hydrodynamic equations is derived in terms of $a_{lm}(\mathbf{k}, t)$. We first differentiate Eq. (AI.1) with respect to time so that momenta densities are eliminated and then by taking Fourier and Laplace transformations, we get the following expression for the Laplace transform of $a_{lm}(\mathbf{k}, t)$ ¹⁻⁴

$$a_{lm}(\mathbf{k}, z) = \frac{a_{lm}(\mathbf{k}, t=0)}{z + \sum_{lm}(k, z)} \quad (\text{AI.5})$$

where $\sum_{lm}(k, z)$ is generalized rate of orientational polarization density relaxation and is given by¹⁻⁴

$$\sum_{lm}(k, z) = \frac{k_B T k^2 f(llm, k)}{M \sigma^2 [z + \Gamma_T(k, z)]} + \frac{k_B T l(l+1) f(llm, k)}{I [z + \Gamma_R(k, z)]} \quad (\text{AI.6})$$

where σ , M and I are the diameter, mass and average moment of inertia of the solvent molecule, respectively. $\Gamma_T(k, z)$ and $\Gamma_R(k, z)$ are the wavenumber and

frequency dependent translational and rotational memory kernels, respectively. $f(lm, k) = 1 - (\rho_d^0 / 4\pi)(-1)^m c(lm, k)$, describes the orientational static structure of the solvent.

Solvent Translational Friction Kernel, $\Gamma_T(k, z)$

The translational memory kernel, $\Gamma_T(k, z)$ is obtained by isotropic ($l=m=0$) component of $a_{lm}(\mathbf{k}, z)$ as¹⁻⁴

$$a_{00}(\mathbf{k}, z) = \frac{a_{00}(\mathbf{k}, t=0)}{z + \frac{k_B T k^2 f(000, k)}{M\sigma^2 [z + \Gamma_T(k, z)]}} \quad (\text{AI.7})$$

By taking its correlation with function $a_{lm}(\mathbf{k}, t=0)$ and ensemble average we get

$$\langle a_{00}(\mathbf{k}, z) a_{00}(\mathbf{k}, t=0) \rangle = \frac{\langle |a_{00}(\mathbf{k}, t=0)|^2 \rangle}{z + \frac{k_B T k^2 f(000, k)}{M\sigma^2 [z + \Gamma_T(k, z)]}} \quad (\text{AI.8})$$

or,

$$S(k, z) = \frac{S(k)}{z + \frac{k_B T k^2 / S(k)}{M\sigma^2 [z + \Gamma_T(k, z)]}} \quad (\text{AI.9})$$

Rearranging the above equation we get

$$\frac{k_B T}{M\sigma^2 [z + \Gamma_T(k, z)]} = \frac{S(k)[S(k) - zS(k, z)]}{k^2 S(k, z)} \quad (\text{AI.10})$$

where $S(k, z)$ and $S(k)$ are wavenumber and frequency dependent isotropic part of solvent dynamic structure factor and static structure factor, respectively. The isotropic solvent static structure factor is often calculated by using Percus-Yevick (PY) hard sphere direct correlation function, $c_{PY}(k)$ as: $S(k) = [1 - \rho_d^0 c_{PY}(k)]^{-1}$. The

wavenumber and time dependent isotropic part of solvent dynamic structure factor, $S(k, t)$, is assumed be given by ¹

$$S(k, t) = L^{-1}[S(k, z)] = L^{-1} \left[\frac{S(k)}{z + \frac{D_T^{Solvent} k^2}{S(k)}} \right] \quad (\text{AI.11})$$

where $D_T^{Solvent}$ is solvent translational diffusion coefficient and can be calculated from its viscosity. L^{-1} is Laplace inversion operator.

Solvent Rotational Friction Kernel, $\Gamma_R(k, z)$

The calculation of rotational memory kernel $\Gamma_R(k, z)$ is complicated and highly nontrivial for all wave numbers. However, an approximate but reliable scheme for the calculating $\Gamma_R(k, z)$ for underdamped liquids has been proposed by Roy and Bagchi²⁻⁴. In this scheme the k-dependence of $\Gamma_R(k, z)$ have been neglected and therefore the kernel $\Gamma_R(k, z)$ is replaced by $\Gamma_R(k=0, z)$. The function $\Gamma_R(k=0, z)$ is directly related to frequency dependent dielectric function $\varepsilon(z)$ through a molecular theory as²⁻⁴

$$\frac{2f(110, k=0)k_B T}{I[z + \Gamma_R(k, z)]} = \frac{z\varepsilon_0[\varepsilon(z) - \varepsilon_\infty]}{\varepsilon_\infty[\varepsilon_0 - \varepsilon(z)]} \quad (\text{AI.12})$$

where ε_0 the static dielectric constant of the medium and ε_∞ is high frequency dielectric constant. $f(110, k=0)$ is the long wave-length of $f(110, k)$.

References

1. B. Bagchi and R. Biswas, Adv. Chem. Phys. **109**, 207 (1999) and references therein.
2. S. Roy and B. Bagchi, J. Chem. Phys. **99**, 1310 (1993).
3. S. Roy and B. Bagchi, J. Chem. Phys. **99**, 9938 (1993).
4. N. Nandi, S. Roy and B. Bagchi, J. Chem. Phys. **102**, 1390 (1995).

Appendix II

Derivation of the Solvent Response Function for a Mobile and Fixed Dipolar Solute

Here we present the solvent response function, $S(t)$, for a mobile (both translationally and rotationally) and fixed dipolar solute using density functional theory. We start with the excess free energy functional for a system of solute dissolved in a solvent given by¹⁻²

$$\begin{aligned}
 \beta\Delta F[\rho_s(\mathbf{r}, \mathbf{\Omega}), \rho_d(\mathbf{r}, \mathbf{\Omega})] = & \int d\mathbf{r}d\mathbf{\Omega} \rho_s(\mathbf{r}, \mathbf{\Omega}) \left[\ln \frac{\rho_s(\mathbf{r}, \mathbf{\Omega})}{\rho_s^0 / 4\pi} - 1 \right] + \int d\mathbf{r}d\mathbf{\Omega} \rho_d(\mathbf{r}, \mathbf{\Omega}) \left[\ln \frac{\rho_d(\mathbf{r}, \mathbf{\Omega})}{\rho_d^0 / 4\pi} - 1 \right] \\
 & - \frac{1}{2} \int d\mathbf{r}d\mathbf{\Omega} d\mathbf{r}'d\mathbf{\Omega}' c_{ss}(\mathbf{r}, \mathbf{\Omega}; \mathbf{r}', \mathbf{\Omega}') \delta\rho_s(\mathbf{r}, \mathbf{\Omega}) \delta\rho_s(\mathbf{r}', \mathbf{\Omega}') \\
 & - \frac{1}{2} \int d\mathbf{r}d\mathbf{\Omega} d\mathbf{r}'d\mathbf{\Omega}' c_{dd}(\mathbf{r}, \mathbf{\Omega}; \mathbf{r}', \mathbf{\Omega}') \delta\rho_d(\mathbf{r}, \mathbf{\Omega}) \delta\rho_d(\mathbf{r}', \mathbf{\Omega}') \\
 & - \int d\mathbf{r}d\mathbf{\Omega} d\mathbf{r}'d\mathbf{\Omega}' c_{sd}(\mathbf{r}, \mathbf{\Omega}; \mathbf{r}', \mathbf{\Omega}') \delta\rho_s(\mathbf{r}, \mathbf{\Omega}) \delta\rho_d(\mathbf{r}', \mathbf{\Omega}')
 \end{aligned} \tag{AII.1}$$

where $\rho_s(\mathbf{r}, \mathbf{\Omega})$ and $\rho_d(\mathbf{r}, \mathbf{\Omega})$ are, respectively, the solute and solvent number density at position \mathbf{r} with orientation $\mathbf{\Omega}$ at any time t . $c_{ss}(\mathbf{r}, \mathbf{\Omega}; \mathbf{r}', \mathbf{\Omega}')$, $c_{dd}(\mathbf{r}, \mathbf{\Omega}; \mathbf{r}', \mathbf{\Omega}')$ and $c_{sd}(\mathbf{r}, \mathbf{\Omega}; \mathbf{r}', \mathbf{\Omega}')$ are the position and orientation dependent solute-solute, solvent-solvent and solute-solvent direct correlation functions, respectively. The fluctuation in solute density ($\delta\rho_s$) over its bulk value, ρ_s^0 , is given by, $\delta\rho_s(\mathbf{r}, \mathbf{\Omega}) = \rho_s(\mathbf{r}, \mathbf{\Omega}) - \rho_s^0 / 4\pi$. $\delta\rho_d(\mathbf{r}, \mathbf{\Omega}) = \rho_d(\mathbf{r}, \mathbf{\Omega}) - \rho_d^0 / 4\pi$ is the space (\mathbf{r}), orientation ($\mathbf{\Omega}$) and time (t) dependent fluctuation in the average number density ρ_d^0 of the pure solvent. Note that in the above functional Taylor expansion of the free energy, the higher order (third, fourth etc) terms are small and so neglected. Now we need the expression for solvation energy which is essentially the effective potential energy of solute due to its interaction with the surrounding solvent molecules. By taking functional derivative of the above free energy functional and equating it equal to zero for equilibrium condition, we get the expression for equilibrium density of solute as^{1,3}

$$\rho_s^{Equil.} = \frac{\rho_s^0}{4\pi} \exp\{-\beta\Delta V_s^{eff}(\mathbf{r}, \mathbf{\Omega})\} \quad (AII.2)$$

where $\beta\Delta V_s^{eff}(\mathbf{r}, \mathbf{\Omega})$ is position and orientation dependent effective potential acting on the solute due to solute-solute, solute-solvent interactions and is given by¹

$$\beta\Delta V_s^{eff}(\mathbf{r}, \mathbf{\Omega}) = -\int d\mathbf{r}'d\mathbf{\Omega}'c_{ss}(\mathbf{r}, \mathbf{\Omega}; \mathbf{r}', \mathbf{\Omega}')\delta\rho_s(\mathbf{r}', \mathbf{\Omega}') - \int d\mathbf{r}'d\mathbf{\Omega}'c_{sd}(\mathbf{r}, \mathbf{\Omega}; \mathbf{r}', \mathbf{\Omega}')\delta\rho_d(\mathbf{r}', \mathbf{\Omega}') \quad (AII.3)$$

However, the probe molecules (solute) that are often used in solvation dynamics experiments are present in infinite dilution. Therefore, the term originating from solute-solute interaction can be neglected. We assume that the temporal evolution of $\beta\Delta V_s^{eff}(\mathbf{r}, \mathbf{\Omega})$ is originated solely from the time dependent fluctuation of position and orientation dependent solvent density. With this assumption we have,

$$\beta\Delta V_s^{eff}(\mathbf{r}, \mathbf{\Omega}, t) = -\int d\mathbf{r}'d\mathbf{\Omega}'c_{sd}(\mathbf{r}, \mathbf{\Omega}; \mathbf{r}', \mathbf{\Omega}')\delta\rho_d(\mathbf{r}', \mathbf{\Omega}', t) \quad (AII.4)$$

The above equation represents the time dependent fluctuating effective potential acting on an immobile solute, both rotationally and translationally. It is shown, however, earlier by Biswas and Bagchi that consideration of solute motions accelerates the rate of its own solvation.^{1,3} The expression for the position (\mathbf{r}), orientation ($\mathbf{\Omega}$) and time (t) dependent fluctuating solvation energy for mobile dipolar solute of density $\rho_s(\mathbf{r}, \mathbf{\Omega})$ can be given as follows^{1,3}

$$\Delta E_{sol}(\mathbf{r}, \mathbf{\Omega}, t) = -k_B T \rho_s(\mathbf{r}, \mathbf{\Omega}; t) \int d\mathbf{r}'d\mathbf{\Omega}'c_{sd}(|\mathbf{r} - \mathbf{r}'|, \mathbf{\Omega}, \mathbf{\Omega}')\delta\rho_d(\mathbf{r}', \mathbf{\Omega}', t) \quad (AII.5)$$

If we define the inverse Fourier transformation as

$$f(\mathbf{r}) = \frac{1}{(2\pi)^3} \int d\mathbf{k} e^{-i\mathbf{k}\cdot\mathbf{r}} f(\mathbf{k}) \quad (AII.6)$$

where $f(\mathbf{r})$ can be $\rho_s(\mathbf{r}, \mathbf{\Omega}, t)$, $c_{sd}(|\mathbf{r} - \mathbf{r}'|, \mathbf{\Omega}, \mathbf{\Omega}')$ and $\delta\rho_d(\mathbf{r}', \mathbf{\Omega}', t)$, and $f(\mathbf{k})$ is their respective Fourier transforms $\rho_s(\mathbf{k}, \mathbf{\Omega}, t)$, $c_{sd}(k, \mathbf{\Omega}, \mathbf{\Omega}')$ and $\delta\rho_d(\mathbf{k}, \mathbf{\Omega}', t)$, then Eq. (AII.5) in wavenumber space can be written as

$$\Delta E_{sol}(\mathbf{q}, \mathbf{\Omega}, t) = -\frac{k_B T}{(2\pi)^3} \int d\mathbf{k} d\mathbf{\Omega}' \rho_s(\mathbf{k}, \mathbf{\Omega}, t) c_{sd}(k, \mathbf{\Omega}, \mathbf{\Omega}') \delta\rho_d(\mathbf{q} - \mathbf{k}, \mathbf{\Omega}', t) \quad (\text{AII.7})$$

The expansion of the angle dependent quantities into spherical harmonics and subsequent integration over angle lead Eq. (AII.7) to take the following form^{1,3}

$$\Delta E_{sol}(\mathbf{q}, \mathbf{\Omega}, t) = -k_B T \sum_{l_1, m_1, l_2, m_2} (-1)^{m_2} Y_{l_1 m_1}(\mathbf{\Omega}) Y_{l_2 m_2}(\mathbf{\Omega}) \int d\mathbf{k} A_{l_1 m_1}(\mathbf{k}, t) c_{sd}(l_2 l_2' m_2, k) a_{l_2 m_2}(\mathbf{q} - \mathbf{k}, t) \quad (\text{AII.8})$$

where $A_{l_1 m_1}(\mathbf{k}, t)$, $c_{sd}(l_2 l_2' m_2, k)$ and $a_{l_2 m_2}(\mathbf{k}, t)$ are the expansion coefficients of solute density $\rho_s(\mathbf{k}, \mathbf{\Omega}, t)$, solute-solvent direct correlation function $c_{sd}(k, \mathbf{\Omega}, \mathbf{\Omega}')$ and fluctuating solvent density $\delta\rho_d(\mathbf{k}, \mathbf{\Omega}', t)$. Using Gaussian decoupling approximation in energy autocorrelation function defined by $C_{EE}(t) = \langle \Delta E_{sol}(t) \Delta E_{sol}(0) \rangle$, in $\mathbf{q} = \mathbf{0}$ limit, we get^{1,3}

$$C_{EE}(t) = 4\pi \frac{(k_B T)^2}{(2\pi)^3} \rho_d^0 \sum_{l, m} \delta_{l, l} [\delta_{m, 0} + 2\delta_{m, 1}] \int_0^\infty dk k^2 S_{solute}^{lm}(k, t) |c_{sd}(l m, k)|^2 S_{solvent}^{lm}(k; t) \quad (\text{AII.9})$$

where $S_{solute}^{lm}(k, t)$ is the $(l, m)^{\text{th}}$ component of the wavenumber dependent self part of the solute dynamic structure factor and is given by

$$S_{solute}^{lm}(k, t) = \langle A_{lm}(k, t) A_{lm}(-k, 0) \rangle \quad (\text{AII.10})$$

and $S_{solvent}^{lm}(k, t)$ is $(l, m)^{\text{th}}$ component of the wavenumber dependent solvent orientational dynamic structure factor defined as

$$S_{solvent}^{lm}(k, t) = \frac{\langle a_{lm}(k, t) a_{lm}(-k, 0) \rangle}{N} \quad (\text{AII.11})$$

where N is the total number of solvent molecules. $\langle \dots \rangle$ denotes the equilibrium ensemble average over all the orientations, Ω .

In our calculation we have adopted the dipolar hard-sphere model for solute and solvent, and used mean spherical approximation (MSA) for obtaining microscopic static correlation functions and solvent orientational structure factors. The fatal error often observed in MSA at $k \rightarrow 0$ and $k \rightarrow \infty$ limits are corrected properly.^{1,3} Combining the expressions of extended hydrodynamic theory and MSA model the final expressions for longitudinal ($S_{solvent}^{10}(k, t)$) and transverse ($S_{solvent}^{10}(k, t)$) components of solvent orientational dynamic structure factor are written as^{1,3}

$$S_{solvent}^{10}(k, t) = S_{solvent}^{10}(k) L^{-1} \left[\frac{1}{z + \sum_{10}(k, z)} \right] = \frac{1}{4\pi 3Y} \left[1 - \frac{1}{\epsilon_L(k)} \right] L^{-1} \left[\frac{1}{z + \sum_{10}(k, z)} \right] \quad (\text{AII.12})$$

and,

$$S_{solvent}^{11}(k, t) = S_{solvent}^{11}(k) L^{-1} \left[\frac{1}{z + \sum_{11}(k, z)} \right] = \frac{[\epsilon_T(k) - 1]}{4\pi 3Y} L^{-1} \left[\frac{1}{z + \sum_{11}(k, z)} \right] \quad (\text{AII.13})$$

Here L^{-1} stands for Laplace inversion. $3Y$ is the polarity parameter of the solvent which is related to the dipole-moment, μ , and density, ρ_d^0 , of the solvent by the relation, $3Y = (4\pi / 3k_B T) \mu^2 \rho_d^0$. $\epsilon_L(k)$ and $\epsilon_T(k)$ are the longitudinal and transverse components of wave number dependent dielectric function. $\sum_{lm}(k, z)$ is the $(l, m)^{th}$ component of the generalized rate of orientational polarization density relaxation of the solvent. The details of the calculation of $\sum_{lm}(k, z)$ can be found in Refs. 1 and 4, and also in Appendix I.

The $(l, m)^{th}$ component of the solute orientational dynamic structure factor which, for a single dipolar solute, is assumed to be given by

$$S_{solute}^{lm}(k, t) = \frac{1}{4\pi} \exp \left[- (l(l+1)D_R^s + k^2 D_T^s) t \right] \quad (\text{AII.14})$$

where the rotational (D_R^s) and translational (D_T^s) diffusion coefficients of the solute are obtained from liquid viscosity using proper hydrodynamic boundary conditions. For an immobile (both rotationally and translationally) solute, $D_R^s = D_T^s = 0$. Therefore, for fixed solute the expression for normalized energy auto correlation function can be written as⁵

$$S(t) = \frac{\int_0^\infty dk k^2 \left\{ |c_{sd}^{10}(k)|^2 \left[1 - \frac{1}{\varepsilon_L(k)} \right] L^{-1} [z + \Sigma_{10}(k, z)]^{-1} + 2 |c_{sd}^{11}(k)|^2 [\varepsilon_T(k) - 1] L^{-1} [z + \Sigma_{11}(k, z)]^{-1} \right\}}{\int_0^\infty dk k^2 \left\{ |c_{sd}^{10}(k)|^2 \left[1 - \frac{1}{\varepsilon_L(k)} \right] + 2 |c_{sd}^{11}(k)|^2 [\varepsilon_T(k) - 1] \right\}} \quad (\text{AII.15})$$

References

5. B. Bagchi and R. Biswas, Adv. Chem. Phys. **109**, 207 (1999) and references therein.
6. B. Bagchi and A. Chandra, Adv. Chem. Phys. **80**, 1 (1991); B. Bagchi, Annu. Rev. Phys. Chem. **40**, 115 (1989).
7. R. Biswas and B. Bagchi, J. Phys. Chem. **100**, 4261 (1996).
8. S. Roy and B. Bagchi, J. Chem. Phys. **99**, 1310 (1993); J. Chem. Phys. **99**, 9938 (1993).
9. H. K. Kashyap, T. Pradhan and R. Biswas, J. Chem. Phys. **125**, 174506 (2006).

Appendix III

Derivation of Solvation Response Function, $S_E(t)$

The total excess free energy functional for a system of dipolar solutes dissolved in a liquid consisting of dipoles and ions can be written as¹

$$\begin{aligned}
 \beta\Delta F[\rho_s(\mathbf{r}, \mathbf{\Omega}), \rho_d(\mathbf{r}, \mathbf{\Omega}), n_\alpha(\mathbf{r})] = & \int d\mathbf{r}d\mathbf{\Omega}\rho_s(\mathbf{r}, \mathbf{\Omega})\left[\ln\frac{\rho_s(\mathbf{r}, \mathbf{\Omega})}{\rho_s^0/4\pi}-1\right] + \int d\mathbf{r}d\mathbf{\Omega}\rho_d(\mathbf{r}, \mathbf{\Omega})\left[\ln\frac{\rho_d(\mathbf{r}, \mathbf{\Omega})}{\rho_d^0/4\pi}-1\right] \\
 & + \sum_{\alpha=1}^2 \int d\mathbf{r}n(\mathbf{r})\left[\ln\frac{n(\mathbf{r})}{n_\alpha^0}-1\right] \\
 & - \frac{1}{2} \int d\mathbf{r}d\mathbf{\Omega}d\mathbf{r}'d\mathbf{\Omega}'c_{ss}(\mathbf{r}, \mathbf{\Omega}; \mathbf{r}', \mathbf{\Omega}')\delta\rho_s(\mathbf{r}, \mathbf{\Omega})\delta\rho_s(\mathbf{r}', \mathbf{\Omega}') \\
 & - \frac{1}{2} \int d\mathbf{r}d\mathbf{\Omega}d\mathbf{r}'d\mathbf{\Omega}'c_{dd}(\mathbf{r}, \mathbf{\Omega}; \mathbf{r}', \mathbf{\Omega}')\delta\rho_d(\mathbf{r}, \mathbf{\Omega})\delta\rho_d(\mathbf{r}', \mathbf{\Omega}') \\
 & - \frac{1}{2} \sum_{\alpha, \beta=1}^2 \int d\mathbf{r}d\mathbf{r}'c_{\alpha\beta}(\mathbf{r}, \mathbf{r}')\delta n_\alpha(\mathbf{r})\delta n_\beta(\mathbf{r}') \\
 & - \int d\mathbf{r}d\mathbf{\Omega}d\mathbf{r}'d\mathbf{\Omega}'c_{sd}(\mathbf{r}, \mathbf{\Omega}; \mathbf{r}', \mathbf{\Omega}')\delta\rho_s(\mathbf{r}, \mathbf{\Omega})\delta\rho_d(\mathbf{r}', \mathbf{\Omega}') \\
 & - \sum_{\alpha=1}^2 \int d\mathbf{r}d\mathbf{\Omega}d\mathbf{r}'c_{d\alpha}(\mathbf{r}, \mathbf{\Omega}; \mathbf{r}')\delta\rho_d(\mathbf{r}, \mathbf{\Omega})\delta n_\alpha(\mathbf{r}') \\
 & - \sum_{\alpha=1}^2 \int d\mathbf{r}d\mathbf{\Omega}d\mathbf{r}'c_{s\alpha}(\mathbf{r}, \mathbf{\Omega}; \mathbf{r}')\delta\rho_s(\mathbf{r}, \mathbf{\Omega})\delta n_\alpha(\mathbf{r}')
 \end{aligned}
 \tag{AIII.1}$$

where $\delta\rho_s(\mathbf{r}, \mathbf{\Omega}) = \rho_s(\mathbf{r}, \mathbf{\Omega}) - \rho_s^0/4\pi$, $\delta\rho_d(\mathbf{r}, \mathbf{\Omega}) = \rho_d(\mathbf{r}, \mathbf{\Omega}) - \rho_d^0/4\pi$,

and $\delta n_\alpha(\mathbf{r}) = n_\alpha(\mathbf{r}) - n_\alpha^0$ are the fluctuations of solute dipole, solvent dipole and ion densities about their bulk values, respectively. In equilibrium,

$\frac{\delta\beta\Delta F[\rho_s(\mathbf{r}, \mathbf{\Omega}), \rho_d(\mathbf{r}, \mathbf{\Omega}), n_\alpha(\mathbf{r})]}{\delta\rho_s(\mathbf{r}, \mathbf{\Omega})} = 0$. Thus, by taking functional derivative of the above

free energy functional and equating it equal to zero for equilibrium condition we get the effective fluctuating potential acting on the solute due to solute (dipole)-solvent (dipole) and solute-ion interactions. Subsequent generalization to time domain allows one to write the following expression for the time dependent fluctuating effective potential energy¹

$$\beta\Delta V_{eff}(\mathbf{r}, \mathbf{\Omega}, t) = -\int d\mathbf{r}'d\mathbf{\Omega}'c_{sd}(\mathbf{r}, \mathbf{\Omega}; \mathbf{r}', \mathbf{\Omega}')\delta\rho_d(\mathbf{r}', \mathbf{\Omega}', t) - \sum_{\alpha=1}^2 \int d\mathbf{r}'c_{s\alpha}(\mathbf{r}, \mathbf{\Omega}; \mathbf{r}')\delta n_{\alpha}(\mathbf{r}', t) \quad (\text{AIII.2})$$

As the probe molecules (solute) used in solvation dynamics experiments are present at infinite dilution, the term originating from solute-solute interaction are neglected. Also, we have assumed that the temporal evolution of $\beta\Delta V_s^{eff}(\mathbf{r}, \mathbf{\Omega}, t)$ is originated solely from the time dependent fluctuation solvent (dipole) and ion densities. Therefore, the expression for the position (\mathbf{r}), orientation ($\mathbf{\Omega}$) and time (t) dependent fluctuating solvation energy of the solute is written as

$$\Delta E_{total}(\mathbf{r}, \mathbf{\Omega}, t) = -k_B T \int d\mathbf{r}'d\mathbf{\Omega}'c_{sd}(\mathbf{r}, \mathbf{\Omega}; \mathbf{r}', \mathbf{\Omega}')\delta\rho_d(\mathbf{r}', \mathbf{\Omega}', t) - k_B T \sum_{\alpha=1}^2 \int d\mathbf{r}'c_{s\alpha}(\mathbf{r}, \mathbf{\Omega}; \mathbf{r}')\delta n_{\alpha}(\mathbf{r}', t) \quad (\text{AIII.3})$$

The above equation represents the time dependent solvation energy of an immobile (both rotationally and translationally) solute. It is shown, however, earlier by Biswas and Bagchi that consideration of solute motions accelerates the rate of its own solvation. The expression for the position (\mathbf{r}), orientation ($\mathbf{\Omega}$) and time (t) dependent solvation energy for mobile dipolar solute with distribution function $\rho_s(\mathbf{r}, \mathbf{\Omega}, t)$ can be written as follows

$$\begin{aligned} \Delta E_{total}(\mathbf{r}, \mathbf{\Omega}, t) &= -k_B T \rho_s(\mathbf{r}, \mathbf{\Omega}, t) \left[\int d\mathbf{r}'d\mathbf{\Omega}'c_{sd}(\mathbf{r}, \mathbf{\Omega}; \mathbf{r}', \mathbf{\Omega}')\delta\rho_d(\mathbf{r}', \mathbf{\Omega}', t) + \sum_{\alpha=1}^2 \int d\mathbf{r}'c_{s\alpha}(\mathbf{r}, \mathbf{\Omega}; \mathbf{r}')\delta n_{\alpha}(\mathbf{r}', t) \right] \\ &= \Delta E_{sd}(\mathbf{r}, \mathbf{\Omega}, t) + \Delta E_{si}(\mathbf{r}, \mathbf{\Omega}, t) \end{aligned} \quad (\text{AIII.4})$$

where, the energy due to dipole-dipole interaction is given by

$$\Delta E_{sd}(\mathbf{r}, \mathbf{\Omega}, t) = -k_B T \rho_s(\mathbf{r}, \mathbf{\Omega}, t) \int d\mathbf{r}'d\mathbf{\Omega}'c_{sd}(\mathbf{r}, \mathbf{\Omega}; \mathbf{r}', \mathbf{\Omega}')\delta\rho_d(\mathbf{r}', \mathbf{\Omega}', t) \quad (\text{AIII.5})$$

and the energy due to dipole-ion interaction is given by

$$\Delta E_{s\alpha}(\mathbf{r}, \mathbf{\Omega}, t) = -k_B T \rho_s(\mathbf{r}, \mathbf{\Omega}, t) \sum_{\alpha=1}^2 \int d\mathbf{r}'c_{s\alpha}(\mathbf{r}, \mathbf{\Omega}; \mathbf{r}')\delta n_{\alpha}(\mathbf{r}', t) \quad (\text{AIII.6})$$

Note that equation (AIII.4) is Eq. 6.1 of chapter 6. Note that incorporation of solute motion via $\rho_s(\mathbf{r}, \mathbf{\Omega}, t)$ in Eq. AIII.6 is somewhat *ad-hoc* but is physically reasonable. The correlation terms (c_{sd} and $c_{s\alpha}$) convolutes with the fluctuating densities ($\delta\rho_d$ and δn_α) to give excess chemical potential, $\Delta\mu_{excess}$ due to the solute-solvent (dipolar and solute-ion) interactions. Therefore, $\rho_s\Delta\mu_{excess}$ represents the total energy density felt by the solute.²

The time dependent total solvation energy for dipolar solute probe averaged over space and angles is, therefore, given by

$$\Delta E_{total}(t) = \int d\mathbf{r}d\mathbf{\Omega}\Delta E_{total}(\mathbf{r}, \mathbf{\Omega}, t) \quad (\text{AIII.7})$$

If we define the inverse Fourier transformation as

$$f(\mathbf{r}) = \frac{1}{(2\pi)^3} \int d\mathbf{k} e^{-i\mathbf{k}\cdot\mathbf{r}} f(\mathbf{k}) \quad (\text{AIII.8})$$

where $f(\mathbf{r})$ can be $c_{sd}(|\mathbf{r}-\mathbf{r}'|, \mathbf{\Omega}, \mathbf{\Omega}')$, $c_{s\alpha}(|\mathbf{r}-\mathbf{r}'|, \mathbf{\Omega})$, $\rho_s(\mathbf{r}, \mathbf{\Omega}, t)$, $\delta\rho_d(\mathbf{r}', \mathbf{\Omega}', t)$ or $\delta n_\alpha(\mathbf{r}, t)$, and $f(\mathbf{k})$ are their respective Fourier transforms $c_{sd}(k, \mathbf{\Omega}, \mathbf{\Omega}')$, $c_{s\alpha}(k, \mathbf{\Omega})$, $\rho_s(\mathbf{k}, \mathbf{\Omega}, t)$, $\delta\rho_d(\mathbf{k}, \mathbf{\Omega}', t)$ or $\delta n_\alpha(\mathbf{k}, t)$, respectively.

Subsequently, Eq. (AIII.7) leads to following expression for the time dependent total solvation energy of a dipolar solute probe

$$\Delta E_{total}(t) = \Delta E_{sd}(t) + \Delta E_{si}(t) \quad (\text{AIII.9})$$

where,

$$\Delta E_{sd}(t) = -\frac{k_B T}{(2\pi)^3} \int d\mathbf{k}d\mathbf{\Omega}d\mathbf{\Omega}' \rho_s(-\mathbf{k}, \mathbf{\Omega}, t) c_{sd}(k, \mathbf{\Omega}; \mathbf{\Omega}') \delta\rho_d(\mathbf{q}-\mathbf{k}, \mathbf{\Omega}', t) \quad (\text{AIII.10})$$

$$\Delta E_{si}(t) = -\frac{k_B T}{(2\pi)^3} \sum_{\alpha=1}^2 \int d\mathbf{k} d\Omega \rho_s(-\mathbf{k}, \Omega, t) c_{s\alpha}(k, \Omega) \delta n_{\alpha}(\mathbf{q} - \mathbf{k}, t) \quad (\text{AIII.11})$$

Now, $\rho_s(\mathbf{k}, \Omega, t)$, $\delta\rho_d(\mathbf{k}, \Omega, t)$, $c_{s\alpha}(k, \Omega)$ and $c_{sd}(k, \Omega, \Omega')$ functions are expanded in spherical harmonics as follows³

$$\rho_s(\mathbf{k}, \Omega, t) = \sum_{l,m} A_{lm}(\mathbf{k}, t) Y_{lm}(\Omega) \quad (\text{AIII.12})$$

$$\delta\rho_d(\mathbf{k}, \Omega, t) = \sum_{l,m} a_{lm}(\mathbf{k}, t) Y_{lm}(\Omega) \quad (\text{AIII.13})$$

$$c_{s\alpha}(k, \Omega) = \sum_{l,m} c_{s\alpha}^{lm}(k) Y_{lm}(\Omega) \quad (\text{AIII.14})$$

$$c_{sd}(k, \Omega, \Omega') = \sum_{l,l',m} c_{sd}^{ll'm}(k) Y_{lm}(\Omega) Y_{l'm}(\Omega') \quad (\text{AIII.15})$$

Here, k is chosen to be parallel to the z -axis of laboratory fixed frame. The expansion of the angle dependent quantities into spherical harmonics, assumed separation of time scales between the fluctuating ion and dipole densities and the choice of time-origin as $t' = 0$, provides the following expression for normalized solvation response function

$$S_E(t) = \frac{\langle \Delta E_{total}(t) \Delta E_{total}(0) \rangle}{\langle |\Delta E_{total}(0)|^2 \rangle} = \frac{\langle |\Delta E_{sd}(0)|^2 \rangle S_{sd}(t)}{\langle |\Delta E_{sd}(0)|^2 \rangle + \langle |\Delta E_{si}(0)|^2 \rangle} + \frac{\langle |\Delta E_{si}(0)|^2 \rangle S_{si}(t)}{\langle |\Delta E_{sd}(0)|^2 \rangle + \langle |\Delta E_{si}(0)|^2 \rangle} \quad (\text{AIII.16})$$

where, $S_{sd}(t)$ and $S_{si}(t)$ are normalized solvation energy auto-correlation function due to the dipole-dipole and dipole-ion interactions, respectively. The above equation is Eq. 6.3 of chapter 6.

The expression for $S_{sd}(t)$ finally takes the following form

$$S_{sd}(t) = \frac{\langle \Delta E_{sd}(t) \Delta E_{sd}(0) \rangle}{\langle |\Delta E_{sd}(0)|^2 \rangle} = \frac{P \int_0^\infty dk k^2 S_{solute}^{10}(k, t) |c_{sd}^{10}(k)|^2 S_{solvent}^{10}(k, t) + 2P \int_0^\infty dk k^2 S_{solute}^{11}(k, t) |c_{sd}^{11}(k)|^2 S_{solvent}^{11}(k, t)}{P \int_0^\infty dk k^2 S_{solute}^{10}(k) |c_{sd}^{10}(k)|^2 S_{solvent}^{10}(k) + 2P \int_0^\infty dk k^2 S_{solute}^{11}(k) |c_{sd}^{11}(k)|^2 S_{solvent}^{11}(k)}$$

(AIII.17)

where P denotes the pre-factor, $2\rho_d^0 \left(\frac{k_B T}{2\pi} \right)^2 \cdot S_{solute}^{lm}(k, t) = \langle A_{lm}(-k, t) A_{lm}(k) \rangle$, is $(l, m)^{th}$ component of solute self-dynamic structure factor. $S_{solvent}^{lm}(k, t) = \langle a_{lm}(-k, t) a_{lm}(k) \rangle / N$, is $(l, m)^{th}$ component of solvent (dipole) orientational dynamic structure factor, N being total number of dipolar particles.

The expression for $S_{si}(t)$ is given as

$$S_{si}(t) = \frac{\langle \Delta E_{si}(t) \Delta E_{si}(0) \rangle}{\langle |\Delta E_{si}(0)|^2 \rangle} = \frac{2 \left(\frac{k_B T}{2\pi} \right)^2 \sum_{\alpha, \beta} \sqrt{n_\alpha^0 n_\beta^0} \int_0^\infty dk k^2 S_{solute}^{10}(k, t) c_{s\alpha}^{10}(k) c_{s\beta}^{10}(-k) S_{\alpha\beta}^{ion}(k, t)}{2 \left(\frac{k_B T}{2\pi} \right)^2 \sum_{\alpha, \beta} \sqrt{n_\alpha^0 n_\beta^0} \int_0^\infty dk k^2 S_{solute}^{10}(k) c_{s\alpha}^{10}(k) c_{s\beta}^{10}(-k) S_{\alpha\beta}^{ion}(k)}$$

(AIII.18)

where $S_{\alpha\beta}^{ion}(k, t) = \frac{\langle \delta n_\alpha(-k, t) \delta n_\alpha(k) \rangle}{\sqrt{N_\alpha N_\beta}}$ is the isotropic ion dynamic structure factor

and N_α the number of α^{th} type ion (cation or anion). Note that equations (AIII.17) and (AIII.18) are respectively the Eqs. 6.4 and 6.5 of chapter 6.

References

1. B. Bagchi and R. Biswas, *Adv. Chem. Phys.* **109**, 207 (1999).
2. (a) A. V. Indrani, S. Ramaswamy, *Phys. Rev. Lett.* **73**, 360 (1994); (b) R. Biswas, S. Roy and B. Bagchi, *Phys. Rev. Lett.* **75**, 1098 (1995).
3. C. G. Grey and K. E. Gubbins, *Theory of Molecular Fluids*, Vol. I, Oxford University: Oxford, 1984.

Table AIII.1: Solvation characteristics of a few imidazolium and phosphonium ionic liquids: Experimental Results

Ionic Liquid	Viscosity of the Ionic Liquid (Poise)	Dynamic Stokes' Shifts (cm^{-1})	Fraction Observed f_{obs}	Average Solvation Time, $\langle \tau_s \rangle$ (ns)	Characteristics of S(t)
DCS+[bmim][PF ₆] ^(a) (Temp. at 298K)	3.10 ^(b)	4240	1.05	1.0±0.20	Biphasic with $\tau_1 \sim 0.3\text{ps}$, $\tau_2 \sim 140\text{ps}$ and $\beta \sim 0.31$
DCS+[bmim][BF ₄] ^(a) (Temp. at 298K)	1.54 ^(c)	4080	1.12	0.34±0.07	Biphasic with $\tau_1 \sim 0.3\text{ps}$, $\tau_2 \sim 130\text{ps}$ and $\beta \sim 0.41$
C153+[P _{14,666}][Br] ^(d) (Temp. at 343K)	1.16	1590	0.99	5.1±0.4	Stretched exponential with single time constant, $\tau \sim 1300\text{ps}$ and $\beta \sim 0.38$
C153+[P _{14,666}][Cl] ^(d) (Temp. at 343K)	1.33	1500	0.93	4.5±0.3	Stretched exponential with single time constant, $\tau \sim 1900\text{ps}$ and $\beta \sim 0.46$
C153+[P _{14,666}][BF ₄] ^(d) (Temp. at 343K)	0.87	1370	1.03	1.98±0.11	Stretched exponential with single time constant, $\tau \sim 1010\text{ps}$ and $\beta \sim 0.51$

(a) Arzhantsev, S.; Jin, H.; Baker, G. A.; Maroncelli, M. *J. Phys. Chem. B* **2007**, *111*, 4978.

(b) Tokuda, H.; Tsuzuki, S.; Susan, M. A. B. H.; Hayamizu, K.; Watanabe, M. *J. Phys. Chem. B* **2006**, *110*, 19593.; Wang, J.; Zhu, A.; Zhou, K.; *J. Solution Chem.* **2005**, *34*, 585.; Dzyuba, S. V.; Bartsch, R. A.; *ChemPhysChem* **2002**, *3*, 161.; Huddelston, J. G.; Visser, A. E.; Reichert, W. M.; Willauer, H. D.; Broker, G. A.; Rogers, R. D.; *Green Chem.* **2001**, *3*, 156.

(c) Nishida, T.; Tashiro, Y.; Yamamoto, M.; *J. Fluorine Chem.* **2003**, *120*, 135.; Huddelston, J. G.; Visser, A. E.; Reichert, W. M.; Willauer, H. D.; Broker, G. A.; Rogers, R. D.; *Green Chem.* **2001**, *3*, 156.; Sanmamed, Y. A.; Gonzalez-Salagado, D.; Troncoso, J.; Cerdeirina, C. A.; Romani, L.; *Fluid Phase Equilib.* **2007**, *252*, 96.

(d) Jin, H.; Baker, G. A.; Arzhantsev, S.; Dong, J.; Maroncelli, M. *J. Phys. Chem. B* **2007**, *111*, 7291.

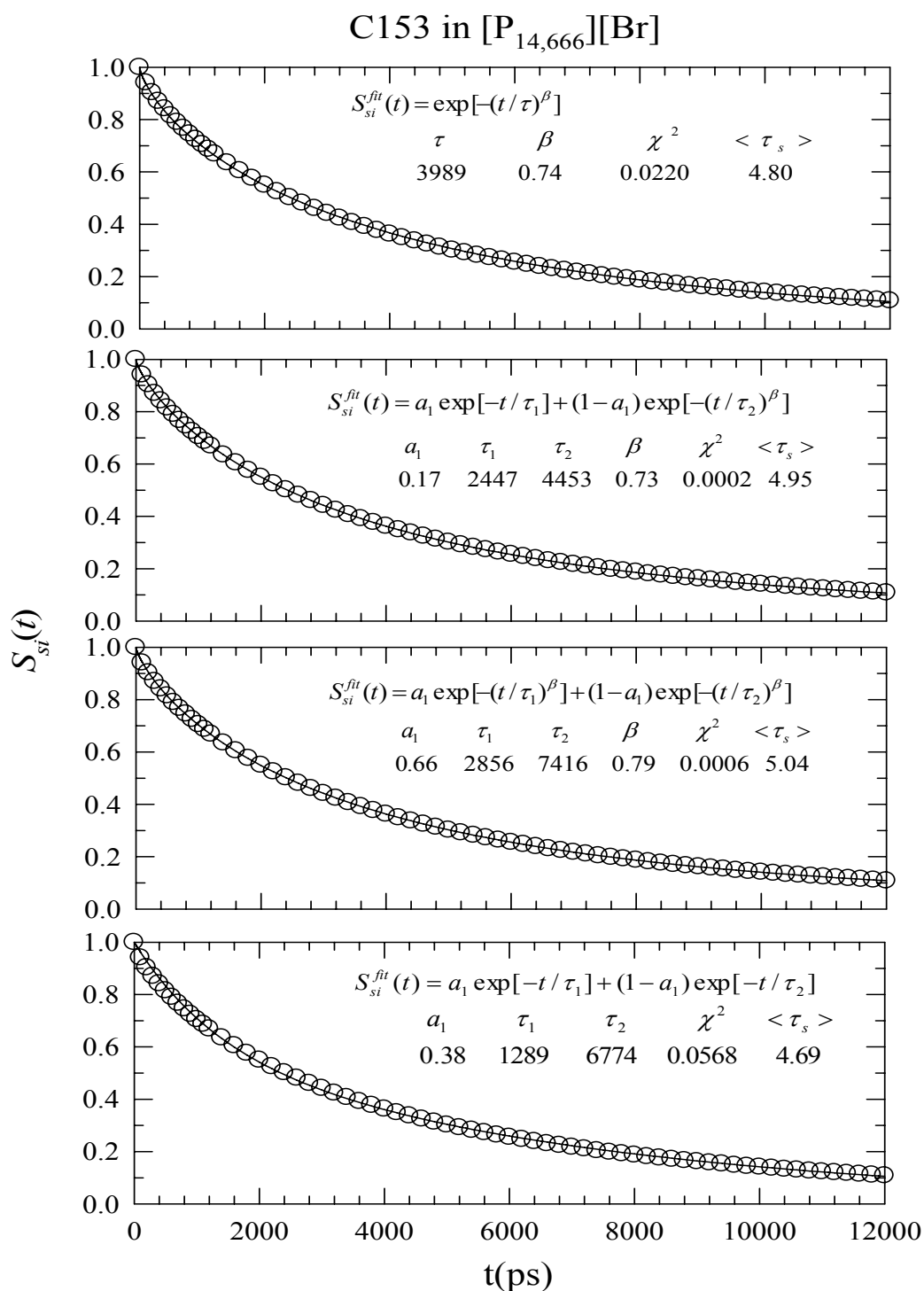


Figure AIII.1: Representative fitting of calculated $S_{si}(t)$ to various types of decay functions. The system shown here is C153 in $[P_{14,666}][Br]$ at 343 K. The calculated results are shown by *circles* and the fitted functions by *solid lines*. The time constants, τ , τ_1 and τ_2 , are all in picoseconds whereas the average solvation times, $\langle \tau_s \rangle$, are in nanoseconds. Note that similar degree of applicability of all these fitting functions has also been observed for other liquids studied here. For more information see text and Ref. 52 of chapter 6.